

THÈSE EN COTUTELLE PRÉSENTÉE  
POUR OBTENIR LE GRADE DE  
**DOCTEUR DE**  
**L'UNIVERSITÉ DE BORDEAUX**  
**ET DE LIÈGE UNIVERSITÉ**

ÉCOLE DOCTORALE SVS

ÉCOLE DOCTORALE GBX-ABT

SPÉCIALITÉ BIOLOGIE CELLULAIRE

Par Jules PETIT

**MEMBRANE TETHERING IN PLANT INTERCELLULAR COMMUNICATION :  
STRUCTURE-FUNCTION OF MULTIPLE C2 DOMAINS AND  
TRANSMEMBRANE REGION PROTEINS (MCTP) AT PLASMODESMATA ER-  
PM MEMBRANE CONTACT SITES**

Sous la direction de Laurence LINS  
et de Emmanuelle M. BAYER

Soutenue le 04 Mars 2022

Membres du jury:

Mme FAUCONNIER Marie-Laure	Professeure, Gbx ABT, ULiège	Présidente
M. VANNI Stefano	Professor, Université de Fribourg	Rapporteur
Mme CAILLAUD Marie Cécile	Chargée de recherche, ENS Lyon	Rapporteuse
M. JOSHI Amit	Assistant professor, University of Tennessee	Examineur
M. BOUTTE Yohann	Chargé de recherche, Université de Bordeaux	Examineur
M. TALY Antoine	Chargé de recherche, UPR9080 CNRS	Examineur



**Title:** Membrane Tethering in Plant Intercellular Communication : Structure-Function of Multiple C2 domains and Transmembrane Region Proteins (MCTP) at Plasmodesmata ER-PM Membrane Contact Sites

**Abstract:** Plant multicellularity relies on intercellular communication in order to transmit information from cell to cell and throughout the entire plant body. In land plants, the major line for such cellular conversations is through plasmodesmata (PD) pores, which are nanoscopic membranous tunnels spanning the pecto-cellulosic cell wall. These pores are indeed involved in the transfer of a wide variety of molecules such as transcription factors, RNAs, hormones and metabolites during all stages of plant life, adaptation and responses to their environment. PD are singular amongst other types of intercellular junctions as they provide a direct continuity of the endoplasmic reticulum (ER), the plasma membrane (PM) and the cytosol between neighboring cells. Their architectural organization can be summarized as followed: a thin strand of constricted ER, called desmotubule, is encased in a tube of PM lining the cell wall. PD are seen as a specialized ER-PM membrane contact sites from the very close apposition (2 to 10 nm) of the ER and PM membranes and the presence of tethering elements bridging the two organelles. In this study, we describe the structural organization and function of several members of the MCTP (Multiple C2 domains and Transmembrane region Protein) family which act as ER-PM tethering elements at PD. We show that these proteins possess molecular features capable of transient interaction with anionic lipids of the PM, through their C2 domains, as well as ER membrane shaping, through their transmembrane region which presents homology to a reticulon domain. We further correlate MCTP function with PD architecture and biogenesis, and investigate on the role of the ER inside PD. Altogether, this work provides original data placing MCTPs as core PD proteins that appear to be crucial in the establishment of PD ultrastructure and associated functions.

**Keywords:** Plant biology; Plasmodesmata; Intercellular communication; Membrane contact sites; MCTP; molecular modeling

---

**Titre:** Rôle des connexions membranaires dans la communication intercellulaire des plantes: Structure-fonction des protéines MCTPs aux sites de contacts membranaires RE-MP des plasmodesmes

**Résumé:** La multicellularité chez les plantes repose sur une communication intercellulaire qui permette le transfert d'informations à travers l'entièreté de l'organisme. Chez les plantes terrestres, la route principale de ces "conversations cellulaires" est assurée par les plasmodesmes (PD), des canaux nanoscopiques qui traversent la paroi pecto-cellulosique. En effet, ces pores sont impliqués dans la circulation d'une très grande variété de molécules, comme des facteurs de transcription, de l'ARN, des hormones et des métabolites et ceci à tous les stades de la vie végétale, permettant réponses et adaptations à l'environnement. Les PD sont particuliers dans le sens où ils forment une continuité du réticulum endoplasmic (RE), de la membrane plasmique (MP) et du cytoplasme entre les cellules adjacentes. Leur architecture est singulière et consiste en un filament de RE, appelé desmotubule, entouré d'un tube de MP qui, lui, longe la paroi. Les PD sont actuellement décrits comme des sites de contact membranaire, du fait du fort accollement des membranes du RE et de la MP (2 à 10 nm) et de la présence de protéines de jonction qui connectent les deux organelles. Dans la présente étude, nous décrivons au niveau structural et fonctionnel plusieurs membres de la famille des MCTPs (protéine avec de multiples domaines C2 et une région transmembranaire) comme protéines assurant la jonction du RE et de la MP dans les PD. Nous démontrons que ces protéines possèdent les caractéristiques moléculaires nécessaires à l'interaction transitoire avec les lipides anioniques de la MP, via leurs domaines C2, ainsi qu'à l'induction de courbure membranaire au RE, via la région transmembranaire qui agit comme un domaine homologue aux protéines réticulons. Ces données nous ont permis de corréliser la fonction des MCTPs à l'architecture et la biogenèse des PD et de réfléchir au rôle du RE à l'intérieur des PD. En conclusion, ce travail a fourni des résultats originaux qui placent les MCTPs comme des protéines centrales dans l'établissement de la structure fine des PD et des fonctions qui y sont associées.

**Mots clés:** Biologie végétale; Plasmodesmes; Communication intercellulaire; Sites de contacts membranaires; MCTP; modélisation moléculaire

---

Laboratoire de biogenèse membranaire, UMR5200-UB, 71 av. Edouard Bourlaux F-33140 Villenave d'Ornon  
Laboratoire de biophysique moléculaire aux interfaces, Gbx-ABT-ULiège, 2 Passage des Déportés B-5030 Gembloux

## **Table of Contents**

Abbreviation glossary

Chapter 1. Introduction **p1**

- 1.1. General introduction **p2**
- 1.2. Aim of the thesis **p3**
- 1.3. Molecular modeling and dynamics **p6**
- 1.4. Plasmodesmata and membrane contact sites **p9**
- 1.5. Collaborations **p11**

Chapter 2. Multiple C2 domains and Transmembrane region Proteins (MCTP) are multifunctional actors at plasmodesmata **p12**

- 2.1. What do we know about the MCTP protein family? **p13**
- 2.2. MCTP proteins tether ER-PM membranes at plasmodesmata **p16**
- 2.3. MCTP transmembrane region is a Reticulon Homology Domain **p18**
  - 2.3.1. Introduction on Reticulon Homology domains **p18**
  - 2.3.2. MCTP TMR is able to shape the cortical ER in vivo **p19**
  - 2.3.3. Sequence analysis and sub-domain delimitation **p23**
  - 2.3.4. 3D modeling of MCTP TMR subdomains **p23**
  - 2.3.5. Membrane simulations of MCTP TMR subdomains **p24**
  - 2.3.6. Bloc assembly and perspectives for full TMR reconstruction **p27**
  - 2.3.7. Mutations in MCTP4 TMR **p27**
- 2.4. The role of MCTP in primary PD biogenesis **p30**
  - 2.4.1. Plant cytokinesis and PD biogenesis: inserting and stabilizing ER strands across the forming cell wall **p30**
  - 2.4.2. Expression and localization of MCTP in dividing cells **p31**
  - 2.4.3. Establishment of TEM-based quantification of PD density in the root meristem **p34**
  - 2.4.4. Searching for defects in PD biogenesis **p35**

Chapter 3. General Discussion **p38**

3.1. MCTP C2 domains: opening Pandora's box **p41**

3.2. MCTP contains RHD, why? **p43**

3.3. MCTP function in primary PD assembly during cytokinesis **p44**

Conclusion and Perspectives **p47**

Material and Methods **p49**

Bibliography **p52**

## **Abbreviations in alphabetic order**

APH	Amphipathic Helix
ER	Endoplasmic Reticulum
E-syt	Extended Synaptotagmin
ET	Electron Tomography
FT	Flowering locus T
HP	Hairpin
MCTP	Multiple C2 domains and Transmembrane region Protein
MCS	Membrane Contact Site
PD	Plasmodesmata
PI4P	Phosphatidylinositol-4-phosphate
PI(4,5)P <sub>2</sub>	Phosphatidylinositol-4,5-biphosphate
PM	Plasma Membranes
RHD	Reticulon Homology Domain
RTN	Reticulon
TEM	Transmission Electron Microscopy
TMR	Transmembrane region
TMD	Transmembrane domain

## Remerciements

Je souhaite, dans cette section, remercier les personnes qui ont été présentes durant ces quatre dernières années, de manière directe dans le cadre de mon projet mais aussi et surtout dans tous les autres aspects de la vie.

Tout d'abord, je remercie du fond de mon coeur Laurence Lins et Emmanuelle Bayer, mes deux promotrices, qui m'ont encouragé, soutenu et aidé de tout leur enthousiasme et de toute leur expertise dans ce projet de recherche. Je les remercie de m'avoir accordé leur confiance et je suis très reconnaissant qu'elles aient apporté autant d'attention bienveillante aux aspects techniques et professionnels qu'aux aspects humains et personnels. Je remercie le F.N.R.S et la bourse FRIA d'avoir soutenu mon travail toutes ces années.

Je suis également extrêmement heureux d'avoir rencontré autant de merveilleuses personnes à travers la vie du laboratoire et avec qui j'ai partagé de très bons moments, parmi elles Magali et Yohann pour les séances d'escalade, Marie pour partager avec moi le bureau et de grandes discussions, Françoise pour sa curiosité, Patrick pour son care et sa force d'esprit, Jessi pour sa joie et son amour, Marija pour la beauté des voyages, Flo pour ses conseils rando et sa douceur, MD pour son entropie, Marguerite pour sa gentillesse, Delphine pour sa confiance, Lucie, Victor, Clément, Andrea, Seb, Carlos, Pepe, ... Je remercie également Lysiane et Melina, avec qui la microscopie devient beaucoup plus que de la microscopie.

Je suis plein de gratitude et d'amour pour les personnes de mon entourage proche et lointain qui ont été là pour moi, ponctuellement ou sur la durée. Je pense, dans le désordre, à Mélina, Nadia, Amine, Nina, Lola, Patrice, Pia, Amandine, Stanislas, Mar, Zoé, Emily, Réal, Estelle, Lucas, Emma, Laura, Roxane, Julien, Loup, Alix, Cécile, Shay, Augustin, Emmanuel, Lucas, Andrea, Annick, Alan, Micka, Jean-Sébastien, Aude, Saeed, Gaëlle, Hélène, Elia, Milou, Esther, Miriam, Aby, Kaya, Louison, Faustine, Marin, Alexia, Hanna, Hayden, Marie-Lou, Emmanuelle, Sonia, Morgane, Ara, Anaïs, Clem, Malou, ...

Pour terminer, je remercie ma mère Virginie qui m'a toujours fait grandir de son amour, et mon père Jean qui m'a toujours soutenu avec fierté. Je pense aussi à mon frère Charles sur qui je sais que je peux compter, à sa femme Thanva et mes nièces Estelle et Rachel.

J'écris ces lignes et clôture cette thèse avec une pensée d'amour et de douceur pour mon père.

**1**

---

**Introduction**



## 1.1. General introduction

Ask a stranger in the street: What is a plant to you? Now, what are the chances they will answer that a plant is a “green living thing” without showing profound interest? And maybe they will have the mental image of the half-dead houseplant they had to water three weeks ago...

Joke aside, we cannot deny that plants exist in a different reality, or, at least, that us humans have the most difficult time to include plants in our reality on Earth, despite the fact that plants are literally everywhere and that our own lives rely on them. This syndrome was nicely denominated “plant blindness” and one of the differences that comes to explain it is the difference in ways of living and associated timescales (“Loving the Alien,” 2019).

In a physical and evolutionary point of view, all living organisms are visco-elastic matters, composed of both liquid and solid molecules. However, there is a big divergence between animals, which could be considered more fluid, in capacity of movement, and plants, which are more static, partly because of the solid nature of the cell walls encasing their cells. From this major difference, plants take advantage of their multicellularity in a completely different way than us in order to maintain the plasticity required for survival (Benítez et al., 2018). Multicellularity relies on developmental processes called dynamical patterning modules that are collections of shared gene networks, their results and the physical forces shaping the cells and their components. In the context of transition from unicellularity, dynamical patterning modules are necessary to integrate the extra layers of complexity arising from multicellularity: the coordination of cell activities in a multicellular organism is more complicated than the simple addition of two cells. In plants, six dynamical patterning modules were proposed and the most important ones being cell to cell adhesion, plans of cell division, spatially dependent differentiation and cell polarity. The third main dynamical patterning module, driven by plasmodesmata intercellular connections, is thought to be critical for the evolution of complex multicellularity in embryophytes (Benítez et al., 2018; Hernández-Hernández et al., 2012). Its importance is easy to imagine when you know that there are hundreds of plasmodesmata at each cell to cell interface, and that, for almost every cell in the whole plant body.

Plasmodesmata are at the center of plant life, whether it is in response to developmental, adaptative or responsive cues, because they are in between worlds of symplastic transport and apoplastic division, between

connection and differentiation of cells throughout the entire plant body, at local and systemic scales (Brunkard et al., 2015; Brunkard & Zambryski, 2017). But in parallel to its key functions, plasmodesmata significance also lies in their structural features. They consist of a continuity of three compartments, namely the endoplasmic reticulum (ER), the plasma membrane (PM) and the cytosol, but also are integral parts of the cell wall (Li et al., 2021). They are organized in a tubular arrangement where the highly constricted ER, the desmotubule, is inserted into a tube of PM lining the cell wall. Inside the pore, between the two membranes, the cytoplasmic sleeve is crossed by tethering elements making ER-PM connections (Nicolas et al., 2017). The closeness of the membranes from the two different organelles and the presence of tethers connecting them lead scientists to envision plasmodesmata as unique areas for ER-PM membrane contact sites (Rosado & Bayer, 2020; Tilsner et al., 2016), thus opening new perspectives of research in the field.

While some physiological events and associated molecular actors occurring at plasmodesmata have already been, and still are, under thorough examination, for instance the role of callose in symplastic regulation (Gaudioso-Pedraza et al., 2018; Han et al., 2019; Yadav et al., 2014), our knowledge remains incomplete due to methodological limitations caused by their nano-scale dimension. Indeed, understanding plasmodesmata-mediated trafficking and regulation of their components at the molecular resolution is important but very challenging as they are a hub of complexity hidden in the cell wall. For this reason, it is vital for us scientists to expand our research using multidisciplinary approaches as it is for instance the case for molecular modeling and cell biology (Deinum et al., 2019; Gronnier et al., 2017; Park et al., 2019).

## **1.2. Aim of the thesis**

As I started my PhD along a pioneer project lead by Emmanuelle Bayer's group, the aim of my thesis began with the rather broad objective of uncovering the function of ER-PM contacts at plasmodesmata. Indeed, the scientific community working on plasmodesmata still lacks understanding on how and why the ER and the PM come together at these cellular junctions, in such a peculiar organization, and, of course, the consequences it has on intercellular communication and thus on plant life and development.

By diving in the topic, the team and I were able to highlight three major intertwined themes at different scales: 1/ the actors and molecular mechanisms regulating organelle tethering at plasmodesmata, 2/ the

dynamics and architecture of the membrane contact sites and the plasmodesmata pores and 3/ the role of the contacts in intercellular communication and plasmodesmata formation.

The first theme was initiated with the search of protein candidates that could act as ER-PM tethers specifically at plasmodesmata, using proteomic assays performed on purified plasmodesmata. From this screen we identified a protein family called Multiple C2 domains and Transmembrane region Proteins (MCTP; 16 members in Arabidopsis) as the prime plasmodesmata-associated tethering candidates (Brault, Petit et al., 2019).

During my PhD I have used molecular dynamics combined with plant cell biology to start uncovering the function and molecular mechanisms of ER-PM membrane tethering at plasmodesmata driven by the MCTP proteins. I have tried to answer the following questions: Do MCTP proteins possess the molecular features necessary for tethering two membranes? If so, how do they interact with the ER and PM and what drives their association with plasmodesmata? Finally, as structural plasmodesmata elements, how do they impact plasmodesmata function and architecture? This last question was legitimate as two MCTP members were already known to be involved in several signaling pathways (see below), thus, can they possess a more structural function as well? If so, are the two connected and how?

The first part of my PhD work consisted in understanding, at the molecular level, how MCTP proteins create bridges between the ER and the PM within plasmodesmata, and their impact on plant development. This work has been published in EMBO Reports in 2019 where i am co-first author (Brault, Petit et al., 2019). In this paper we showed that MCTP members are core plasmodesmata components that insert in the ER through a C-terminal transmembrane region (TMR) and dock to the PM through anionic lipid interaction via their N-terminal C2 domains (3 to 4 domains depending on the members). Double loss-of-function mutant *mctp3,4* displays strong growth and developmental phenotype linked with cell-to-cell trafficking defects. This work unveils for the first time the molecular identity of tether proteins acting specifically inside plasmodesmata intercellular junctions.

Toward the middle of my thesis, new questions emerged in conjunction with the role of the MCTP TMR, which anchors the protein in the ER membrane. We found out that, similar to human MCTP (Joshi et al., 2021), Arabidopsis MCTP TMR displays homology to reticulon domains, a motif known to shape the ER into tubules. This hypothetical ER-shaping MCTP-associated function is relevant to plasmodesmata

structure, which presents a highly constricted form of ER. In the second part of my PhD, I have therefore tried to address the following questions: Are MCTP capable of shaping the ER into the narrow desmotubule that spans plasmodesmata? How could the structural motif of MCTP TMR be responsible for shaping and plasmodesmata association? *In planta*, MCTP3 and 4 TMRs are able to shape the cortical ER when overexpressed. Molecular modeling of the MCTP4 TMR enabled the prediction of five subdomains (two amphipathic helices, two hairpin transmembrane helices and one putative transmembrane domain). This data allowed the generation of single-domain deletion TMR constructs. Their expression *in planta* demonstrates redundancy in cortical ER-shaping but shows that they are all necessary for plasmodesmata targeting of the full-length MCTP.

Last, as structural elements bridging the ER to the PM, we wonder whether MCTP proteins could be involved in the establishment of plasmodesmata and the plant intercellular network. Plasmodesmata are initiated during the cell division but we have little details on the molecular mechanisms driving their insertion across the new cell wall. In the last months of my PhD, I have tried to understand the molecular mechanisms and functions that could be associated with the MCTP transmembrane region and then integrate it, together with the role the C2 domains and MCTP tethering ability, in the context of the building of plasmodesmata pore architecture (a tube within a tube). During primary plasmodesmata formation at cytokinesis, ER strands are inserted across the expanding cell plate and their contacts with the cell plate membrane have to be actively controlled (Seguí-Simarro et al., 2004). Are MCTPs the tethering elements involved in this critical step of connecting the ER to the PM during plasmodesmata biogenesis? How could both the C2 domains and the transmembrane region work collaboratively to perform such a task?

To unravel these questions, I used a combination of molecular modeling, cell biology and electron microscopy techniques. Working on loss-of-function *mctp* mutant backgrounds allowed us to compare plasmodesmata-associated defects with the wild type and correlate them with MCTP functions during plasmodesmata assembly. Live imaging of fluorescent-tagged MCTP3 and 4 in dividing cells in root meristem show a gradual transition from ER signal to nascent PD accumulation at the cell plate. In the same tissues, PD density in *mctp* mutants is significantly decreased (30 to 40%) compared to the wild type. Electron tomography data brings evidence that the ER-cell plate connections are central to PD formation.

These results place MCTP as early and important actors in PD biogenesis, possibly by connecting the ER to the cell plate.

### **1.3. Molecular modeling and simulation**

In this project, I used bio-informatic tools to explore and partly answer the questions mentioned above. Bio-informatics are a very broad term to talk about computer techniques applied to the field of life sciences. They include, for example, the handling and analysis of big and complex data (Vilsker et al., 2019) or the computation prediction/modeling of systems (Gabler et al., 2020). The recent development of novel machine learning algorithms is noteworthy since it is greatly enhancing the potential and reliability of existing tools, and has a very promising future (Cao et al., 2020; Chmiela et al., 2018; Jumper et al., 2021; Shastry & Sanjay, 2020; J. Wang et al., 2019). During my PhD, I performed molecular modeling and simulations in two independent experimental contexts, but linked together as both were focused on MCTP proteins. The first approach was the prediction and modeling of the MCTP C2 domains while the second was the prediction and modeling of the MCTP TMR. Both of these works involved lipid-protein interactions, hence also the modeling of lipid bilayers.

It is nowadays well established that biological membranes are fundamental elements of cell life and that they are a complex assembly of lipids, proteins and carbohydrates (Lombard, 2014; Singer & Nicolson, 1972). Research on lipid-protein interactions, linked with their involvements in membrane organization and function, is thus fundamental to understand many cellular processes such as trafficking, transport, signaling, metabolism, ... Considering the diversity of lipids and proteins, together with their small size and fast dynamics, scientists can only rely on structural biology (X-Ray, Cryo-EM, MD), molecular sorting/analysis (isolation, mass spectrometry, FRET) and single molecule tracking technologies (Sych et al., 2022). Structure prediction and molecular simulation has been a growing technique during the last 20 years thanks to the development of computational technologies. Today, several methods provide a window for molecular simulation, both in time and size, that spans from atomic interactions to membrane fusion events, making

this technique widely accessible for multi-scale characterization of lipid-protein interactions (Chavent et al., 2016; Enkavi et al., 2019; Goossens & De Winter, 2018; Muller et al., 2019).

Before presenting the three types of lipid-protein interactions I am interested in, namely peripheral proteins, amphipathic helices and transmembrane proteins, I believe important to introduce how structural prediction can be performed and how membranes can be simulated.

Protein structural predictions are computational methods that consist in calculating the 3D model of a protein of interest from its amino acid sequence and it is usually done when structural data are not available or not possible to access easily. Originally, there are two main methods. On one hand, template-based modeling, also called structural homology modeling, is done when the protein of interest share enough sequence identity with proteins of known structures (X-Ray, NMR, Cryo-EM). The modeling relies on sequence and structural alignments, taking in consideration the differences of residues between the target and the templates. On the other hand, template-free modeling, also called *de novo* modeling, uses conformational sampling based on energy functions. Peptides and small proteins can spontaneously fold into the right conformation. This intrinsic property is exploited and the energy landscapes of the models is monitored to find structures with minimal potential energy. Bigger proteins are usually dissected in fragments, which undergo such sampling, assembled together and the structure is finally refined. These two methods are now commonly hybridized, for example template-based models can be refined with energy minimization steps while machine learning is able to enhance *de novo* modeling by using fragment-based sampling information from existing structural databases (Kuhlman & Bradley, 2019).

The simulation of biological membranes is challenging, considering the diversity of lipids molecules and of their intrinsic properties (Harayama & Riezman, 2018). It is thus common to perform simulations using simplified membrane compositions, sometimes down to very few lipid species, to form bilayer models. During the past decade however, the development of lipid model databases (Crowet et al., 2021) and membrane builders (Wu et al., 2014), allows the modeling of more complex and realistic membranes. The choice of membrane complexity, and its size, also depends on the computational power that is available. Indeed, the simulation of lipid bilayers results in rapid increase in the size of the system and in the total number of particles, implying a need for increase computational power. Nowadays, methods are available to

increase both speed and size while reducing the computational cost, by simplification of the models, but at the price of reduced resolution and accuracy (Marrink et al., 2019). Aside from being aware of the models limitations (Javanainen et al., 2017), researchers constantly work in improving these methods, to gain accuracy and resolution while maintaining affordable costs. This can be done by improving the models themselves (Souza et al., 2021), by charge scaling (Duboué-Dijon et al., 2020) and also by using hybrid multiscale particle fields that can efficiently combine mesoscale potentials and atomic representations, which can resolve biologically relevant membrane dynamics and shapes (Pezeshkian & Marrink, 2021; Soares et al., 2017).

As tethering elements, MCTP possess specific domains for membrane interactions. On one side, the C2 domain bloc is able to interact transiently with specific lipids through electrostatic bonds, and, on the other side, the transmembrane region anchors the protein stably within the ER membrane. Taken individually, these domains and subdomains can be classified into three types of lipid-protein interactions: C2 domains are peripheral proteins and the transmembrane region is composed of amphipathic and transmembrane domains. These three classes of interactions are commonly found in living organisms and we have many examples of researches that have studied them. I will hereafter briefly present them, with a focus on predictive and computational modeling studies.

Peripheral proteins are proteins that are recruited to membranes and interact at the surface of lipid bilayers in more or less specific manners. Their are critical components of numerous biological processes and are involved in the regulation of local lipid composition, membrane dynamics and inter-protein coordination, through a variety of molecular mechanisms (Whited & Johs, 2015). By definition, peripheral proteins are transient, meaning they can reversibly bind and detach from the membrane. This implies a coordination of interaction specificity and strength, in order to be recruited to specific membrane locations during the necessary amount of time. Molecular dynamics are very welcome to better understand these specific lipid-protein interactions, because they can provide information that is still challenging to access via *in vitro* structural or live-cell experiments, due to their furtiveness. Simulations can bring insights in the nature of the interactions but also on the diffusion behavior of the protein in the membrane plane and the impact it has on lipid clustering or membrane shaping for example (Geragotelis et al., 2021; Andreas H Larsen et al., 2022; Andreas Haahr Larsen & Sansom, 2021; Yamamoto et al., 2020).

Amphipathic helices are protein domains which present a face of hydrophobic residues, whereas the other face is composed of polar residues. Therefore, these helices usually localize at the interface between the acyl moieties and the solvated polar heads of the lipids. However, aside from this property, their sequence is variable and their function can be diverse. Nonetheless, prediction of such elements is possible (Gautier et al., 2008), as well as their modeling (Bhaskara et al., 2019).

Transmembrane proteins are integral parts of membranes in which they are embedded deeply and sometimes span the bilayer. Many proteins are intrinsically transmembrane, such as signaling receptors and transporters, but there are also proteins that possess partial membrane anchorage and thus transmembrane domains. The prediction of transmembrane protein topology is very important in biology and many algorithms have been developed and refined (Tsirigos et al., 2018; Yang et al., 2022). With the development of isolation and purification methods, together with *in vitro* structural biology evolution, we also witness increase in resolved structures (Overduin & Esmaili, 2019) and associated databases (Bittrich et al., 2022). Our understanding of transmembrane proteins/domains structure and function can be enhanced by molecular simulation combined with *in vitro* and live-cell experimentation (Bhaskara et al., 2019; Siggel et al., 2021). Incorporation of membrane proteins is also important in the simulation of realistic membranes, in order to unveil altogether lipid-lipid, lipid-protein and protein-protein interactions (Marrink et al., 2019).

Alongside the development of prediction tools, models and *in silico* methods, specific packages are made to analyze the simulated trajectories and extract relevant biological information that can be linked with other experimental data. These tools can be homemade for specific purposes, but many are published and shared within the community: some are specific to study the properties of the bilayer itself (Allen et al., 2009; Gautier et al., 2018; Guixà-González et al., 2014), others are helpful for the description of the lipid-protein interactions (Sejdiu & Tieleman, 2021), and others are more global and can be useful for detailed description of protein conformation (Gowers et al., 2016).

## **1.4. Plasmodesmata and Membrane Contact Sites**

Now that some technical aspects are made clearer, and before leaping into the results of my thesis, I believe it is important to consider the biological and biophysical context of my research in more details. To



do that, I am hereafter presenting two review articles, where I am first author, published in 2019 and 2020 (Petit et al., 2019, 2020).

The first article, published in *Current Opinion in Plant Biology*, where I am first author, is a review of the latest research in the plasmodesmata field, with a focus on results of remarkable interest. The paper starts with stating novel breakthroughs in plasmodesmata-mediated short and long-distance signaling. Then, it gives insights in the relationship between plasmodesmata structure and plasmodesmata function, explaining why understanding plasmodesmata architecture is so important to completely understand its functional components. This section is followed by an examination of MCTPs as proteins acting at the ER-PM interface. Finally, the last chapter considers plasmodesmata as dynamic signaling platforms undergoing constant remodeling in response to internal and external cues, far from the concept of immalleable and neutral holes piercing through the cell wall.

Jules D. Petit, Ziqiang Patrick Li, William J. Nicolas, Magali S. Grison & Emmanuelle M. Bayer. *Dare to change, the dynamics behind plasmodesmata-mediated cell-to-cell communication*. COPB (2020), vol. 53, p 80-89.

The second article, published in *Frontiers in Plant Science*, where I am first and co-corresponding author, is reviewing the mode of action of Membrane Contact Sites (MCS) from the point of view of the biophysical properties of their molecular actors: lipids and proteins. I here illustrate how lipids are able to create unique environments that can define specialized membrane territories, engaging specific proteins and hence functions, establishing and regulating MCSs. The role of lipid exchange at MCS is then discussed before an opening on the definition and meaning of MCS at plasmodesmata. The review ends on a section promoting the importance of multidisciplinary research in the uncovering of MCS dynamics and actors.

Jules D. Petit, Françoise Immel, Laurence Lins & Emmanuelle M. Bayer, *Lipids or Proteins: Who Is Leading the Dance at Membrane Contact Sites?* Front. Plant Sci. (2019), vol. 10, article 198, p 1-10.

## 1.5. Collaborations

My co-supervised PhD was funded by the belgian F.N.R.S.- F.R.I.A grant (N°1.E.096.18) and was also integrated in the ERC consolidator grant (BRIDGING-772103) obtained by Emmanuelle Bayer (LBM, UB). The presented work has therefore no solid substance without the works of the numerous people I have been collaborating with, and I want to clearly convey in this section the ins and outs of each major collaboration I had the pleasure to experience.

I worked in pair with Marie Brault (LBM) in the data collection and establishment of the “MCTP tether membranes at plasmodesmata” article published in EMBO Reports where Marie Brault and I are co-first authors (Brault, Petit et al., 2019). My collaboration with Patrick Ziqiang Li (LBM) started with the plasmodesmata biogenesis project and ER shaping function of MCTPs. Patrick worked on the generation of the plant material (Arabidopsis mutants, complementation lines expressing MCTPs tagged with fluorescent marker, co-expression with different subcellular markers) and realized the high resolution photonic microscopy data while I was focused on molecular modeling and electron microscopy techniques. We currently work collaboratively in the establishment of a research article where Patrick and I will be co-first authors.

I also worked with Françoise Immel in the attempt to purify AtMCTP4 C2 domains. Marie Glavier (LBM) and Lysiane Brocard (Bordeaux Imaging Center) were fundamental support in my learning of all techniques revolving around electron microscopy but also very important fellow researchers with whom I was able to share expertise and discuss about the interpretations of the micrographs and tomograms. Jean-Marc Crowet initiated me to molecular modeling and dynamics during my master thesis and helped me at the beginning of my PhD for the analysis of the MCTP C2 domains simulations. Antoine Taly was of great support and advice during the modeling of the MCTP4 TMR. More recently, I work in collaboration with Melina Petrel (Bordeaux Imaging Center) for the development of scanning transmission electron microscopy-based electron tomography on thick biological sections and with Etienne Gontier (Bordeaux Imaging Center) for the development of the serial bloc face scanning electron microscopy technique on plant root material.

## **Multiple C2 domains and Transmembrane region Proteins are multifunctional actors at plasmodesmata**

## 2.1. What do we know about the MCTP protein family?

The realm of multiple C2 domain-containing proteins is a vast eukaryotic structural family playing various functions associated with membrane trafficking and cell signaling. Among them we find synaptotagmins (Ishikawa et al., 2020; Wolfes & Dean, 2020), extended-synaptotagmins (Saheki & De Camilli, 2017), ferlins (Bulankina & Thoms, 2020), tricalbins (Collado et al., 2019; Hoffmann et al., 2019) and MCTPs. MCTPs are only present in higher eukaryotes. In metazoans, we can distinguish two groups: the chordates, which possess two MCTPs, MCTP1 and MCTP2, and the non-chordates, which only have one MCTP (Shin et al., 2005). In plants, MCTPs are present in larger families, for instance sixteen members were described in *Arabidopsis thaliana* (Liu, Li, Liang, et al., 2018) and thirteen in rice (Zhu et al., 2020). In both metazoan and plants, MCTPs share similar structural features consisting of three or four C2 domains at the N-terminal part of the protein and one or two transmembrane domains at the C-terminal end.

In *Drosophila*, MCTP is proposed to act as an ER-localized calcium sensor protein and a potential source of calcium-dependent feedback, regulating the baseline neurotransmitter release and presynaptic homeostatic plasticity in motoneurons (Genç et al., 2017). In *C. elegans*, *MCTP1* locus produces four splicing variants under the control of two promoters that leads to differential expression in neurons and spermatheca. In neurons, it is suggested that *MCTP1* plays a role in the modulation of neurotransmitter release rate through the control of vesicle exocytosis (Téllez-Arreola et al., 2020). It is however not limited to this role, as demonstrate the results of Joshi et al., 2018 where *MCTP1* deletion leads to a decrease in lipid droplet number and size in the worm intestine. In the zebra fish, four *MCTP* genes are expressed during all the fish life stages and tissues, and localize in the ER, lysosomes and endosomes (Espino-Saldaña et al., 2020).

In humans, Single Nucleotide Polymorphism in *MCTP1* and *MCTP2* are associated with neuropsychiatric diseases (Djurovic et al., 2009; Scott et al., 2009). The bipolar disorder caused by *MCTP1* mutation is possibly a consequence of a defect in the regulation of synaptic vesicle recycling in neurons and synapses of the central nervous system (Qiu et al., 2015). More recently, mammalian *MCTP1* and *MCTP2* were shown to localize at specialized ER subdomains to promote lipid droplet formation and control their growth (Joshi et al., 2018, 2021). In this context, the MCTP transmembrane domain is described to act as a reticulon homology domain capable of tubulating the ER membrane, supporting lipid droplet biogenesis by promoting

membrane curvature. On the other hand, the cytosolic C2 domains are able to bind charged phospholipids, likely mediating ER-lipid droplet contacts to regulate lipid droplet size (Joshi et al., 2021). Interestingly, it is discussed in the same article that MCTP, by being present at several ER-organelle MCSs (lipid droplets, peroxisomes, endosomes, mitochondria), could, in a more general way and similarly to other multiple C2 domains-containing proteins, be involved in organelle biogenesis, remodeling and signaling. This idea is in line with data reviewed above, showing that MCTP expression is correlated with various functions, in the different tissues and organelles of the studied organisms.

In plants, studies also describe many functions associated with MCTPs in the context of plasmodesmata cell to cell communication. In the case of embryophytes, this diversity of function might also be linked to the broader genetic diversity. In *Arabidopsis thaliana*, the most examined MCTP is QUIRKY (QKY, MCTP15), which was shown to interact with the PM-localized leucine-rich-repeat receptor-like kinase STRUBBELIG (SUB, SCRAMBLED) to mediate organ and tissue morphogenesis, cellular patterning and growth anisotropy (Fulton et al., 2009; Trehin et al., 2013; Vaddepalli et al., 2014). QKY is mostly localized at the PM (Liu, Li, Liang, et al., 2018; J. H. Song et al., 2019; Trehin et al., 2013) and plasmodesmata (Vaddepalli et al., 2014). In root epidermal cells, QKY stabilizes SUB at the PM and indirectly facilitates the import of CAPRICE transcription factor, leading to its accumulation at H-position epidermal cells. Through direct interaction with SUB, QKY also hampers its ubiquitination and vacuolar degradation (J. H. Song et al., 2019). Finally, QKY was found to play a role in the regulation of novel and alternative route for florigen transport. Together with SYNTAXIN OF PLANTS121 (SYP121), QKY forms a protein complex with FLOWERING LOCUS T (FT) at endosomal vesicles. This route is proposed to drive FT accumulation at the companion cell PM, thus facilitating its transport, through plasmodesmata, into the sieve elements of the phloem (Liu et al., 2019). The first route to be described for FT transport, through plasmodesmata and at the same cellular interface, is mediated by another MCTP member, called FTIP1 (MCTP1), which localizes in the ER and at plasmodesmata (Liu et al., 2012). MCTP6, localized partly at plasmodesmata, is also capable of interaction with FT and with TWIN SISTER OF FT, potentially playing additive roles in FT regulation (Liu, Li, Liang, et al., 2018). Since FT is required for flowering, FT and FT-associated genes are linked with photoperiodic stimulus – MCTP1 regulates flowering under long days (Liu et al., 2012) together with MCTP6 (Liu, Li, Liang, et al., 2018) – but also temperature (Liu et al., 2020). The rice and lotus homologs OsFTIP1 and

NnFTIP1 are also involved in the export of FT from companion cell to the sieve elements, suggesting an evolutionary conserved role of FTIP1 across flowering plants (S. Song et al., 2017; Zhang et al., 2021). Other members, FTIP3 (MCTP3) and FTIP4 (MCTP4), play a role in the shoot apical meristem development by preventing SHOOTMERISTEMLESS (STM) intracellular trafficking through direct protein-protein interaction at endosomes (Liu, Li, Song, et al., 2018). The rice homolog, OsFTIP7, (Zhu et al., 2020) is associated with auxin-mediated anther dehiscence. The presence of OsFTIP7 in the cytosol leads to the sequestration of the KNOX protein OSH1 (homolog of STM in arabidopsis) in the nucleus, which in turns blocs the transcription of the OsYUCCA4 gene involved in auxin biosynthesis.

In conclusion, some MCTP members have been associated with plasmodesmata *in planta*, namely FTIP1, QKY, MCTP6, and are involved in cell to cell signaling pathways and impact molecular transport. The other MCTP members were not described as plasmodesmata-associated (Liu, Li, Liang, et al., 2018; Liu, Li, Song, et al., 2018). However, proteomic data associated with plasmodesmata show the presence of MCTP6 and MCTP4 in arabidopsis leaves (Kraner et al., 2017) and MCTP3 and MCTP6 in populus cell cultures (Leijon et al., 2018). One study, on Carbohydrate Partitioning Defective33 (CPD33), the QKY homolog in maize, shows a relationship between MCTP and plasmodesmata density (Tran et al., 2019), but the MCTP function as plasmodesmata-specific ER-PM tether was never investigated. Actually, before our work, no plasmodesmata-specific ER-PM tethers were described at all. For this reason, our work, aiming to link MCTP to plasmodesmata ER-PM MCS structure-function, is original in the plasmodesmata field and may open a plethora of perspectives.

## 2.2. MCTP proteins tether ER-PM membranes at plasmodesmata

Since the first electron microscope acquisition of plasmodesmata (PD), plant biologists using this technology observed electron-dense spokes connecting the ER to the PM along the entire length of the PD pores (Nicolas et al., 2017). Yet, their molecular identity has remained a matter of debate in the community (C. Chen et al., 2021; Li et al., 2021).

To investigate this question and identify the proteins responsible for ER-PM contacts specifically at PD, Bayer group's comparative semi-quantitative proteomic profiling from purified PD generated a list of PD-associated proteins candidates (about 115 proteins). Among the most enriched ones, we found well described PD proteins such as members of the plasmodesmata-located protein and plasmodesmata callose-binding protein families (R. E. Sager & Lee, 2018) but also proteins from the MCTP family (Brault, Petit et al., 2019). Several MCTP members (MCTP3-7, MCTP9-10, MCTP14-16) were present in this refined proteome, being highly enriched and abundant in our PD-membrane fractions. These data were however in conflict with some published data, as only some members (MCTP1,6,15) had been shown to associate with PD while others were described as non-PD associated (Liu, Li, Liang, et al., 2018; Liu, Li, Song, et al., 2018). Very interestingly, MCTPs are structurally related to known ER-PM tethers such as Synaptotagmins and Extended-synaptotagmins, presenting multiple lipid binding modules (C2) and a C-terminal complex transmembrane region. MCTPs were therefore perfect candidates for ER-PM tethering function inside PD. In the following EMBO reports research article (Brault, Petit et al., 2019), where I am co-first author, we describe MCTPs as tethering elements connecting the ER to the PM inside PD. Main findings can be summarized as followed:

- 1 MCTPs are core PD constituents, enriched in PD with tight ER-PM junctions.
- 2 MCTP3 and 4 (two prevalent members) are critical to plant development, with loss-of-function *mctp3,4* Arabidopsis mutants presenting severe and pleiotropic defects (including a dwarf phenotype and a root meristem disorganization).
- 3 *mctp3,4* also presents defect in cell-cell trafficking.

4 MCTP possess the typical properties of membrane tethers: an ER-inserted C-terminal transmembrane region and several N-terminal C2 domains for PM docking. Both the ER-anchor and C2 domains are necessary for PD association.

5 MCTPs are integral ER-membrane proteins, which cluster and are immobilised at PD.

6 Using molecular dynamics, we showed that the C2 domains of MCTP3 and 4 have the ability to bind PI4P (main phosphoinositide of the PM in plants). Short term depletion of PI4P abolishes MCTP4 association with PD and mimics *mctp3,4* root phenotype.

I contributed in the article with the molecular modeling and dynamic simulations, the confocal subcellular localization of the fluorescent tagged full length and truncated mutants as well as the calculation of the PD indexes (quantifying a protein enrichment at PD), the phenylarsine oxide experiment, the transmission electron microscopy (TEM) immunogold assay and I also helped with the correlative light-electron microscopy and the yeast complementation quantification.

Following this research article, I wrote a review article in COPB (Petit et al., 2020) where I discuss the potential role and function of MCS and MCTPs in regulating cell to cell trafficking. I also co-wrote a method article about quantifying protein localization at PD (M. Grison et al., 2020).

Marie L. Brault\*, Jules D. Petit\*, Françoise Immel, William J. Nicolas, Marie Glavier, Lysiane Brocard, Amélia Gaston, Mathieu Fouché, Timothy J. Hawkins, Jean-Marc Crowet, Magali S. Grison, Véronique Germain, Marion Rocher, Max Kraner, Vikram Alva, Stéphane Claverol, Andrea Paterlini, Ykä Helariutta, Magali Deleu, Laurence Lins, Jens Tilsner & Emmanuelle M. Bayer. *Multiple C2 domains and transmembrane region proteins (MCTPs) tether membranes at plasmodesmata*. EMBO Reports (2019), e47182.



## **2.3. MCTP transmembrane region is a Reticulon Homology Domain**

### ***2.3.1. Introduction on Reticulon Homology domains***

RHD are domains found in eukaryote membrane-shaping proteins such as reticulons (RTNs), reticulon-like proteins (RTNLs), receptor expression enhancing proteins (REEPs), Yop1, Pex30, ATG40 and FAM134B. They are generally involved in constriction, fission and/or dynamic patterning and remodeling of the ER membrane network (Espadas et al., 2019; West et al., 2011) as well as in ER-phagy (Bhaskara et al., 2019; D'Eletto et al., 2020; Jiang et al., 2020; Siggel et al., 2021) and organelle biogenesis (Joshi et al., 2018; S. Wang et al., 2018).

A study on AtRNTL-B13 suggests that the ER shaping properties of the RTN family relies on the presence of a conserved amphipathic helix (APH) able to sense membrane curvature ((Breeze et al., 2016; Brooks et al., 2021)). Following a similar idea, a most recent and extensive description of RHD was performed by molecular modeling and dynamic simulations on FAM134B ER-phagy receptor (Bhaskara et al., 2019; Siggel et al., 2021). The first article demonstrates the role of the two transmembrane helical hairpins and the two APHs in the induction of the membrane curvature but also in the self-sorting of the RHD toward already curved membrane regions. The second article goes further by showing how several FAM134B RHDs are capable of clustering through curvature sensing and enhance the membrane curvature to the point of driving spontaneous budding and vesicle fission. An opposite role has been proposed in the case of RTN: their shaping activity presumably provides membrane flexibility and stability, hence reducing mechanical stress induced by the escape of large macromolecular protein complexes out of the ER membrane (Y. J. Chen et al., 2020).

Within PD, the ER undergoes extreme constriction to form the desmotubule, a thin ER strand devoided of luminal space. The generation and stabilization of such energetically unfavorable high-curvature tubule (~17 nm) requires significant accumulation of shaping factors (Hu et al., 2008). In plants, AtRTNL-B3 and AtRTNL-B6 have been proposed to constrict the ER during primary PD formation (Knox et al., 2015). Based on our observations, however, RTNL-B3 and RTNL-B6 do not seem to be specifically enriched at PD, questioning their function in ER-shaping inside the pores.

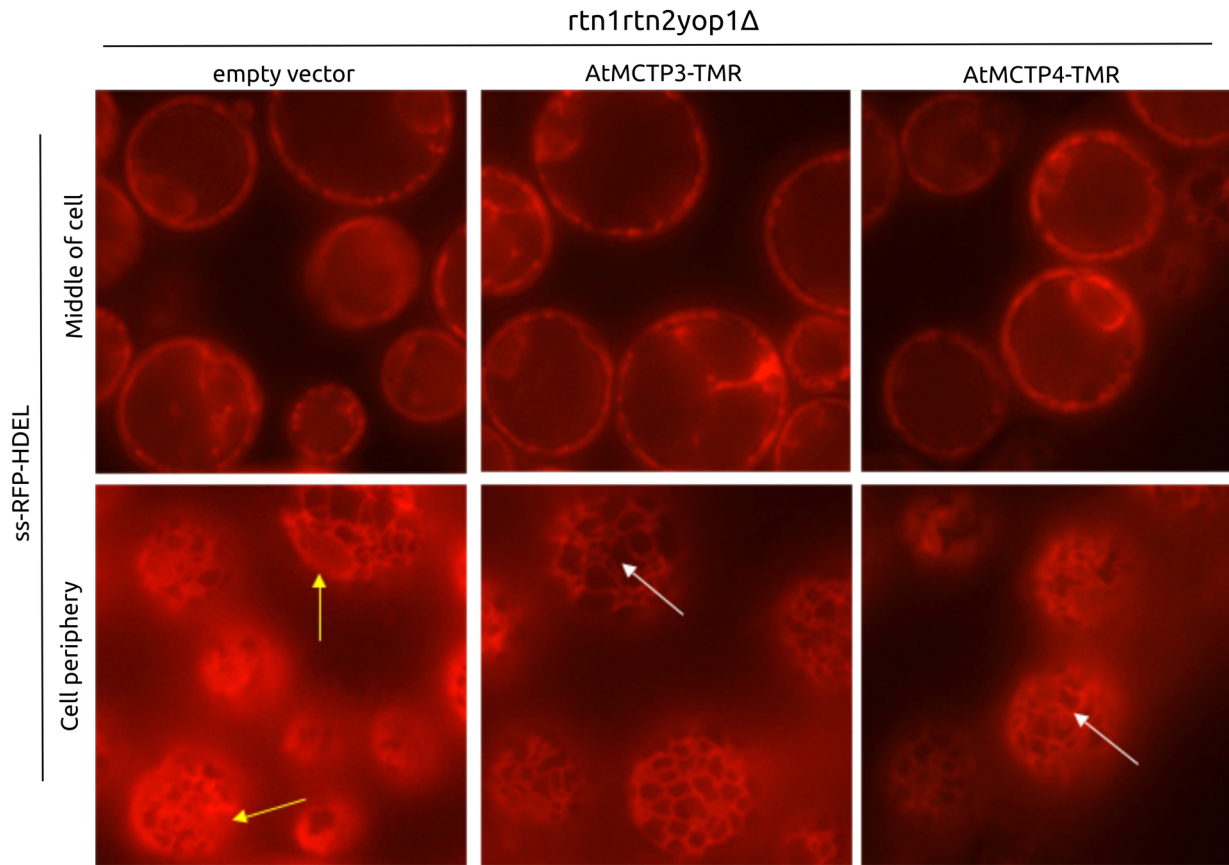
In this result section, I show that *Arabidopsis* PD-associated MCTPs harbor a reticulon homology domain (RHD) at their C-terminus. Overexpression of MCTP3, 4 and 6 TMR results in cortical ER constriction *in planta*. Using molecular dynamics, I assembled model for MCTP4 RHD, which consists of five distinct subdomains: a C-term amphipathic helix (APH1), followed by a transmembrane domain (TMD0), and two hairpins (HP1 and HP2) linked together by another amphipathic helix (APH2). Similar to FAM134B RHD, the two hairpins induce membrane thinning at their vicinity, a feature proposed to be linked with their shaping activity.

### ***2.3.2. MCTP TMR is able to shape the cortical ER in vivo***

The transmembrane region (TMR) of MCTPs is a ~200 residues-long sequence conserved throughout the entire family and annotated with two hydrophobic transmembrane domains (TMD). Since HsMCTP TMRs were described as RHD (Joshi et al., 2018, 2021) and plant MCTPs share structural similarity with them, we decided to draw our attention on this region with the objective of highlighting additional functions beyond simple ER membrane attachment.

This idea started a discussion, followed by a collaboration, with William Prinz and Amit Joshi, to complement the yeast *rtn1rtn2yop1Δ* mutant background with *Arabidopsis* MCTP3 and 4 TMRs. This yeast is defective in ER tubule shaping proteins and consequently displays defects in ER tubularization. As in Joshi et al., 2018 with HsMCTP2 TMR, the expression of AtMCTP3 TMR and AtMCTP4 TMR was able to rescue the ER tubules in the mutant, thus establishing solid preliminary data to further investigate MCTP TMR as an ER-shaping motif (Figure 1).

**Figure 1 :** In a yeast background defective in ER shaping proteins (RTN1, RTN2, YOP1), AtMCTP3 and AtMCTP4 TMRs are able partially complement the cisternae phenotype (yellow arrows) back into a reticulated ER network (white arrows). This work was performed by Amit Joshi and in collaboration with William Prinz.



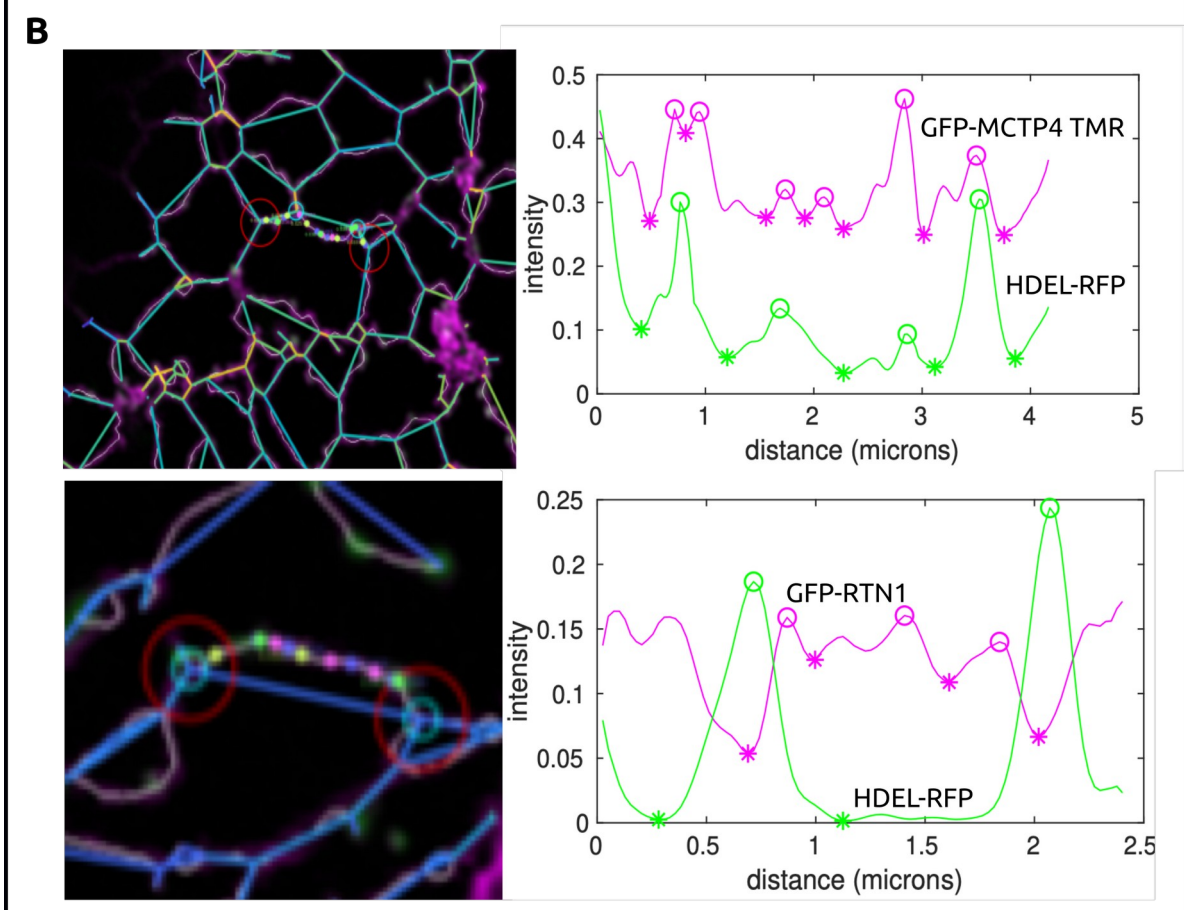
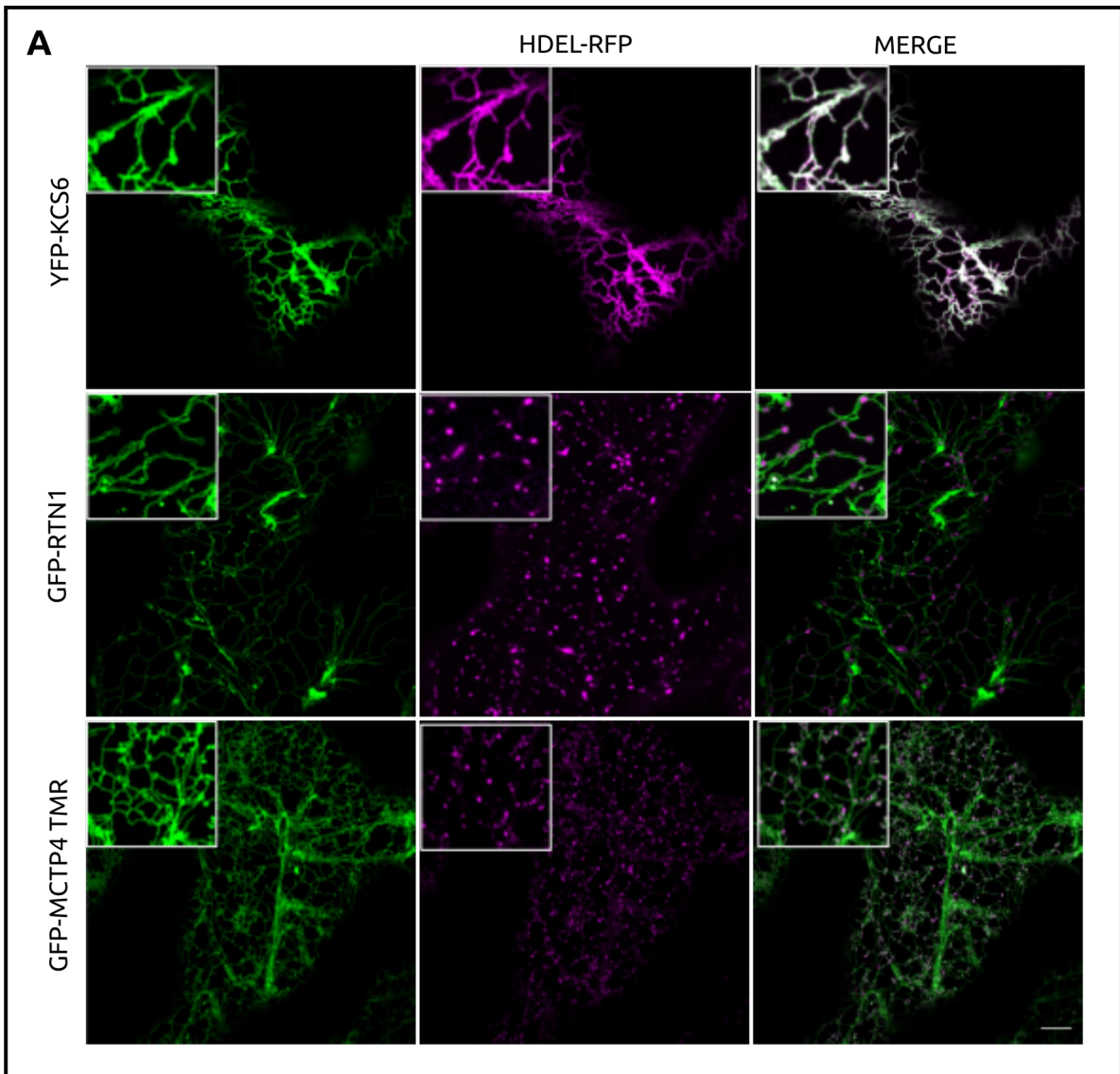
Following this assay in yeast, with the help of Patrick Li, we performed transient overexpression of YFP-MCTP3, 4 and 6 TMRs in *Nicotiana benthamiana* leaves together with the ER luminal marker RFP-HDEL. ER constriction was observed in epidermal cells expressing the two constructs, as the HDEL signal was disrupted into small pockets of ER, displaying a “droplet” pattern instead of the usual reticulated network. This phenomenon is also observed when overexpressing RTN1 (positive control) but not KCS6 (negative control), an ER localized protein without shaping properties (Figure 2A). Using specialized analysis tools (Pain et al., 2019), a difference is however noticeable between RTN1 and MCTP TMR. As a matter of fact, RTN are mainly localized in tubular ER subdomains, curving them even more, whereas MCTP TMRs were seen to localize along the entire ER network (tubular and cisternae regions) and even at nuclear envelop, and are able to induce constriction everywhere (Figure 2B). The behavior of RTN is already known from the literature and can be explained by the fact that they are both membrane curvature sensing proteins and membrane shaping proteins (Brooks et al., 2021). In the case of *Arabidopsis* MCTP3,4,6 TMR, membrane shaping activity seems to be conserved but may lack curvature sensing property. Lastly, results of co-

immunoprecipitation experiments on ER-associated MCTPs (unpublished) performed by Jessica Perez-Sancho show interaction between full length MCTP3, 4 and 6 as well as between MCTP3, 4 and 6 TMRs. Similar to reticulon motifs (Shibata et al., 2008; Sparkes et al., 2010), MCTPs are likely to interact through their RHD and possibly oligomerize.

All this data opens novel putative MCTP functions and we needed to get insights into the molecular mechanisms of MCTP-driven ER shaping. To do that, because we don't have purified MCTP proteins under our hands and because resolving experimentally the 3D structure of transmembrane proteins is tedious, we decided to use molecular modeling and dynamics as a first approach. The modeling of undescribed protein domains is however tricky, involving a lot of trials-and-errors. Complete accuracy cannot be stated in the following work but construction of step-by-step pipelines with validation steps aimed at reducing biases. This method still opens possibilities to answer questions on MCTP TMR structure-function, such as: What are the structural modules of MCTP TMR involved in the shaping of the ER membrane? Do they work collaboratively to promote constriction? What molecular interactions with the membrane drive its curvature?

The work described in sections below consists in setting foundations and already gives partial answers by identifying the shaping modules and observing their individual interactions with a simple lipid bilayer. For molecular dynamics, we have decided to focus on AtMCTP4 as it is one of the most abundant MCTP member at PD. Loss-of-function *mctp4* Arabidopsis mutant does not show any obvious phenotype but *mctp3,4* double mutant presents strong developmental and growth defects. The amino acid sequence identity between AtMCTP4 and AtMCTP3 is very high (92.8% identity and 98.7% similarity; Brault et al., 2019), explaining the redundancy of function and enabling us to work on one member only.

**Figure 2** : MCTP4 TMR is able to shape the cortical ER membrane. A. MCTP4 TMR localises at the ER and induce constriction. The HDEL marker is squeezed out of the luminal space and forms a characteristic pattern, similar to reticulon (RTN1). B. Unlike RTN1, MCTP4 TMR is not only inducing curvature at specialized ER domains (where HDEL is excluded), but seems to drive curvature in the entire network.



### **2.3.3. Sequence analysis and subdomain delimitation**

Because sequence-based predictive bioinformatic servers give variable results in the delimitation of transmembrane helices and APH, we studied MCTP4 TMR using a combination of tools. Hydrophobic Cluster Analysis (HCA) (Gaboriaud et al., 1987) gave a general idea of the organization of the residue properties along the sequence while predictive tools such as  $\Delta G$  predictor (Hessa et al., 2007), PSIPRED (Buchan et al., 2013) and Heliquet (Gautier et al., 2008) provided more specific information about the secondary structure as well as the ability to cross membranes and amphipathicity of the helices.

I could identify five putative subdomains in the ~200 residue sequence of the AtMCTP4 TMR: an N-term amphipathic helix (APH1), a putative transmembrane domain (TMD0), a hairpin transmembrane (HP1) composed of two transmembrane helices (TM1 and TM2), a second, longer, amphipathic helix (APH2) and another hairpin transmembrane (HP2) composed of two transmembrane helices (TM3 and TM4) (Figure 3A).

The predictions regarding TMD0 are not unequivocal, putting, for now, this subdomain's properties somewhere in between a transmembrane helix and an unusual amphipathic helix.

Patrick Li relied on this delimitation prediction to generate MCTP TMR single-domain deletion mutant and check ER and PD localization as well as ER-shaping functions (see section 2.3.7.). Other members of the E. Bayer's group used these predictions, and my expertise, to produce additional MCTP mutant constructions that still require investigation.

### **2.3.4. 3D modeling of MCTP TMR subdomains**

Because of the complete lack of available 3D models from homologous proteins, and the relative small size of the sub-domains, the modeling work was done using *ab initio* folding method on Robetta Server (Raman et al., 2009). To avoid inaccurate constrained folding, due to the presence of many hydrophobic strands in the sequence, and the absence of lipid bilayer-mimicking force field in this method, the TMR was split in three overlapping parts: APH1-TMD0-HP1, HP1-APH2-HP2 and HP2-Cterm. Overlapping subdomains gave similar intrinsic conformations. Each sub-domain was then separated from the others and processed individually.

At this stage, various trials of molecular dynamics were done on APH1, TMD0 and APH2. They were set in solvent and simulated all-atom for 200ns in the attempt to grasp a stable model for later membrane simulation work. To make a long story short, none of the simulations were giving promising models and the “freedom” given to the peptides in solution lead to various degree of unfolding and/or rearrangements. We thus decided to use the initial models for the next step.

Each model was also run through IMPALA (Ducarme et al., 1998) before performing membrane simulations and results supported the predicted properties.

### ***2.3.5. Membrane simulations of MCTP TMR subdomains***

Simulating system containing a membrane bilayer is quite demanding if performed in all-atom force field. For that reason, I transformed all subdomains into coarse grained representation. The use of coarse grain forcefield is a simplification but it enables us to work on big systems and compute much longer trajectories. Each subdomain secondary structure was constrained using ElNeDyn (Periole et al., 2009) and refined using DomELNEDIN (Siuda & Thøgersen, 2013). I then followed two different pipelines depending on the subdomain properties: amphipathic domains were initially placed in the solvent above the membrane to monitor the docking dynamics (similarly to the work on the C2 domains in Brault et al., 2019) whereas the transmembrane hairpins were embedded in the bilayer before the start of the simulation.

A short note here to say that I started to perform these simulations in two different membrane compositions, one neutral phosphatidylcholine (PC) and one with phosphatidylethanolamine (PE) in a PC:PE (4:1) ratio, in the attempt to potentially observe different behaviors. The PC-only membrane is commonly used in molecular dynamics as it is easier to understand a protein's behavior in a simple and neutral environment. The PC-PE bilayer aimed to approximate the ER lipid composition while staying in a relatively simple system. As preliminary results were similar, and to gain time and computational power, I pursued with the PC-only bilayer and thus will only display these results. Because of its “in-between” properties, TM0 was processed following both amphipathic and transmembrane pipelines in parallel.

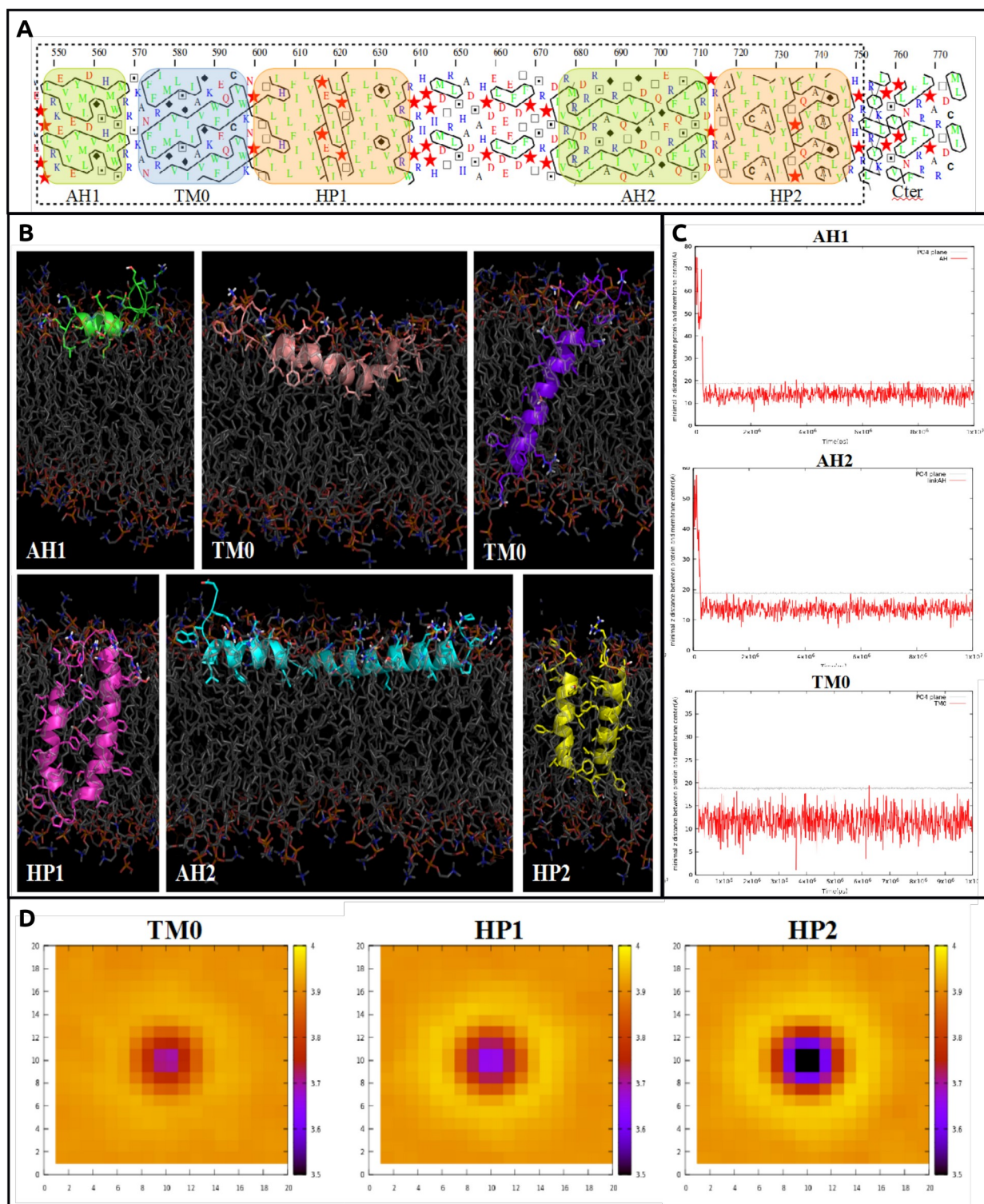
During 10  $\mu$ s simulations, APH placed in the solvent above the bilayer rapidly docked onto the membrane and stabilized themselves horizontally, at the hydrophobic/hydrophilic interface of the membrane leaflet they

approached (Figure 3C). The HP, embedded vertically in the bilayer, underwent 30  $\mu$ s simulations to sample the interactions between the two helices and the associated conformations. Because HP1 and HP2 are composed of short helices, I analyzed their impact on the membrane thickness using GridMAT (Allen et al., 2009). The results for HP1 and more especially HP2 show a similar effect on the membrane as observed in Bhaskara et al., 2019, for the ER-phagy receptor FAM134B RHD. The membrane is squeezed vertically at the vicinity of the protein, resulting in a local thinning of the bilayer, a property associated with membrane curvature induction (Figure 3D). TMD0, placed above the membrane, show APH-like interaction but falls deeper within the leaflet and seems unstable. Embedded vertically in the bilayer, TMD0 was very stable for all 15  $\mu$ s of the simulation. It however has very little to no impact on the membrane thickness compared to the HPs (Figure 3C, D).

Following these CG simulations, backmapping (meaning the reverse transformation from coarse grained to all-atom representation) was performed on each subdomain-bilayer system taken from the most representative subdomain structural conformation using cluster analysis (Figure 3B). All-atom simulations were then run for 50 ns to allow structural equilibration. Stability was assessed by calculation of the root mean square deviation (assessing the structural deformation of the protein along the simulation time) and following the secondary structure over time.

**Figure 3** : MCTP4 TMR delimitation and molecular modeling. A. Hydrophobic Cluster Analysis layout of the TMR sequence. The subdomains are highlighted in different colors : amphipathichelices in green, transmembrane domain 0 in blue, hairpin transmembrane helices in orange. B. Molecular interaction between the subdomains and the membrane at the end of the coarse grained simulation and after backmapping. C. Docking analysis of the amphipathic helices along simulation time. Grey line represents the lipid phosphate plane. Red line is the minimal distance between the protein and the membrane center. D. GridMAT results for the transmembrane domain showing the impact of the proteins on the lipid bilayer thickness. The membrane is shown from above and protein is centered in the middle (not displayed). The color represents the membrane thickness.





### **2.3.6. Bloc assembly and perspectives for full TMR reconstruction**

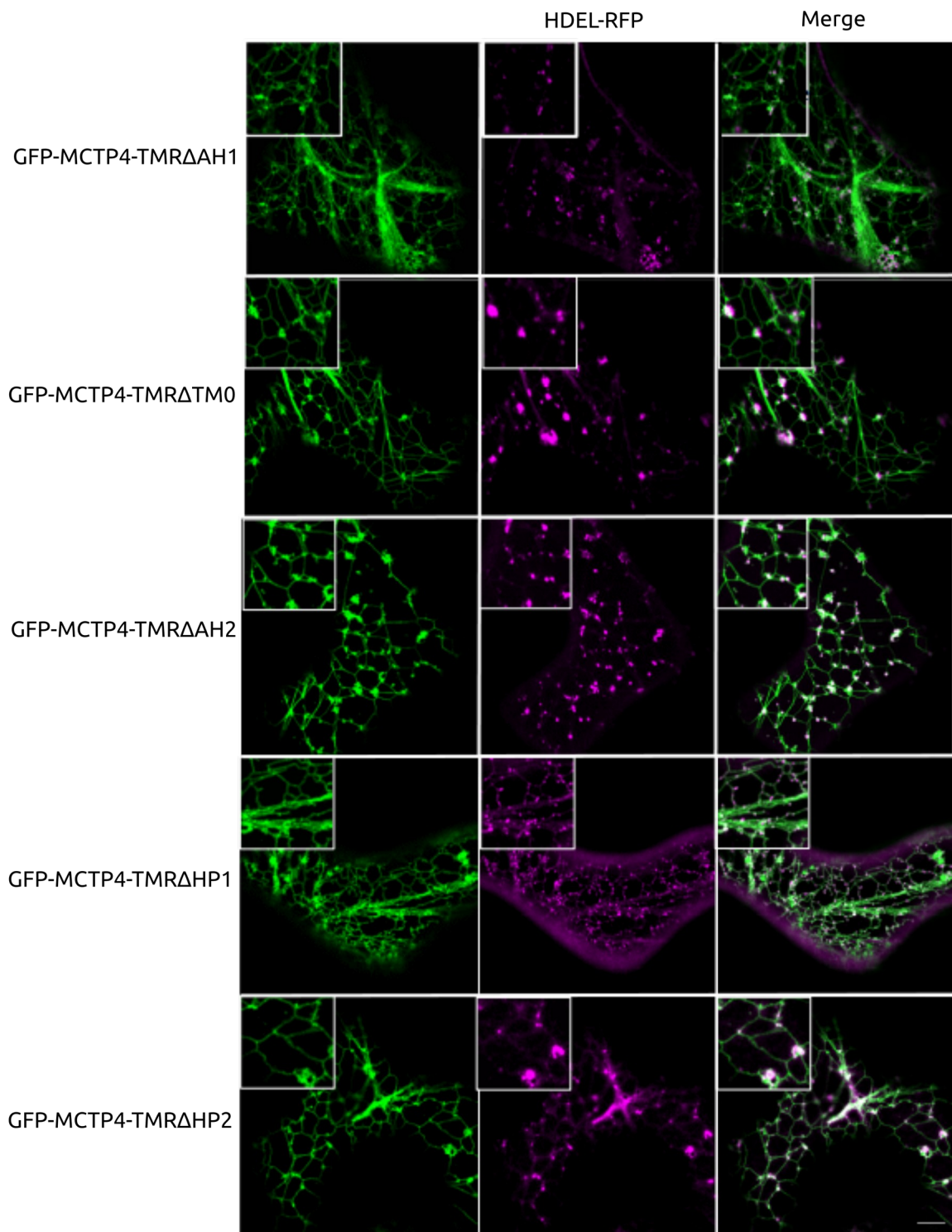
Cluster analysis was done on each subdomain-membrane system and average structures from the main cluster were computed. These structures can be used as base modules to reconstruct the full TMR. I already started the manual assembly of intermediate blocs, using PyMOL (<https://pymol.org>) and MODELLER (Eswar et al., 2008), to study the interactions between the subdomains and the consequences they have on the individual subdomain behaviors during dynamic simulations. Since two conformational predictions exist for TMD0, two MCTP TMR topologies are possible. To discriminate between the two, bimolecular fluorescence complementation experiment could be done *in planta*. The presence of a large linker between HP1 and APH2 lead us to reconstruct the TMR in two blocs, in a first hand, to uncover the degree of freedom of the subdomains within these smaller blocs, before building the full TMR. This work is currently under investigation.

### **2.3.7. Mutations in MCTP4 TMR**

Based on the delimitation and description of the subdomains of MCTP4 TMR described above, TMR mutants lacking single subdomains were generated by Patrick Li and tested for cortical ER association and shaping in *N. benthamiana* leaves. Interestingly, all single-deletion MCTP4 TMR mutants retained ER localization and resulted in the same constriction of the ER network as the native protein, proving structural and functional redundancy in terms of shaping (Figure 4). However, preliminary data on full-length MCTP4 with mutated TMR show a loss of their ability to target PD.

These results highlight the robustness of MCTP4 TMR in shaping the cortical ER membrane thanks to the repetition and redundancy of shaping modules composing it. Nonetheless, these same modules seem to work collaboratively to specifically target MCTP4 at PD, as deletion of any one of them prevents MCTP enrichment at PD.

**Figure 4** : MCTP4 TMR single subdomain deletion mutants is able to shape the cortical ER membrane in transient expression in *N. benthamiana* leaves. In each of the following constructs, one of the five subdomain was removed from the sequence. This work was performed by Patrick Ziqiang Li (LBM).



## **2.4. The role of MCTP in primary PD biogenesis**

### ***2.4.1. Plant cytokinesis and PD biogenesis: inserting and stabilizing ER strands across the forming cell wall***

In plants, cytokinesis is special in the sense that the separation is not complete: daughter cells keep organelle continuities across the new cell wall thanks to the formation of PD (Buschmann & Müller, 2019). It is important to understand that the establishment of these continuities takes place during the division itself, when ER strands are actively trapped across the cell plate, establishing membrane contacts with the cell membrane and are later constricted into a desmotubule while PD are being formed (Nicolas et al., 2017; Seguí-Simarro et al., 2004). To date, the molecular mechanisms of PD assembly remain undisclosed.

The plant cell division can be seen as a construction process. In the middle of the mother cell, a complex network of cytoskeletal polymers, membranes and proteins, called phragmoplast, drives the cell plate assembly. It's the mason. The cell plate consists in PM/cell wall components that are being put together (like bricks) to partition the cytoplasm after nuclear division and that will later mature into the cell wall between the two daughter cells. This construction process can be divided in different stages based on the middle-to-side growing of the phragmoplast and cell plate: disk phragmoplast, ring phragmoplast, discontinuous phragmoplast and cross-wall. This last stage marks the “complete” division between the daughter cells, when the cell plate has reached and fused with the parental cell wall (Smertenko et al., 2017). From previous work, PD were reported to assemble during the cytokinesis process but the timing of PD assembly, ER-cell plate tethering, ER constriction and the molecular players involved are not known.

Here, we want to tackle the question of how plant cells build up PD and maintain post-cytokinesis ER cell-cell continuity. Our hypothesis relies on the action of MCTP for favouring and/or maintaining the ER strands crossing the cell plate through their tethering abilities with the PM while potentially simultaneously stabilizing it. The ER-PM tethering ability of MCTPs in mature PD was already showed in our previous research article (Brault, Petit et al., 2019) and seems to rely on the presence of anionic lipids. Research in the field of plant division suggests that phosphoinositides, especially PI4P and PI(4,5)P<sub>2</sub>, play critical role in the assembly of the cell plate (Caillaud, 2019; Lin et al., 2019; Simon et al., 2016) by defining cell plate

membrane docking sites for protein interaction (tethers, cytoskeletal and trafficking regulators) and ensuring their correct spacio-temporal recruitment through dynamic patterning. In this context, it is legitimate to hypothesize that MCTP could tether the ER to the PM thanks to the early accumulation of PI4P at the cell plate.

#### **2.4.2. Expression and localization of MCTP in dividing cells**

Analysis of the single-cell transcriptomic data from arabidopsis root by Wendrich et al., 2020 gave us insights on the expression of the different MCTP members in the different cell layers in the root. By linking the expression of markers of cell division we identified co-expressed MCTP proteins at this precise stage of cell life. MCTP3, 4, and 6 are expressed in all cell types except the lateral root cap and trichoblasts. They are also the main members expressed during cell division, together with MCTP7 (Figure 5D).

In parallel to my work, Patrick Li observed, using live imaging, the subcellular localization pattern of MCTP3, 4 and 6 during cell division in root epidermis in an actively dividing zone call the division zone under native and UBQ10 promoter. He observed that MCTP3,4 and 6 were localized to the expanding cell plate, where they first display a typical ER pattern (similar to HDEL-GFP for instance) but then become concentrated at punctae within the cell plate at cross-wall stage (Figure 5B, C)

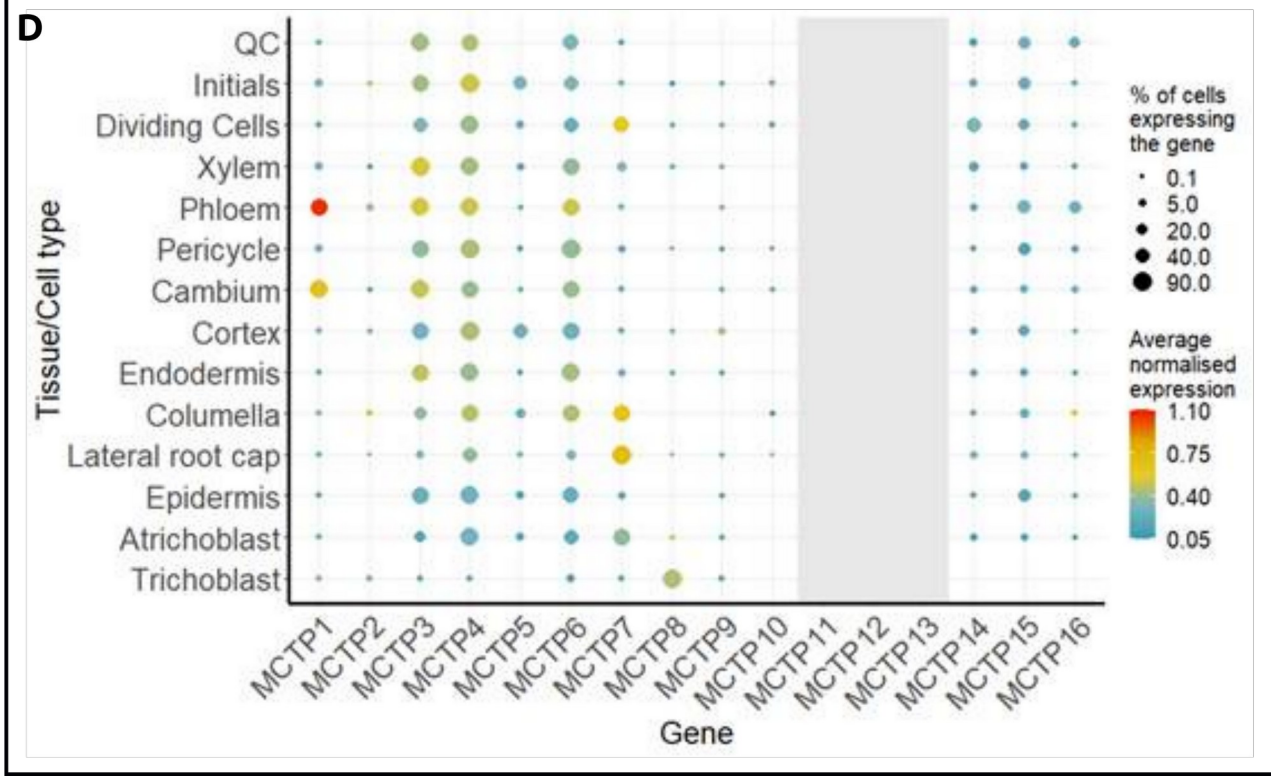
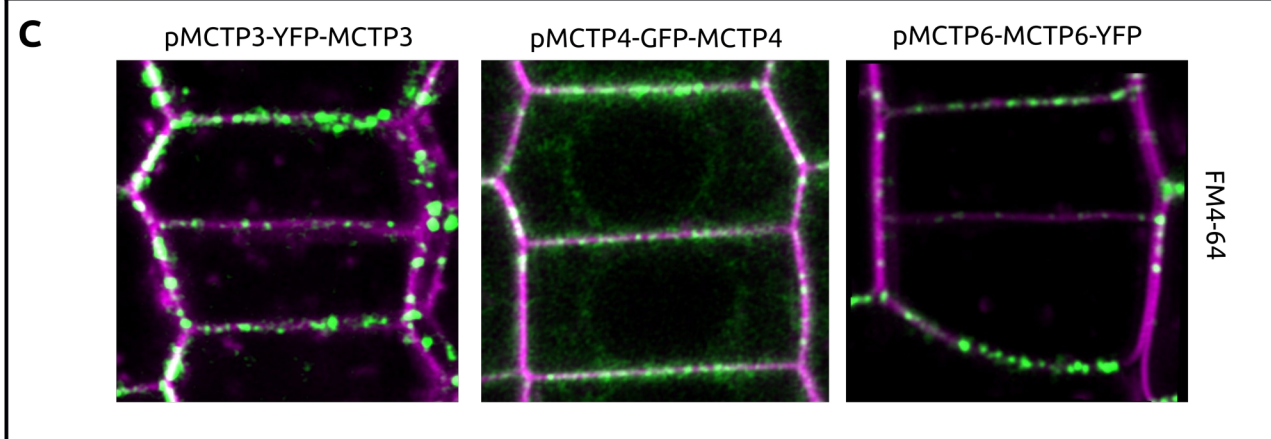
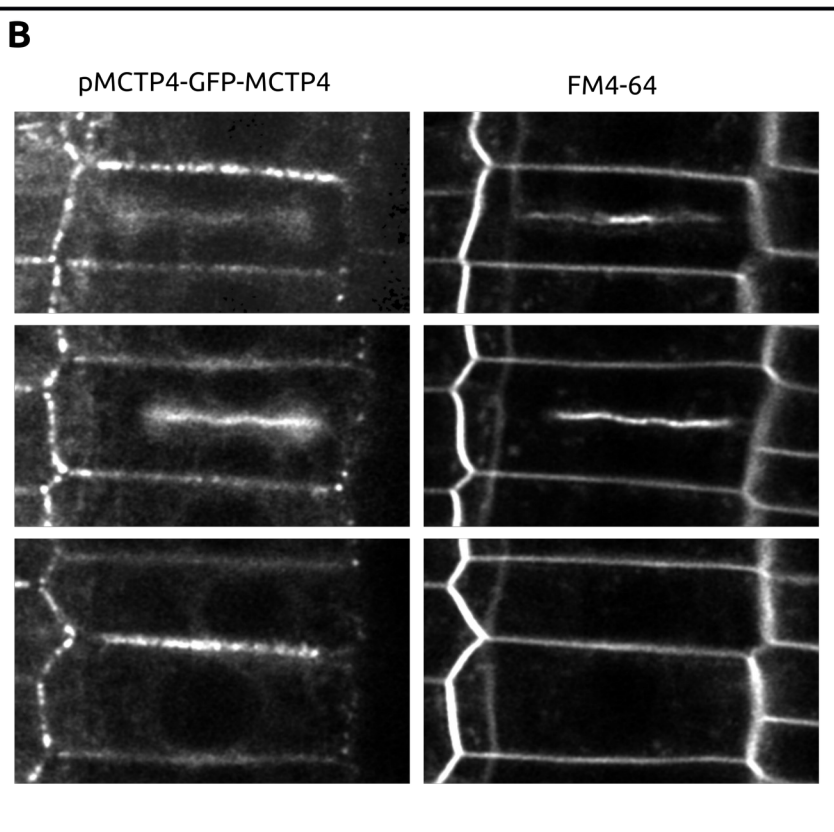
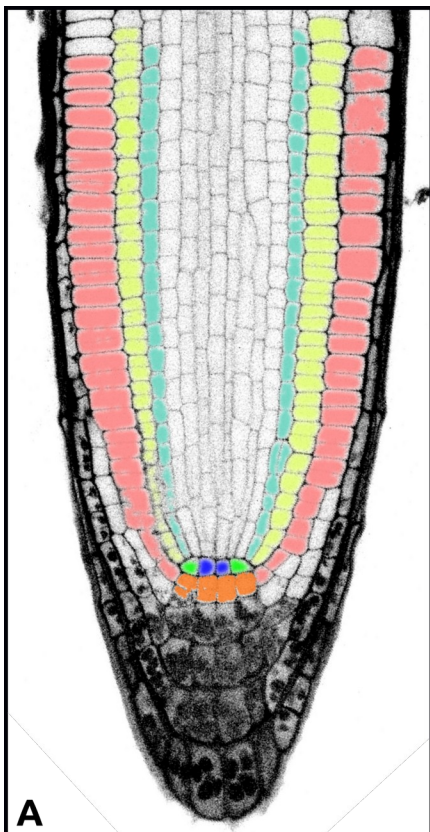
From the data above, as well as for technical reasons, we decided to focus our research on the division zone of the root apical meristem of arabidopsis. This zone, in young seedlings, will provide fresh cell walls with newly formed primary PD, along with cells at cytokinesis stage (Figure 5A). On this tissue, we decided to execute a systematic approach consisting in a comparison between the following genotypes: Col-0, the double *mctp3,4* and the triple *mctp3,4,6* loss-of-function mutants. We evaluated;

- 1) the number of PD at apico-basal cell-cell interfaces (i.e. freshly divided cell walls) across three cell layers: epidermis, cortex and endodermis. My objective here was to provide robust and quantitative analysis on potential defects in PD biogenesis in *mctp* mutant background.

- 2) the detailed cellular events leading to PD formation during cell plate expansion from ring phragmoplast to cross-wall stage and mature walls, in Col-0 and *mctp* mutants.

Considering our objectives, electron microscopy is the most suited way to access this information with enough resolution and accuracy.

**Figure 5** : MCTPs are associated with the cell plate during cell division. A. Representation of an arabidopsis root meristem (image courtesy of Jessica Perez-Sancho), the quiescent center is labelled in blue, the columella initials in brown, the cortex/endodermis initials in green, the epidermis in red, the cortex in yellow and the endodermis in light blue. B. Live imaging of MCTP4 showing its association pattern with the cell plate at different stages of division (top : early phragmoplast, middle : late phragmoplast, bottom : cross-wall ; images from Ziqiang Patrick Li). C. Cross-wall stage association of MCTP3,4 and 6 showing punctae corresponding to nascent plasmodesmata (images from Ziqiang Patrick Li). D. Table of the expression of MCTP members in the root meristem based on single-cell RNA sequencing (data from Wendrich et al. 2020 ; analysis by Andrea Paterlini)





### **2.4.3. Establishment of TEM-based quantification of PD density in the root meristem**

Counting the number of primary PD and observe potential defects, in relationship with the maintenance of the ER in PD assembly, in several genotypes and cell layers, is not an easy and quick task. To realize this, I first had to find a protocol allowing us to fix many samples and that would sufficiently contrast the ER membranes (which can be difficult to see when using high pressure freezing approach (Seguí-Simarro et al., 2004)). For these reasons, I decided to use the chemical fixation and staining protocol from Hepler (Hepler, 1981) and adapted it to 4 days-old arabidopsis roots. This protocol uses a combination of osmium tetroxide and potassium ferricyanide to heavily stain the membranes, in particular the ER (Figure 6B).

I prepared 5 roots per genotype (Col-0, *mctp3,4*, *mctp3,4,6*) and realized ultra-thin longitudinal sections (90 nm) at the root surface and deeper in the tissues using an ultra-microtome. For individual root, I then imaged five to fifteen young mature cell walls in three consecutive cell layers – epidermis, cortex and endodermis – in the root meristem division zone and at X11000 magnification to have a sufficient resolution and be able to see global PD structures. Depending on the cell type, several acquisitions were sometime required to capture the entire wall. All the images were then manually assembled with MosaicJ (ImageJ; <https://imagej.nih.gov/ij/>) to reconstruct each cell wall, before its length could be measured and PD counted. The PD density was then calculated from these two information and results were plotted and analyzed with a mixed linear model in R (with the help of Andrea Paterlini; Figure 6A).

Results show a substantial 30 to 40% decrease of the PD density in the *mctp3,4* and *mctp3,4,6* mutants in the epidermis and endodermis compared to the wild type. Please note that the statistical significance of the decrease in the epidermis in the double *mctp3,4* mutant isn't established. The cortex displays no significant difference in the PD density between any of the three genotypes.

The method used here is very time-consuming, thus to have a more systematic way to quantify primary PD density, I am developping Serial-Bloc-Face Scanning-Electron-Microscopy, in collaboration with Etienne Gontier (Bordeaux Imaging Center). This technique, once settled, will enable the counting of PD throughout a much larger volume of the root tissue and acquire several cell walls, and maybe cell types, simultaneously.

In this manner, we will have more extensive data on each root and accurate densities (calculated on several  $\mu\text{m}$  instead of 90 nm) for individual cell walls.

Finally, it's important to note that while realizing the PD quantification on the TEM images, ER strands were observed entering the pores in all PD, even in the *mctp* mutant backgrounds.

#### **2.4.4. Searching for defects in PD biogenesis**

During the PD quantification described above, the mature PD observed in the *mctp* mutants did not show any obvious defects in their ultrastructure, in the sense that we didn't observe PD without ER or incomplete half-PD. We hypothesized that the origin of the decrease in density in the mutants could be associated with their biogenesis during the cell cytokinesis, and could be due to a reduction in the number of "trapped" ER strands and/or failure to maintain a PD pore when the cell plate expands.

In the aim to access such information, we decided to perform electron tomography (ET) on the same samples as for the quantification. Screening of the sections enabled us to locate several events of cell division in the Col-0 and *mctp3,4,6* genotypes. Overview of the dividing cell allowed us to estimate the stage of cytokinesis. Having said that, late stages of cell division, when, based on our observations, PD "mature", can last 2-3 hours (von Wangenheim et al., 2017). The first attempts of ET were done on 90 nm thick sections, a thickness usually large enough to capture mature PD. However, the fenestrae present in the cell plate are much larger than PD and we had to capture events on thicker sections to be able to reconstruct more volume and access more information. We pursued with 120 nm sections, the maximal thickness for a 120kV TEM but we still thought that we could do better. We finally decided to use 300 nm sections with a 200kV TEM, using the scanning transmission (STEM) mode to acquire the tomograms to enhance resolution. This STEM-ET work is done in collaboration with Melina Petrel (Bordeaux Imaging Center).

The acquisitions are still on-going but the first data are very promising. The resolution is sufficient to visualize the ER tubules surrounding the phragmoplast vesicles and the forming vesicles but also tubules of ER passing through fenestrae (Figure 6C).

From the preliminary data we conclude that:

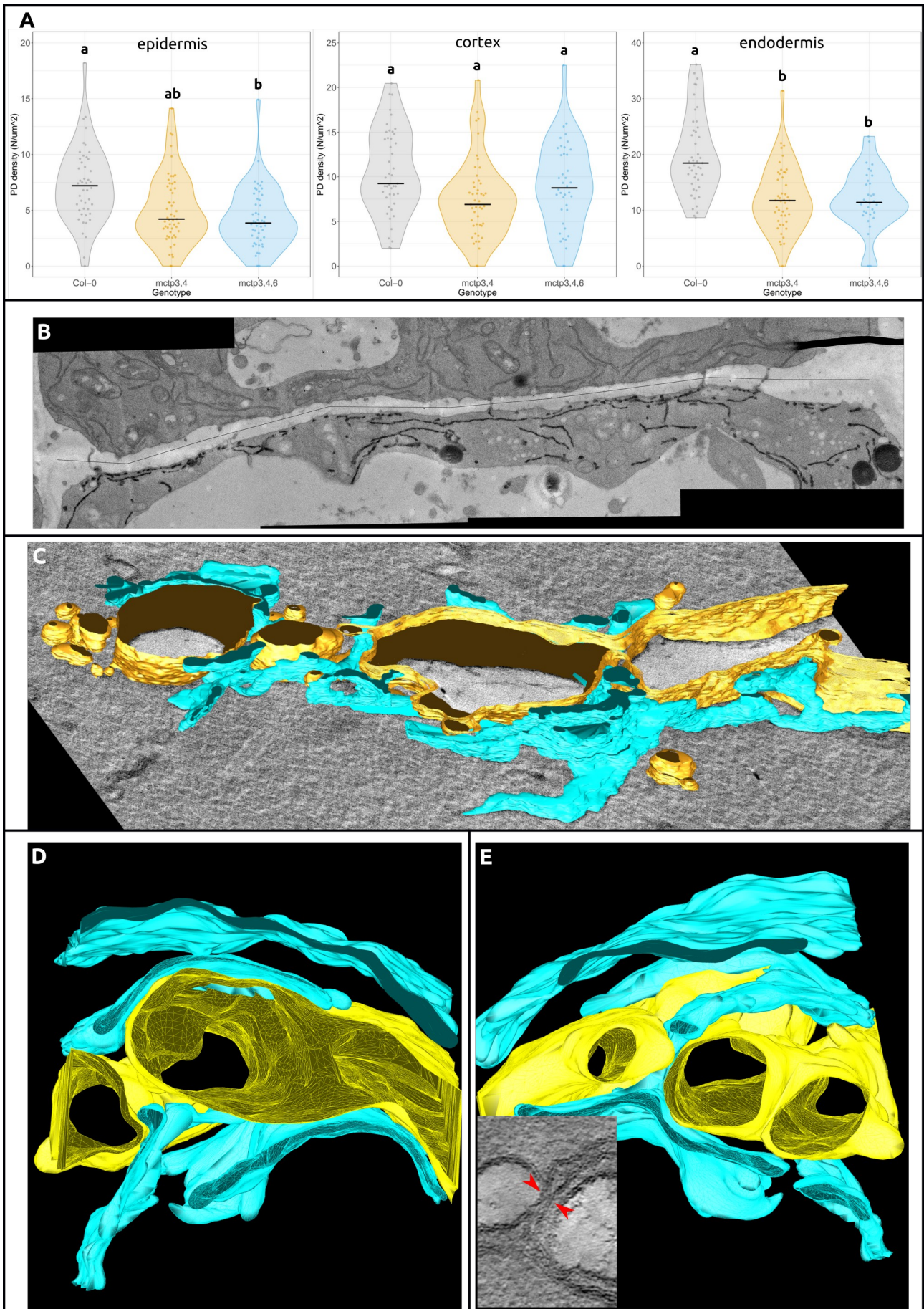
1) the ER network is intertwined with cell-plate-derived vesicles from the very first stage of cytokinesis (ring phragmoplast), presumably establishing membrane contacts. This suggests that the establishment of the ER continuity between daughter cells (hence the intercellular network) is likely initiated at this early stage. However, in early phragmoplast events, no PD-like structures are seen but rather an interconnected/intricated ER-vesicular network with large fenestrae (Figure 6C).

2) PD like structures are visible at later stage of the cytokinesis, i.e. cross-cell wall stage. It is at this stage only that we were able to observed PD-like structure characterised by tight junctions (down to 20 nm PM-PM in diameter) with a constricted ER and tight ER-cell plate membrane contact giving an impression of tight ER-PM membrane zipping (Figure 6E). Although, during the cross-wall stage, different stages of PD "maturation" co-exist with, for instance, constricted and non-constricted ER.

3) in the Col-0 wild type, at cross-wall stage, we observed events where the ER connection seemed lost between the daughter cells. In these events, the ER strands seem to penetrate the plane of the cell plate from each side but do not join (Figure 6D).

**Figure 4** : A. Comparative analysis of the PD density between three genotypes (Col0, *mctp3,4* and *mctp3,4,6*) and in three cell layers (epidermis, cortex, endodermis) based on transmission electron microscopy data. B. Electron micrograph of a Col0 epidermal cell wall. The ER network is highly contrasted and can be seen going through several plasmodesmata. This image is one of the images used for the quantification of plasmodesmata density described in (A.) The line represents the measured cell wall length. C. Electron tomography-based segmentation of a Col-0 cell plate edge (yellow) with the associated ER network (blue) (section of 120 nm). D. Electron tomography-based segmentation of a Col-0 cell plate (yellow) and discontinuous ER (blue) not crossing it (section of 300nm, segmentation by E. Bayer). E. Electron tomography-based segmentation of a Col-0 cell plate (yellow) and continuous ER (blue) forming a nascent plasmodesmata. Insert shows ER-PM contact and simultaneous ER lateral constriction (red arrows ; section of 300nm, segmentation by E. Bayer).

This work is still on going and still has to be finalized to pinned point key stages of PD assembly and defects in the *mctp* mutant background.



# 3

---

## General Discussion

The results presented in the three previous chapters set up a baseline in the operating mode of MCTP proteins at PD, linking their intrinsic structure with functions *in vivo in planta*. While discovering their features and some of their associated capabilities, we unlocked a plethora of questions that remain to be answered. Hereafter, I discuss the results presented in previous chapters and some hypothesis regarding the roles of MCTPs at PD.

Beforehand, it is worth noticing that two research articles were published from Hao Yu's laboratory in Singapore (Liu, Li, Liang, et al., 2018; Liu, Li, Song, et al., 2018) on Arabidopsis MCTPs during the course of my PhD, some of them showing discrepancies with our own data in terms of subcellular localisation.

The first article (Liu, Li, Liang, et al., 2018) was published in *Plant Physiol.* In 2018 and is giving an overview of MCTP family, defining all 16 members with tissue expression patterns and sub-cellular localization. They performed phylogenetic classification of the MCTP family, establishing relationships with plant protein homologs. In our article (Brault, Petit et al., 2019), we show a structural homology screening of the Arabidopsis MCTP against eukaryotic proteins (plants, yeast and animals). This difference illustrates completely different views and objectives of research between them and us. The second article of Liu et al. (Liu, Li, Song, et al., 2018) published in *Cell Reports* in 2018, focuses on two members, MCTP3 and 4. There, they show that both proteins are key regulators of the equilibrium between maintenance of shoot stem cells and their differentiation by controlling the subcellular localization and preventing trafficking of the SHOOT MERISTEMLESS (STM) protein. In this article, they also isolate the double *mctp3,4* knock-out mutant and describe similar dwarf and bushy phenotype.

The main discrepancy between Liu et al. works and our data concerns MCTP3 and 4 enrichment at plasmodesmata. In both papers, the authors do not see enrichment of MCTP3 and 4 at plasmodesmata whereas our work clearly suggest they are core plasmodesmata constituents. Our conclusion are based from semi-comparative proteomic analyses of plasmodesmata fraction and subcellular localization of functional GFP tagged MCTPs ((Brault, Petit et al., 2019 and unpublished data). In our hands, both members associate with the ER but very strongly accumulate at plasmodesmata. Loss-of-function *mctp3,4* Arabidopsis mutant displays a dwarf shoot phenotype which can be rescued upon expression of N-terminal (but not C-terminal) GFP tagged MCTP3 or 4.

In the work of Liu et al., the authors used similarly to us both transient expression in *N. benthamiana* and stable *Arabidopsis* transformants, using a combination of N and C terminus as well as internal tagging (Liu, Li, Liang, et al., 2018; Liu, Li, Song, et al., 2018). In the sub-cellular localization section of the *Plant Physiol.*, none of the GFP-MCTPs was described at plasmodesmata (Fig 7). Later however, in Fig 10, GFP-MCTP6 (the same construct as in Fig 7) is now shown to localize at plasmodesmata (colocalization with callose). Based on transient expression, they group MCTP proteins depending on their subcellular localization: MCTP1,5,10,11,12,16 are associated with the ER, MCTP3,4,6,9,13,15 are observed in the cytosol and at the PM, MCTP7,8,14 localize in small structures inside the cell and MCTP2 is at the PM. Then, they co-localize MCTP3,4,6,7 partially at endosomes and MCTP14,15 partially in the Golgi. They attribute this diversity of localization to potentially distinct functions. To confirm and strengthen our data concerning plasmodesmata enrichment, we decided to perform repetitions and quantification for plasmodesmata association in transient expression and in transgenic *Arabidopsis* lines.

In their second paper, Liu et al. focuses on MCTP3 and 4. As already stated, they observe a similar phenotype than us in double *Arabidopsis* mutant background but once again they do not see any plasmodesmata localization. This major discrepancy with our work was discussed in the EMBO Report (p15). In particular, we raised the issue of the fusion tag placement together with protein localization and functionality. GFP-MCTP3 and 4, transiently expressed in *N. benthamiana* leaves, is shown at the PM and in cytosol, with partial co-localization with endosomal compartments. MCTP4-GFP also localizes in similar organelles but also in Golgi. MCTP3-RFP and MCTP4-GFP localize in the entire cytoplasm in *Arabidopsis* SAM. Immunogold assay of 4HA-gMCTP4 display wide labeling throughout the intracellular compartments, including vesicles and PM but is absent of the nucleus. Using various techniques and tagging, the MCTP3 and 4 localization pattern they observe in these two studies is very wide (cytosol, PM, endosomes, Golgi, vesicles). In comparison, we observe a very consistent ER/plasmodesmata association in both transient expression and stable transgenic lines.

In order to confirm plasmodesmata association, we further investigated their localization by immunogold labelling assays and Correlative Light-Electron Microscopy. Both approaches confirmed the presence of MCTP3 and 4 with plasmodesmata. It is also worth mentioning that other plasmodesmata proteomic work in

Arabidopsis had, similar to us, identified MCTP3 and 4 as PD associated (Fernandez-calvino et al., 2011; Kraner et al., 2017).

During the revision of our manuscript, *Populus* proteomic data (Leijon et al., 2018) supported our own Arabidopsis data regarding MCTP protein enrichment at plasmodesmata. Shortly after the publication of our article, work on maize CPD33 protein also supported a link between MCTPs and PD (Tran et al., 2019).

### **3.1. MCTP C2 domains, opening Pandora's box**

The lipid-binding properties of the MCTP C2 domains shown in Brault, Petit et al., 2019 are important features, conserved in other MCS tethers. From our work we postulated that anionic lipid binding allows MCTP3,4 to dock and interact with the PM inside PD, while the TMR anchors the protein at the ER. The fact that MCTP C2 domains are able to interact with anionic lipids but not stably with neutral membranes puts forward the ideas of transient and dynamic bridging and/or remodeling of the ER-PM MCS, as discussed in (Petit et al., 2020). Since MCTP tether the ER and the PM inside PD, they could easily control the space between the two membranes, like E-Syts (Bian et al., 2018; Ge et al., 2021). This space, the cytoplasmic sleeve, is believed to be the main route for molecular trafficking from cell to cell. By adjusting it, potentially in response to changes in membrane composition and/or cytosolic calcium levels, MCTPs could regulate molecular fluxes passing through PD. This hypothesis is supported by unpublished data from Magali Grison (E. Bayer group), showing enhanced macromolecular trafficking in the epidermis, cortex and endodermis in *mctp3,4* mutant compared to the Col-0, using a photoactivable cytosolic DRONPA marker (Gerlitz et al., 2018). This is counter-intuitive as it occurs at the same cell layers where I demonstrated a decrease of PD density. It is however possible that PD that are still formed at these cellular interfaces, lacking MCTPs, are no able to maintain proper ER-PM contacts, thus facilitating the passage of molecules. This working hypothesis is supported by results from Marie Glavier (E. Bayer group), who also observed more extreme ER-PM detachments in the *mctp3,4,6* mutant in root epidermis PD. More interestingly, this increased intercellular movement of macromolecules isn't correlated with a default in callose accumulation (data from Magali Grison, E. Bayer group). Callose is a glucan polymer of the cell wall and a master regulator of cell-cell trafficking through its accumulation/degradation at the necks of PD pores, regulating the size exclusion



limit (R. Sager & Lee, 2014). The question emerges on whether ER-PM tethering is an alternative, yet complementary, mechanism to callose in the control of PD size exclusion limit.

We still lack lots of information on the specificity of MCTP C2 domains. First, we do not know if the lipid-binding property is specific to the nature of precise lipids, such as PI4P, or if it is charge-dependent and can also bind other PIPs. In the molecular dynamics work published in EMBO Reports, we chose to work on PI4P because, in plants, this lipid constitutes one of the main anionic lipid of the inner PM leaflet (Simon et al., 2016), we however have very little information about PIP composition of the PM inside PD (M. S. Grison et al., 2015). Opening the discussion on this topic, liposome sedimentation assays show interaction of purified MCTP4 C2B with liposomes containing PI(4,5)P<sub>2</sub> (please note that the individual C2 of MCTP4 were purified in bacteria but only the C2B was soluble). Secondly, C2 domains are well known for interacting with calcium ions and some MCTP C2 domains possess a conserved calcium binding site. In the same liposome sedimentation assay, C2B show more stable binding to the liposomes in presence of calcium, indicating a potential role of calcium for stronger membrane interaction. Such investigation could be performed by dynamic simulations but requires the confirmation of localization of the predicted calcium-binding sites. During my master thesis, I used a machine learning-based program called FEATURE (ref) to predict and model the C2 domain loops together with calcium ions, using a database consisting of calcium-bound structures and unbound structures. Similar method, as well as the fast development of AlphaFold methodology (ref), could bring information on MCTP calcium binding while MCTP C2 domains are being purified and assays like Langmuir Though and Isothermal Titration Calorimetry could be done. Thirdly, we have knowledge of C2-C2 interactions in other multiple C2 domain-containing tethering proteins, in link with auto-inhibition and tethering regulation. These protein-protein interactions can also be regulated by the presence of calcium (Bian et al., 2018). C2 domains can additionally interact with other proteins, and data from E. Bayer group showed that MCTP3,4 and 6 interact to form a complex, adding more capabilities and maybe complexity in their modes of actions.

The modeling work I have performed during this project was simply scratching the surface. My methodology had flaws because of computational limitations. It was, for example, impossible for me to realize extensive modeling and sampling, for example to observe the effect of initial positioning of the C2s and, by extension, to characterize deeply the protein-lipid interactions. Moreover, the usage of Martini 2 in

the docking simulations is now debatable in terms of accuracy, since this forcefield is known to enhance/favor molecular interactions (Javanainen et al., 2017). The simulations should be done again with Martini 3 or using mesoscale hybrid models in order to validate the published data (Soares et al., 2017; Souza et al., 2021).

Nonetheless, the modeling work enabled us to get access to information we couldn't get access otherwise but also open our minds through a different point of view on biological questions.

### **3.2. MCTP contains RHD, why?**

During my PhD work I uncovered a new function of PD associated MCTPs, related to membrane shaping. The TMR regions of MCTP3 and 4 are RHDs capable of shaping the cortical ER when present in high amounts (in our case, when overexpressed). Its domain organization is a repetition of shaping modules: APHs and HP transmembranes. Furthermore, we have evidence that MCTP3,4 and 6 TMRs are able to form homomers and heteromers in the cortical ER.

The first questions arising is why do MCTPs possess such features? And, does it have a function at PD? While these functions are of great interest in the context of PD, please note that the *in planta* data described in chapter 2 where obtained in the cortical ER and not at PD, thus, for now, we can only elaborate on putative roles related to their shaping activity inside PD. However, considering the enrichment of MCTP at PD, potentially in correlation with their oligomerization propensity (Jessica Perez-Sancho, unpublished), they could play a role in the high constriction of the ER into the desmotubule, as well as stabilizing it by creating a protein scaffold structuring the strand and preventing fission. Supporting this hypothesis, our electron tomography work that shows ER constriction within the forming pore at cross-wall stage, the exact same stage where live-cell fluorescent microscopy show MCTP accumulation at punctae, likely nascent PD.

In the context of MCS, recent work has shown that extreme ER membrane shaping activity mediated by tricalbins in yeasts and E-Syts in animal results in the formation of ER-peak at ER-PM MCS, which is proposed to drive directional transfer of lipids from the ER to the PM in yeast (Bian et al., 2018; Hoffmann

et al., 2019). For the time being, we do not know if PD are sites for non-vesicular lipid exchange between membranes and what role it would play in regulation cell to cell trafficking.

The fact that single-domain deletion TMR protein mutant (i.e. individual subdomain removal) maintain ER shaping activity but loose PD localization opens discussion on other-than-shaping specificity of this domain at PD. All TMR subdomains might be necessary for effective oligomerization or interaction with other proteins inside PD. It could also be correlated with a membrane specificity/organization at the desmotubule. For example, the desmotubule severe constriction with two ER membranes closely apposed could drive molecular rearrangements in the TMR region where every module works in synchronicity with the others.

Modeling work on the nano-fluidic flows possibly occurring in PD predict a strong effect of the ER shape and position inside PD in the regulation of diffusive and pressure-driven transport (Christensen et al., 2021). This article demonstrates that radial harmonic fluctuation of the ER is strongly affecting bulk flow through the pore. Scaffolding of the ER into a straight narrow tubule (i.e. of constant width) would considerably enhance transport capabilities. It is easy to imagine that MCTPs could have a role, considering their shaping and oligomerization properties, in the maintenance/relaxation of such geometry on the ER desmotubule, thus directly influencing the transport mediated by the cytoplasmic sleeve.

Here again, the modeling work cannot be seen as a strong base but rather as a tool that is getting us moving forward in the exploration of MCTP structure-function. Indeed, I faced similar limitations as the ones described previously, and the “divide and conquer” methodology I used is now confronted to the growth of AlphaFold (Jumper et al., 2021)(although this revolutionary tool’s complete reliability is still a debate in the scientific community). Regarding MCTP TMR, I believe my work can facilitate the comprehension of the protein structure and the development of new modeling and simulations. The exploration of MCTP structure-function by molecular modeling is now taken over within an ANR project in collaboration with the team of Antoine Taly.

### **3.3. MCTP function in primary PD assembly during cytokinesis**

In the last result section, we have discovered that MCTP3,4,6 localize at the phragmoplast and that they accumulate at punctae along the cell plate at cross-wall stage, when PD-like structures are first visible. This data initiated a reflection on the function of MCTP in primary PD biogenesis.

To verify this, we performed TEM and ET on chemically fixed samples of wild type, *mctp3,4* and *mctp3,4,6* mutant seedlings. The quantification of PD density in the apico-basal cell walls of the root meristem epidermis and endodermis shows significant decrease (30 to 40%) in PD numbers in the mutant backgrounds. Supporting the data, reduction of PD density was already observed in the *cpd33* mutant in maize (Tran et al., 2019). Many questions arise in this context: How MCTPs act to drive PD formation and maturation? What happens to the mutant that leads to a reduction of primary PD? Is it because of defects in the attachments between the ER and the PM during the expansion of the cell wall? Is it because less ER strands are spanning the cell plate beforehand? Are some PD aborted during fenestrae closure and PD constriction because they are not stabilized? It is still difficult to answer these questions, yet we are currently performing ET on events occurring at this crucial step of constriction of the ER-fenestrae system into PD, both in *Col-0* and *mctp* mutants. One hypothesis is that the lack of MCTP in the mutant leads to the rupture of the ER crossing the fenestrae. Computational modeling of the cell plate expansion and maturation demonstrates the need of a spreading force acting on the cell plate vesicles in order to transition into a fenestrae state (Jawaid et al., 2020). The impossibility of ER stabilization by both the zipping/tethering to the PM and the construction of a protein scaffold around it, potentially mediated by shaping elements, could be the reason why nearly half of the PD are not maintained in the *mctp* mutant.

Another question then comes to mind: why do we still have some PD left? Do they display visible defects? From our classical transmission electron micrographs, we do not see clear differences between PD in *mctp* and wild type background. It seems that all PD, even in the mutants, possess an ER strand and they also seem to cross over the wall effectively connecting daughter cells. In plants however, MCTP proteins are numerous, and we cannot rule out that structural redundancy is able to partly complement the PD loss in our mutants. To answer this point, inducible CRISPR knock-out lines are currently on going in the lab. Our ET data on forming cell plate show both fenestrae with and without ER crossing them (including events where ER strands are intruding but without ER continuity across the cell plate). We postulate that these later events may correspond to abscission events where ER continuity is not maintained across the cell plate, resulting in aborting PD. This phenomenon may occur at a higher rate in our *mctp* mutant background. If true, this also mean that the presence of ER could then be a necessary condition to form PD in land plants.

Lastly, it is also interesting to think about the diversity of PD: this hypothesis has never been investigated, but considering the narrowness of PD and the significant number of molecular actors, signaling pathways and physiological events occurring at or relying on PD, it is legitimate to wonder if several PD populations exist, with different compositions and functions.

## Conclusion and Perspectives

Overall, my work brought new insights on the role of ER-PM contacts in cell to cell trafficking mediated by PD and in PD biogenesis. It brings novel perspectives on callose-independent symplastic transport regulation by proposing a role of ER-PM connections in the control of the PD size exclusion limit. It also highlights new molecular mechanisms possibly in action during the formation of PD during plant cell division. We propose that these functions is assured by members of the MCTP family, tethering proteins capable of connecting the ER to the PM inside the PD pore.

The main dataset collected during my project was the structural description of the MCTP domains in correlation with their functions at PD. First, we started with the description of the MCTP C2 domains, acting as peripheral proteins capable of anionic lipid-dependant interaction with the plasma membrane. This function enabled us to describe MCTP proteins as tethering elements enriched at PD ER-PM MCS and potentially capable of modulating molecular trafficking and signaling though dynamic and transient bridging between the ER and the PM inside PD (Brault, Petit et al., 2019). Then, we leaned over the other “termini” of the MCTPs, the TMR. This region of MCTP possesses the structural features of RHD and has ER shaping properties. Both these tethering and shaping properties lead us to investigate on the role of MCTP during PD biogenesis in post-cytokinesis walls. Indeed, MCTP could zip the ER to the PM while mediating its tubular constriction, hence providing a protein scaffold that could resist the physical forces in play during cell plate growth. The integration of this work puts MCTP as incredibly multi-task proteins and supports their function as core elements of PD, yet it as also opened many many doors.

Work still needs to be done regarding the C2 domains of MCTP in order to understand they specificity of action and decipher the impact of lipid binding on PD-mediated molecular fluxes. The purification of soluble individual C2 domain (in progress), will allow us to refine their interaction potential with specific lipids, in the presence and absence of calcium, using *in vitro* assays and biophysical techniques. The presence of phosphorylation sites on MCTPs also brings interesting perspectives for future research. Similarly, a better understanding of the TMR and ER shaping inside PD is needed to understand how the two could be involved in PD biogenesis but also transport through the cytosol in mature PD (Christensen et al., 2021).

Despite the limitations of molecular dynamics, we can still rely on them in complementation with experimental data. The revolution induced by AlphaFold structure prediction (Jumper et al., 2021) will allow us to study and compare MCTP structures across the family. Together with the work we already performed, it will bring information on the structure-function similarities/differences for C2 domains and TMRs. To further look into the behavior analysis of the C2 domains, the work of Mark Sansom on peripheral proteins may be of great interest (Andreas Haahr Larsen & Sansom, 2021). For the TMR, many simulations can be performed to understand its function as a whole domain as well as together with other TMRs (as in Bhaskara et al., 2019; Siggel et al., 2021). These assays should obviously be developed based on the biological context we want to decipher. In this context, the development of MARTINI3 coarse grain force field (Souza et al., 2021) will enable more accurate predictions in the molecular interaction occurring during the molecular dynamic simulations.

## Material and Methods

As I relied on multidisciplinary approaches to tackle the research question of my thesis, various techniques were used. Some of them are already published in the EMBO Reports research article (Brault et al., 2019), in Bio-protocol (M. Grison et al., 2020) and in a chapter of Methods in Molecular Biology (in press).

More recent material and methods, used for the acquisition of the data in parts 2 and 3 of this thesis, will be described in more details below.

### ***Quantification of protein enrichment at plasmodesmata using live-cell imaging***

Magali S. Grison, Jules D. Petit, Marie Glavier & Emmanuelle M. Bayer.  
*Quantification of protein enrichment at plasmodesmata*. Bio-protocol (2020), vol. 10 (05), e3545.

### ***Determination of plasmodesmata ultrastructure using electron tomography***

Jules D. Petit, Marie Glavier, Lysiane Brocard & Emmanuelle M. Bayer.  
*Plasmodesmata ultrastructure determination using electron tomography*. In: Benitez-Alfonso (eds) Plasmodesmata. Methods in Molecular Biology (Methods and Protocols). Humana Press, New York, NY. (in press)

### ***Molecular modeling and simulations of MCTP4 TMR***

AtMCTP4 sequence was analyzed using Hydrophobic Cluster Analysis, Psipred, HeliQuest, CCTOP and  $\Delta G$  predictor to predict amphipathic and transmembrane domains and secondary structures. AtMCTP4 TMR 3D model was built using the *ab initio* method of the Robetta server. To prevent bias from the lack of lipid bilayer during the folding, the TMR sequence was not modeled as one but was fragmented in smaller blocks. Domains were prepared for coarse grain simulation using martinize.py script with the elnedyn22 network set on backbone atoms of  $\alpha$ -helices. Hairpin transmembrane were refined using domELNEDIN.tcl script on VMD in order to remove the elastic network in between the two helices. HPs were oriented with the main vector along the Z axis and embedded in a PC membrane using insane.py (-dm0, -box 12,12,10).



Amphipathic helices were oriented parallel to the membrane surface and placed 6 nm above the bilayer center.

For each domain, structural clusters were calculated using gmx cluster tool with the gromos method and a cutoff of 0.15nm when overall RMSD  $\leq$  0.25nm (APH1, TMD0 as TM, HP1 and HP2) or 0.20nm when overall RMSD  $\geq$  0.25nm (APH2, TMD0 as APH). Average structure for the main cluster (most abundant and stable) in interaction with the bilayer was selected for domain assembly.

Block construction was performed first using PyMol: 8 PC molecules at the 4 corners of the box (4 top, 4 bottom) were selected for each object. PC molecules from the two objects were then superimposed automatically using pair\_fit command. Protein domains were then placed in the most “open” conformation relative to one another using rotate and translate command without disrupting the bilayer superimposition. Once close enough and in an optimal conformation, linker “loose ends” from both sides of the secondary structures that need to be reattached were deleted. Protein fragments were saved as one pbd file without lipids.

Final block assembly was performed using a MODELLER loop construction python script directed on linker regions that needed to be built (to avoid movement of whole domains). Blocs were prepared for coarse grain simulation using martinize.py script with the elnodyn22 network set on backbone atoms and refined using domELNEDIN.tcl script on VMD in order to remove the elastic network in between domains. Blocs were oriented using gmx editconf using the -princ option on the amphipathic helices and -rotate option to align the hairpin to the Z axis. Membrane insertion was done with insane.py script using option -dm 1.5 in a 20x20x10nm box.

### ***Arabidopsis root chemical fixation for TEM-based quantification and ET***

4 days old seedlings growing on ½ MS 1% sucrose media on vertical plates were fixed in a fixation buffer (Sodium Cacodylate 0.1M (pH7.4), Glutaraldehyde 2.5%, Paraformaldehyde 2%, CaCl<sub>2</sub> 10mM) for 2h at room temperature. They were then rinsed 3 times for 5-10min with a rinsing buffer (Sodium Cacodylate 0.1M (pH7.4), CaCl<sub>2</sub> 10mM) before the staining solution was added (Sodium Cacodylate 0.1M (pH7.4), Osmium tetroxide 2%, Potassium ferricyanide 0,8%, CaCl<sub>2</sub> 10mM). Staining was realized overnight at 4°C. Washing buffer (Sodium Cacodylate 0.1M (pH 7.4) was used to rinse the staining solution 3 times, followed

by 3 distilled water washes. Dehydration steps were done with a gradient of ethanol/water solutions until seedlings were set in ultrapure ethanol. The ethanol was then substituted with ultrapure acetone and finally in gradient of Spurr resin in acetone. Once in 100% Spurr, the samples were placed in moulds and polymerized at 70°C for 16h.

## References

- Allen, W. J., Lemkul, J. A., & Bevan, D. R. (2009). GridMAT-MD: a grid-based membrane analysis tool for use with molecular dynamics. *Journal of Computational Chemistry*, *30*, 1952–1958. <https://doi.org/10.1002/jcc>
- Benítez, M., Hernández-Hernández, V., Newman, S. A., & Niklas, K. J. (2018). Dynamical patterning modules, biogeneric materials, and the evolution of multicellular plants. *Frontiers in Plant Science*, *9*(July), 1–16. <https://doi.org/10.3389/fpls.2018.00871>
- Bhaskara, R. M., Grumati, P., Garcia-Pardo, J., Kalayil, S., Covarrubias-Pinto, A., Chen, W., Kudryashev, M., Dikic, I., & Hummer, G. (2019). Curvature induction and membrane remodeling by FAM134B reticulon homology domain assist selective ER-phagy. *Nature Communications*, *10*(1). <https://doi.org/10.1038/s41467-019-10345-3>
- Bian, X., Saheki, Y., & De Camilli, P. (2018). Ca<sup>2+</sup> releases E-Syt1 autoinhibition to couple ER-plasma membrane tethering with lipid transport. *The EMBO Journal*, *37*(2), 219–234. <https://doi.org/10.15252/embj.201797359>
- Bittrich, S., Rose, Y., Segura, J., Lowe, R., Westbrook, J. D., Duarte, J. M., & Burley, S. K. (2022). RCSB Protein Data Bank: improved annotation, search and visualization of membrane protein structures archived in the PDB. *Bioinformatics*, *38*(5), 1452–1454. <https://doi.org/10.1093/bioinformatics/btab813>
- Brault, M. L., Petit, J. D., Immel, F., Nicolas, W. J., Glavier, M., Brocard, L., Gaston, A., Fouché, M., Hawkins, T. J., Crowet, J., Grison, M. S., Germain, V., Rocher, M., Kraner, M., Alva, V., Claverol, S., Paterlini, A., Helariutta, Y., Deleu, M., ... Bayer, E. M. (2019). Multiple C<sub>2</sub> domains and transmembrane region proteins (MCTPs) tether membranes at plasmodesmata. *EMBO Reports*, 1–26. <https://doi.org/10.15252/embr.201847182>
- Breeze, E., Dzimitrowicz, N., Kriechbaumer, V., Brooks, R., Botchway, S. W., Brady, J. P., Hawes, C., Dixon, A. M., Schnell, J. R., Fricker, M. D., & Frigerio, L. (2016). A C-terminal amphipathic helix is necessary for the in vivo tubule-shaping function of a plant reticulon. *Proceedings of the National Academy of Sciences of the United States of America*, *113*(39), 10902–10907. <https://doi.org/10.1073/pnas.1605434113>
- Brooks, R. L., Mistry, C. S., & Dixon, A. M. (2021). Curvature sensing amphipathic helix in the C-terminus of RTNLB13 is conserved in all endoplasmic reticulum shaping reticulons in *Arabidopsis thaliana*. *Scientific Reports*, *11*(1), 1–11. <https://doi.org/10.1038/s41598-021-85866-3>
- Brunkard, J. O., Runkel, A. M., & Zambryski, P. C. (2015). The cytosol must flow: Intercellular transport through plasmodesmata. *Current Opinion in Cell Biology*, *35*, 13–20. <https://doi.org/10.1016/j.ceb.2015.03.003>
- Brunkard, J. O., & Zambryski, P. C. (2017). Plasmodesmata enable multicellularity: new insights into their evolution, biogenesis, and functions in development and immunity. *Current Opinion in Plant Biology*, *35*, 76–83. <https://doi.org/10.1016/j.pbi.2016.11.007>
- Buchan, D. W. A., Minneci, F., Nugent, T. C. O., Bryson, K., & Jones, D. T. (2013). Scalable web service for the PSIPRED Protein Analysis Workbench. *Nucleic Acids Research*, *41*, 349–357.

- Bulankina, A. V., & Thoms, S. (2020). Functions of Vertebrate Ferlins. In *Cells* (Vol. 9, Issue 3). <https://doi.org/10.3390/cells9030534>
- Buschmann, H., & Müller, S. (2019). Update on plant cytokinesis: rule and divide. *Current Opinion in Plant Biology*, 52, 97–105. <https://doi.org/10.1016/j.pbi.2019.07.003>
- Caillaud, M. C. (2019). Anionic lipids: A pipeline connecting key players of plant cell division. *Frontiers in Plant Science*, 10(April), 1–11. <https://doi.org/10.3389/fpls.2019.00419>
- Cao, Y., Geddes, T. A., Yang, J. Y. H., & Yang, P. (2020). Ensemble deep learning in bioinformatics. *Nature Machine Intelligence*, 2(9), 500–508. <https://doi.org/10.1038/s42256-020-0217-y>
- Chavent, M., Duncan, A. L., & Sansom, M. S. P. (2016). Molecular dynamics simulations of membrane proteins and their interactions : from nanoscale to mesoscale. *Current Opinion in Structural Biology*, 40, 8–16. <https://doi.org/10.1016/j.sbi.2016.06.007>
- Chen, C., Vanneste, S., & Chen, X. (2021). Review: Membrane tethers control plasmodesmal function and formation. *Plant Science*, 304, 110800. <https://doi.org/10.1016/j.plantsci.2020.110800>
- Chen, Y. J., Williams, J. M., Arvan, P., & Tsai, B. (2020). Reticulon protects the integrity of the ER membrane during ER escape of large macromolecular protein complexes. *Journal of Cell Biology*, 219(2), 1–13. <https://doi.org/10.1083/jcb.201908182>
- Chmiela, S., Sauceda, H. E., Müller, K. R., & Tkatchenko, A. (2018). Towards exact molecular dynamics simulations with machine-learned force fields. *Nature Communications*, 9(1). <https://doi.org/10.1038/s41467-018-06169-2>
- Christensen, A. H., Stone, H. A., & Jensen, K. H. (2021). Diffusion and flow across shape-perturbed plasmodesmata nanopores in plants. *European Physical Journal Plus*, 136(8). <https://doi.org/10.1140/epjp/s13360-021-01727-y>
- Collado, J., Kalemánov, M., Campelo, F., Bourgoing, C., Thomas, F., Loewith, R., Martínez-Sánchez, A., Baumeister, W., Stefan, C. J., & Fernández-Busnadiego, R. (2019). Tricalbin-Mediated Contact Sites Control ER Curvature to Maintain Plasma Membrane Integrity. *Developmental Cell*, 51(4), 476-487.e7. <https://doi.org/10.1016/j.devcel.2019.10.018>
- Crowet, J. M., Buchoux, S., Belloy, N., Sarazin, C., Lins, L., & Dauchez, M. (2021). LIMONADA: A database dedicated to the simulation of biological membranes. *Journal of Computational Chemistry*, 42(14), 1028–1033. <https://doi.org/10.1002/jcc.26511>
- D’Eletto, M., Oliverio, S., & Di Sano, F. (2020). Reticulon Homology Domain-Containing Proteins and ER-Phagy. *Frontiers in Cell and Developmental Biology*, 8(February), 1–6. <https://doi.org/10.3389/fcell.2020.00090>
- Deinum, E. E., Benitez-alfonso, Y., & Mulder, B. M. (2019). *From plasmodesma geometry to effective symplastic permeability through biophysical modelling.*
- Djurovic, S., Le Hellard, S., Kähler, A. K., Jönsson, E. G., Agartz, I., Steen, V. M., Hall, H., Wang, A. G., Rasmussen, H. B., Melle, I., Werge, T., & Andreassen, O. A. (2009). Association of MCTP2 gene variants with schizophrenia in three independent samples of Scandinavian origin (SCOPE). *Psychiatry Research*, 168(3), 256–258. <https://doi.org/10.1016/j.psychres.2008.08.007>

- Duboué-Dijon, E., Javanainen, M., Delcroix, P., Jungwirth, P., & Martinez-Seara, H. (2020). A practical guide to biologically relevant molecular simulations with charge scaling for electronic polarization. *Journal of Chemical Physics*, 153(5). <https://doi.org/10.1063/5.0017775>
- Ducarme, P., Rahman, M., & Brasseur, R. (1998). Impala: A simple constraint field to simulate the biological membrane in molecular structure studies. *Journal de Pharmacie de Belgique*, 53(2), 106. [https://doi.org/10.1002/\(sici\)1097-0134\(19980301\)30:4<357::aid-prot3>3.3.co;2-8](https://doi.org/10.1002/(sici)1097-0134(19980301)30:4<357::aid-prot3>3.3.co;2-8)
- Enkavi, G., Javanainen, M., Kulig, W., Róg, T., & Vattulainen, I. (2019). Multiscale Simulations of Biological Membranes: The Challenge To Understand Biological Phenomena in a Living Substance. *Chemical Reviews*, 119(9), 5607–5774. <https://doi.org/10.1021/acs.chemrev.8b00538>
- Espadas, J., Pendin, D., Bocanegra, R., Escalada, A., Misticoni, G., Trevisan, T., Velasco del Olmo, A., Montagna, A., Bova, S., Ibarra, B., Kuzmin, P. I., Bashkirov, P. V., Shnyrova, A. V., Frolov, V. A., & Daga, A. (2019). Dynamic constriction and fission of endoplasmic reticulum membranes by reticulon. *Nature Communications*, 10(1), 1–11. <https://doi.org/10.1038/s41467-019-13327-7>
- Espino-Saldaña, A. E., Durán-Ríos, K., Olivares-Hernandez, E., Rodríguez-Ortiz, R., Arellano-Carbajal, F., & Martínez-Torres, A. (2020). Temporal and spatial expression of zebrafish mctp genes and evaluation of frameshift alleles of mctp2b. *Gene*, 738(September 2019). <https://doi.org/10.1016/j.gene.2020.144371>
- Eswar, N., Eramian, D., Webb, B., Shen, M.-Y., & Sali, A. (2008). Protein Structure Modeling with MODELLER. In B. Kobe, M. Guss, & T. Huber (Eds.), *Structural Proteomics* (pp. 145–159). Humana Press. [https://doi.org/10.1007/978-1-60327-058-8\\_8](https://doi.org/10.1007/978-1-60327-058-8_8)
- Fernandez-calvino, L., Faulkner, C., Walshaw, J., Saalbach, G., Benitez-alfonso, Y., & Maule, A. (2011). Arabidopsis Plasmodesmal Proteome. *Plos One*, 6(4). <https://doi.org/10.1371/journal.pone.0018880>
- Fulton, L., Batoux, M., Vaddepalli, P., Kishor, R., Busch, W., Andersen, S. U., Jeong, S., Lohmann, J. U., & Schneitz, K. (2009). DETORQUEO, QUIRKY, and ZERZAUST Represent Novel Components Involved in Organ Development Mediated by the Receptor-Like Kinase STRUBBELIG in Arabidopsis thaliana. *Plos Genetics*, 5(1). <https://doi.org/10.1371/journal.pgen.1000355>
- Gabler, F., Nam, S. Z., Till, S., Mirdita, M., Steinegger, M., Söding, J., Lupas, A. N., & Alva, V. (2020). Protein Sequence Analysis Using the MPI Bioinformatics Toolkit. *Current Protocols in Bioinformatics*, 72(1), 1–30. <https://doi.org/10.1002/cpbi.108>
- Gaboriaud, C., Bissery, V., Benchetrit, T., & Mornon, J. P. (1987). Hydrophobic cluster analysis : an efficient new way to compare and analyse amino acid sequences. *FEBS Letters*, 224(1), 149–155.
- Gaudioso-Pedraza, R., Beck, M., Frances, L., Kirk, P., Ripodas, C., Niebel, A., Oldroyd, G. E. D., Benitez-Alfonso, Y., & de Carvalho-Niebel, F. (2018). Callose-Regulated Symplastic Communication Coordinates Symbiotic Root Nodule Development. *Current Biology*, 28(22), 3562-3577.e6. <https://doi.org/10.1016/j.cub.2018.09.031>
- Gautier, R., Bacle, A., Tiberti, M. L., Fuchs, P. F., Vanni, S., & Antonny, B. (2018). PackMem: A Versatile Tool to Compute and Visualize Interfacial Packing Defects in Lipid Bilayers. *Biophysical Journal*, 115(3), 436–444. <https://doi.org/10.1016/j.bpj.2018.06.025>

- Gautier, R., Douguet, D., Antony, B., & Drin, G. (2008). HELIQUEST: A web server to screen sequences with specific  $\alpha$ -helical properties. *Bioinformatics*, *24*(18), 2101–2102. <https://doi.org/10.1093/bioinformatics/btn392>
- Ge, J., Bian, X., Ma, L., Cai, Y., Li, Y., Yang, J., Karatekin, E., & Di Camilli, P. (2021). Stepwise membrane binding of the C2 domains of the extended synaptotagmins revealed by optical tweezers. *Research Square*.
- Genç, Ö., Dickman, D. K., Ma, W., Tong, A., Fetter, R. D., & Davis, G. W. (2017). MCTP is an ER-resident calcium sensor that stabilizes synaptic transmission and homeostatic plasticity. *ELife*, *6*(e22904), 1–23. <https://doi.org/10.7554/eLife.22904>
- Geragotelis, A. D., Freitas, J. A., & Tobias, D. J. (2021). Anomalous Diffusion of Peripheral Membrane Signaling Proteins from All-Atom Molecular Dynamics Simulations. *Journal of Physical Chemistry B*, *125*(35), 9990–9998. <https://doi.org/10.1021/acs.jpcc.1c04905>
- Gerlitz, N., Gerum, R., Sauer, N., & Stadler, R. (2018). Photoinducible DRONPA-s: a new tool for investigating cell-cell connectivity. *The Plant Journal*, *94*(5), 751–766.
- Goossens, K., & De Winter, H. (2018). Molecular Dynamics Simulations of Membrane Proteins: An Overview. *Journal of Chemical Information and Modeling*, *58*(11), 2193–2202. <https://doi.org/10.1021/acs.jcim.8b00639>
- Gowers, R. J., Linke, M., Barnoud, J., Reddy, T. J. E., Melo, M. N., Seyler, S. L., Dotson, D. L., Domanski, J., Buchoux, S., Kenney, I. M., & Beckstein, O. (2016). MDAnalysis: A Python Package for the Rapid Analysis of Molecular Dynamics Simulations. In I. S. B. and S. Rostrup (Ed.), *Proceedings of the 15th Python in Science Conference* (pp. 102–109). SciPy.
- Grison, M., Petit, J., Glavier, M., & Bayer, E. (2020). Quantification of Protein Enrichment at Plasmodesmata. *Bio-Protocol*, *10*(5), 1–10. <https://doi.org/10.21769/bioprotoc.3545>
- Grison, M. S., Brocard, L., Fouillen, L., Nicolas, W., Wewer, V., & Dörmann, P. (2015). Specific Membrane Lipid Composition Is Important for Plasmodesmata Function in Arabidopsis. *The Plant Cell*, *27*, 1228–1250. <https://doi.org/10.1105/tpc.114.135731>
- Gronnier, J., Crowet, J.-M., Habenstein, B., Nasir, M. N., Bayle, V., Hosy, E., Platre, M. P., Gougnet, P., Raffaele, S., Martinez, D., Grelard, A., Loquet, A., Simon-Plas, F., Gerbeau-Pissot, P., Der, C., Bayer, E. M., Jaillais, Y., Deleu, M., Germain, V., ... Mongrand, S. (2017). Structural basis for plant plasma membrane protein dynamics and organization into functional nanodomains. *ELife*, *6*(e26404), 1–24. <https://doi.org/10.7554/eLife.26404>
- Guixà-González, R., Rodríguez-Espigares, I., Ramírez-Angueta, J. M., Carrió-Gaspar, P., Martínez-Seara, H., Giorgino, T., & Selent, J. (2014). MEMBPLUGIN: Studying membrane complexity in VMD. *Bioinformatics*, *30*(10), 1478–1480. <https://doi.org/10.1093/bioinformatics/btu037>
- Han, X., Huang, L. J., Feng, D., Jiang, W., Miu, W., & Li, N. (2019). Plasmodesmata-related structural and functional proteins: The long sought-after secrets of a cytoplasmic channel in plant cell walls. *International Journal of Molecular Sciences*, *20*(12). <https://doi.org/10.3390/ijms20122946>
- Harayama, T., & Riezman, H. (2018). Understanding the diversity of membrane lipid composition. *Nature Reviews Molecular Cell Biology*, *19*(5), 281–296. <https://doi.org/10.1038/nrm.2017.138>

- Hepler, P. K. (1981). The structure of the endoplasmic reticulum revealed by osmium tetroxide-potassium ferricyanide staining. *European Journal of Cell Biology*, 26(1), 102–111. <http://europepmc.org/abstract/MED/6173219>
- Hernández-Hernández, V., Niklas, K. J., Newman, S. A., & Benítez, M. (2012). Dynamical patterning modules in plant development and evolution. *International Journal of Developmental Biology*, 56(9), 661–674. <https://doi.org/10.1387/ijdb.120027mb>
- Hessa, T., Meindl-Beinker, N. M., Bernsel, A., Kim, H., Sato, Y., Lerch-Bader, M., Nilsson, I., White, S. H., & Von Heijne, G. (2007). Molecular code for transmembrane-helix recognition by the Sec61 translocon. *Nature*, 450(7172), 1026–1030. <https://doi.org/10.1038/nature06387>
- Hoffmann, P. C., Bharat, T. A. M., Wozny, M. R., Boulanger, J., Miller, E. A., & Kukulski, W. (2019). Tricalbins Contribute to Cellular Lipid Flux and Form Curved ER-PM Contacts that Are Bridged by Rod-Shaped Structures. *Developmental Cell*, 51(4), 488-502.e8. <https://doi.org/10.1016/j.devcel.2019.09.019>
- Hu, J., Shibata, Y., Voss, C., Shemesh, T., Li, Z., Coughlin, M., Kozlov, M. M., Rapoport, T. A., & Prinz, W. A. (2008). Membrane proteins of the endoplasmic reticulum induce high-curvature tubules. *Science*, 319(5867), 1247–1250. <https://doi.org/10.1126/science.1153634>
- Ishikawa, K., Tamura, K., Fukao, Y., & Shimada, T. (2020). Structural and functional relationships between plasmodesmata and plant endoplasmic reticulum–plasma membrane contact sites consisting of three synaptotagmins. *New Phytologist*, 226(3), 798–808. <https://doi.org/10.1111/nph.16391>
- Javanainen, M., Martinez-Seara, H., & Vattulainen, I. (2017). Excessive aggregation of membrane proteins in the Martini model. *Plos One*, 12(11), 1–20. <https://doi.org/10.5281/zenodo.1019733>
- Jawaid, M. Z., Sinclair, R., Cox, D., & Drakakaki, G. (2020). A Biophysical Model for Plant Cell Plate Development. <https://doi.org/10.1101/2020.05.21.109512>
- Jiang, X., Wang, X., Ding, X., Du, M., Li, B., Weng, X., Zhang, J., Li, L., Tian, R., Zhu, Q., Chen, S., Wang, L., Liu, W., Fang, L., Neculai, D., & Sun, Q. (2020). FAM 134B oligomerization drives endoplasmic reticulum membrane scission for ER -phagy . *The EMBO Journal*, 39(5), 1–14. <https://doi.org/10.15252/embj.2019102608>
- Joshi, A. S., Nebenfuehr, B., Choudhary, V., Satpute-Krishnan, P., Levine, T. P., Golden, A., & Prinz, W. A. (2018). Lipid droplet and peroxisome biogenesis occur at the same ER subdomains. *Nature Communications*, 9(2940), 1–12. <https://doi.org/10.1038/s41467-018-05277-3>
- Joshi, A. S., Ragusa, J. V., Prinz, W. A., & Cohen, S. (2021). Multiple C2 domain-containing transmembrane proteins promote lipid droplet biogenesis and growth at specialized endoplasmic reticulum subdomains. *Molecular Biology of the Cell*, 32(12), 1147–1157. <https://doi.org/10.1091/MBC.E20-09-0590>
- Jumper, J., Evans, R., Pritzel, A., Green, T., Figurnov, M., Ronneberger, O., Tunyasuvunakool, K., Bates, R., Žídek, A., Potapenko, A., Bridgland, A., Meyer, C., Kohl, S. A. A., Ballard, A. J., Cowie, A., Romera-Paredes, B., Nikolov, S., Jain, R., Adler, J., ... Hassabis, D. (2021). Highly accurate protein structure prediction with AlphaFold. *Nature*, 596(7873), 583–589. <https://doi.org/10.1038/s41586-021-03819-2>
- Knox, K., Wang, P., Kriechbaumer, V., Tilsner, J., Frigerio, L., Sparkes, I., Hawes, C., & Oparka, K. (2015). Putting the Squeeze on Plasmodesmata : A Role for Reticulons in Primary Plasmodesmata Formation 1. *Plant Physiology*, 168, 1563–1572. <https://doi.org/10.1104/pp.15.00668>

- Kraner, M. E., Müller, C., & Sonnewald, U. (2017). Comparative proteomic profiling of the choline transporter-like1 (CHER1) mutant provides insights into plasmodesmata composition of fully developed *Arabidopsis thaliana* leaves. *The Plant Journal*, *92*, 696–709. <https://doi.org/10.1111/tpj.13702>
- Kuhlman, B., & Bradley, P. (2019). Advances in protein structure prediction and design. *Nature Reviews Molecular Cell Biology*, *20*(11), 681–697. <https://doi.org/10.1038/s41580-019-0163-x>
- Larsen, Andreas H, John, L. H., Sansom, M. S. P., & Corey, R. A. (2022). Specific interactions of peripheral membrane proteins with lipids: what can molecular simulations show us? *Under Review*.
- Larsen, Andreas Haahr, & Sansom, M. S. P. (2021). Binding of Ca<sup>2+</sup>-independent C2 domains to lipid membranes: A multi-scale molecular dynamics study. *Structure*, *29*(10), 1200-1213.e2. <https://doi.org/10.1016/j.str.2021.05.011>
- Leijon, F., Melzer, M., Zhou, Q., Srivastava, V., & Bulone, V. (2018). Proteomic Analysis of Plasmodesmata From Populus Cell Suspension Cultures in Relation With Callose Biosynthesis. *Frontiers in Plant Science*, *9*(1681), 1–14. <https://doi.org/10.3389/fpls.2018.01681>
- Li, Z. P., Paterlini, A., Glavier, M., & Bayer, E. M. (2021). Intercellular trafficking via plasmodesmata: molecular layers of complexity. *Cellular and Molecular Life Sciences*, *78*(3), 799–816. <https://doi.org/10.1007/s00018-020-03622-8>
- Lin, F., Krishnamoorthy, P., Schubert, V., Hause, G., Heilmann, M., & Heilmann, I. (2019). A dual role for cell plate-associated PI4K $\beta$  in endocytosis and phragmoplast dynamics during plant somatic cytokinesis. *The EMBO Journal*, *38*(4), 1–26. <https://doi.org/10.15252/emboj.2018100303>
- Liu, L., Li, C., Liang, Z., & Yu, H. (2018). Characterization of Multiple C2 Domain and Transmembrane. *Plant Physiology*, *176*(March), 2119–2132. <https://doi.org/10.1104/pp.17.01144>
- Liu, L., Li, C., Norman, W., Zhang, B., & Yu, H. (2019). The MCTP-SNARE Complex Regulates Florigen Transport in Arabidopsis. *Plant Cell*. <https://doi.org/10.1105/tpc.18.00960>
- Liu, L., Li, C., Song, S., Teo, Z. W. N., Shen, L., Wang, Y., Jackson, D., & Yu, H. (2018). FTIP-Dependent STM Trafficking Regulates Shoot Meristem Development in Arabidopsis. *Cell Reports*, *23*, 1879–1890. <https://doi.org/10.1016/j.celrep.2018.04.033>
- Liu, L., Liu, C., Hou, X., Xi, W., Shen, L., Tao, Z., Wang, Y., & Yu, H. (2012). FTIP1 is an essential regulator required for florigen transport. *Plos Biology*, *10*(4).
- Liu, L., Zhang, Y., & Yu, H. (2020). Florigen trafficking integrates photoperiod and temperature signals in Arabidopsis. *Journal of Integrative Plant Biology*, *62*(9), 1385–1398. <https://doi.org/10.1111/jipb.13000>
- Lombard, J. (2014). Once upon a time the cell membranes: 175 years of cell boundary research. *Biology Direct*, *9*(1), 32. <https://doi.org/10.1186/s13062-014-0032-7>
- Loving the alien. (2019). *Nature Plants*, *5*(6), 551. <https://doi.org/10.1038/s41477-019-0463-3>
- Marrink, S. J., Corradi, V., Souza, P. C. T., Ingólfsson, H. I., Tieleman, D. P., & Sansom, M. S. P. (2019). Computational Modeling of Realistic Cell Membranes. *Chemical Reviews*, *119*(9), 6184–6226. <https://doi.org/10.1021/acs.chemrev.8b00460>



- Muller, M. P., Jiang, T., Sun, C., Lihan, M., Pant, S., Mahinthichaichan, P., Trifan, A., & Tajkhorshid, E. (2019). Characterization of Lipid-Protein Interactions and Lipid-Mediated Modulation of Membrane Protein Function through Molecular Simulation. *Chemical Reviews*, *119*(9), 6086–6161. <https://doi.org/10.1021/acs.chemrev.8b00608>
- Nicolas, W. J., Grison, M. S., Trépout, S., Gaston, A., Fouché, M., Cordelières, F. P., Oparka, K., Tilsner, J., Brocard, L., & Bayer, E. M. (2017). Architecture and permeability of post-cytokinesis plasmodesmata lacking cytoplasmic sleeves. *Nature Plants*, *3*(17082), 1–11. <https://doi.org/10.1038/nplants.2017.82>
- Overduin, M., & Esmaili, M. (2019). Structures and Interactions of Transmembrane Targets in Native Nanodiscs. *SLAS Discovery*, *24*(10), 943–952. <https://doi.org/10.1177/2472555219857691>
- Pain, C., Kriechbaumer, V., Kittelmann, M., Hawes, C., & Fricker, M. (2019). Quantitative analysis of plant ER architecture and dynamics. *Nature Communications*, *10*(1), 1–15. <https://doi.org/10.1038/s41467-019-08893-9>
- Park, K., Knoblauch, J., Oparka, K., & Jensen, K. H. (2019). Controlling intercellular flow through mechanosensitive plasmodesmata nanopores. *Nature Communications*, *10*(1). <https://doi.org/10.1038/s41467-019-11201-0>
- Periole, X., Cavalli, M., Marrink, S., & Ceruso, M. A. (2009). Combining an Elastic Network With a Coarse-Grained Molecular Force Field : Structure , Dynamics , and Intermolecular Recognition. *Journal of Chemical Theory and Computation*, *5*, 2531–2543.
- Petit, J. D., Immel, F., Lins, L., & Bayer, E. M. (2019). Lipids or Proteins : Who Is Leading the Dance at Membrane Contact Sites ? *Frontiers in Plant Science*, *10*(February), 1–10. <https://doi.org/10.3389/fpls.2019.00198>
- Petit, J. D., Li, Z. P., Nicolas, W. J., Grison, M. S., & Bayer, E. M. (2020). Dare to change, the dynamics behind plasmodesmata-mediated cell-to-cell communication. *Current Opinion in Plant Biology*, *53*, 80–89. <https://doi.org/10.1016/j.pbi.2019.10.009>
- Pezeshkian, W., & Marrink, S. J. (2021). Simulating realistic membrane shapes. *Current Opinion in Cell Biology*, *71*, 103–111. <https://doi.org/10.1016/j.ceb.2021.02.009>
- Qiu, L., Yu, H., & Liang, F. (2015). Multiple C2 domains transmembrane protein 1 is expressed in CNS neurons and possibly regulates cellular vesicle retrieval and oxidative stress. *Journal of Neurochemistry*, *135*(3), 492–507. <https://doi.org/10.1111/jnc.13251>
- Raman, S., Vernon, R., Thompson, J., Tyka, M., Sadreyev, R., Pei, J., Kim, D., Kellogg, E., Dimairo, F., Lange, O., Kinch, L., Sheffler, W., Kim, B. H., Das, R., Grishin, N. V., & Baker, D. (2009). Structure prediction for CASP8 with all-atom refinement using Rosetta. *Proteins: Structure, Function and Bioinformatics*, *77*(SUPPL. 9), 89–99. <https://doi.org/10.1002/prot.22540>
- Rosado, A., & Bayer, E. M. (2020). *Short title : Shaping and function of membrane contact sites.*
- Sager, R. E., & Lee, J.-Y. (2018). Plasmodesmata at a glance. *Journal of Cell Science*, *131*(11), jcs209346. <https://doi.org/10.1242/jcs.209346>
- Sager, R., & Lee, J. (2014). Plasmodesmata in integrated cell signalling : insights from development and environmental signals and stresses. *Journal of Experimental Botany*, *65*(22), 6337–6358. <https://doi.org/10.1093/jxb/eru365>

- Saheki, Y., & De Camilli, P. (2017). The Extended-Synaptotagmins. *BBA - Molecular Cell Research*, 1864(9), 1490–1493. <https://doi.org/10.1016/j.bbamcr.2017.03.013>
- Scott, L. J., Muglia, P., Kong, X. Q., Guan, W., Flickinger, M., Upmanyu, R., Tozzi, F., Li, J. Z., Burmeister, M., Absher, D., Thompson, R. C., Francks, C., Meng, F., Antoniadis, A., Southwick, A. M., Schatzberg, A. F., Bunney, W. E., Barchas, J. D., Jones, E. G., ... Boehnke, M. (2009). Genome-wide association and meta-analysis of bipolar disorder in individuals of European ancestry. *Proceedings of the National Academy of Sciences of the United States of America*, 106(18), 7501–7506. <https://doi.org/10.1073/pnas.0813386106>
- Seguí-Simarro, J. M., Austin, J. R., White, E. A., & Staehelin, L. A. (2004). Electron tomographic analysis of somatic cell plate formation in meristematic cells of arabidopsis preserved by high-pressure freezing. *Plant Cell*, 16(4), 836–856. <https://doi.org/10.1105/tpc.017749>
- Sejdiu, B. I., & Tieleman, D. P. (2021). ProLint: A web-based framework for the automated data analysis and visualization of lipid-protein interactions. *Nucleic Acids Research*, 49(W1), W544–W550. <https://doi.org/10.1093/nar/gkab409>
- Shastri, K. A., & Sanjay, H. A. (2020). *Machine Learning for Bioinformatics BT - Statistical Modelling and Machine Learning Principles for Bioinformatics Techniques, Tools, and Applications* (K. G. Srinivasa, G. M. Siddesh, & S. R. Manisekhar (Eds.); pp. 25–39). Springer Singapore. [https://doi.org/10.1007/978-981-15-2445-5\\_3](https://doi.org/10.1007/978-981-15-2445-5_3)
- Shibata, Y., Voss, C., Rist, J. M., Hu, J., Rapoport, T. A., Prinz, W. A., & Voeltz, G. K. (2008). The reticulon and Dp1/Yop1p proteins form immobile oligomers in the tubular endoplasmic reticulum. *Journal of Biological Chemistry*, 283(27), 18892–18904. <https://doi.org/10.1074/jbc.M800986200>
- Shin, O. H., Hau, W., Wang, Y., & Südhof, T. C. (2005). Evolutionarily conserved multiple C2 domain proteins with two transmembrane regions (MCTPs) and unusual Ca<sup>2+</sup> binding properties. *Journal of Biological Chemistry*, 280(2), 1641–1651. <https://doi.org/10.1074/jbc.M407305200>
- Siggel, M., Bhaskara, R. M., Moesser, M. K., Dikić, I., & Hummer, G. (2021). FAM134B-RHD Protein Clustering Drives Spontaneous Budding of Asymmetric Membranes. *Journal of Physical Chemistry Letters*, 12(7), 1926–1931. <https://doi.org/10.1021/acs.jpcclett.1c00031>
- Simon, M. L. A., Platre, M. P., Marquès-bueno, M. M., Armengot, L., Stanislas, T., Bayle, V., Caillaud, M., & Jaillais, Y. (2016). A PtdIns(4)P-driven electrostatic field controls cell membrane identity and signalling in plants. *Nature Plants*, 1–10. <https://doi.org/10.1038/nplants.2016.89>
- Singer, S. J., & Nicolson, G. L. (1972). The fluid mosaic model of the structure of cell membranes. *Science (New York, N.Y.)*, 175(4023), 720–731. <https://doi.org/10.1126/science.175.4023.720>
- Siuda, I., & Thøgersen, L. (2013). Conformational flexibility of the leucine binding protein examined by protein domain coarse-grained molecular dynamics. *Journal of Molecular Modeling*, 19(11), 4931–4945. <https://doi.org/10.1007/s00894-013-1991-9>
- Smertenko, A., Assaad, F., Baluška, F., Bezanilla, M., Buschmann, H., Drakakaki, G., Hauser, M. T., Janson, M., Mineyuki, Y., Moore, I., Müller, S., Murata, T., Otegui, M. S., Panteris, E., Rasmussen, C., Schmit, A. C., Šamaj, J., Samuels, L., Staehelin, L. A., ... Žárský, V. (2017). Plant Cytokinesis: Terminology for Structures and Processes. *Trends in Cell Biology*, 27(12), 885–894. <https://doi.org/10.1016/j.tcb.2017.08.008>

- Soares, T. A., Vanni, S., Milano, G., & Cascella, M. (2017). Toward Chemically Resolved Computer Simulations of Dynamics and Remodeling of Biological Membranes. *Journal of Physical Chemistry Letters*, 8(15), 3586–3594. <https://doi.org/10.1021/acs.jpcllett.7b00493>
- Song, J. H., Kwak, S. H., Nam, K. H., Schiefelbein, J., & Lee, M. M. (2019). QUIRKY regulates root epidermal cell patterning through stabilizing SCRAMBLED to control CAPRICE movement in Arabidopsis. *Nature Communications*, 10(1). <https://doi.org/10.1038/s41467-019-09715-8>
- Song, S., Chen, Y., Liu, L., Wang, Y., Bao, S., Zhou, X., Teo, Z. W. N., Mao, C., Gan, Y., & Yu, H. (2017). OsFTIP1-mediated regulation of florigen transport in rice is negatively regulated by the ubiquitin-like domain kinase OsUbDKy4. *Plant Cell*, 29(3), 491–507. <https://doi.org/10.1105/tpc.16.00728>
- Souza, P. C. T., Alessandri, R., Barnoud, J., Thallmair, S., Faustino, I., Grünwald, F., Patmanidis, I., Abdizadeh, H., Bruininks, B. M. H., Wassenaar, T. A., Kroon, P. C., Melcr, J., Nieto, V., Corradi, V., Khan, H. M., Domański, J., Javanainen, M., Martinez-Seara, H., Reuter, N., ... Marrink, S. J. (2021). Martini 3: a general purpose force field for coarse-grained molecular dynamics. *Nature Methods*, 18(4), 382–388. <https://doi.org/10.1038/s41592-021-01098-3>
- Sparkes, I., Tolley, N., Aller, I., Svozil, J., Osterrieder, A., Botchway, S., Mueller, C., Frigerio, L., & Hawes, C. (2010). Five Arabidopsis Reticulon Isoforms Share Endoplasmic Reticulum Location , Topology , and Membrane-Shaping Properties. *The Plant Cell*, 22, 1333–1343. <https://doi.org/10.1105/tpc.110.074385>
- Sych, T., Levental, K. R., & Sezgin, E. (2022). Lipid–Protein Interactions in Plasma Membrane Organization and Function. *Annual Review of Biophysics*, 51(1), 135–156. <https://doi.org/10.1146/annurev-biophys-090721-072718>
- Télliez-Arreola, J. L., Silva, M., & Martínez-Torres, A. (2020). MCTP-1 modulates neurotransmitter release in *C. elegans*. *Molecular and Cellular Neuroscience*, 107(July), 103528. <https://doi.org/10.1016/j.mcn.2020.103528>
- Tilsner, J., Nicolas, W., Rosado, A., & Bayer, E. M. (2016). Staying Tight : Plasmodesmal Membrane Contact Sites and the Control of Cell-to-Cell Connectivity in Plants. *Annual Review Plant Biology*, 67, 337–364. <https://doi.org/10.1146/annurev-arplant-043015-111840>
- Tran, T. M., Mccubbin, T. J., Bihmidine, S., Julius, B. T., Baker, R. F., Schauflinger, M., Weil, C., Springer, N., Chomet, P., Wagner, R., Woessner, J., Grote, K., Peevers, J., Slewinski, T. L., & Braun, D. M. (2019). Maize Carbohydrate Partitioning Defective33 Encodes an MCTP Protein and Functions in Sucrose Export from Leaves. *Molecular Plant*, 12(9), 1278–1293. <https://doi.org/10.1016/j.molp.2019.05.001>
- Trehin, C., Schrempp, S., Chauvet, A., Berne-dedieu, A., Thierry, A., Faure, J., Negrutiu, I., & Morel, P. (2013). QUIRKY interacts with STRUBBELIG and PAL OF QUIRKY to regulate cell growth anisotropy during Arabidopsis gynoecium development. *The Company of Biologists Ltd - Development*, 140, 4807–4817. <https://doi.org/10.1242/dev.091868>
- Tsirigos, K. D., Govindarajan, S., Bassot, C., Västermark, Å., Lamb, J., Shu, N., & Elofsson, A. (2018). Topology of membrane proteins — predictions, limitations and variations. *Current Opinion in Structural Biology*, 50(November 2017), 9–17. <https://doi.org/10.1016/j.sbi.2017.10.003>
- Vaddepalli, P., Herrmann, A., Fulton, L., Oelschner, M., Hillmer, S., Stratil, T. F., Fastner, A., Hammes, U. Z., Ott, T., Robinson, D. G., & Schneitz, K. (2014). The C2-domain protein QUIRKY and the receptor-

like kinase STRUBBELIG localize to plasmodesmata and mediate tissue morphogenesis in *Arabidopsis thaliana*. *The Company of Biologists Ltd - Development*, 141, 4139–4148.  
<https://doi.org/10.1242/dev.113878>

- Vilsker, M., Moosa, Y., Nooij, S., Fonseca, V., Ghysens, Y., Dumon, K., Pauwels, R., Alcantara, L. C., Vanden Eynden, E., Vandamme, A. M., Deforche, K., & De Oliveira, T. (2019). Genome Detective: An automated system for virus identification from high-throughput sequencing data. *Bioinformatics*, 35(5), 871–873. <https://doi.org/10.1093/bioinformatics/bty695>
- von Wangenheim, D., Hauschild, R., Fendrych, M., Barone, V., Benková, E., & Friml, J. (2017). Live tracking of moving samples in confocal microscopy for vertically grown roots. *ELife*, 6.  
<https://doi.org/10.7554/eLife.26792>
- Wang, J., Olsson, S., Wehmeyer, C., Pérez, A., Charron, N. E., De Fabritiis, G., Noé, F., & Clementi, C. (2019). Machine Learning of Coarse-Grained Molecular Dynamics Force Fields. *ACS Central Science*, 5(5), 755–767. <https://doi.org/10.1021/acscentsci.8b00913>
- Wang, S., Idrissi, F. Z., Hermansson, M., Grippa, A., Ejsing, C. S., & Carvalho, P. (2018). Seipin and the membrane-shaping protein Pex30 cooperate in organelle budding from the endoplasmic reticulum. *Nature Communications*, 9(1), 1–12. <https://doi.org/10.1038/s41467-018-05278-2>
- Wendrich, J. R., Yang, B. J., Vandamme, N., Verstaen, K., Smet, W., Velde, C. Van de, Minne, M., Wybouw, B., Mor, E., Arents, H. E., Nolf, J., van Duyse, J., van Isterdael, G., Maere, S., Saeys, Y., & Rybel, B. De. (2020). Vascular transcription factors guide plant epidermal responses to limiting phosphate conditions. *Science*, 370(6518). <https://doi.org/10.1126/science.aay4970>
- West, M., Zurek, N., Hoenger, A., & Voeltz, G. K. (2011). A 3D analysis of yeast ER structure reveals how ER domains are organized by membrane curvature. *Journal of Cell Biology*, 193(2), 333–346.  
<https://doi.org/10.1083/jcb.201011039>
- Whited, A. M., & Johs, A. (2015). The interactions of peripheral membrane proteins with biological membranes. *Chemistry and Physics of Lipids*, 192, 51–59.  
<https://doi.org/10.1016/j.chemphyslip.2015.07.015>
- Wolfes, A. C., & Dean, C. (2020). The diversity of synaptotagmin isoforms. *Current Opinion in Neurobiology*, 63, 198–209. <https://doi.org/10.1016/j.conb.2020.04.006>
- Wu, E. L., Cheng, X., Jo, S., Rui, H., Song, K. C., Dávila-Contreras, E. M., Qi, Y., Lee, J., Monje-Galvan, V., Venable, R. M., Klauda, J. B., & Im, W. (2014). CHARMM-GUI membrane builder toward realistic biological membrane simulations. *Journal of Computational Chemistry*, 35(27), 1997–2004.  
<https://doi.org/10.1002/jcc.23702>
- Yadav, S. R., Yan, D., Sevilem, I., & Helariutta, Y. (2014). Plasmodesmata-mediated intercellular signaling during plant growth and development. *Frontiers in Plant Science*, 5(February), 1–7.  
<https://doi.org/10.3389/fpls.2014.00044>
- Yamamoto, E., Domański, J., Naughton, F. B., Best, R. B., Kalli, A. C., Stansfeld, P. J., & Sansom, M. S. P. (2020). Multiple lipid binding sites determine the affinity of PH domains for phosphoinositide-containing membranes. *Science Advances*, 6(8). <https://doi.org/10.1126/sciadv.aay5736>
- Yang, Y., Yu, J., Liu, Z., Wang, X., Wang, H., Ma, Z., & Xu, D. (2022). An Improved Topology Prediction of Alpha-Helical Transmembrane Protein Based on Deep Multi-Scale Convolutional Neural Network.

*IEEE/ACM Transactions on Computational Biology and Bioinformatics*, 19(1), 295–304.  
<https://doi.org/10.1109/TCBB.2020.3005813>

Zhang, L., Zhang, F., Liu, F., Shen, J., Wang, J., Jiang, M., Zhang, D., Yang, P., Chen, Y., & Song, S. (2021). The lotus NnFTIP1 and NnFT1 regulate flowering time in Arabidopsis. *Plant Science*, 302(October 2020), 110677. <https://doi.org/10.1016/j.plantsci.2020.110677>

Zhu, M., Yan, B., Hu, Y., Cui, Z., & Wang, X. (2020). Genome-wide identification and phylogenetic analysis of rice FTIP gene family. *Genomics*, 112(5), 3803–3814. <https://doi.org/10.1016/j.ygeno.2020.03.003>



# Dare to change, the dynamics behind plasmodesmata-mediated cell-to-cell communication

Jules D Petit<sup>1,2</sup>, Ziqiang Patrick Li<sup>1</sup>, William J Nicolas<sup>1,3</sup>,  
Magali S Grison<sup>1</sup> and Emmanuelle M Bayer<sup>1</sup>

Plasmodesmata pores control the entry and exit of molecules at cell-to-cell boundaries. Hundreds of pores perforate the plant cell wall, connecting cells together and establishing direct cytosolic and membrane continuity. This ability to connect cells in such a way is a hallmark of plant physiology and is thought to have allowed sessile multicellularity in *Plantae* kingdom. Indeed, plasmodesmata-mediated cell-to-cell signalling is fundamental to many plant-related processes. In fact, there are so many facets of plant biology under the control of plasmodesmata that it is hard to conceive how such tiny structures can do so much. While they provide ‘open doors’ between cells, they also need to guarantee cellular identities and territories by selectively transporting molecules. Although plasmodesmata operating mode remains difficult to grasp, little by little plant scientists are divulging their secrets. In this review, we highlight novel functions of cell-to-cell signalling and share recent insights into how plasmodesmata structural and molecular signatures confer functional specificity and plasticity to these unique cellular machines.

## Addresses

<sup>1</sup>Laboratoire de Biogenèse Membranaire, UMR5200 CNRS, Université de Bordeaux, Villenave d’Ornon, France

<sup>2</sup>Laboratoire de Biophysique Moléculaire aux Interfaces, TERRA Research Centre, GX ABT, Université de Liège, Gembloux, Belgium

Corresponding author:

Bayer, Emmanuelle M ([emmanuelle.bayer@u-bordeaux.fr](mailto:emmanuelle.bayer@u-bordeaux.fr))

<sup>3</sup> Present address: Division of Biology and Biological Engineering, California Institute of Technology, Pasadena, USA.

**Current Opinion in Plant Biology** 2020, **53**:80–89

This review comes from a themed issue on **Growth and development**

Edited by **Marcus Heisler** and **Alexis Maizel**

For a complete overview see the [Issue](#) and the [Editorial](#)

Available online 2nd December 2019

<https://doi.org/10.1016/j.pbi.2019.10.009>

1369-5266/© 2019 Published by Elsevier Ltd.

## Introduction

All forms of multicellularity depend on two fundamental pillars: cell-to-cell contact and cell-to-cell communication. Both functions have emerged independently and multiple times throughout evolution, resulting in the development of different forms of connections with diversified molecular

strategies [1]. In plants, cell-to-cell communication is largely assisted by plasmodesmata intercellular pores, which ensure concerted cellular actions during tissue growth, development and response to environmental cues [2]. In concert with the vascular system, plasmodesmata support long-range signalling to integrate local responses at the organism level [3,4–6]. These unique cellular machines can be viewed as gates through the plant cell wall, providing cytosolic and membrane continuity from cell-to-cell and eventually throughout the whole plant body. They are involved in multiple tasks like conveying organic nutrients [7,8], regulating crucial steps during organ initiation and growth [9,10], assisting tissue patterning by conveying positional information [11], acting as signalling hubs and contributing to defence response [12,13,14–17]. Despite their central role in plant physiology, their operating mode remains elusive. Yet, they keep on fascinating and intriguing scientists. In this review, we recapitulate recent and significant advances in our understanding of plasmodesmata-mediated cell-to-cell communication and their central function for plant biology.

## Reaching out further: new insights into plasmodesmata-mediated short-distance and long-distance signalling

A wide range of developmental and physiological processes depends on symplastic communication. Examples include shoot meristem maintenance [18–21], tissue patterning and organ growth [9,10], bud dormancy [22], defence signalling [5,6,16], adaptation to environmental stresses [12,13,14,15] and exchange of nutrients between cells and organs [7,8,23]. In the last two years, the realm of symplastic communication has grown even bigger and it now embraces symbiotic interaction [24], calcium-based long-distance signalling [6] and unfolded protein response (UPR) [3].

Transcription factors (TFs) were amongst the first endogenous factors to be shown to act non-cell autonomously through plasmodesmata, a decisive condition for both tissue patterning and meristem maintenance [10,11,18,21]. Since then, a growing number of signalling molecules, from RNAs [4,25,26] to hormones [27] and even lipids [5,16], were reported to move through plasmodesmata. In all cases, and regardless of the trafficking mechanisms (selective or passive), these signalling gradients are tightly controlled both spatially and temporally. A recent study, by Helariutta and De Rybel’s teams [11], illustrates how, through a complex feed-back loop between TFs, miRNAs and

hormones, spatial information can be generated to create sharp boundaries. During radial growth initiation in root procambial tissues, cytokinin promotes the expression of the mobile PHLOEM EARLY DOF (PEAR) TFs, which then form a short-range gradient and activate genes promoting radial growth at protophloem sieve elements. PEAR action is in turn antagonised by class III HOMEODOMAIN LEUCINE ZIPPER (HD-ZIP III) transcription factors, their expression being controlled by auxin, miRNA165/166 and PEAR TFs [11<sup>\*\*</sup>]. Not only movement but also the transcription of PEARs must be regulated to achieve proper growth pattern. This work perfectly illustrates the complexity of intercellular communication networks where both intra-cellular and inter-cellular processes are integrated at a multiscale level, and where symplastic trafficking is only one of the many key components.

Information exchange between distant organs is crucial to prime integrated responses at the body level. This is often achieved by combining cell-to-cell transport through plasmodesmata and long-distance trafficking via the phloem [4–6,16,26,28,29]. A well-established example is the florigen, Flowering Locus T, which moves from the leaves into the phloem to reach out the shoot apex and reprogram leaf production into flowers [28–32]. Failure in moving through plasmodesmata results in late flowering [29–32]. Plant stress responses also rely on long-distance communication. Herbivore feeding triggers glutamate-dependent calcium signalling at the wounded site, which rapidly propagates to distant leaves to presumably activate defence responses in non-damaged regions [6]. Calcium itself is unlikely to move long distances. Instead, calcium waves may require a relay-based system, potentially coupled with reactive oxygen species (ROS) [33]. Likewise, the ER-embedded UPR response, which until recently has been regarded as a cell-autonomous process, acts systemically through non-cell autonomous signalling and long-range movement of bZIP60 TF [3<sup>\*</sup>]. By combining short-range and long-distance movement, plants can perceive and prime stress responses in regions far away from initiation sites. Plasmodesmata crucial functions also rely on their capacity to integrate a wide range of environmental and developmental signals and accordingly regulate the movement of many different classes of molecules at specific interfaces. The molecular mechanisms regulating transport across plasmodesmata rely, for a large part, on their structural and functional plasticity.

### Plasmodesmal structure defines plasmodesmal function

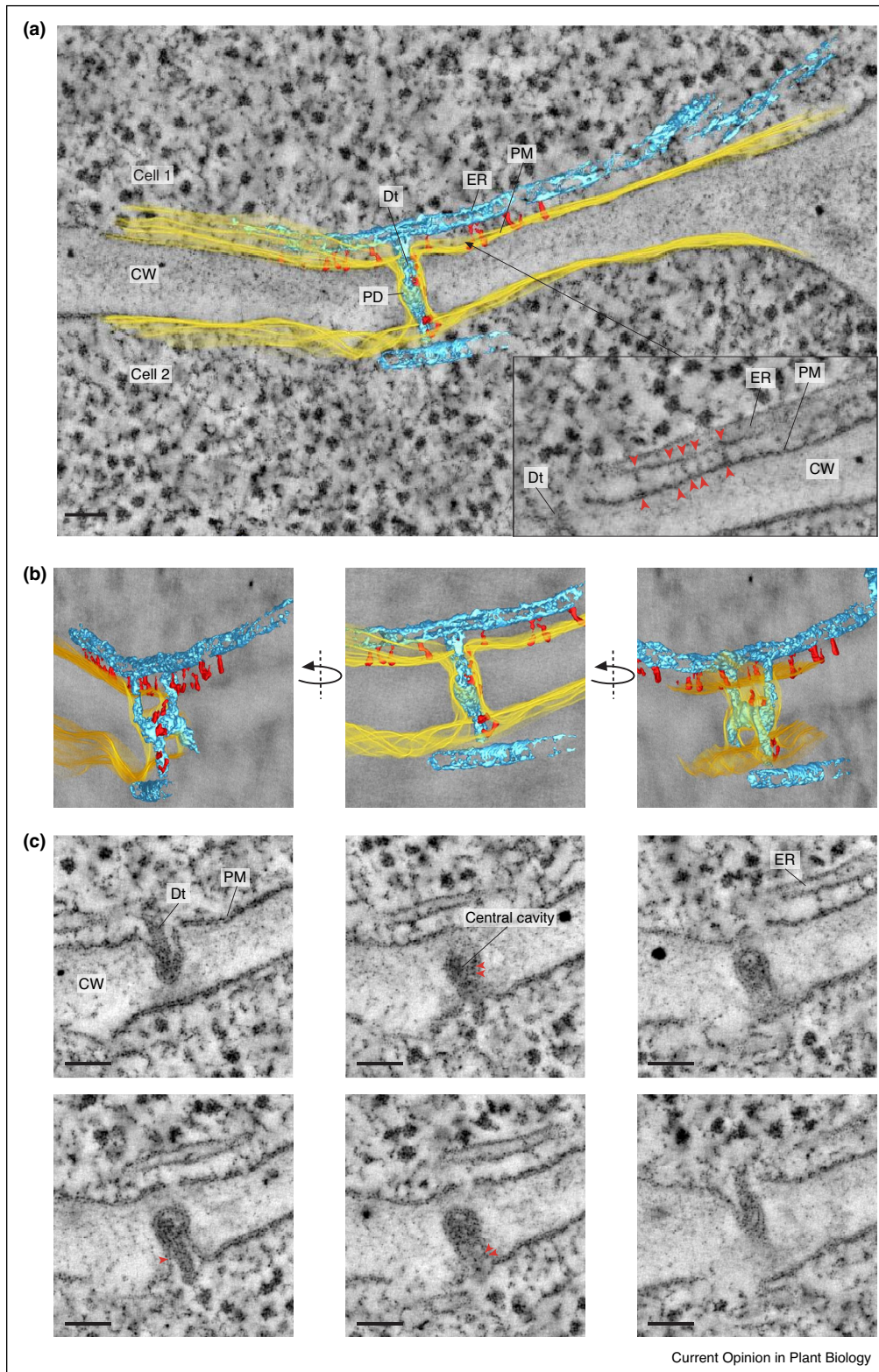
Plasmodesmata bridge cells across the wall creating physical continuity between three compartments: the plasma membrane (PM), the cytoplasm and the endoplasmic reticulum (ER) (Figure 1) [2,34]. Distinguished by its lipid profile, membrane curvature, and protein composition, the PM lining plasmodesmata is considered as a specialized microdomain, which dictates plasmodesmata-specific function. For example, enrichment of distinctive sterol and

sphingolipid species participate in the recruitment of cell-wall remodelling enzymes which create a unique cell wall environment and impacts on plasmodesmata permeability [35]. In apposition to the PM, and as it enters the pores, the ER becomes tightly constricted into a highly differentiated ER subdomain called the desmotubule. Constriction of the ER inside plasmodesmata presumably restricts cell-to-cell diffusion of ER-associated molecules. Inside and at the entry of the pores, the desmotubule/ER establishes contacts with the PM through tethering elements, which function and molecular identity have remained unknown until recently (see next section) [35,37]. Altogether, membranes and the immediate wall environment present a unique molecular signature, supporting plasmodesmata function [12<sup>\*</sup>,13<sup>\*</sup>,14,16,31,35,36<sup>\*\*</sup>,37–39].

So far, no consensus plasmodesmata targeting motif has been identified and the emerging picture is that plants rely on a diversity of strategies to regulate symplastic trafficking. Both passive and selective transports occur, with the latter implying direct interaction between mobile factors and plasmodesmata ‘receptors’ to facilitate movement [16,30,31,39–41]. Dynamic cell-to-cell communication is also achieved through the controlled opening or closure of plasmodesmata. In canonical models, molecules traffic through the cytoplasmic sleeve and the size exclusion limit (SEL) of the pores is defined by the ER-PM gap [42]. In other words, the wider is the gap, the more transport there is. This model has however been recently challenged by two independent studies [7<sup>\*</sup>,34]. Using electron tomography Nicolas *et al.* showed that post-cytokinesis plasmodesmata (called Type I), previously shown to offer high transport capacity, present a very narrow cytoplasmic sleeve not exceeding 2–3 nm. Later during cell growth/differentiation, the ER-PM gap extends to 8–10 nm leading to open-sleeved Type II plasmodesmata. *Arabidopsis* plants missing the *Phloem Unloading Modulator (PLM)* gene, present a defect in Type I to Type II transition at the phloem-pole-pericycle/endodermis interface, which results in higher symplastic unloading capacity. These data indicate that very narrow-sleeved plasmodesmata are actually more conductive than wide-sleeved ones, questioning the current trafficking model.

Over the years, callose has emerged as a chief regulator of plasmodesmata SEL and dynamically modulates the pore conductivity in response to environmental and developmental cues [13<sup>\*</sup>,14,15,22,24<sup>\*</sup>,37,42]. Although its mode of action remains poorly understood, the current model proposes that local callose synthesis at the plasmodesmata neck region forms an extracellular ring, which squeezes the PM against the ER, contracting the cytoplasmic sleeve [37]. This model, however, implies that the PM can accommodate rapid local deformation through stretching, an unlikely event for lipid bilayers, which present limited elastic properties [43]. Such local deformation would imply membrane remodelling

Figure 1



Current Opinion in Plant Biology

Plasmodesmata viewed by electron tomography. 3D segmentation (a, b) and reconstructed sections (c) of a branched plasmodesma at the phloem pole pericycle-endodermis interface in *Arabidopsis* root. (a) Plasmodesmata are embedded within the cell wall (CW) and create PM (yellow) and ER (blue) continuity from cell-to-cell. Tethering elements (red) are visible between the ER and the PM within and outside the pores. Inset represents a reconstructed micrograph section showing tether elements (red arrowheads) at the entrance of the pore. (b) Different views of



through lipid redistribution and possibly the action of membrane-shaping proteins. Callose accumulation could also lead to the re-organisation of PM-located callose-binding proteins and their interacting partners, thus changing not only immediate PM environment but also the ER-PM interface.

Using callose-cellulose biopolymer mixture, Abou-Saleh *et al.* recently suggested that, at certain concentrations, callose could in fact increase the elasticity rather than rigidify the wall matrix, leaving open the question of how this polymer could influence the properties of the cell wall at plasmodesmata and the conductive properties of the pores [44]. Aside from callose, the 'I' shape ER that passes through the pore has recently been proposed to control rapid plasmodesmata closure upon osmotic pressure through mechanosensing [45]. According to this model, the tether elements bridging the ER to the PM offer physical elasticity which in turn determines the sensibility to the pressure-induced movement of the desmotubule. This interesting piece of work revealed an alternative option for plasmodesmata regulation that directly take into account the mechanics associated with the desmotubule positioning in the context of cell–cell junction.

Besides plasmodesmata SEL, many additional elements influence symplastic trafficking. These include, plasmodesmata density at cellular interface [8,46], wall thickness [47], expression level of mobile factors [11], ability for a given molecule to 'enter' the symplastic pathway, which can be influenced by complex formation [19,20,48] or binding to a membrane-compartment [49,50]. Ultimately, these diversified strategies, which rely on both the structural and functional properties of plasmodesmata, need to operate synergistically to precisely regulate symplastic trafficking and integrate a complex network of signalling pathways.

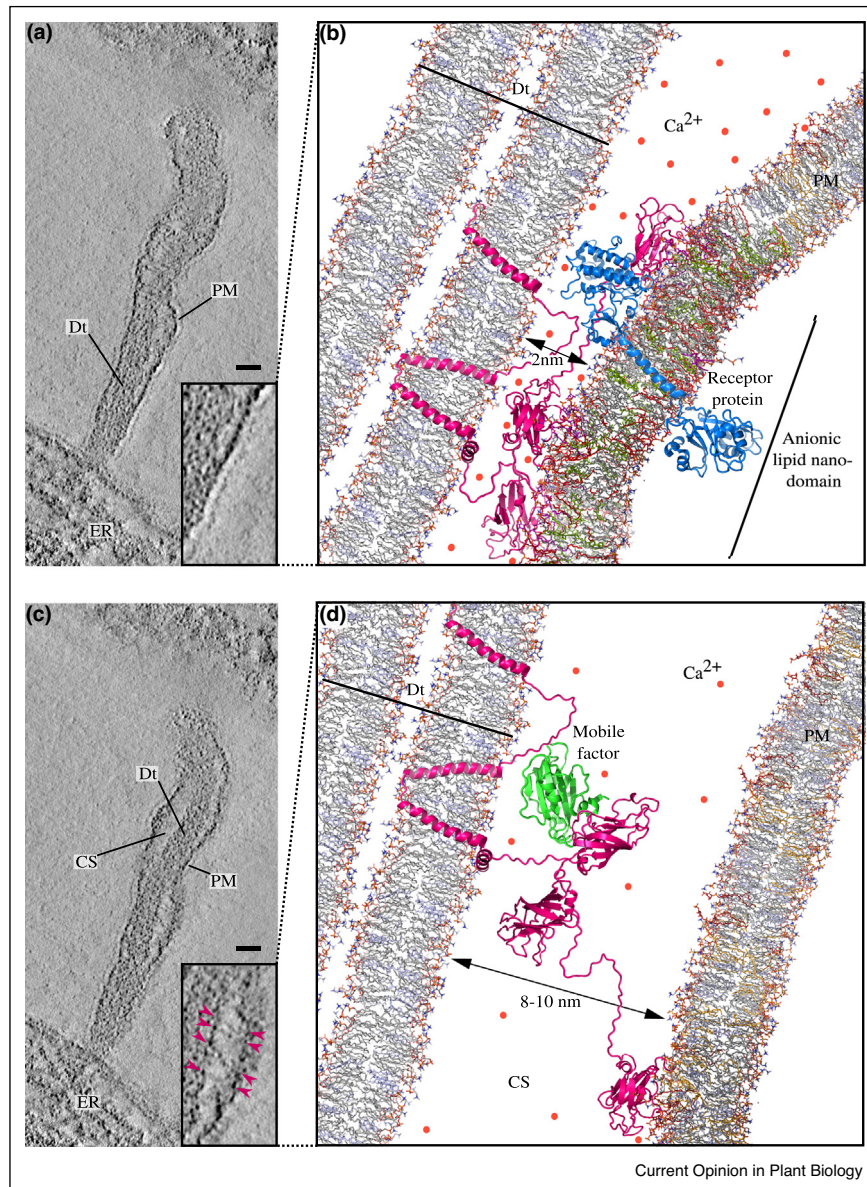
### Acting at the ER-PM interface: the multiple C2 domains transmembrane region protein family

An additional way of considering plasmodesmata is to view them as specialised ER-PM membrane contact sites [2,51]. The gap between the two membranes inside the pore is remarkably flexible and presumably impacts intercellular trafficking (Figure 2) [7,34]. Now, to the questions as to what elements regulate this structural plasticity, we still have no answer. Historically the molecular identity of the elements bridging the ER to the PM was in favour of cytoskeletal proteins such as actin or myosin, but their function in membrane tethering still remains hypothetical [34,51]. Recently, the Multiple C2 domains and Transmembrane region Proteins (MCTPs)

have emerged as plasmodesmata-specific ER-PM tethers [36]. MCTPs are a conserved family in higher eukaryotes, yet, while *Homo sapiens* and *Drosophila* spp. only have two members, the *Arabidopsis* genome contains 16 members, suggesting a larger functional diversity. At least six members of the *Arabidopsis* family cluster at plasmodesmata, where they seem to serve different functions detailed below [8,31,36,38,39,52]. MCTPs present the structural organisation of a typical tether, with a C-terminal transmembrane region, which inserts into the ER and three to four C2 domains, which act as PM docking sites through anionic lipid-binding [36] (Figure 2). Unlike other tethers, MCTPs are not only involved in bridging membranes, they also regulate intercellular trafficking of non-cell autonomous signals. AtMCTP1/FT-interacting protein 1 (FTIP1) interacts with Flowering locus T to promote its transfer at the companion cell-sieve element interface [31]. AtMCTP3 and AtMCTP4 antagonise the movement of the TF SHOOT MERISTEM LESS, although here it is not clear whether they act from endosomes or directly at plasmodesmata [36,50]. Nevertheless, loss-of-function *mctp3/4 Arabidopsis* mutants display pleiotropic developmental defects [36,50], reduced SEL and altered plasmodesmata protein composition [36]. In *Arabidopsis*, MCTP15/QUIRKY regulates CAPRICE movement and root epidermis patterning by directly modulating the activity and stability of the receptor-like kinase STRUBBELIG/ SCRAMBLED and downstream cell-to-cell signalling [39]. In maize, the AtMCTP15 homologue, Carbohydrate Partitioning Defective 33, promotes symplastic transport of carbohydrates into sieve elements, possibly by regulating plasmodesmata formation at the companion cell–sieve element interface [8]. From their optimal position at the ER-PM interface, MCTPs appear to control multiple aspects of plasmodesmata-mediated cell-to-cell communication, including 1) selective transport of mobile factors, 2) activation of receptor-mediated cell-to-cell signalling, 3) plasmodesmata SEL, hence passive transport and 4) formation/stabilisation of the pores. This multifaceted function of MCTPs may partially be attributable to the diversity of actions of their multiple C2 domains. Similar to other ER-PM tethers [53,54], the C2 domains of AtMCTP4 and 15/QUIRKY most likely interact with anionic lipids, potentially in a calcium-dependant manner. This implies that the surface charges of the plasmodesmal PM and/or calcium could influence membrane docking inside the pores in a conditional and reversible manner, which in turn could change the cytoplasmic sleeve conducting properties (Figure 2). Furthermore, the same C2 cytosolic regions of AtMCTP15/QUIRKY, AtMCTP3/4

(Figure 1 Legend Continued) the 3D segmentation depicted in (a) showing the branched-structure with a central cavity where the two desmotubules are connected. (c) Reconstructed sections through the volume of the tomogram shown in panels (a, b). Tether elements are visible along the pore and in the central cavity (red arrowheads). PD: plasmodesmata, CW: cell wall, Dt: desmotubule. Scale bar is 50 nm.

Figure 2



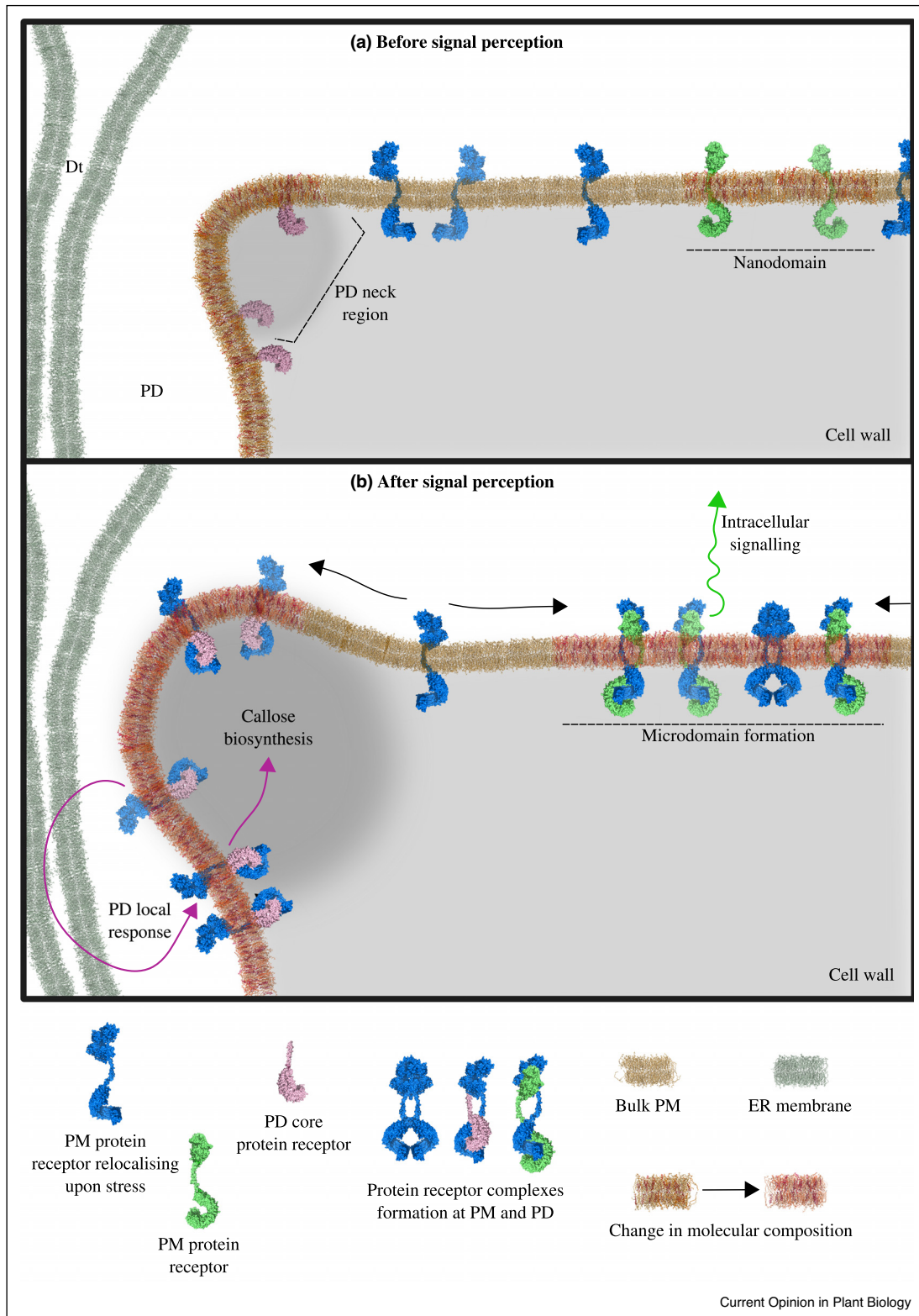
Hypothetical model of MCTP operating mode at the plasmodesmal ER-PM interface. **(a, c)** Two reconstructed sections at a  $\sim 2.5$  nm interval of an electron tomogram of a plasmodesma in *Arabidopsis* root tip. The spacing between the desmotubule (Dt) and the PM varies from very close contacts with no observable electron-lucent cytoplasmic sleeve (CS) (inset in panel (a)), to larger gap with electron-lucent readily identifiable CS and spoke-like tethering elements connecting the two membranes (inset in panel (c), pink arrowheads indicate tethers). Scale bar is 20 nm.

**(b, d)** Molecular representation of MCTP with three C2 domains (pink) connecting the Dt to the PM inside the pores in tight  $\sim 2$  nm (b) and 'open'  $\sim 8$ – $10$  nm (d) CS configurations. MCTPs insert into the ER/Dt membrane through their transmembrane region and interact with the PM in the presence of anionic lipids. The molecular re-arrangement of MCTP cytoplasmic tail in response to calcium (orange beads) and/or changes in membrane lipid composition influences the ER-PM gap inside the pore and the conductive properties of the CS. (b) Upon elevated local calcium concentration and the presence of anionic lipids, all C2 domains dock to the PM, restricting the ER-PM gap. C2 domains interaction with the PM could then stabilise/re-enforce anionic lipid nanodomains, changing the PM surface charge inside plasmodesmata and recruiting/activating/stabilising receptor proteins (blue). Note that calcium could also compete with C2 domains by shielding the polar heads of anionic lipids (not represented). (d) Upon low calcium concentration, PM lipid modification or binding to mobile factors (green), some C2 domains dissociate from the PM leading to the opening of the ER-PM gap.

and AtMCTP1/FTIP are known to be involved in protein–protein interactions [30,31,38,39,50\*]. By analogy with Extended-Synaptotagmins [53\*], it is tempting to speculate that MCTPs protein-binding and lipid docking

functions work together to regulate transport (Figure 2). By uniting intercellular and inter-organellar functions, MCTPs are one-of-a-kind tethers, playing a master regulator function at plasmodesmata.

Figure 3



Putative model illustrating signal-triggered dynamic re-organisation of receptor-complexes induces local and distinct responses at plasmodesmata versus the PM. **(a)** The PM lining the plasmodesmata pores and the PM nanodomains provide a membrane environment distinct from the bulk PM, with a unique set of lipids and proteins, including protein receptors, and function as signalling platforms. **(b)** Biotic and abiotic-derived signals induce a re-organisation of PM protein receptors, which includes changes in localisation, protein-protein interactions, and clustering in

### Plasmodesmata define membrane nanoterritories, which serve as dynamic signalling platforms

Plasmodesmata act at the interface between intra-cellular and extra-cellular compartments. As such, they are ideally located to integrate apoplastic, symplastic and endomembrane signalling to coordinate cellular responses. The PM lining plasmodesmata hosts receptor-like activities, which sense developmental and environmental apoplastic signals and regulate symplastic exchanges [12\*,13\*,14,15,17,55]. Some receptors are shared components between the PM and plasmodesmata, but they orchestrate distinct signalling pathways by assembling into different complexes depending on their localisation. For example, the receptor-kinases CLAVATA1 (CLV1) and CRINKLY4 (ACR4), which function in stem cell maintenance, have variable complex composition depending on if they locate at the bulk PM or plasmodesmata [55]. Likewise, STRUBBELIG/SCRAMBLED associates with the PM but only forms heteromeric complex with AtMCTP15/QUIRKY at plasmodesmata, from where it initiates non-cell autonomous signalling [38].

Conventionally, plasmodesmata-signalling was believed to be exerted exclusively by plasmodesmata-located receptors. However, recent studies show that PM receptors can conditionally relocate to plasmodesmata to trigger local response (Figure 3). The Cysteine-Rich Receptor-like kinase 2 (CRK2), strictly located at the PM, associates to plasmodesmata within 30 min after salt treatment and promotes callose deposition [13\*]. CRK2 re-organisation depends on Phospholipase D  $\alpha$ 1, indicating that changes in membrane lipid composition is instrumental to recruit receptors to plasmodesmata [13\*]. Upon osmotic stress, the PM-associated Leucine-Rich repeat RLKs Qian Shou Kinase 1 (QSK1) and Inflorescence Meristem Kinase 2 (IMK2) rapidly relocate, within less than 2 min, to plasmodesmata and into PM-nanodomains [12\*]. Similar to CRK2, the recruitment of QSK1 to plasmodesmata is correlated with callose-accumulation and also partially depends on its phosphorylation [12\*]. Stimuli-dependant re-organisations of receptor-like activities at plasmodesmata are therefore frequent events and may in fact be a common strategy to modulate symplastic trafficking. In a similar fashion, the immune fungal elicitor chitin induces redistribution of the chitin-receptor complex at both PM and plasmodesmata [14]. Upon chitin sensing at the PM, the CHITIN ELICITOR RECEPTOR KINASE 1 (CERK1) interacts with LysM receptor-like kinase LYK5, which initiates intracellular defence responses [14,17]. Simultaneously, LYSIN MOTIF DOMAIN CONTAINING

GLYCOSYLPHOSPHATIDYLINOSITOL-ANCHORED PROTEIN (LYM2) accumulates to plasmodesmata, where it associates with LYK4 to promote localised callose synthesis [14]. Taken together, these data indicate that the molecular composition of plasmodesmata is rapidly modified through either biotic or abiotic stresses to induce cellular responses.

Inherent to its role as a barrier, the PM constitutes an optimal interface for signal perception and intracellular signal transduction. The nanoscale composition and segregation of the PM contribute to the emergence of distinct membrane territories, which not only directly impact on receptor activation/deactivation, but also differentiate signalling pathways sharing common components [56–58]. Likewise, plasmodesmata create PM subdomains with a unique protein/lipid signature and facilitate localised and specific responses. In addition, signalling events triggered at the PM also need to be coordinated with local responses at plasmodesmata to specifically and independently regulate cell-to-cell communication. Until now, callose deposition-mediated plasmodesmata closure has been the main signalling output but other local responses could also be triggered in parallel. These could include changes in plasmodesmata membrane electrostatic signature, re-arrangement of plasmodesmata tethers which could then change the cytoplasmic sleeve conducting properties. Furthermore, we can wonder what are the molecular mechanisms underlying the rapid mobility of receptors between PM and plasmodesmata, but also how the system deactivates such processes.

### Concluding remarks

Recent years have seen remarkable progress in our structural and functional understanding of plasmodesmata-mediated cell-to-cell communication and how these structures can create dynamic areas of cell-to-cell connectivity in response to a wide range of developmental and environmental signals. They have also highlighted the complexity of plant inter-cellular communication and the intricacies of short and long-range communication networks, where hormone-signalling, receptor-signalling and symplastic-signalling pathways intersect in a very dynamic manner to create coherent responses at the organism level. Challenges in studying plasmodesmata also lie in their nanoscale dimensions and their high plasticity, making it hard to pin down particular morphological states and link them to functional/physiological states. A comprehensive understanding of symplastic transport will benefit from multidisciplinary approaches that combine emerging fields and technologies such as *in silico*

(Figure 3 Legend Continued) microdomains. Alongside, a specific set of PM-associated receptors are rapidly and actively recruited to plasmodesmata where they accumulate and interact with plasmodesmal receptor proteins to induce local responses, such as callose deposition. With the receptor protein moving between the PM and plasmodesmata, perception of one signal can translate into both intracellular signalling cascades at the PM (green arrow) and local plasmodesmata responses (pink arrow), facilitated by the local protein interactors. PD: Plasmodesmata, Dt: Desmotubule, ER: Endoplasmic Reticulum, PM: Plasma Membrane.

molecular dynamics, electron microscopy, super resolution light microscopy and *in vitro* biophysical analyses with more classical genetics and cell biology approaches. Without doubt, future research will continue to uncover the fascinating and multifaceted mechanisms that govern plasmodesmata intercellular communication.

## Conflict of interest statement

Nothing declared.

## Acknowledgements

We apologize to any authors whose relevant work on plasmodesmata has not been cited owing to length constraints. We thank Dr Christine Faulkner (John Innes Centre, Norwich U.K.), Dr Jens Tilsner (Saint Andrew University/The James Hutton Institute, U.K.) and Dr Yoselin Benitez-Alfonso (University of Leeds, U.K.) for comments on the manuscript, Andrea Paterlini (The Sainsbury Laboratory, University of Cambridge, U.K.) for the help with electron tomography segmentation and Marie Brault for helping with the figures. This work was supported by the European Research Council (ERC) under the European Union's Horizon 2020 research and innovation programme (grant agreement No 772103-BRIDGING) to E.M.B and the EMBO Young Investigator Program. J.D.P. is funded by a PhD fellowship from the Belgian "Formation à la Recherche dans l'Industrie et l'Agriculture" (FRIA grant no. 1.E.096.18).

## References and recommended reading

Papers of particular interest, published within the period of review, have been highlighted as:

- of special interest
- of outstanding interest

1. Mittelbrunn M, Sánchez-Madrid F: **Intercellular communication: diverse structures for exchange of genetic information.** *Nat Rev Mol Cell Biol* 2012, **13**:328-335.
  2. Tilsner J, Nicolas W, Rosado A, Bayer EM: **Staying tight: plasmodesmal membrane contact sites and the control of cell-to-cell connectivity in plants.** *Annu Rev Plant Biol* 2016, **67**:337-364.
  3. Lai YS, Stefano G, Zemelis-Durfee S, Ruberti C, Gibbons L, Brandizzi F: **Systemic signaling contributes to the unfolded protein response of the plant endoplasmic reticulum.** *Nat Commun* 2018, **9**:3918
- This paper demonstrates how plant employs its long-distance and plasmodesmata-mediated cell-to-cell transportation to induce a systemic ER stress response through the root-to-shoot movement of a UPR transcriptional factor, ZIP60.
4. Zhang Z, Zheng Y, Ham BK, Chen J, Yoshida A, Kochian LV, Fei Z, Lucas WJ: **Vascular-mediated signalling involved in early phosphate stress response in plants.** *Nat Plants* 2016, **2**:16033.
  5. Chanda B, Xia Y, Mandal MK, Yu K, Sekine KT, Gao QM, Selote D, Hu Y, Stromberg A, Navarre D *et al.*: **Glycerol-3-phosphate is a critical mobile inducer of systemic immunity in plants.** *Nat Genet* 2011, **43**:421-429.
  6. Toyota M, Spencer D, Sawai-Toyota S, Jiaqi W, Zhang T, Koo AJ, Howe GA, Gilroy S: **Glutamate triggers long-distance, calcium-based plant defense signaling.** *Science* 2018, **361**:1112-1115.
  7. Yan D, Yadav SR, Paterlini A, Nicolas WJ, Belevich I, Grison MS, Vaten A, Karami L, Lee J, Murawska GM *et al.*: **PLM modulates phloem unloading through sphingolipid biosynthesis and plasmodesmal ultrastructure.** *Nat Plants* 2019, **5**:604-615
- This study sheds light on the function prospective of the structural transition from Type-I to Type-II plasmodesmata, showing such a transition adjusts macromolecule unloading at the phloem pole pericycle-endodermis interface, and identifying sphingolipids with very-long-chain fatty acids as elements influencing plasmodesmata structural transition.
8. Tran TM, McCubbin TJ, Bihmidine S, Julius BT, Baker RF, Schauffinger M, Weil C, Springer N, Chomet P, Wagner R *et al.*: **Maize carbohydrate partitioning defective33 encodes a MCTP protein and functions in sucrose export from leaves.** *Mol Plant* 2019, **12**:1278-1293
- This paper identifies QUIRKY homologue in maize, CPD33, through a genetic screen and shows it is essential for plasmodesmata formation and sucrose export from leaves. CPD33 localises to ER, PM and plasmodesmata, a puzzling observation that supports plant MCTP protein action at PM-ER and PD MCS.
9. Liu Y, Xu M, Liang N, Zheng Y, Yu Q, Wu S: **Symplastic communication spatially directs local auxin biosynthesis to maintain root stem cell niche in Arabidopsis.** *Proc Natl Acad Sci U S A* 2017, **114**:4005-4010.
  10. Wu S, O'Lexy R, Xu M, Sang Y, Chen X, Yu Q, Gallagher KL: **Symplastic signaling instructs cell division, cell expansion, and cell polarity in the ground tissue of Arabidopsis thaliana roots.** *Proc Natl Acad Sci U S A* 2016, **113**:11621-11626.
  11. Miyashima S, Roszak P, Sevilem I, Toyokura K, Blob B, Heo J, Mellor N, Help-Rinta Rahko H, Otero S, Smet W *et al.*: **Mobile PEAR transcription factors integrate positional cues to prime cambial growth.** *Nature* 2019, **565**:490-494
- This paper elegantly illustrates how signal communication between mother and daughter cells through plasmodesmata helps to establish cell identities and boundaries during ontogenesis in procambium cells. PEAR TFs mark the active dividing protophloem-sieve-elements and move to neighbour cells to promote procambial cell division. In the daughter cells, target of PEAR proteins, HD ZIP III antagonizes PEAR function and mobility to specify the un-dividing cell population.
12. Grison MS, Kirk P, Brault M, Na Wu X, Schulze WX, Benitez-Alfonso Y, Immel F, Bayer EM: **Plasma membrane associated receptor like kinases relocate to plasmodesmata in response to osmotic stress.** *Plant Physiol* 2019, **181**:142-160
- In this paper, the authors demonstrate the fast (2–3 min) re-localisation of the LRR receptor-like kinases QSK1 and IMK2 from the PM to plasmodesmata in response to osmotic stress and link it to callose deposition and plasmodesmata closure. QSK1 association with plasmodesmata is dependent on its phosphorylation pattern.
13. Hunter K, Kimura S, Rokka A, Tran HC, Toyota M, Kukkonen JP, Wrzaczek M: **CRK2 enhances salt tolerance by regulating callose deposition in connection with PLD $\alpha$ 1.** *Plant Physiol* 2019, **180**:2004-2021
- In this paper, the authors show that re-localization of cysteine-rich receptor-kinase, CRK2 from PM to plasmodesmata regulates callose deposition and salt stress responses. Genetic and pharmacological experiments suggest that calcium, phospholipase D and CRK2 kinase activities are involved in the process.
14. Cheval C, Johnston M, Samwald S, Liu X, Bellandi A, Breakspear A, Kadota Y, Zipfel C, Faulkner C: **Chitin perception in plasmodesmata identifies subcellular, context-specific immune signalling in plants.** *bioRxiv* 2019 <http://dx.doi.org/10.1101/611582>.
  15. O'Lexy R, Kasai K, Clark N, Fujiwara T, Sozzani R, Gallagher KL: **Exposure to heavy metal stress triggers changes in plasmodesmal permeability via deposition and breakdown of callose.** *J Exp Bot* 2018, **69**:3715-3728.
  16. Lim GH, Shine MB, De Lorenzo L, Yu K, Cui W, Navarre D, Hunt AG, Lee JY, Kachroo A, Kachroo P: **Plasmodesmata localizing proteins regulate transport and signaling during systemic acquired immunity in plants.** *Cell Host Microbe* 2016, **19**:541-549.
  17. Faulkner C, Petutschnig E, Benitez-Alfonso Y, Beck M, Robotzek S, Lipka V, Maule AJ: **LYM2-dependent chitin perception limits molecular flux via plasmodesmata.** *Proc Natl Acad Sci U S A* 2013, **110**:9166-9170.
  18. Lucas WJ, Bouche-Pillon S, Jackson DP, Nguyen L, Baker L, Ding B, Hake S, Bouché-Pillon S, Jackson DP, Nguyen L *et al.*: **Selective trafficking of KNOTTED1 homeodomain protein and its mRNA through plasmodesmata.** *Science* 1995, **270**:1980-1983.
  19. Xu XM, Wang J, Xuan Z, Goldshmidt A, Borrill PGM, Hariharan N, Kim JY, Jackson D: **Chaperonins facilitate KNOTTED1 cell-to-cell trafficking and stem cell function.** *Science* 2011, **333**:1141-1144.
  20. Daum G, Medzihradsky A, Suzuki T, Lohmann JU: **A mechanistic framework for non-cell autonomous stem cell induction in Arabidopsis.** *Proc Natl Acad Sci U S A* 2014, **111**:14619-14624.

21. Balkunde R, Kitagawa M, Xu XM, Wang J, Jackson D: **SHOOT MERISTEMLESS trafficking controls axillary meristem formation, meristem size and organ boundaries in Arabidopsis.** *Plant J* 2017, **90**:435-446.
22. Tylewicz S, Petterle A, Marttila S, Miskolczi P, Azeez A, Singh RK, Immanen J, Mähler N, Hvidsten TR, Eklund DM *et al.*: **Photoperiodic control of seasonal growth is mediated by ABA acting on cell-cell communication.** *Science* 2018, **360**:212-215.
23. Ross-Elliott TJ, Jensen KH, Haaning KS, Wager BM, Knoblauch J, Howell AH, Mullendore DL, Monteith AG, Paultre D, Yan D *et al.*: **Phloem unloading in Arabidopsis roots is convective and regulated by the phloem-pole pericycle.** *eLife* 2017, **6**:e24125.
24. Gaudioso-Pedraza R, Beck M, Frances L, Kirk P, Ripodas C, Niebel A, Oldroyd GED, Benitez-Alfonso Y, de Carvalho-Niebel F: **Callose-regulated symplastic communication coordinates symbiotic root nodule development.** *Curr Biol* 2018, **28**:3562-3577
- This study shows how callose turn-over at plasmodesmata influences root nodulation in *Medicago truncatula*. Rhizobia infection induces the expression of MtBG2, a  $\beta$ -1,3-Glucanase, to promote symplastic communication and transcriptional activation of key symbiotic regulators, which are blocked when callose ectopically accumulates at plasmodesmata.
25. Skopelitis DS, Hill K, Klesen S, Marco CF, von Born P, Chitwood DH, Timmermans MCP: **Gating of miRNA movement at defined cell-cell interfaces governs their impact as positional signals.** *Nat Commun* 2018, **9**:3107.
26. Thieme CJ, Rojas-Triana M, Stecyk E, Schudoma C, Zhang W, Yang L, Minambres M, Walther D, Schulze WX, Paz-Ares J *et al.*: **Endogenous Arabidopsis messenger RNAs transported to distant tissues.** *Nat Plants* 2015, **1**:15025.
27. Han X, Hyun TK, Zhang M, Kumar R, Koh EJ, Kang BH, Lucas WJ, Kim JY: **Auxin-callose-mediated plasmodesmal gating is essential for tropic auxin gradient formation and signaling.** *Dev Cell* 2014, **28**:132-146.
28. Tamaki S, Matsuo S, Wong HL, Yokoi S, Shimamoto K: **Hd3a protein is a mobile flowering signal in rice.** *Science* 2007, **316**:1033-1036.
29. Corbesier L, Vincent C, Jang S, Fornara F, Fan Q, Searle L, Giakountis A, Farrona S, Gissot L, Turnbull C, Coupland G: **FT protein movement contributes to long-distance signalling in floral induction of Arabidopsis.** *Science* 2007, **316**:1030-1033.
30. Song S, Chen Y, Liu L, Wang Y, Bao S, Zhou X, Teo ZWN, Mao C, Gan Y, Yu H: **OsFTIP1-mediated regulation of florigen transport in rice is negatively regulated by the ubiquitin-like domain kinase OsUbdK $\gamma$ 4.** *Plant Cell* 2017, **29**:491-507.
31. Liu L, Liu C, Hou X, Xi W, Shen L, Tao Z, Wang Y, Yu H: **FTIP1 is an essential regulator required for florigen transport.** *PLoS Biol* 2012, **10**:e1001313.
32. Zhu Y, Liu L, Shen L, Yu H: **NaKR1 regulates long-distance movement of FLOWERING LOCUS T in Arabidopsis.** *Nat Plants* 2016, **2**:16075.
33. Evans MJ, Choi W-G, Gilroy S, Morris RJ: **A ROS-assisted calcium wave dependent on the AtRBOHD NADPH oxidase and TPC1 cation channel propagates the systemic response to salt stress.** *Plant Physiol* 2016, **171**:1771-1784.
34. Nicolas WJ, Grison MS, Trépout S, Gaston A, Fouché M, Cordelières FP, Oparka K, Tilsner J, Brocard L, Bayer EM: **Architecture and permeability of post-cytokinesis plasmodesmata lacking cytoplasmic sleeves.** *Nat Plants* 2017, **3**:17082.
35. Grison MS, Brocard L, Fouillen L, Nicolas W, Wewer V, Dörmann P, Nacir H, Benitez-Alfonso Y, Claverol S, Germain V *et al.*: **Specific membrane lipid composition is important for plasmodesmata function in Arabidopsis.** *Plant Cell* 2015, **27**:1228-1250.
36. Brault ML, Petit JD, Immel F, Nicolas WJ, Glavier M, Brocard L, Gaston A, Fouché M, Hawkins TJ, Crowet J *et al.*: **Multiple C2 domains and transmembrane region proteins (MCTPs) tether membranes at plasmodesmata.** *EMBO Rep* 2019, **20**:e47182
- Combining label-free proteomics, cell biology, genetics and molecular dynamics, this study identifies the MCTP family as plasmodesmata-specific

ER-PM tethers, that bridge the two membranes through their transmembrane region and C2 lipid-binding domains. It further demonstrates that MCTP3/4 are core plasmodesmal proteins which are involved in multiple perspectives of plant development, and influence plasmodesmata connectivity and molecular specification. This is the first study identifying structural plasmodesmal proteins acting at the ER-PM interface.

37. Amsbury S, Kirk P, Benitez-Alfonso Y: **Emerging models on the regulation of intercellular transport by plasmodesmata-associated callose.** *J Exp Bot* 2017, **69**:105-115.
38. Vaddepalli P, Herrmann A, Fulton L, Oelschner M, Hillmer S, Stratil TF, Fastner A, Hammes UZ, Ott T, Robinson DG *et al.*: **The C2-domain protein QUIRKY and the receptor-like kinase STRUBBELIG localize to plasmodesmata and mediate tissue morphogenesis in Arabidopsis thaliana.** *Development* 2014, **141**:4139-4148.
39. Song JH, Kwak SH, Nam KH, Schiefelbein J, Lee MM: **QUIRKY regulates root epidermal cell patterning through stabilizing SCRAMBLED to control CAPRICE movement in Arabidopsis.** *Nat Commun* 2019, **10**:1744.
40. Amari K, Boutant E, Hofmann C, Schmitt-Keichinger C, Fernandez-Calvino L, Didier P, Lerich A, Mutterer J, Thomas CL, Heinlein M *et al.*: **A family of plasmodesmal proteins with receptor-like properties for plant viral movement proteins.** *PLoS Pathog* 2010, **6**:e1001119.
41. Levy A, Zheng JY, Lazarowitz SG: **Synaptotagmin SYTA forms ER-plasma membrane junctions that are recruited to plasmodesmata for plant virus movement.** *Curr Biol* 2015, **25**:2018-2025.
42. Vatén A, Dettmer J, Wu S, Stierhof YD, Miyashima S, Yadav SR, Roberts CJ, Campilho A, Bulone V, Lichtenberger R *et al.*: **Callose biosynthesis regulates symplastic trafficking during root development.** *Dev Cell* 2011, **21**:1144-1155.
43. Zimmerberg J, Kozlov MM: **How proteins produce cellular membrane curvature.** *Nat Rev Mol Cell Biol* 2006, **7**:9-19.
44. Abou-Saleh RH, Hernandez-Gomez MC, Amsbury S, Paniagua C, Bourdon M, Miyashima S, Helariutta Y, Fuller M, Budtova T, Connell SD *et al.*: **Interactions between callose and cellulose revealed through the analysis of biopolymer mixtures.** *Nat Commun* 2018, **9**:4538
- This paper investigates, using an *in vitro* model, the physical impact of callose deposition in the cell wall, especially in regards to its interaction with cellulose. The inter-molecule interaction between callose and cellulose dictates the elasticity of the whole, a feature that has not been considered before and raises interesting questions of how these physical features would impact on plasmodesmata function.
45. Park K, Knoblauch J, Oparka K, Jensen KH: **Controlling intercellular flow through mechanosensitive plasmodesmata nanopores.** *Nat Commun* 2019, **10**:3564
- At the plasmodesmata entry sites, ER-PM contacts leave a small annular gap for molecules to enter the pores. This paper brings a new perspective on how plasmodesmata ER-PM tethers, that position the ER-Desmotubule complex, could possibly function as mechanical sensor to fine-tune the lateral movement of ER-desmotubule hence PD transport through the cytoplasmic sleeve upon rapid osmotic pressure changes.
46. Zhu T, O'Quinn RL, Lucas WJ, Rost TL: **Directional cell-to-cell communication in the Arabidopsis root apical meristem II. Dynamics of plasmodesmata formation.** *Protoplasma* 1998, **204**:84-93.
47. Deinum EE, Benitez-Alfonso Y, Mulder BM: **From plasmodesma geometry to effective symplastic permeability through biophysical modelling.** *eLife* 2019, **8**:e49000.
48. Lee JY, Yoo BC, Rojas MR, Gomez-Ospina N, Staehelin LA, Lucas WJ: **Selective trafficking of non-cell-autonomous proteins mediated by NtNCAPP1.** *Science* 2002, **229**:392-396.
49. Ishikawa K, Hashimoto M, Yusa A, Koinuma H, Kitazawa Y, Netsu O, Yamaji Y, Namba S: **Dual targeting of a virus movement protein to ER and plasma membrane subdomains is essential for plasmodesmata localization.** *PLoS Pathog* 2017, **13**:e1006463.
50. Liu L, Li C, Song S, Teo ZWN, Shen L, Wang Y, Jackson D, Yu H: **FTIP-dependent STM trafficking regulates shoot meristem development in Arabidopsis.** *Cell Rep* 2018, **23**:1879-1890

In this paper, the authors report that FTIP3/4, also called MCTP3/4, localise to endosomes and recruit the TF SHOOT MERSITEMLESS through direct interaction to balance its subcellular localisation and mobility through plasmodesmata.

51. Tilsner J, Amari K, Torrance L: **Plasmodesmata viewed as specialised membrane adhesion sites.** *Protoplasma* 2011, **248**:39-60.
52. Liu L, Li C, Liang Z, Yu H: **Characterization of multiple C2 domain and transmembrane region proteins in arabidopsis.** *Plant Physiol* 2018, **176**:2119-2132.
53. Bian X, Saheki Y, De Camilli P: **Ca<sup>2+</sup> releases E-Syt1**
  - **autoinhibition to couple ER-plasma membrane tethering with lipid transport.** *EMBO J* 2018, **37**:219-234

With elegant *in vitro* assays, this paper demonstrates how C2 domains of E-Syt1 can adopt multiple regulatory roles through inter-domain interaction, calcium binding and calcium-dependent lipid transfer functions.
54. Giordano F, Saheki Y, Idevall-Hagren O, Colombo SF, Pirruccello M, Milosevic I, Gracheva EO, Bagriantsev SN, Borgese N, De Camilli P: **PI(4,5)P(2)-dependent and Ca(2+)-regulated ER-PM interactions mediated by the extended synaptotagmins.** *Cell* 2013, **153**:1494-1509.
55. Stahl Y, Grabowski S, Bleckmann A, Kühnemuth R, Weidtkamp-Peters S, Pinto KG, Kirschner GK, Schmid JB, Wink RH, Hülsewede A *et al.*: **Moderation of arabidopsis root stemness by CLAVATA1 and ARABIDOPSIS CRINKLY4 receptor kinase complexes.** *Curr Biol* 2013, **23**:362-371.
56. Saka SK, Honigmann A, Eggeling C, Hell SW, Lang T, Rizzoli SO: **Multi-protein assemblies underlie the mesoscale organization of the plasma membrane.** *Nat Commun* 2014, **5**:4509.
57. Hohmann U, Lau K, Hothorn M: **The structural basis of ligand perception and signal activation by receptor kinases.** *Annu Rev Plant Biol* 2017, **68**:109-137.
58. Bücherl CA, Jarsch IK, Schudoma C, Segonzac C, Mbengue M, Robatzek S, MacLean D, Ott T, Zipfel C: **Plant immune and growth receptors share common signalling components but localise to distinct plasma membrane nanodomains.** *eLife* 2017, **6**:e25114.



# Lipids or Proteins: Who Is Leading the Dance at Membrane Contact Sites?

Jules D. Petit<sup>1,2\*</sup>, Françoise Immel<sup>1</sup>, Laurence Lins<sup>2\*</sup> and Emmanuelle M. Bayer<sup>1\*</sup>

<sup>1</sup> UMR5200 CNRS, Laboratory of Membrane Biogenesis, University of Bordeaux, Villenave d'Ornon, France, <sup>2</sup> Laboratoire de Biophysique Moléculaire aux Interfaces, TERRA Research Centre, GX ABT, Université de Liège, Liège, Belgium

## OPEN ACCESS

### Edited by:

Antia Rodriguez-Villalon,  
ETH Zürich, Switzerland

### Reviewed by:

Miguel A. Botella,  
Universidad de Málaga, Spain  
Roman Pleskot,  
Ghent University, Belgium

### \*Correspondence:

Jules D. Petit  
jules.petit@u-bordeaux.fr  
Laurence Lins  
l.lins@uliege.be  
Emmanuelle M. Bayer  
emmanuelle.bayer@u-bordeaux.fr

### Specialty section:

This article was submitted to  
Plant Cell Biology,  
a section of the journal  
Frontiers in Plant Science

**Received:** 10 December 2018

**Accepted:** 05 February 2019

**Published:** 21 February 2019

### Citation:

Petit JD, Immel F, Lins L and  
Bayer EM (2019) Lipids or Proteins:  
Who Is Leading the Dance  
at Membrane Contact Sites?  
*Front. Plant Sci.* 10:198.  
doi: 10.3389/fpls.2019.00198

Understanding the mode of action of membrane contact sites (MCSs) across eukaryotic organisms at the near-atomic level to infer function at the cellular and tissue levels is a challenge scientists are currently facing. These peculiar systems dedicated to inter-organellar communication are perfect examples of cellular processes where the interplay between lipids and proteins is critical. In this mini review, we underline the link between membrane lipid environment, the recruitment of proteins at specialized membrane domains and the function of MCSs. More precisely, we want to give insights on the crucial role of lipids in defining the specificity of plant endoplasmic reticulum (ER)-plasma membrane (PM) MCSs and we further propose approaches to study them at multiple scales. Our goal is not so much to go into detailed description of MCSs, as there are numerous focused reviews on the subject, but rather try to pinpoint the critical elements defining those structures and give an original point of view by considering the subject from a near-atomic angle with a focus on lipids. We review current knowledge as to how lipids can define MCS territories, play a role in the recruitment and function of the MCS-associated proteins and in turn, how the lipid environment can be modified by proteins.

**Keywords:** membrane contact sites, plants, lipids, tether proteins, plasmodesmata, biophysics

## INTRODUCTION

From an evolutionary perspective, membrane contact sites (MCSs) have been suggested to be the first contacts between archeon and protobacterium, leading to the emergence of eukaryotic cells (Jain and Holthuis, 2017). More generally, MCSs are described as a very close apposition (10–30 nm gap) of membranes of usually two different organelles (intra-organellar MCSs also exist), with specific lipid and protein populations (Bayer et al., 2017; Wang et al., 2017). MCSs create micro-environments that are under tight spatial and temporal control. Their main function is to promote fast inter-organellar communication through direct exchange of molecules such as lipids or calcium and through coordinated actions, for instance, with proteins acting in *trans* on the adjacent membrane to control receptor signaling or lipid synthesis (Eden et al., 2010; Haj et al., 2012; Himschoot et al., 2017; Muallem et al., 2017; Henrich et al., 2018). MCSs' capacity to create and modulate micro-environments but also macro-environment at larger scales in the cell, is determined by high regulation of lipids and proteins, both in composition and distribution (Eisenberg-Bord et al., 2016; Gatta and Levine, 2017; Muallem et al., 2017). Many research have been made on the diversity of membrane lipids and the consequences of their heterogeneous distributions along and across the bilayer (Cacas et al., 2016; Sezgin et al., 2017; Gronnier et al., 2018; Harayama and Riezman, 2018). There is also increasing knowledge about the identity and function



of MCS-associated proteins (Eisenberg-Bord et al., 2016; Wong et al., 2018). The exact definition of the MCSs is still being discussed but an emerging consensus is that they are (1) involved in the bulk lipid distribution and/or the fine regulation of membrane lipid composition through (but not only) direct lipid transfer which in turn is critical for local and organellar cellular processes and (2) characterized with the presence of tethering elements to hold the membranes close to each other but without undergoing fusion. Lipid transfer proteins (LTPs) are locally found at MCSs and, in addition to lipid transfer, some are also able to act as tethers (Lahiri et al., 2015; Eisenberg-Bord et al., 2016; Quon et al., 2018; Tong et al., 2018). In turn, the lipids are one of the main actors for LTP/tether recruitment, hence stability and function of MCSs (Bian et al., 2018; Wong et al., 2018). In such an environment, it is challenging to understand the dynamics and relationships between proteins and lipids but also interactions between lipid-lipid and protein-protein inside these confined areas filled with such a dynamic complexity.

We chose here to give a global view and additional thoughts on the role of lipids at plant MCSs, mainly at endoplasmic reticulum (ER)-plasma membrane (PM) MCSs (EPCSs). In this review, we will first describe the different ways lipids can define specific regions and regulate protein complexes through the formation of lipid domains, the regulation of membrane curvature and membrane electrostatics. Secondly, we will look at the importance of lipid exchange at MCSs. Thirdly, we will open a discussion about the particularity of plasmodesmata MCSs and their potential implications in organelle crosstalk, cell-to-cell communication and trafficking regulation. Finally, we list a number of multidisciplinary approaches that could be used to provide a complete view of these structures at (near) atomic and molecular levels.

## MEMBRANE LIPIDS CREATE UNIQUE ENVIRONMENTS THAT DEFINE AND REGULATE MCSs

MCSs have specific molecular compositions in both lipids and proteins, which define nano- and microdomains within the organelle. These subdomains are very important for the cellular polarization of signaling events via the formation of protein complexes, notably receptor complexes that are as such spatially and temporally regulated, driving acute signaling pathways (Burkart and Stahl, 2017; Gronnier et al., 2018). The molecular mechanisms leading to subcompartmentalization in general terms are gradually being uncovered and have been shown to involve lipids, membrane biophysical properties and the concerted action of specific protein machineries. Membrane subdivision is arising from the combination of membrane biophysical properties – such as fluidity, thickness, curvature and electrostatics – and has consequences in the recognition pattern of a plethora of lipid environment-sensing protein domains (Prévost et al., 2015; Strahl et al., 2015; Pérez-Lara et al., 2016; Lorent et al., 2017; Platre et al., 2018; Wong et al., 2018).

## Membrane Fluidity and Domains

There are two main elements playing a role in membrane fluidity and lipid domain formation and conservation. A very general feature is the liquid-liquid phase separation, caused by the tendency of sterols to associate with saturated lipids or proteins and form sterol-enriched ordered domains (liquid ordered Lo versus liquid disordered Ld domains) and of unsaturated lipids to tune the phase separation stability (Levental et al., 2016; Javanainen et al., 2017; Weiner and Feigenson, 2018). More precisely, in plants, a model of PM nanodomain has been proposed to involve plant-specific sphingolipids called Glycosyl Inositol Phospho Ceramides (GIPCs). GIPCs possess very long saturated acyl chains and presumably locate in the outer leaflet of the PM. Poly glycosylated GIPCs tend to increase the size of phytosterol-dependent ordered domains through cooperative interactions (Figure 1A; Grosjean et al., 2015), which likely mirrors poly phosphoinositides-enriched domains in the inner leaflet, possibly through interdigitation; i.e., interaction through very long fatty acyl chains between outer and inner leaflet lipids (Raghupathy et al., 2015; Cacas et al., 2016; Gronnier et al., 2016).

The natural segregation of lipids into domains, caused by their intrinsic properties is used, controlled and balanced by the cell through the action of proteins in order to build functional entities capable of molecular and cellular operations such as signaling (Sezgin et al., 2017). The rigidity/fluidity of the membrane partially derives from the proportion of sterols present in the bilayer, as their stiff planar structure is constraining the acyl chains of neighboring lipids (Dufourc, 2008). As a consequence, the presence of nanodomains and membrane-associated cytoskeleton is directly impacting the mobility of peripheral and anchored protein. This so-called anomalous diffusion of membrane-associated proteins and lipids could be as important as membrane compartmentalization for mesoscopic dynamics (100–1000 nm) (Wu et al., 2016). In addition, the sterol enrichment together with the orderliness and length of the lipid acyl chains are associated with the thickness of the bilayer (Javanainen et al., 2017). One example of protein sorting associated to lipid nano-domain formation is the distribution of transmembrane domains via the hydrophobic mismatch; i.e., the properties of the transmembrane domain is correlated to specific lipid domains (Figure 1B; Milovanovic et al., 2015; Lorent et al., 2017). A recent study describing the plasmodesmata proteome of *Populus trichocarpa* shows an increase in the length of the transmembrane domains of plasmodesmata-associated proteins in comparison with membrane-associated proteins (Leijon et al., 2018). This observation is in correlation with the specificity of the membrane composition described at post cytokinesis plasmodesmata (Grison et al., 2015) and pointing toward a thick “raft-like” membrane.

In animals, MCSs between the ER and the *trans*-Golgi network are critical for the regulation of the sterol and sphingolipid transfer, mediated by the Ceramide Transport Protein (CERT) and the Oxysterol Binding Protein (OSBP), which is very important for the control of *trans*-Golgi lipid composition, hence PM lipid composition (Yamaji et al., 2008; Olkkonen, 2015; Jain and Holthuis, 2017; Hanada, 2018). GIPCs being plant-specific

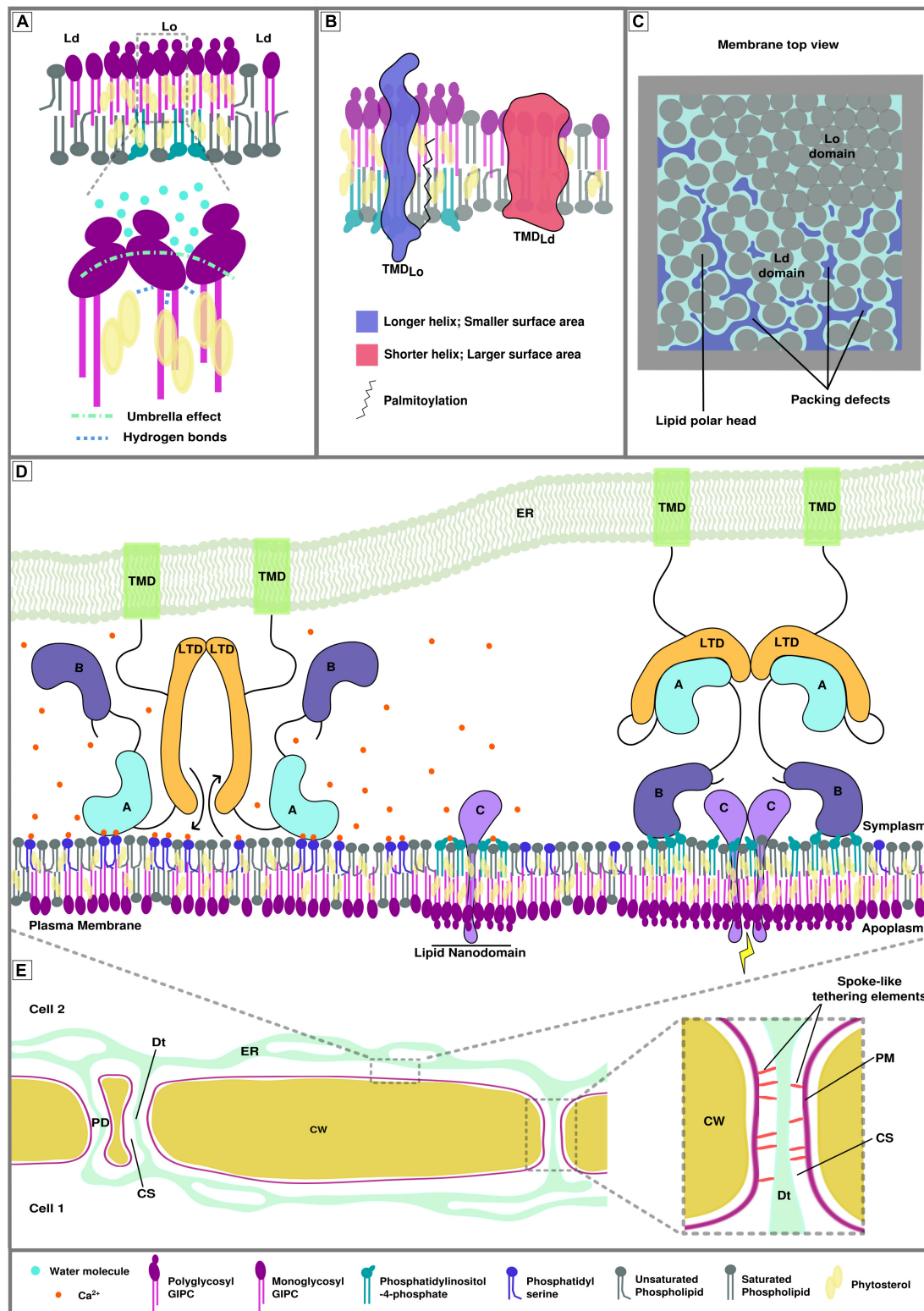


**FIGURE 1 |** Membrane biophysical properties and lipid-protein interplay at membrane contact sites (MCSs). **(A)** Poly glycosylated GIPCs tend to increase the size and rigidity of phytosterol-dependent ordered membrane domains (Lo) through hydrogen bonding between the hydroxyl group of the sterols and the polarized groups of the GIPCs located at the polar/hydrophobic interface. This interaction is also favored by the umbrella effect of the big GIPCs' polar moiety, which prevents water molecules to interact deeper into the bilayer (Grosjean et al., 2015). **(B)** Transmembrane protein distribution between different lipid domains relies on transmembrane length, surface area and palmitoylation (adapted from Lorent et al., 2017). **(C)** Representation of the lipid packing of membrane domains. (Continued)

**FIGURE 1 | Continued**

Liquid ordered domain are more tightly packed than liquid disordered domains (Ld) because of the nature of the lipids and degree of their acyl chain saturation. Lipid packing defects arise in liquid disordered domains. **(D)** Hypothetical model of calcium-dependent regulation of protein-plasma membrane interaction at endoplasmic reticulum-plasma membrane MCS (EPCS). This hypothetical model gathers the possible interactions involving proteins, lipids and ions that could occur at MCS during signaling events. Its goal is to illustrate the complexity of lipid/protein/ion interactions. The protein illustrated here represents a lipid transfer protein/tether element that specifically locates to EPCS upon homodimerization. **Left.** In presence of calcium, domain A is able to interact with phosphatidylserine, the inter-membrane gap is reduced, allowing the exchange of lipids by the lipid transfer domains (LTDs). Domain B cannot interact with the phosphatidylinositol phosphates of the lipid nanodomains as they are shielded by the calcium ions **(Middle).** **Right.** In the absence of calcium, domain A is released from the membrane, increasing the inter-membrane gap, and binds to the LTD, inhibiting lipid exchange between organelles. Domain B docks onto the lipid nanodomains via electrostatic interactions with anionic PIPs and leads to the formation of bigger lipid domains where protein C can interact with one another and initiate/relay a signal. There are two main domain types allowing peripheral binding of proteins, the anionic lipid and/or calcium-dependent C2 domains (such as domain A in this figure) and the anionic lipid dependent PH domains (such as domain B in this figure). **(E)** Schematic view of plant cell-to-cell junction showing the cell wall (CW), the endoplasmic reticulum (ER) network, plasma membrane (PM) and several plasmodesmata (PD). The **right** insert shows the PD ultrastructure. The close vicinity between the PM and the desmotubule (Dt; a lumen-free tubule of ER), connected by spoke-like tethering elements, leaves a small inter-membrane gap between the two membranes, called the cytoplasmic sleeve (CS).

sphingolipids, understanding their role in membranes and how they could indirectly act at MCS by modulating lipid composition would be a major step forward in cell biology. Although some studies have shown enrichment of sphingolipids and phytosterols at some plant MCSs (Fujimoto et al., 2011; Grison et al., 2015), we currently don't know the role of inter-organellar exchange in maintaining these local lipid environments. The remaining enigma behind the role of leaflet interdigitation mediated by the GIPCs' very long chain fatty acids and more globally the asymmetrical distribution of lipids between the inner and outer leaflets of the PM is also worth our attention (Cacas et al., 2016; Gronnier et al., 2016).

## Membrane Curvature and Lipid Packing

Another major component of the establishment of specialized membrane domains is membrane curvature and lipid packing. The latter can be described as the orderliness of the lipid arrangement: lipid packing defects arise when cavities in the membrane are formed at the interface with water, exposing aliphatic carbons (**Figure 1C**; Jackson et al., 2016; Gautier et al., 2018). This property of the bilayer relies upon a balance between the size of the lipid polar head and the degree of lipid unsaturation (Bigay and Antonny, 2012) but also upon the curvature of the bilayer itself (Harayama and Riezman, 2018). Other studies also suggest the formation of lipid packing defects at Lo/Ld boundaries (Tripathy et al., 2018). These membrane biophysical properties can drive membrane adsorption of various peripheral proteins which recognize lipid packing defects through, for instance, amphipathic helices in membrane curvature-sensing proteins (Cui et al., 2011; Vanni et al., 2013; Simunovic et al., 2015). In addition, the curvature itself can drive autonomous sorting of molecules depending on their properties, as it was shown for lipids (Baoukina et al., 2018) and transmembrane proteins (Aimon et al., 2014). In the context of MCSs, highly negatively curved membranes, such as PM inside plasmodesmata intercellular pores, could cluster small polar head lipids like phosphatidic acid (PA) and/or specific proteins, to potentially regulate the function of the MCS.

Other proteins or local production/degradation of specific lipids have been shown to induce membrane curvature (Tilsner et al., 2016; Choudhary et al., 2018; Ramakrishnan et al., 2018). The transmembrane region of human MCTP2 (Multiple

C2 domains and Transmembrane region Protein 2), a protein that is suspected to act as a tether at EPCS in neurons (Genç et al., 2017), was notably shown to act as a reticulon domain, constraining the ER network into narrow tubules by inducing curvature (Joshi et al., 2018). An interesting question to ask is whether tether proteins can also shape membranes at MCSs and how this could be linked with inter-organellar exchange. Does the curvature induced by these tethers aim to facilitate lipid extraction for transfer? Sterol extraction could indeed be facilitated at positively curved membranes (Bigay and Antonny, 2012) and maybe more stably incorporated into membranes with no lipid packing defect such as negatively curved membranes, possibly providing a driving force for directional movement.

## Membrane Electrostatics and Ions

The third main element defining membrane and domain identity is the charge carried by the lipid polar heads, more precisely anionic lipids. In plants, phosphatidylinositol-4-phosphate (PI4P) is the major anionic lipid that drives the electrostatic identity of the PM inner leaflet (Simon et al., 2016) but a more recent research shows that the electrostatic field is actually controlled by a combination of several charged lipids, namely PI4P, PA and phosphatidylserine (PS) (Platre et al., 2018). This three-way electrostatic landscape of plant PM is critical for the creation of specific local charges and thus the recruitment and function of cationic proteins involved in cellular responses, such as the brassinosteroid transport regulator BRI1 KINASE INHIBITOR1 (BKI1) and auxin polarity modulators AGC kinases PINOID and D6-PROTEIN KINASE (D6PK) (Barbosa et al., 2016; Simon et al., 2016; Platre et al., 2018).

Negatively charged lipids are also critical elements of EPCSs, acting as co-factors for membrane tethering through direct interaction with tether proteins. Few examples are tricalbins (Tcb1-3) and Ist2 proteins in yeast (Manford et al., 2012), extended-synaptotagmins (E-Syt1-3), TMEM16, junctophilins and STIM1 in humans and finally synaptotagmin 1/A (Syt1) and MCTPs in plants (Henne et al., 2015; Tilsner et al., 2016; Brault et al., 2018). Indeed, many LTPs/tethering elements possess pleckstrin homology (PH) or C2 domains, which are known anionic lipid-interacting domains (Wong et al., 2018). In

animals, MCS tether proteins presenting a series of C2 domains (like E-Syt1) were shown to have conditional environment-mediated structural modifications, which initiate or relay a signal at the MCS scale: decrease of inter-membrane gap, lipid exchange, protein complex formation/loosening (Saheki and De Camilli, 2017; Zhou et al., 2017; Bian et al., 2018). In plants, we are running late on understanding the dynamic molecular mechanisms occurring at MCSs but still, Syt1 C2 domains were shown to interact with anionic lipids (Schapire et al., 2008; Pérez-Sancho et al., 2015) and new insights on the function of MCTP family at plasmodesmata EPCS might give us some clues as their C2 domains also have the capacity to interact with PS and PI4P (Brault et al., 2018).

Local lipid modifications, pH and gradients/local concentrations of ions must also be taken into account in the regulation of the membrane electrostatic signature and thus the ability of anionic lipid-protein interactions. We know that MCSs are places of calcium exchange and anionic lipid concentration (Muallem et al., 2017). It is important to consider how the two are related and the consequences it has on MCS functions. For instance, the function of E-Syt1, which relies on the membrane docking ability of its C2 domains with anionic lipids, can be directly modulated by the presence of calcium ions (Idevall-hagren et al., 2015; Bian et al., 2018) but the latter can also shield PIP polar heads and prevent protein binding at places undergoing signaling (Seo et al., 2015; Bilkova et al., 2017; Himschoot et al., 2017; **Figure 1D**). Recent work has also demonstrated the effect of local concentrations of bivalent cations, mainly calcium, on the shaping of membranes containing anionic lipids: the clustering of PS and PI(4,5)P<sub>2</sub> caused by ion interactions drives a negative curvature and tubulation of the bilayer (Doosti et al., 2017; Graber et al., 2017). A last element that is able to determine a spatiotemporal electrostatic signature is the pH, which can act on anionic lipids, mainly PA (Shin et al., 2011; Tanguy et al., 2018). It is possible that the pH at MCS could differ from the bulk cytosol and studying its variations at these areas by using pH probes could be interesting.

## LIPID EXCHANGE AT MCS

At MCS, we observe an alternative transport to vesicular trafficking: a direct shuttle/exchange of lipids between membranes. This exchange seems to be a way to guarantee robust mechanism of lipid transfer and regulation between compartments as it results in organellar lipid modifications and plays a major role in cellular events such insulin response (Lees et al., 2017) and neuronal growth (Petkovic et al., 2014). This fast and efficient crosstalk is performed by a specialized group of proteins, the lipid transfer proteins (LTPs) and relies on protein membrane binding through lipid interaction (mainly anionic lipid and/or calcium-dependent C2 domains and anionic lipid-dependent PH domains), but also on the close proximity of the two membranes (**Figure 1D**; Wong et al., 2018). Non-vesicular transport of lipids by LTPs is important for the regulation of membrane composition in tight places, which cannot be achieved

by vesicles. It may also play an essential role in controlling the bulk lipid distribution of organelles.

For example, the OSBP and OSBP-Related Proteins (ORP, Osh) associate with vesicle-associated membrane protein-associated proteins (VAPs) at ER MCSs to specifically exchange sterols, PS and PIP molecules (Olkkonen, 2015; Moser von Filseck and Drin, 2016). Osh4 uses the PI4P imbalance created at the ER by PI4P phosphatase Sac1p to exchange PI4P extracted from the *trans*-Golgi network with sterols. This counter-flow process results in sterol enrichment at the *trans*-Golgi network and PI4P pool maintenance at the ER (Saint-jean et al., 2011). Interestingly, maintaining this PI4P pool at the ER allows the recruitment of CERT in order to transport ceramide from the ER to the *trans*-Golgi (Yamaji et al., 2008; Moser von Filseck and Drin, 2016). This trafficking of sterols and sphingolipids to the *trans*-Golgi leads to the indirect regulation of the PM lipid composition. ORP5/8 also contributes to build the PM lipid signature by counter-flowing PS to it, in exchange of PI4P and more efficiently PI(4,5)P<sub>2</sub> from the ER (Chung et al., 2015; Ghai et al., 2017). Overall, it becomes clear that the transport of sterols, sphingolipids and anionic lipids is critical for the definition of membrane signature and control of lipid composition. This leads us to believe that lipid exchange at MCSs is at the basis of membrane identity by shaping their properties through the transfer of specific lipids. It also allows the creation and maintenance of lipid gradients needed for the function of molecular machineries during cellular actions. However, our knowledge on how plant lipid transfer at MCS is able to tune organellar function and respond to signaling pathways remains limited.

## MCS AT PLASMODESMATA, OPENINGS ON A VERY CONFINED SPACE

Plasmodesmata are plant-specific channels crossing cell walls and enabling cell-to-cell communication (Brunkard and Zambryski, 2017). They are unique as they allow continuity of PM, ER and cytosol between cells (**Figure 1E**) and provide a direct cytosolic road for cell-to-cell molecular trafficking of metabolites, transcription factors, RNAs and calcium, and their membranes also host signaling pathways' machineries with receptor-like proteins (Kim et al., 2005; Rutschow et al., 2011; Furuta et al., 2012; Brunkard et al., 2015; Chen et al., 2016a; Tilsner et al., 2016; Brunkard and Zambryski, 2017). New insights into the plasmodesmata ultrastructure have revealed extremely tight vicinity (down to 3 nm) between the ER and the PM inside the pores, with spoke-like tethering elements connecting the two (**Figure 1E**), and highlighted the plasticity of these membrane junctions during cell growth and development (Nicolas et al., 2017). To some extent, this observation leads to the re-consideration of plasmodesmata as specialized EPCS and questions the function of ER-PM contacts at plasmodesmata (Tilsner et al., 2016; Nicolas et al., 2017). While plasmodesmata are structurally related to MCSs, being sites of ER-PM contacts, we do not know if they are involved in inter-organellar communication yet. Plasmodesmata are,

however, well-established sites of intercellular communication and, over the last decade, they have emerged as important signaling hubs playing a role in ever growing aspects of plant physiology. Merging these two elements results in the possibility of plasmodesmata to be a unique kind of MCS, acting as a node for both inter-organelle and cell-to-cell communication. Indeed, organelle crosstalk would clearly play a role in plasmodesmata function and local lipid transfer activity between the membranes would be conceivable since plasmodesmata are usually 500nm long channels and reaching inside the pore for vesicles is challenging, especially in mature tissues where the cell wall will be thicker.

Plasmodesmata are also singular amongst MCSs as they present a unique structural organization and membrane biophysical properties. Inside the pore, both the ER and the PM present extreme curvature, both positive and negative. So instead of two “flat” membrane segments tethered together, plasmodesmata MCS features two membrane tubes nested into each other and sitting at cell interfaces (which is neither inside the cell, neither part of the extracellular matrix). The extremely confined space between the ER and the PM (2–3 nm) is also not usual for MCSs and tight connection between the PM and cell wall components might lead us to someday talk about WALL-PM-ER MCSs.

A global view of protein population at plasmodesmata is starting to emerge (Fernandez-calvino et al., 2011; Salmon

and Bayer, 2013; Kraner et al., 2017; Brault et al., 2018) and few lipidomics, showing specific lipid composition of plasmodesmata-enriched biochemical fraction, have been performed (Grison et al., 2015). However, we currently have little understanding on how the lipid and protein populations are regulating each other and how they play a role in plasmodesmata dynamics. A glimpse on the identity, structure and mode of action of plasmodesmata-associated tethering elements could open the door on understanding the molecular mechanisms taking place at plasmodesmata and potentially bridge extracellular, PM and endomembrane signaling.

## UNDERSTANDING THE MCS AND ITS DYNAMICS REQUIRE INTERDISCIPLINARY APPROACHES

Understanding the dynamics of MCSs and its actors (lipid-protein, lipid-lipid and protein-protein interactions) requires bridging across scales from atomic (or near-atomic) to cellular and tissue levels, to get a comprehensive picture of MCSs. While cellular and tissue-level events can be tackled by classical cell biology (such as confocal microscopy) and genetic tools, their limits in terms of resolution encourage the use of *in silico*, biophysical-based tools and electron microscopy for understanding MCSs at atomic/macromolecular-levels. Many

**TABLE 1** | Non-extensive list of tools usable for atomic/macromolecular-level study of MCSs.

Technique	Usage	Reference
<i>In silico</i>		
Hypermatrix	Energy-based calculation of lipid-ligand interactions and 3D arrangements	Deleu et al., 2014; Cacas et al., 2016
IMPALA	Energy-based prediction of the insertion of molecules in lipid bilayers	Basyn et al., 2001; Lins et al., 2001; Cacas et al., 2016
Molecular dynamics	Atomic and coarse grained simulations to study the behavior over time of lipids bilayers and proteins	Deleu et al., 2014; Yamamoto et al., 2016; Duncan et al., 2017; Gronnier et al., 2017
<i>In vitro</i>		
PIP Strips	Determination of protein ability to interact with specific anionic lipids	Pérez-Sancho et al., 2016
Liposome flotation/sedimentation assays	Determination of protein ability to interact with a lipid bilayer	Schapiro et al., 2008; Pérez-Sancho et al., 2016; Meca et al., 2018
Tubule formation by optical tweezers on liposome	Study of membrane curvature-induced sorting of proteins	Aimon et al., 2014; Prévost et al., 2015; Chen et al., 2016b
<i>In vitro</i> tethering to reconstitute simplified MCS with isolated protein and controlled lipid and ion environment.	Characterization of the ability of a protein to tether two liposomes using dynamic light scattering and the inter-liposome distance by FRET. Visualize the tethering ultrastructure using cryo-electron microscopy	Mesmin et al., 2013; Lin et al., 2014; Diao et al., 2015
Isothermal Titration Calorimetry (ITC)	Determination of the affinity constant and thermodynamics parameters for the interaction between proteins and liposomes.	Ghai et al., 2012
Langmuir Trough	Determination of the kinetics of adsorption and affinity parameters of proteins for lipid monolayers	Eeman et al., 2006; Calvez et al., 2011; Gronnier et al., 2017
Solid state NMR	Study lipid-protein interactions and the deformation of the lipid membrane caused by the interaction at atomic level	Huster, 2014; Gronnier et al., 2017
<i>In situ</i>		
(Cryo) electron tomography	Visualize MCS architecture at macromolecular scale	Collado and Fernández-Busnadiego, 2017; Nicolas et al., 2017

options are possible but a number of approaches are especially interesting in the context of protein/lipid interaction, hence MCSs (see **Table 1**). For example, molecular modeling and dynamic simulations are relatively easy-accessible ways to study, simultaneously or not, the structure and function of proteins and lipid bilayers at a molecular/atomic level and often bring evidences on questions that could not be answered by other means (Javanainen et al., 2017). Currently, the increasing computational power and the development of efficient coarse grained force fields for an increasing number of molecules<sup>1</sup> (Marrink et al., 2007) allow the simulation of bigger and more complex systems during longer time scales (up to the micro-scale) (Duncan et al., 2017; Hsu et al., 2017), which fit MCS scales.

The study of a system closely related to MCSs, the SNARE (Soluble NFS attachment protein receptor)-mediated membrane fusion, involved for example in the highly regulated release of neurotransmitters at the synapse in animals (Chen and Scheller, 2001), proves the need for multidisciplinary tools to understand the molecular operations and underlying subtleties. Animal synaptotagmin 1 (Syt1), a tether protein that possesses a transmembrane domain and two C2 domains, is a major actor of SNARE as it is implicated in each step of the neurotransmitter release process. For example, the role of PIP, PS and calcium in PM docking of Syt1 C2 domains and bridging of the membranes was revealed by using isothermal titration calorimetry (ITC), fluorescence energy transfer (FRET) and vesicle sedimentation assays, NMR and computational modeling (Lin et al., 2014; Pérez-Lara et al., 2016). Understanding the causes and function of the ring-like oligomerization of Syt1 and the role of tandem C2 domain interaction was performed using electron microscopy, circular dichroism, ITC, atomic force microscopy, floatation, and sedimentation assays (Evans et al., 2016; Zanetti et al., 2016). Comprehending the nature of the Syt1-SNARE complex interaction was possible mainly through NMR and molecular modeling and dynamics (Brewer et al., 2015). All these techniques brought an integrated vision of the dynamic molecular mechanisms occurring at this crucial interface. We believe that employing similar resources for MCS-associated processes would undoubtedly bring us new and original insights in these peculiar systems of cell biology.

## CONCLUSION

There is still a lot to be done in the understanding of plant EPCS function and the molecular mechanisms involved in their

<sup>1</sup> <http://cgmartini.nl/>

## REFERENCES

- Aimon, S., Callan-Jones, A., Berthaud, A., Pinot, M., Toombes, G. E. S., and Bassereau, P. (2014). Membrane shape modulates transmembrane protein distribution. *Dev. Cell* 28, 212–218. doi: 10.1016/j.devcel.2013.12.012
- Baoukina, S., Ingólfsson, H. I., Marrink, S. J., and Tieleman, D. P. (2018). Curvature-induced sorting of lipids in plasma membrane tethers. *Biophys. J.* 1:1800034. doi: 10.1002/adts.201800034

dynamics and regulation. Important questions concern the function and role of membrane compartmentalization (lipid nanodomains, inner/outer leaflet composition, interdigitation), the molecular mechanisms associated with the tethering machinery at MCSs (tethers' identity, effect of tethering in lipid transfer and signaling pathways) and the roles of the lipid environment in the definition of MCSs (regulation, dynamics). However, increasing technical resources have helped to grasp pieces of the puzzle that we are only now starting to assemble. The complexity arising from the incredible diversity in lipids and proteins and, over all, the complex relationships that interconnect them are not making the task easy to accomplish. The biophysical properties of the membrane derived from the intrinsic nature of a plethora of lipids species and their mutual interactions, is impacting on the recruitment and function of proteins, which in turn are fine tuning their lipid environment. The effects of this cycle are expected to get even more intertwined inside very confined environments, such as MCSs, and the entanglement is such that every molecule and every interaction is part of the dance, driving short or long-term consequences on MCS function.

## AUTHOR CONTRIBUTIONS

JP did the writing, figure, and table. FI and LL did the corrections and advised on the manuscript content. EB supervised the writing and did the corrections and comments.

## FUNDING

This work was supported by the National Agency for Research (Grant ANR-14-CE19-0006-01 to EB), the European Research Council (ERC) under the European Union's Horizon 2020 research and innovation program (Grant Agreement No. 772103-BRIDGING to EB), "Osez l'interdisciplinarité" Centre National Recherche Scientifique to EB, Fonds National de la Recherche Scientifique (NEAMEMB PDR T.1003.14 and BRIDGING CDR J.0114.18 to LL). JP was funded by a Ph.D. fellowship from the Belgian "Formation à la Recherche dans l'Industrie et l'Agriculture" (FRIA grant n° 1.E.096.18).

## ACKNOWLEDGMENTS

We thank Sebastien Mondgrand for his critics and comments during the redaction of this review.

- Barbosa, I. C. R., Shikata, H., Zourelidou, M., Heilmann, M., Heilmann, I., and Schwechheimer, C. (2016). Phospholipid composition and a polybasic motif determine D6 PROTEIN KINASE polar association with the plasma membrane and tropic responses. *Development* 143, 4687–4700. doi: 10.1242/dev.137117
- Basyn, F., Charletoaux, B., Thomas, A., and Brasseur, R. (2001). Prediction of membrane protein orientation in lipid bilayers: a theoretical approach. *J. Mol. Graph. Model.* 20, 235–244. doi: 10.1016/S1093-3263(01)00114-0

- Bayer, E. M., Sparkes, I., Vanneste, S., and Rosado, A. (2017). From shaping organelles to signalling platforms: the emerging functions of plant ER-PM contact sites. *Curr. Opin. Plant Biol.* 40, 89–96. doi: 10.1016/j.pbi.2017.08.006
- Bian, X., Saheki, Y., and De Camilli, P. (2018). Ca<sup>2+</sup> releases E-Syt1 autoinhibition to couple ER-plasma membrane tethering with lipid transport. *EMBO J.* 37, 219–234. doi: 10.15252/embj.201797359
- Bigay, J., and Antonny, B. (2012). Curvature, lipid packing, and electrostatics of membrane organelles: defining cellular territories in determining specificity. *Dev. Cell* 23, 886–895. doi: 10.1016/j.devcel.2012.10.009
- Bilkova, E., Pleskot, R., Rissanen, S., Sun, S., Czogalla, A., Cwiklik, L., et al. (2017). Calcium directly regulates phosphatidylinositol 4,5-bisphosphate headgroup conformation and recognition. *J. Am. Chem. Soc.* 139, 4019–4024. doi: 10.1021/jacs.6b11760
- Braut, M., Petit, J. D., Immel, F., Nicolas, W. J., Brocard, L., Gaston, A., et al. (2018). Multiple C2 domains and transmembrane region proteins (MCTPs) tether membranes at plasmodesmata. *bioRxiv* [Preprint]. doi: 10.1101/423905
- Brewer, K. D., Bacaj, T., Cavalli, A., Camilloni, C., Swarbrick, J. D., Liu, J., et al. (2015). Dynamic binding mode of a Synaptotagmin-1-SNARE complex in solution. *Nat. Struct. Mol. Biol.* 22, 555–564. doi: 10.1038/nsmb.3035
- Brunkard, J. O., Runkel, A. M., and Zambryski, P. C. (2015). The cytosol must flow: intercellular transport through plasmodesmata. *Curr. Opin. Cell Biol.* 35, 13–20. doi: 10.1016/j.ceb.2015.03.003
- Brunkard, J. O., and Zambryski, P. C. (2017). Plasmodesmata enable multicellularity: new insights into their evolution, biogenesis, and functions in development and immunity. *Curr. Opin. Plant Biol.* 35, 76–83. doi: 10.1016/j.pbi.2016.11.007
- Burkart, R. C., and Stahl, Y. (2017). Dynamic complexity: plant receptor complexes at the plasma membrane. *Curr. Opin. Plant Biol.* 40, 15–21. doi: 10.1016/j.pbi.2017.06.016
- Cacas, J.-L., Buré, C., Grosjean, K., Gerbeau-Pissot, P., Lherminier, J., Rombouts, Y., et al. (2016). Revisiting plant plasma membrane lipids in tobacco: a focus on sphingolipids. *Plant Physiol.* 170, 367–384. doi: 10.1104/pp.15.00564
- Calvez, P., Demers, E., Boisselier, E., and Salses, C. (2011). Analysis of the contribution of saturated and polyunsaturated phospholipid monolayers to the binding of proteins. *Langmuir* 27, 1373–1379. doi: 10.1021/la104097n
- Chen, X., Yao, Q., Gao, X., Jiang, C., Harberd, N. P., and Fu, X. (2016a). Shoot-to-root mobile transcription factor HY5 coordinates plant carbon and nitrogen acquisition. *Curr. Biol.* 26, 640–646. doi: 10.1016/j.cub.2015.12.066
- Chen, Z., Atefi, E., and Baumgart, T. (2016b). Membrane shape instability induced by protein crowding. *Biophys. J.* 111, 1823–1826. doi: 10.1016/j.bpj.2016.09.039
- Chen, Y. A., and Scheller, R. H. (2001). SNARE-mediated membrane fusion. *Nature* 2, 98–106.
- Choudhary, V., Golani, G., Joshi, A. S., Cottier, S., Schneiter, R., Prinz, W. A., et al. (2018). Architecture of lipid droplets in endoplasmic reticulum is determined by phospholipid intrinsic curvature. *Curr. Biol.* 28:915-926.e9. doi: 10.1016/j.cub.2018.02.020
- Chung, J., Torta, F., Masai, K., Lucast, L., Czaplá, H., Tanner, L. B., et al. (2015). PI4P/phosphatidylserine countertransport at ORP5- and ORP8-mediated ER-plasma membrane contacts. *Science* 349, 428–432. doi: 10.1126/science.aab1370
- Collado, J., and Fernández-Busnadiego, R. (2017). Deciphering the molecular architecture of membrane contact sites by cryo-electron tomography. *Biochim. Biophys. Acta Mol. Cell Res.* 1864, 1507–1512. doi: 10.1016/j.bbamcr.2017.03.009
- Cui, H., Lyman, E., and Voth, G. A. (2011). Mechanism of membrane curvature sensing by amphipathic helix containing proteins. *Biophys. J.* 100, 1271–1279. doi: 10.1016/j.bpj.2011.01.036
- Deleu, M., Crowet, J. M., Nasir, M. N., and Lins, L. (2014). Complementary biophysical tools to investigate lipid specificity in the interaction between bioactive molecules and the plasma membrane: a review. *Biochim. Biophys. Acta Biomembr.* 1838, 3171–3190. doi: 10.1016/j.bbamem.2014.08.023
- Diao, J., Liu, R., Rong, Y., Zhao, M., Zhang, J., Lai, Y., et al. (2015). ATG14 promotes membrane tethering and fusion of autophagosomes to endolysosomes. *Nature* 520, 563–566. doi: 10.1038/nature14147
- Doosti, B. A., Pezeshkian, W., Bruhn, D. S., Ipsen, J. H., Khandelia, H., Jeffries, G. D. M., et al. (2017). Membrane tubulation in lipid vesicles triggered by the local application of calcium ions. *Langmuir* 33, 11010–11017. doi: 10.1021/acs.langmuir.7b01461
- Dufourc, E. J. (2008). Sterols and membrane dynamics. *J. Chem. Biol.* 1, 63–77. doi: 10.1007/s12154-008-0010-6
- Duncan, A. L., Reddy, T., Koldso, H., Hélie, J., Fowler, P. W., Chavent, M., et al. (2017). Protein crowding and lipid complexity influence the nanoscale dynamic organization of ion channels in cell membranes. *Sci. Rep.* 7:16647. doi: 10.1038/s41598-017-16865-6
- Eden, E. R., White, I. J., Tsapara, A., and Futter, C. E. (2010). Membrane contacts between endosomes and ER provide sites for PTP1B-epidermal growth factor receptor interaction. *Nat. Cell Biol.* 12, 267–272. doi: 10.1038/ncb2026
- Eeman, M., Berquand, A., Dufrière, Y. F., Paquot, M., Dufour, S., and Deleu, M. (2006). Penetration of surfactin into phospholipid monolayers: nanoscale interfacial organization. *Langmuir* 22, 11337–11345. doi: 10.1021/la061969p
- Eisenberg-Bord, M., Shai, N., Schuldiner, M., and Bohnert, M. (2016). A tether is a tether: tethering at membrane contact sites. *Dev. Cell* 39, 395–409. doi: 10.1016/j.devcel.2016.10.022
- Evans, C. S., He, Z., Bai, H., Lou, X., Jeggle, P., Sutton, R. B., et al. (2016). Functional analysis of the interface between the tandem C2 domains of synaptotagmin-1. *Mol. Biol. Cell* 27, 979–989. doi: 10.1091/mbc.E15-07-0503
- Fernandez-calvino, L., Faulkner, C., Walshaw, J., Saalbach, G., Benitez-alfonso, Y., and Maule, A. (2011). Arabidopsis plasmodesmal proteome. *PLoS One* 6:e018880. doi: 10.1371/journal.pone.0018880
- Fujimoto, M., Hayashi, T., and Su, T. P. (2011). The role of cholesterol in the association of endoplasmic reticulum membranes with mitochondria. *Biochem. Biophys. Res. Commun.* 417, 635–639. doi: 10.1016/j.bbrc.2011.12.022
- Furuta, K., Lichtenberger, R., and Helariutta, Y. (2012). The role of mobile small RNA species during root growth and development. *Curr. Opin. Cell Biol.* 24, 211–216. doi: 10.1016/j.ceb.2011.12.005
- Gatta, A. T., and Levine, T. P. (2017). Piecing together the patchwork of contact sites. *Trends Cell Biol.* 27, 214–229. doi: 10.1016/j.tcb.2016.08.010
- Gautier, R., Bacle, A., Tiberti, M. L., Fuchs, P. F., Vanni, S., and Antonny, B. (2018). PackMem: a versatile tool to compute and visualize interfacial packing defects in lipid bilayers. *Biophys. J.* 115, 436–444. doi: 10.1016/j.bpj.2018.06.025
- Genç, Ö., Dickman, D. K., Ma, W., Tong, A., Fetter, R. D., and Davis, G. W. (2017). MCTP is an ER-resident calcium sensor that stabilizes synaptic transmission and homeostatic plasticity. *eLife* 6:e22904. doi: 10.7554/eLife.22904
- Ghai, R., Du, X., Wang, H., Dong, J., Ferguson, C., Brown, A. J., et al. (2017). ORP5 and ORP8 bind phosphatidylinositol-4,5-bisphosphate (PtdIns(4,5)P<sub>2</sub>) and regulate its level at the plasma membrane. *Nat. Commun.* 8:757. doi: 10.1038/s41467-017-00861-5
- Ghai, R., Falconer, R. J., and Collins, B. M. (2012). Applications of isothermal titration calorimetry in pure and applied research survey of the literature from 2010. *J. Mol. Recognit.* 25, 32–52. doi: 10.1002/jmr.1167
- Graber, Z. T., Shi, Z., and Baumgart, T. (2017). Cations induce shape remodeling of negatively charged phospholipid membranes. *Phys. Chem. Chem. Phys.* 19, 15285–15295. doi: 10.1039/c7cp00718c
- Grisson, M. S., Brocard, L., Fouillen, L., Nicolas, W., Wewer, V., Dörmann, P., et al. (2015). Specific membrane lipid composition is important for plasmodesmata function in Arabidopsis. *Plant Cell* 27, 1228–1250. doi: 10.1105/tpc.114.135731
- Gronnier, J., Crowet, J.-M., Habenstein, B., Nasir, M. N., Bayle, V., Hosy, E., et al. (2017). Structural basis for plant plasma membrane protein dynamics and organization into functional nanodomains. *eLife* 6:e26404. doi: 10.7554/eLife.26404
- Gronnier, J., Gerbeau-Pissot, P., Germain, V., Mongrand, S., and Simon-Plas, F. (2018). Divide and rule: plant plasma membrane organization. *Trends Plant Sci.* 23, 899–917. doi: 10.1016/j.tplants.2018.07.007
- Gronnier, J., Germain, V., Gouguet, P., Cacas, J. L., and Mongrand, S. (2016). GIPC: glycosyl inositol phospho ceramides, the major sphingolipids on earth. *Plant Signal. Behav.* 11:e1152438. doi: 10.1080/15592324.2016.1152438
- Grosjean, K., Mongrand, S., Beney, L., Simon-Plas, F., and Gerbeau-Pissot, P. (2015). Differential effect of plant lipids on membrane organization specificities of phytosphingolipids and phytosterols. *J. Biol. Chem.* 290, 5810–5825. doi: 10.1074/jbc.M114.598805
- Haj, F. G., Sabet, O., Kinkhabwala, A., Wimmer-Kleikamp, S., Roukos, V., Han, H. M., et al. (2012). Regulation of signaling at regions of cell-cell contact by endoplasmic reticulum-bound protein-tyrosine phosphatase 1B. *PLoS One* 7:e0036633. doi: 10.1371/journal.pone.0036633

- Hanada, K. (2018). Lipid transfer proteins rectify inter-organelle flux and accurately deliver lipids at membrane contact sites. *J. Lipid Res.* 59, 1341–1366. doi: 10.1194/jlr.R085324
- Harayama, T., and Riezman, H. (2018). Understanding the diversity of membrane lipid composition. *Nat. Rev. Mol. Cell Biol.* 19, 281–296. doi: 10.1038/nrm.2017.138
- Henne, W. M., Liou, J., and Emr, S. D. (2015). Molecular mechanisms of inter-organelle ER – PM contact sites. *Curr. Opin. Cell Biol.* 35, 123–130. doi: 10.1016/j.ccb.2015.05.001
- Henrich, E., Löhr, F., Pawlik, G., Peetz, O., Dötsch, V., Morgner, N., et al. (2018). Lipid conversion by cell-free synthesized phospholipid methyltransferase opi3 in defined nanodisc membranes supports an in trans mechanism. *Biochemistry* 57, 5780–5784. doi: 10.1021/acs.biochem.8b00807
- Himschoot, E., Pleskot, R., Van Damme, D., and Vanneste, S. (2017). The ins and outs of Ca<sup>2+</sup>-in plant endomembrane trafficking. *Curr. Opin. Plant Biol.* 40, 131–137. doi: 10.1016/j.pbi.2017.09.003
- Hsu, P. C., Samsudin, F., Shearer, J., and Khalid, S. (2017). It is complicated: curvature, diffusion, and lipid sorting within the two membranes of *Escherichia coli*. *J. Phys. Chem. Lett.* 8, 5513–5518. doi: 10.1021/acs.jpcclett.7b02432
- Huster, D. (2014). Solid-state NMR spectroscopy to study protein-lipid interactions. *Biochim. Biophys. Acta Mol. Cell Biol. Lipids* 1841, 1146–1160. doi: 10.1016/j.bbalip.2013.12.002
- Idevall-hagen, O., Lü, A., Xie, B., and De Camilli, P. (2015). Triggered Ca<sup>2+</sup>-influx is required for extended synaptotagmin 1-induced ER-plasma membrane tethering. *EMBO J.* 34, 2291–2305. doi: 10.15252/embj.201591565
- Jackson, C. L., Walch, L., and Verbavatz, J. (2016). Lipids and their trafficking: an integral part of cellular organization. *Dev. Cell* 39, 139–153. doi: 10.1016/j.devcel.2016.09.030
- Jain, A., and Holthuis, J. C. M. (2017). Membrane contact sites, ancient and central hubs of cellular lipid logistics. *Biochim. Biophys. Acta Mol. Cell Res.* 1864, 1450–1458. doi: 10.1016/j.bbamer.2017.05.017
- Javanainen, M., Martinez-Seara, H., and Vattulainen, I. (2017). Nanoscale membrane domain formation driven by cholesterol. *Sci. Rep.* 7, 1143. doi: 10.1038/s41598-017-01247-9
- Joshi, A. S., Nebenfuhr, B., Choudhary, V., Satpute-Krishnan, P., Levine, T. P., Golden, A., et al. (2018). Lipid droplet and peroxisome biogenesis occur at the same ER subdomains. *Nat. Commun.* 9:2940. doi: 10.1038/s41467-018-05277-3
- Kim, I., Cho, E., Crawford, K., Hempel, F. D., and Zambryski, P. C. (2005). Cell-to-cell movement of GFP during embryogenesis and early seedling development in Arabidopsis. *PNAS* 102, 2227–2231. doi: 10.1073/pnas.0409193102
- Kraner, M. E., Müller, C., and Sonnewald, U. (2017). Comparative proteomic profiling of the choline transporter-like 1 (CHERT) mutant provides insights into plasmodesmata composition of fully developed *Arabidopsis thaliana* leaves. *Plant J.* 92, 696–709. doi: 10.1111/tj.13702
- Lahiri, S., Toulmay, A., and Prinz, W. A. (2015). Membrane contact sites, gateways for lipid homeostasis. *Curr. Opin. Cell Biol.* 33, 82–87. doi: 10.1016/j.ccb.2014.12.004
- Lees, J. A., Messa, M., Sun, E. W., Wheeler, H., Torta, F., Wenk, M. R., et al. (2017). Lipid transport by TMEM24 at ER-plasma membrane contacts regulates pulsatile insulin secretion. *Science* 355:eaah6171. doi: 10.1126/science.aah6171
- Leijon, F., Melzer, M., Zhou, Q., Srivastava, V., and Bulone, V. (2018). Proteomic analysis of plasmodesmata from populus cell suspension cultures in relation with callose biosynthesis. *Front. Plant Sci.* 9:1681. doi: 10.3389/fpls.2018.01681
- Levental, K. R., Lorent, J. H., Lin, X., Skinkle, A. D., Surma, M. A., Stockenbojer, E. A., et al. (2016). Polyunsaturated lipids regulate membrane domain stability by tuning membrane order. *Biophys. J.* 110, 1800–1810. doi: 10.1016/j.bpj.2016.03.012
- Lin, C. C., Seikowski, J., Pérez-Lara, A., Jahn, R., Höbartner, C., and Walla, P. J. (2014). Control of membrane gaps by synaptotagmin-Ca<sup>2+</sup>-measured with a novel membrane distance ruler. *Nat. Commun.* 5:5859. doi: 10.1038/ncomms6859
- Lins, L., Charlotteaux, B., Thomas, A., and Bresseur, R. (2001). Computational study of lipid-destabilizing protein fragments: towards a comprehensive view of tilted peptides. *Proteins Struct. Funct. Genet.* 44, 435–447. doi: 10.1002/prot.1109
- Lorent, J. H., Diaz-Rohrer, B., Lin, X., Spring, K., Gorfé, A. A., Levental, K. R., et al. (2017). Structural determinants and functional consequences of protein affinity for membrane rafts. *Nat. Commun.* 8, 1219. doi: 10.1038/s41467-017-01328-3
- Manford, A. G., Stefan, C. J., Yuan, H. L., Macgurn, J. A., and Emr, S. D. (2012). ER-to-plasma membrane tethering proteins regulate cell signaling and morphology. *Dev. Cell* 23, 1129–1140. doi: 10.1016/j.devcel.2012.11.004
- Marrink, S. J., Risselada, H. J., Yefimov, S., Tieleman, D. P., and De Vries, A. H. (2007). The martini force field: coarse grained model for biomolecular simulations. *J. Phys. Chem. B* 111, 7812–7824. doi: 10.1021/jp071097f
- Meca, J., Massoni-laporte, A., Martinez, D., Sartorel, E., Loquet, A., and Mccusker, D. (2018). Avidity-driven polarity establishment via multivalent lipid – GTPase module interactions. *EMBO J.* 38:e99652. doi: 10.15252/embj.201899652
- Mesmin, B., Bigay, J., Moser Von Filseck, J., Lacas-Gervais, S., Drin, G., and Antonny, B. (2013). A four-step cycle driven by PI(4)P hydrolysis directs sterol/PI(4)P exchange by the ER-Golgi tether OSBP. *Cell* 155, 830–843. doi: 10.1016/j.cell.2013.09.056
- Milovanovic, D., Honigmann, A., Koike, S., Göttfert, F., Pähler, G., Junius, M., et al. (2015). Hydrophobic mismatch sorts SNARE proteins into distinct membrane domains. *Nat. Commun.* 6:5984. doi: 10.1038/ncomms6984
- Moser von Filseck, J., and Drin, G. (2016). Running up that hill: how to create cellular lipid gradients by lipid counter-flows. *Biochimie* 130, 115–121. doi: 10.1016/j.biochi.2016.08.001
- Muallem, S., Chung, W. Y., Jha, A., and Ahuja, M. (2017). Lipids at membrane contact sites: cell signaling and ion transport. *EMBO Rep.* 18:e201744331. doi: 10.15252/embr.201744331
- Nicolas, W. J., Grison, M. S., Trépot, S., Gaston, A., Fouché, M., Cordelières, F. P., et al. (2017). Architecture and permeability of post-cytokinesis plasmodesmata lacking cytoplasmic sleeves. *Nat. Plants* 3, 17802. doi: 10.1038/nplants.2017.82
- Olkkonen, V. M. (2015). OSBP-related protein family in lipid transport over membrane contact sites. *Lipid Insights* 8(Suppl. 1), 1–9. doi: 10.4137/Lpi.s31726
- Pérez-Lara, Á., Thapa, A., Nyenhuis, S. B., Nyenhuis, D. A., Halder, P., Tietzel, M., et al. (2016). PtdInsP2 and PtdSer cooperate to trap synaptotagmin-1 to the plasma membrane in the presence of calcium. *eLife* 5:e15886. doi: 10.7554/eLife.15886
- Pérez-Sancho, J., Schapiro, A. L., Botella, M. A., and Rosado, A. (2016). “Analysis of protein-lipid interactions using purified C2 domains,” in *Methods in Molecular Biology. Plant Signal Transduction: Methods and Protocols*, eds J. R. Botella and M. A. Botella (New York, NY: Springer), 175–187.
- Pérez-Sancho, J., Vanneste, S., Lee, E., Mcfarlane, H. E., Esteban del Valle, A., Valpuesta, V., et al. (2015). The arabidopsis synaptotagmin1 is enriched in endoplasmic reticulum-plasma membrane contact sites and confers cellular resistance to mechanical stresses 1 [ OPEN ]. *Plant Physiol.* 168, 132–143. doi: 10.1104/pp.15.00260
- Petkovic, M., Jemaiel, A., Daste, F., Specht, C. G., Izeddin, I., Vorkel, D., et al. (2014). The SNARE Sec22b has a non-fusogenic function in plasma membrane expansion. *Nat. Cell Biol.* 16, 434–444. doi: 10.1038/ncb2937
- Platre, M. P., Noack, L. C., Doumane, M., Bayle, V., Simon, M. L. A., Maneta-Peyret, L., et al. (2018). A combinatorial lipid code shapes the electrostatic landscape of plant endomembranes. *Dev. Cell* 45, 465–480. doi: 10.1016/j.devcel.2018.04.011
- Prévost, C., Zhao, H., Manzi, J., Lemichez, E., Lappalainen, P., Callan-Jones, A., et al. (2015). IRSp53 senses negative membrane curvature and phase separates along membrane tubules. *Nat. Commun.* 6:8529. doi: 10.1038/ncomms9529
- Quon, E., Sere, Y. Y., Chauhan, N., Johansen, J., Sullivan, D. P., Dittman, J. S., et al. (2018). Endoplasmic reticulum-plasma membrane contact sites integrate sterol and phospholipid regulation. *PLoS Biol.* 16:e2003864. doi: 10.1371/journal.pbio.2003864
- Raghupathy, R., Anilkumar, A. A., Polley, A., Singh, P. P., Yadav, M., Johnson, C., et al. (2015). Transbilayer lipid interactions mediate nanoclustering of lipid-anchored proteins. *Cell* 161, 581–594. doi: 10.1016/j.cell.2015.03.048
- Ramakrishnan, N., Bradley, R. P., Tourdot, R. W., and Radhakrishnan, R. (2018). Biophysics of membrane curvature remodeling at molecular and mesoscopic length scales. *J. Phys. Condens. Matter* 30:273001. doi: 10.1088/1361-648X/30/27/aac702
- Rutschow, H. L., Baskin, T. I., and Kramer, E. M. (2011). Regulation of solute flux through plasmodesmata in the root meristem. *Plant Physiol.* 155, 1817–1826. doi: 10.1104/pp.110.168187
- Saheki, Y., and De Camilli, P. (2017). The Extended-Synaptotagmins. *Biochim. Biophys. Acta Mol. Cell Res.* 1864, 1490–1493. doi: 10.1016/j.bbamer.2017.03.013

















- Saint-jean, M., De Delfosse, V., Douguet, D., Chicanne, G., Payrastra, B., Bourguet, W., et al. (2011). Osh4p exchanges sterols for phosphatidylinositol 4-phosphate between lipid bilayers. *J. Cell Biol.* 195, 965–978. doi: 10.1083/jcb.201104062
- Salmon, M. S., and Bayer, E. M. F. (2013). Dissecting plasmodesmata molecular composition by mass spectrometry-based proteomics. *Front. Plant Sci.* 3:307. doi: 10.3389/fpls.2012.00307
- Schapiro, A. L., Voigt, B., Jasik, J., Rosado, A., Lopez-Cobollo, R., Menzel, D., et al. (2008). Arabidopsis synaptotagmin 1 is required for the maintenance of plasma membrane integrity and cell viability. *Plant Cell* 20, 3374–3388. doi: 10.1105/tpc.108.063859
- Seo, J. B., Jung, S. R., Huang, W., Zhang, Q., and Koh, D. S. (2015). Charge shielding of PIP2 by cations regulates enzyme activity of phospholipase C. *PLoS One* 10:e0144432. doi: 10.1371/journal.pone.0144432
- Sezgin, E., Levental, I., Mayor, S., and Eggeling, C. (2017). The mystery of membrane organization: composition, regulation and roles of lipid rafts. *Nat. Rev. Mol. Cell Biol.* 18, 361–374. doi: 10.1038/nrm.2017.16
- Shin, J. J. H., Loewen, C. J. R., Shin, J. J. H., and Loewen, C. J. R. (2011). Putting the pH into phosphatidic acid signaling. *BMC Biol.* 9:85. doi: 10.1186/1741-7007-9-85
- Simon, M. L. A., Platre, M. P., Marqués-Bueno, M. M., Armengot, L., Stanislas, T., Bayle, V., et al. (2016). A PtdIns(4)P-driven electrostatic field controls cell membrane identity and signalling in plants. *Nat. Plants* 2:16089. doi: 10.1038/NPLANTS.2016.89
- Simunovic, M., Voth, G. A., Callan-Jones, A., and Bassereau, P. (2015). When physics takes over: bar proteins and membrane curvature. *Trends Cell Biol.* 25, 780–792. doi: 10.1016/j.tcb.2015.09.005
- Strahl, H., Ronneau, S., González, B. S., Klutsch, D., Schaffner-Barbero, C., and Hamoen, L. W. (2015). Transmembrane protein sorting driven by membrane curvature. *Nat. Commun.* 6:8728. doi: 10.1038/ncomms9728
- Tanguy, E., Kassas, N., and Vitale, N. (2018). Protein–phospholipid interaction motifs: a focus on phosphatidic acid. *Biomolecules* 8:20. doi: 10.3390/biom8020020
- Tilsner, J., Nicolas, W., Rosado, A., and Bayer, E. M. (2016). Staying tight: plasmodesmal membrane contact sites and the control of cell-to-cell connectivity in plants. *Annu. Rev. Plant Biol.* 67, 337–364. doi: 10.1146/annurev-arplant-043015-111840
- Tong, J., Manik, M. K., and Im, Y. J. (2018). Structural basis of sterol recognition and nonvesicular transport by lipid transfer proteins anchored at membrane contact sites. *Proc. Natl. Acad. Sci. U.S.A.* 115, E856–E865. doi: 10.1073/pnas.1719709115
- Tripathy, M., Iyer, S. S., and Srivastava, A. (2018). Molecular origin of spatiotemporal heterogeneity in biomembranes with coexisting liquid phases: insights from topological rearrangements and lipid packing defects. *Adv. Biomed. Lipid Self-Assembly* 28, 87–114. doi: 10.1016/bs.abl.2018.06.001
- Vanni, S., Vamparys, L., Gautier, R., Drin, G., Etchebest, C., Fuchs, P. F. J., et al. (2013). Amphipathic lipid packing sensor motifs: probing bilayer defects with hydrophobic residues. *Biophys. J.* 104, 575–584. doi: 10.1016/j.bpj.2012.11.3837
- Wang, P., Hawes, C., and Hussey, P. J. (2017). Plant endoplasmic reticulum–plasma membrane contact sites. *Trends Plant Sci.* 22, 289–297. doi: 10.1016/j.tplants.2016.11.008
- Weiner, M. D., and Feigenson, G. W. (2018). Presence and role of midplane cholesterol in lipid bilayers containing registered or antiregistered phase domains. *J. Phys. Chem. B* 122, 8193–8200. doi: 10.1021/acs.jpcc.8b03949
- Wong, L. H., Gatta, A. T., and Levine, T. P. (2018). Lipid transfer proteins: the lipid commute via shuttles, bridges and tubes. *Nat. Rev. Mol. Cell Biol.* 20, 85–101. doi: 10.1038/s41580-018-0071-5
- Wu, H. M., Lin, Y. H., Yen, T. C., and Hsieh, C. L. (2016). Nanoscopic substructures of raft-mimetic liquid-ordered membrane domains revealed by high-speed single-particle tracking. *Sci. Rep.* 6:20542. doi: 10.1038/srep20542
- Yamaji, T., Kumagai, K., Tomishige, N., and Hanada, K. (2008). Two sphingolipid transfer proteins, CERT and FAPP2: their roles in sphingolipid metabolism. *IUBMB Life* 60, 511–518. doi: 10.1002/iub.83
- Yamamoto, E., Kalli, A. C., Yasuoka, K., and Sansom, M. S. P. (2016). Interactions of pleckstrin homology domains with membranes: adding back the bilayer via high-throughput molecular dynamics. *Struct. Des.* 24, 1421–1431. doi: 10.1016/j.str.2016.06.002
- Zanetti, M. N., Bello, O. D., Wang, J., Coleman, J., Cai, Y., Sindelar, C. V., et al. (2016). Ring-like oligomers of synaptotagmins and related C2 domain proteins. *eLife* 5:e17262. doi: 10.7554/eLife.17262
- Zhou, Q., Zhou, P., Wang, A. L., Wu, D., Zhao, M., Südhof, T. C., et al. (2017). The primed SNARE-complexin-synaptotagmin complex for neuronal exocytosis. *Nature* 548, 420–425. doi: 10.1038/nature23484

**Conflict of Interest Statement:** The authors declare that the research was conducted in the absence of any commercial or financial relationships that could be construed as a potential conflict of interest.

Copyright © 2019 Petit, Immel, Lins and Bayer. This is an open-access article distributed under the terms of the Creative Commons Attribution License (CC BY). The use, distribution or reproduction in other forums is permitted, provided the original author(s) and the copyright owner(s) are credited and that the original publication in this journal is cited, in accordance with accepted academic practice. No use, distribution or reproduction is permitted which does not comply with these terms.

# Multiple C2 domains and transmembrane region proteins (MCTPs) tether membranes at plasmodesmata

Marie L Brault<sup>1,¶</sup>, Jules D Petit<sup>1,2,¶</sup> , Françoise Immel<sup>1</sup> , William J Nicolas<sup>1,†</sup> , Marie Glavier<sup>1</sup> , Lysiane Brocard<sup>3</sup>, Amèlia Gaston<sup>1,‡</sup> , Mathieu Fouché<sup>1,‡</sup>, Timothy J Hawkins<sup>4</sup>, Jean-Marc Crowet<sup>2,§</sup> , Magali S Grison<sup>1</sup> , Véronique Germain<sup>1</sup>, Marion Rocher<sup>1</sup>, Max Kraner<sup>5</sup>, Vikram Alva<sup>6</sup> , Stéphane Claverol<sup>7</sup>, Andrea Paterlini<sup>8</sup> , Ykä Helariutta<sup>8</sup> , Magali Deleu<sup>2</sup> , Laurence Lins<sup>2</sup> , Jens Tilsner<sup>9,10,\*</sup>  & Emmanuelle M Bayer<sup>1,\*\*</sup> 

## Abstract

In eukaryotes, membrane contact sites (MCS) allow direct communication between organelles. Plants have evolved a unique type of MCS, inside intercellular pores, the plasmodesmata, where endoplasmic reticulum (ER)–plasma membrane (PM) contacts coincide with regulation of cell-to-cell signalling. The molecular mechanism and function of membrane tethering within plasmodesmata remain unknown. Here, we show that the multiple C2 domains and transmembrane region protein (MCTP) family, key regulators of cell-to-cell signalling in plants, act as ER-PM tethers specifically at plasmodesmata. We report that MCTPs are plasmodesmata proteins that insert into the ER via their transmembrane region while their C2 domains dock to the PM through interaction with anionic phospholipids. A *Atmctp3/Atmctp4* loss of function mutant induces plant developmental defects, impaired plasmodesmata function and composition, while MCTP4 expression in a yeast  $\Delta$ tether mutant partially restores ER-PM tethering. Our data suggest that MCTPs are unique membrane tethers controlling both ER-PM contacts and cell-to-cell signalling.

**Keywords** ER-PM membrane contact sites; intercellular communication in plants; multiple C2 domains and transmembrane region proteins; plasmodesmata

**Subject Categories** Membrane & Intracellular Transport; Plant Biology  
**DOI** 10.15252/embr.201847182 | Received 3 October 2018 | Revised 28 May 2019 | Accepted 6 June 2019 | Published online 9 July 2019  
**EMBO Reports (2019) 20: e47182**

## Introduction

Intercellular communication is essential for the establishment of multicellularity, and evolution gave rise to distinct mechanisms to facilitate this process. Plants have developed singular intercellular pores—the plasmodesmata—which span the cell wall and interconnect nearly every single cell, establishing direct membrane and cytoplasmic continuity throughout the plant body [1]. Plasmodesmata are indispensable for plant life. They control the intercellular trafficking of non-cell-autonomous signals such as transcription factors, small RNAs, hormones and metabolites during key growth and developmental events [1–11]. Over the past few years, plasmodesmata have emerged as key components of plant defence signalling [12–14]. Mis-regulation of plasmodesmata function can lead to severe defects in organ growth and tissue patterning but also generate inappropriate responses to biotic and abiotic stresses [7,8,12,15–17]. Plasmodesmata not only serve as conduits, but act as

1 Laboratoire de Biogenèse Membranaire, UMR5200, CNRS, Université de Bordeaux, Villenave d'Ornon, France  
 2 Laboratoire de Biophysique Moléculaire aux Interfaces, TERRA Research Centre, GX ABT, Université de Liège, Gembloux, Belgium  
 3 Bordeaux Imaging Centre, Plant Imaging Platform, UMS 3420, INRA-CNRS-INSERM-University of Bordeaux, Villenave-d'Ornon, France  
 4 Department of Biosciences, University of Durham, Durham, UK  
 5 Division of Biochemistry, Department of Biology, Friedrich-Alexander University Erlangen-Nuremberg, Erlangen, Germany  
 6 Department of Protein Evolution, Max Planck Institute for Developmental Biology, Tübingen, Germany  
 7 Proteome Platform, Functional Genomic Center of Bordeaux, University of Bordeaux, Bordeaux Cedex, France  
 8 The Sainsbury Laboratory, University of Cambridge, Cambridge, UK  
 9 Biomedical Sciences Research Complex, University of St Andrews, Fife, UK  
 10 Cell and Molecular Sciences, The James Hutton Institute, Dundee, UK  
 \*Corresponding author. Tel: +44 1334 464829; E-mail: jt58@st-andrews.ac.uk  
 \*\*Corresponding author. Tel: +33 55712 2539; E-mail: emmanuelle.bayer@u-bordeaux.fr  
 †These authors contributed equally to this work  
 ‡Present address: Division of Biology and Biological Engineering, California Institute of Technology, Pasadena, CA, USA  
 §Present address: UMR 1332 BFP, INRA, University of Bordeaux, Bordeaux, France  
 §Present address: Matrice Extracellulaire et Dynamique Cellulaire MEDyC, UMR7369, CNRS, Université de Reims-Champagne-Ardenne, Reims, France

specialised signalling hubs, capable of generating and/or relaying signals from cell to cell through plasmodesmata-associated receptor activity [18–21].

Plasmodesmata are structurally unique [22,23]. They contain a strand of ER, continuous through the pores, tethered extremely tightly (~10 nm) to the PM by spoke-like elements [24,25] whose function and identity are unknown. Inside plasmodesmata, specialised subdomains of the ER and the PM co-exist, each being characterised by a unique set of lipids and proteins, both critical for proper function [6,12,26–31]. Where it enters the pores, the ER becomes constricted to a 15-nm tube (the desmotubule) leaving little room for luminal trafficking. According to current models, transfer of molecules occurs in the cytoplasmic sleeve between the ER and the PM. Constriction of this gap, by the deposition of callose ( $\beta$ -1,3 glucan), in the cell wall around plasmodesmata, is assumed to be the main regulator of the pore size exclusion limit [4,32]. Recent work, however, suggests a more complex picture where the plasmodesmal ER-PM gap is not directly related to pore permeability and may play additional roles [22,25]. Newly formed plasmodesmata (type I) exhibit such close contact (~2–3 nm) between the PM and the ER that no electron-lucent cytoplasmic sleeve is observed [25]. During subsequent cell growth and differentiation, the pore widens, separating the two membranes, which remain connected by visible electron-dense spokes, leaving a cytosolic gap (type II). This transition has been proposed to be controlled by protein tethers acting at the ER-PM interface [22,33]. Counterintuitively, type I plasmodesmata with no apparent cytoplasmic sleeve are open to macromolecular trafficking and recent data indicate that tight ER-PM contacts may in fact favour transfer of molecules from cell to cell [25,34].

The close proximity of the PM and ER within the pores and the presence of tethers qualify plasmodesmata as a specialised type of ER-to-PM membrane contact site (MCS) [1,33]. MCS are structures found in all eukaryotic cells which function in direct interorganellar signalling by promoting fast, non-vesicular transfer of molecules and allowing collaborative action between the two membranes [35–46]. In yeast and mammalian cells, MCS protein tethers are known to physically bridge the two organelles, to control the intermembrane gap and to participate in organelle cross-talk. Their molecular identity/specificity dictate structural and functional singularity to different types of MCS [47,48]. To date, the plasmodesmal membrane tethers remain unidentified, but by analogy to other types of MCS, it seems likely that they play important roles in plasmodesmal structure and function, and given their unique position within a cell-to-cell junction may link intra- and intercellular communication.

Here, we have reduced the complexity of the previously published *Arabidopsis* plasmodesmal proteome [49] through the combination of a refined purification protocol [28,50,54] and semi-quantitative proteomics, to identify 115 proteins highly enriched in plasmodesmata and identify tether candidates. Amongst the most abundant plasmodesmal proteins, members of the multiple C2 domains and transmembrane region proteins (MCTPs) were enriched in post-cytokinetic plasmodesmata with tight ER-PM contact compared to mature plasmodesmata with wider cytoplasmic gap and sparse spokes, and exhibit the domain architecture characteristic of membrane tethers, with multiple lipid-binding C2 domains in the N-terminal and multiple transmembrane domains in the C-terminal region. Two MCTP members, AtMCTP1/Flower Locus T

Interacting Protein (FTIP) and AtMCTP15/QUIRKY (QKY), have previously been localised to plasmodesmata in *Arabidopsis* and are involved in cell-to-cell signalling [20,51]. However, two recent studies indicate that other MCTP members, including AtMCTP3, AtMCTP4 and AtMCTP9, which show high plasmodesmata enrichment in our proteome, do not associate with the pores *in vivo* [52,53]. Using confocal live cell imaging, 3D structured illumination super-resolution microscopy, correlative light and electron microscopy, immunogold labelling and genetic approaches, we provide evidence that MCTPs, including AtMCTP3 and 4, localise and function at plasmodesmata pores. We further show that *Atmctp3/Atmctp4* loss of function *Arabidopsis* mutant, which displays developmental phenotypic defects, shows reduced cell-to-cell trafficking and a significantly altered plasmodesmata proteome. By combining confocal imaging of truncated MCTP mutants, molecular dynamics and yeast complementation, our data indicate that MCTP properties are consistent with a role in ER-PM membrane tethering at plasmodesmata. As several MCTP members have been identified as important components of plant intercellular signalling [20,51], our data suggest a link between interorganelle contacts at plasmodesmata and intercellular communication in plants.

## Results

### Identification of plasmodesmal ER-PM tethering candidates

To identify putative plasmodesmal MCS tethers, we decided to screen the plasmodesmata proteome for ER-associated proteins (a general trait of ER-PM tethers [47,48]) with structural features enabling bridging across two membranes. A previously published plasmodesmata proteome reported the identification of more than 1,400 proteins in *Arabidopsis* [49], making the discrimination of true plasmodesmata-associated from contaminant proteins a major challenge. To reduce the proteome complexity and identify core plasmodesmata protein candidates, we used a refined plasmodesmata purification technique [28,50,54] together with label-free comparative quantification (Appendix Fig S1A). Plasmodesmata and likely contaminant fractions, namely the PM, microsomal, total cell and cell wall fractions, were purified from 6-day-old *Arabidopsis* suspension culture cells and simultaneously analysed by liquid chromatography–tandem mass spectrometry (LC-MS/MS). For each protein identified, its relative enrichment in the plasmodesmata fraction versus “contaminant” fractions was determined (Appendix Fig S1B; Appendix Table S1). Enrichment ratios for selecting plasmodesmal candidates were set based on previously characterised plasmodesmal proteins (see Materials and Methods for details). This refined proteome dataset was reduced to 115 unique proteins, cross-referenced with two published ER proteomes [55,56] and used as a basis for selecting MCS-relevant candidates.

Alongside, we also analysed changes in protein abundance during the ER-PM tethering transition from very tight contacts in post-cytokinetic plasmodesmata (type I) to larger ER-PM gap and sparse tethers in mature plasmodesmata (type II) [25]. For this, we obtained a similar semi-quantitative proteome from 4- and 7-day-old culture cells, enabling a comparison of plasmodesmata composition during the tethering transition [25] (Appendix Fig S2).

A survey of our refined proteome identified several members of the multiple C2 domains and transmembrane region proteins (MCTPs) family, namely AtMCTP3-7, AtMCTP9, AtMCTP10 and 14–16, as both abundant and highly enriched at plasmodesmata (Appendix Fig S1B, Appendix Table S1). In addition to being plasmodesmata-enriched proteins, our data also suggest that MCTPs are differentially regulated during the ER-PM tethering transition from post-cytokinetic to mature plasmodesmata [25] (Appendix Fig S2). Amongst the 47 plasmodesmal proteins differentially enriched, all MCTPs were more abundant (1.4–3.6 times) in type I (tight ER-PM contacts) compared with type II (open cytoplasmic sleeves) plasmodesmata (Appendix Fig S2).

### MCTPs are ER-associated proteins located at plasmodesmata and present structural features of membrane tethers

MCTPs are structurally reminiscent of the ER-PM tether families of mammalian extended-synaptotagmins (HsE-Syts) and *Arabidopsis* synaptotagmins (AtSYTs) [57,58], possessing lipid-binding C2 domains at one end and multiple transmembrane domains (TMDs) at the other, a domain organisation consistent with the function of membrane tethers (Appendix Fig S3). Unlike HsE-Syts and AtSYTs, the transmembrane region of MCTPs is located at the C-terminus and three to four C2 domains at the N-terminus (Fig 1A; Appendix Fig S3). Two members of the *Arabidopsis* MCTP family, AtMCTP1/Flower Locus T Interacting Protein (FTIP) and AtMCTP15/QUIRKY (QKY), have previously been localised to plasmodesmata in *Arabidopsis* and implicated in cell-to-cell trafficking of developmental signals [20,51]. However, two recent studies indicate that other MCTP members, including AtMCTP3, AtMCTP4 and AtMCTP9, which show high plasmodesmata enrichment in our proteome, do not associate with the pores *in vivo* [52,53].

We investigated the *in vivo* localisation of MCTPs identified in our proteomic screen by transiently expressing N-terminal fusions with fluorescent proteins in *Nicotiana benthamiana* leaves. As the MCTP family is conserved in *N. benthamiana* (Appendix Fig S4) and to avoid working in a heterologous system, we also examined the localisation of NbMCTP7, whose closest homolog in *Arabidopsis* was also identified as highly enriched in plasmodesmata fractions (AtMCTP7; Appendix Fig S1). Confocal imaging showed that all selected MCTPs, namely AtMCTP3, AtMCTP4, AtMCTP6, AtMCTP9 and NbMCTP7, displayed a similar subcellular localisation, with a

faint ER-like network at the cell surface and a punctate distribution along the cell periphery at sites of epidermal cell-to-cell contacts (Fig 1B and C). Time-lapse imaging showed that peripheral fluorescent punctae were immobile, which contrasted with the high mobility of the ER-like network (Movie EV1). Co-localisation with RFP-HDEL confirmed MCTPs association with the cortical ER, while the immobile spots at the cell periphery perfectly co-localised with the plasmodesmal marker mCherry-PDCB1 ([27,29]; Fig 1C). Co-labelling with general ER-PM tethers such as VAP27.1-RFP and SYT1-RFP [57,59] showed partial overlap with GFP-NbMCTP7, while co-localisation with mCherry-PDCB1 was significantly higher (Appendix Fig S5). To further quantify and ascertain MCTP association with plasmodesmata, we measured a plasmodesmal enrichment ratio, hereafter named “plasmodesmata index”. For this, we calculated fluorescence intensity at plasmodesmata pit fields (indicated by mCherry-PDCB1 or aniline blue) versus cell periphery. All MCTPs tested displayed a high plasmodesmata index, ranging from 1.85 to 4.15, similar to PDLP1 (1.36) and PDCB1 (1.45), two well-established plasmodesmata markers [29,60] (Fig 1D), confirming enrichment of MCTPs at pit fields. When stably expressed in *Arabidopsis thaliana* under the moderate promoter UBIQUITIN10 or 35S promoter AtMCTP3, AtMCTP4, AtMCTP6 and AtMCTP9 were found mainly restricted to plasmodesmata (Appendix Fig S6A, white arrows), as indicated by an increase in their plasmodesmata index compared with transient expression in *N. benthamiana* (Appendix Fig S6B). A similar increase in the plasmodesmata index is seen with PDLP1.RFP when stably expressed in *Arabidopsis* (Appendix Fig S6B). A weak but consistent ER localisation was also visible in stably transformed *Arabidopsis* (Appendix Fig S6A red stars).

To get a better understanding of MCTP distribution within the plasmodesmal pores, we further analysed transiently expressed GFP-NbMCTP7 by 3D structured illumination super-resolution microscopy (3D-SIM) [61] (Fig 1E). We found that NbMCTP7 is associated with all parts of plasmodesmata including the neck regions and central cavity, as well as showing continuous fluorescence throughout the pores. In some cases, lateral branching of plasmodesmata within the central cavity was resolved. The very faint continuous fluorescent threads connecting neck regions and central cavity correspond to the narrowest regions of the pores and may indicate association with the central desmotubule (Fig 1E, white arrows).

### Figure 1. MCTPs are ER-associated proteins located at plasmodesmata.

Localisation of AtMCTP3, AtMCTP4, AtMCTP6, AtMCTP9 and NbMCTP7 in *N. benthamiana* epidermal cells visualised by confocal microscopy. MCTPs were tagged at their N-terminus with YFP or GFP and expressed transiently under 35S (NbMCTP7) or UBIQUITIN10 promoters (AtMCTP3, AtMCTP4, AtMCTP6 and AtMCTP9).

- Schematic representation of MCTP domain organisation, with three to four C2 domains at the N-terminus and multiple transmembrane domains (TMD) at the C-terminus.
- GFP-NbMCTP7 associates with punctae at the cell periphery (white arrowheads) and labels a reticulated network at the cell surface resembling the cortical ER. Maximum projection of z-stack. Scale bar, 2  $\mu$ m.
- Single optical sections at cell surface (left) or cell-to-cell interface (right), showing the co-localisation between MCTPs and the ER marker RFP-HDEL (left) and the plasmodesmata marker mCherry-PDCB1 (right). Intensity plots along the white dashed lines are shown for each co-localisation pattern. Scale bars, 2  $\mu$ m.
- The plasmodesmata (PD) index of individual MCTPs is above 1 (red dashed line) and similar to known plasmodesmata markers (aniline blue, PDCB1, PDLP1) confirming enrichment at plasmodesmata. By comparison, the PM-localised proton pump ATPase PMA2 and the ER marker HDEL that are not enriched at plasmodesmata have a PD index below 1. In the box plot, median is represented by horizontal line, values between quartiles 1 and 3 are represented by box ranges, and minimum and maximum values are represented by error bars. Three biological replicates were analysed.
- 3D-SIM images (individual z-sections) of GFP-NbMCTP7 within three different pit fields (panels 1-2, 3-4 and 5, respectively) showing fluorescence signal continuity throughout the pores, enrichment at plasmodesmal neck regions (1-2, arrowheads in 1), central cavity (3-4, arrowhead in 3) and branching at central cavity (5, arrow). Dashed lines indicate position of cell wall borders. Scale bars, 500 nm.

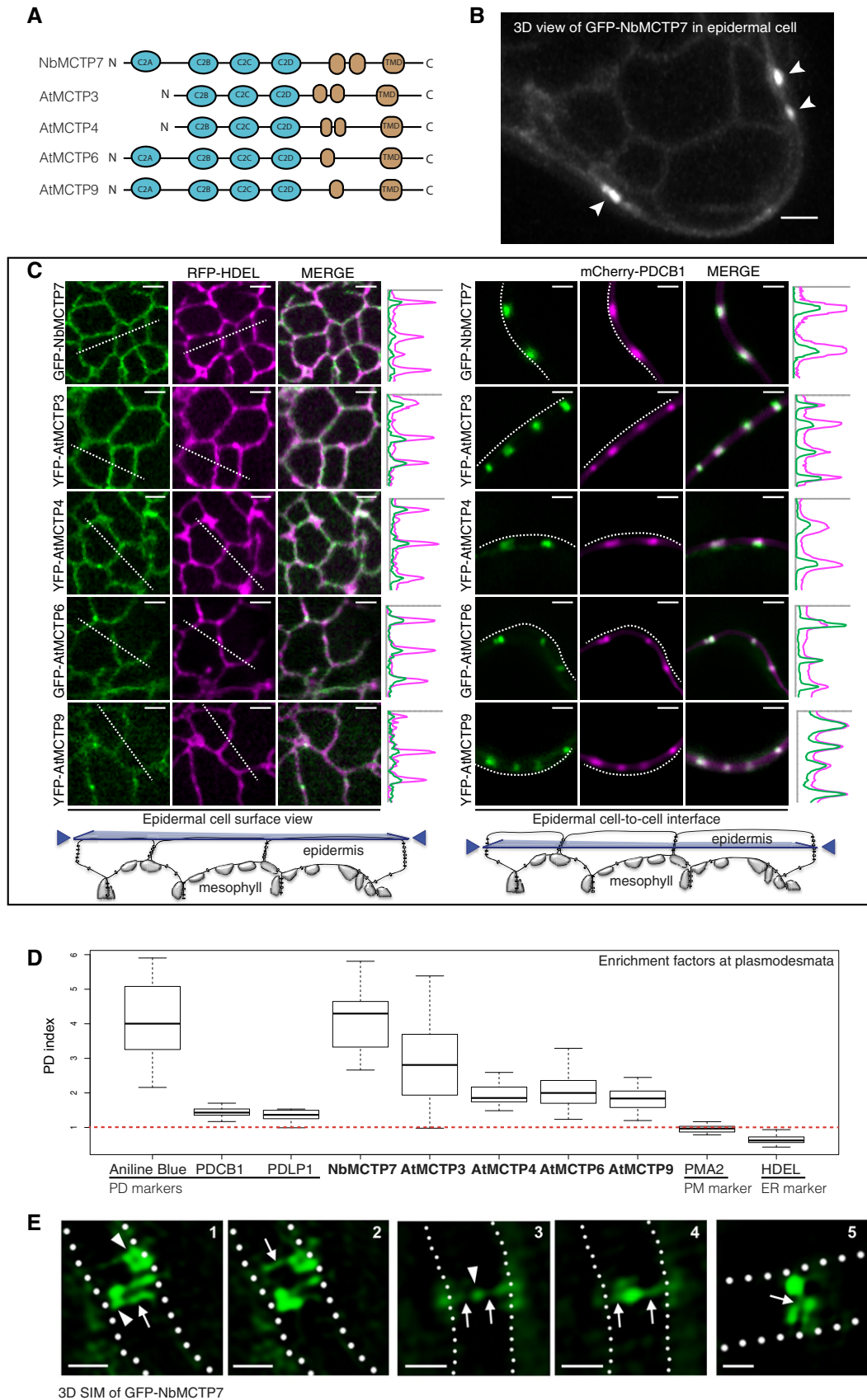
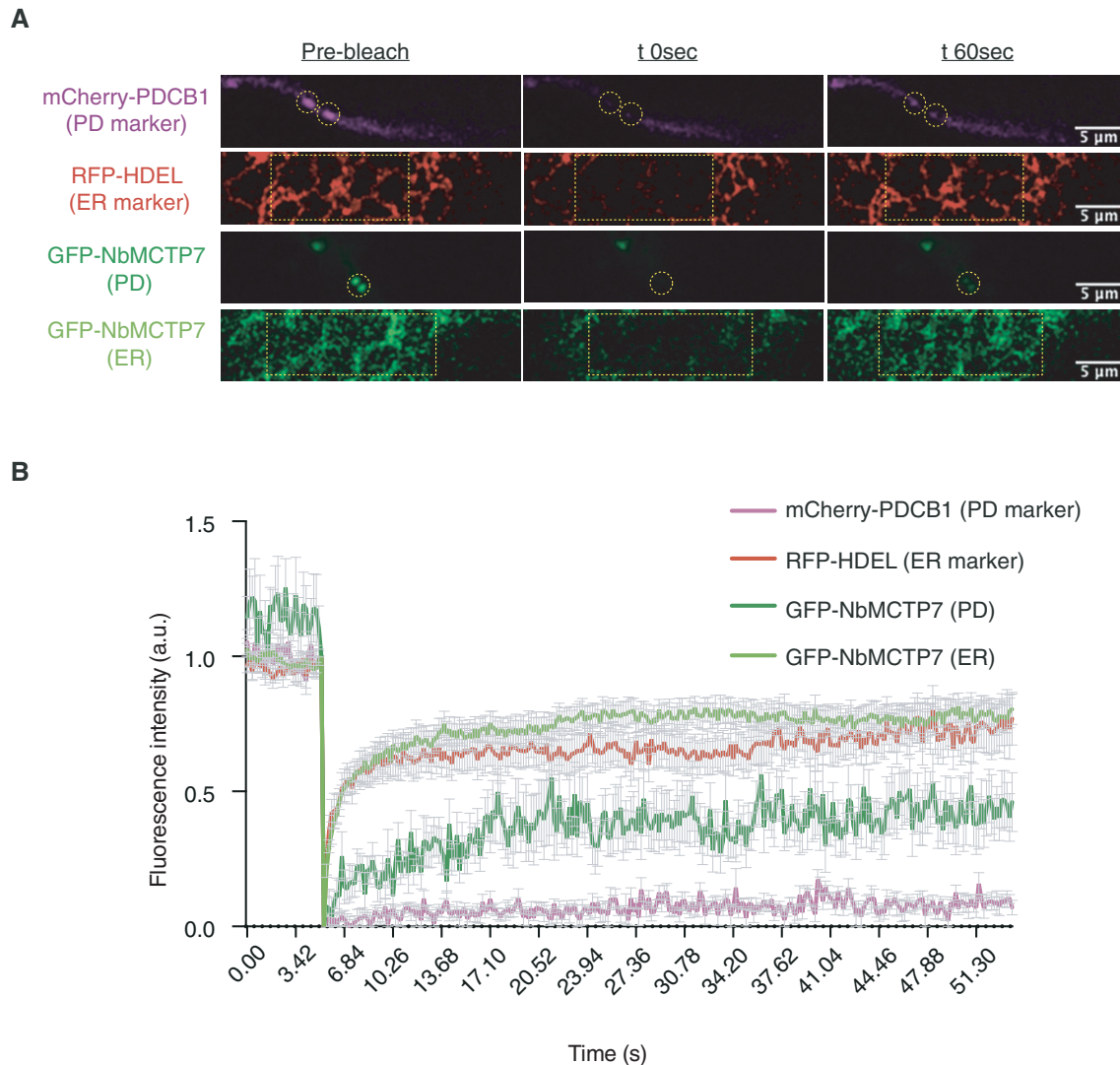


Figure 1.



**Figure 2. NbMCTP7 mobility at plasmodesmata is reduced compared to cortical ER. FRAP analysis of NbMCTP7 in *N. benthamiana* leaf epidermal cells.**

A Representative pre-bleach and post-bleach images for mCherry-PDCB1 (purple; plasmodesmata marker), RFP-HDEL (red; ER marker) and GFP-NbMCTP7 at plasmodesmata (dark green) and at the cortical ER (light green). Yellow dashed boxes or circles indicate the bleach region.

B FRAP comparing the mobility of GFP-NbMCTP7 at plasmodesmata (dark green) and at the cortical ER (light green) to that of RFP-HDEL (red) and mCherry-PDCB1 (purple). NbMCTP7 is highly mobile when associated with the ER as indicated by fast fluorescent recovery but shows reduced mobility when associated with plasmodesmata. Data are averages of at least 3 separate experiments; error bars indicate standard error.

Using fluorescence recovery after photobleaching (FRAP), we then assessed the mobility of NbMCTP7. We found that, when associated with the cortical ER, the fluorescence recovery rate of GFP-NbMCTP7 was extremely fast and similar to RFP-HDEL with half-times of 1.16 and 0.99 s, respectively (Fig 2A and B). By contrast, when GFP-NbMCTP7 was associated with plasmodesmata, the recovery rate slowed down to a half-time of 4.09 s, indicating restricted mobility, though still slightly faster than for the cell wall-localised plasmodesmal marker mCherry-PDCB1 (5.98 s). Overall, these results show that NbMCTP7 mobility is high at the cortical ER but becomes restricted inside the pores.

From our data, we concluded that MCTPs are ER-associated proteins, whose members specifically and stably associate with plasmodesmata. They display the structural features required for ER-PM

tethering and are differentially associated with the pores during the transition in ER-PM contacts.

#### Loss of function *mctp3/mctp4* double mutant shows pleiotropic developmental defects, reduced cell-to-cell trafficking and an altered plasmodesmata proteome

We next focused on AtMCTP4, which according to our proteomic screen appears as one of the most abundant proteins associated with plasmodesmata-enriched fractions (Appendix Table S1). The implication of AtMCTP4 association with plasmodesmata is that the protein contributes functionally to cell-to-cell signalling. Given the importance of plasmodesmata in tissue patterning and organ growth, a loss-of-function mutant is expected to show defects in

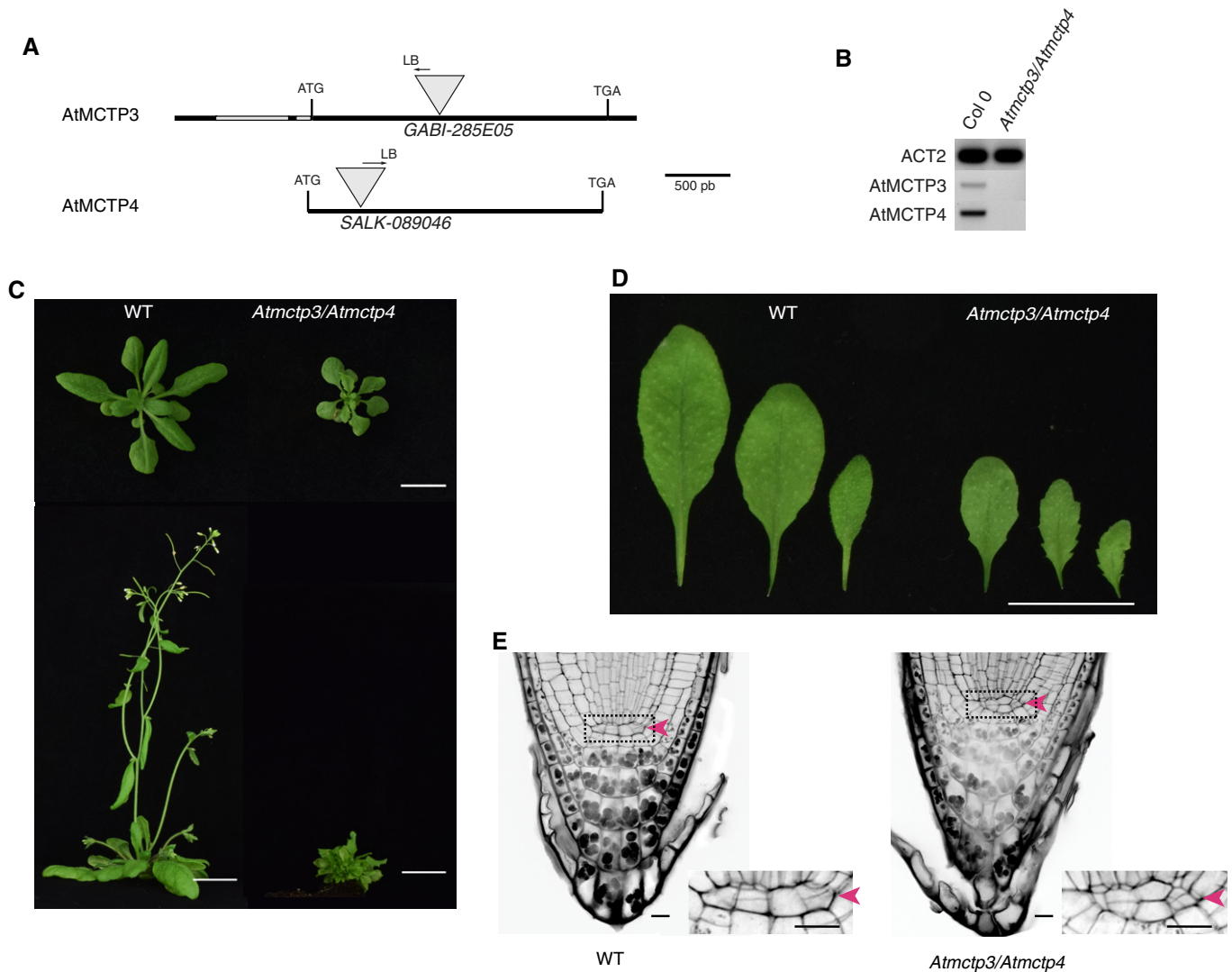


**Figure 3. *Atmctp3/Atmctp4* loss of function double mutant shows severe defects in development.**

A–E Characterisation of *Atmctp3/Atmctp4* double mutant in *Arabidopsis*. (A) Schematic representation of T-DNA insertions in *AtMCTP3* and *AtMCTP4*. LB, left border. (B) RT-PCR analysis of *AtMCTP3*, *AtMCTP4* and *Actin2* (ACT2) transcripts in Col-0 wild-type (WT) and *Atmctp3/Atmctp4* double mutant showing the absence of full-length transcripts in the *Atmctp3/Atmctp4* double mutant. (C) Rosette and inflorescence stage phenotypes of *Atmctp3/Atmctp4* double mutant compared to Col-0 WT. Scale bar, 2 cm. (D) Leaf phenotypes of *Atmctp3/Atmctp4* double mutant compared to WT. Scale bar, 2 cm. (E) Pseudo-Schiff propidium iodide method-stained root tips of WT and *Atmctp3/Atmctp4* double mutant. Defect in quiescent centre (QC, red arrowheads) cell organisation was observed in 20 out of 20 plants examined. Scale bars, 10  $\mu$ m.

plant development. We first obtained T-DNA insertion lines for *AtMCTP4* and its closest homolog *AtMCTP3*, which share 92.8% identity and 98.7% similarity in amino acids with *AtMCTP4*, but both single knockouts showed no apparent phenotypic defects (Appendix Fig S7). We therefore generated an *Atmctp3/Atmctp4* double mutant, which presented pleiotropic developmental defects with a severely dwarfed and bushy phenotype, twisted leaves with increased serration (Fig 3A–D) and multiple inflorescences (Appendix Fig S7). The phenotype was fully complemented by YFP-*AtMCTP3* expression (Appendix Fig S7). While preparing this manuscript, another paper describing the *Atmctp3/Atmctp4* mutant was published [50], reporting similar developmental defects. We noted additional phenotypic defects in particular aberrant

patterning in the root apical meristem, specifically within the quiescent centre (QC) and columella cells (Fig 3E, Appendix Fig S14). Instead of presenting the typical four-cell layer organisation, we observed asymmetrical divisions in the QC of the *Atmctp3/Atmctp4*, suggesting that both proteins may play a general role in cell stem niche maintenance [50]. To further investigate the role of *AtMCTP3* and *AtMCTP4* in plasmodesmata function, we performed intercellular trafficking assays by monitoring GFP-sporamin (47 kDa) [62] movement from single-cell transformation sites in fully expanded leaves. Compared to wild-type Col-0 or *Atmctp3* and *Atmctp4* single mutants, *Atmctp3/Atmctp4* double mutant presented a significant reduction of GFP-sporamin spread, indicating reduced plasmodesmata-mediated macromolecular

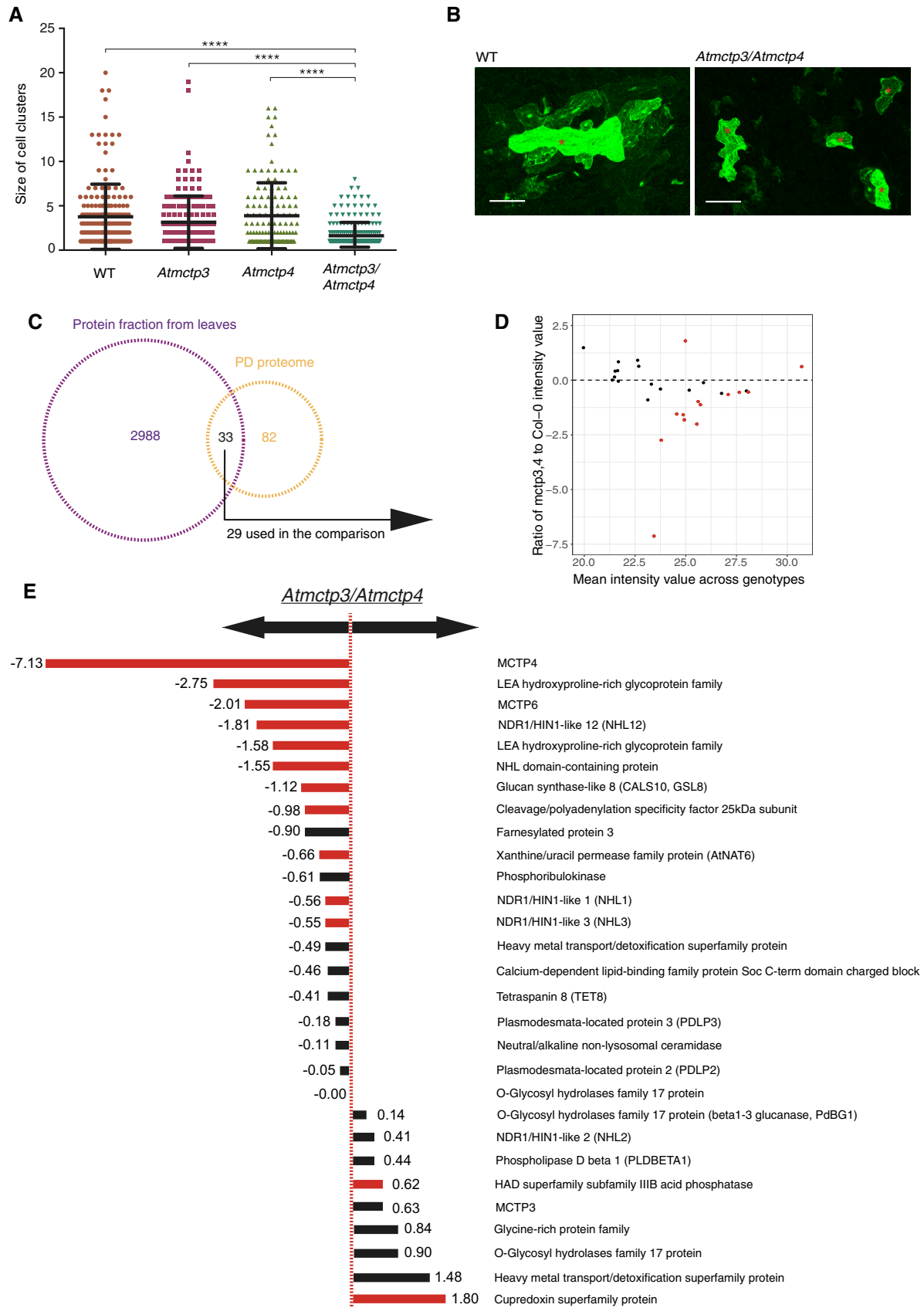


Figure 4.



**Figure 4. Plasmodesmata function and composition are altered in *Atmctp3/Atmctp4* *Arabidopsis* mutant.**

A, B Macromolecular trafficking through plasmodesmata is reduced in *Atmctp3/Atmctp4* *Arabidopsis* mutant. Leaves of Col-0, *Atmctp3*, *Atmctp4* single mutants and *Atmctp3/Atmctp4* double mutant were bombarded with a GFP-sporamin (47 kDa) expression plasmid. Diffusion of GFP-sporamin to surrounding cells 72 h after bombardment was used as a measure of plasmodesmata molecular trafficking. (A) Scatter plot representation with the black lines representing the mean value (middle) and SD. (B) Representative GFP-sporamin fluorescent foci observed by confocal microscopy 72 h after bombardment. Bombarded cells are indicated by a red star.  $n = 50$  foci for Col-0;  $n = 37$  foci for *Atmctp3* single mutant;  $n = 33$  foci for *Atmctp4* single mutant; and  $n = 48$  foci for *Atmctp3/Atmctp4* double mutant (3 biological replicates). Pairwise comparisons by Wilcoxon test, \*\*\*\* $P < 0.0001$ . Scale bar, 100  $\mu\text{m}$ .

C–E Comparative proteomic analysis of *Atmctp3/Atmctp4* and Col-0. (C) Intersection between the protein identities obtained from leaf tissue and those in the plasmodesmata proteome (Appendix Table S1). Only proteins appearing in at least 3/5 samples were employed for the comparison (29). (D) Plot of the log<sub>2</sub> ratios of the average plasmodesmata protein intensities in *Atmctp3/Atmctp4* relative to Col-0. Dashed line indicates no change ( $0 = \log_2(1)$ ), above the line enrichments, below the line depletions. (E) List of plasmodesmata proteins detected in leaf tissue and their ratios of abundance in *Atmctp3/Atmctp4* relative to Col-0. Please note that we detected AtMCTP3 unique peptides at relatively high abundance in the *Atmctp3/Atmctp4* mutant. These peptides are located before the T-DNA insertion, and it is therefore likely that a truncated non-functional protein is still translated at levels similar to the wild-type (see Appendix Fig S8). Bars for the proteins whose differential abundance is supported by statistical testing ( $t$ -test with  $P$ -value correction for false discovery rate.  $P < 0.05$ ) are in red. Bars for other proteins are in black.

trafficking (Fig 4A and B). To complement the trafficking assays, we performed comparative proteomic profiling of the *Atmctp3/Atmctp4* mutant and wild-type Col-0. For this, we analysed cell wall extracts from fully expanded leaves using quantitative high-resolution mass spectrometry [63]. Comparative data analysis showed that about one-third (13 out of 29) of the proteins identified as plasmodesmata-associated according to our “refined” proteome were differentially regulated in *Atmctp3/Atmctp4* mutant compared to wild-type Col-0 (Fig 4C–E). This indicates that the molecular composition of plasmodesmata is substantially altered in the *Atmctp3/Atmctp4* mutant. Altogether, these data indicate that *Atmctp3/Atmctp4* loss of function is detrimental for plasmodesmata function and composition, and this probably contributes to developmental defects observed in the mutant.

**AtMCTP4 is a plasmodesmata-associated protein**

To further verify plasmodesmata association of AtMCTP4, we expressed the N-terminal GFP fusion under its own promoter (pAtMCTP4:GFP-AtMCTP4). At the tissue level, the expression pattern of this construct in stable *Arabidopsis* lines was consistent with the phenotypic defects we observed in the *Atmctp3/Atmctp4* mutant, as strong expression was observed in the inflorescence shoot apical meristem (Fig 5A), root tip (including QC), lateral root primordia and young leaf primordia (Appendix Fig S9A), i.e., the tissues showing developmental defects in the mutant (Fig 3; [50]). However, AtMCTP4 has recently been reported as an endosomal-localised protein [52], which is in conflict with our data indicating plasmodesmata association. We analysed localisation pattern of pAtMCTP4:GFP-AtMCTP4 at the subcellular level in *Arabidopsis* stable lines. Similar to transient expression experiments (Fig 1), we found that pAtMCTP4:GFP-AtMCTP4 was located at stable punctate spots at the cell periphery (Fig 5A white arrows; Movie EV2), in all tissues examined, i.e. leaf epidermal and spongy mesophyll cells, hypocotyl epidermis, lateral root primordia, root tip and inflorescence shoot apical meristem. These immobile dots co-localised perfectly with aniline blue indicating plasmodesmata association (Fig 5A top row), which was also evident in leaf spongy mesophyll cells where the dotted pattern of pAtMCTP4:GFP-AtMCTP4 was present on adjoining walls (containing plasmodesmata), but absent from non-adjoining walls (without plasmodesmata) (Fig 5A white arrowheads). Furthermore, localisation of pAtMCTP4:GFP-AtMCTP4 at interfaces between epidermal pavement cells and stomata guard

cells, where plasmodesmata are only half-formed on the pavement cell side [64], is similar to that of the viral movement protein cucumber mosaic virus (CMV 3a) (Appendix Fig S9B). We also observed a weak but consistent ER association of AtMCTP4 (Fig 5A, red stars).

To investigate further AtMCTP4 association with plasmodesmata, we performed immunogold labelling on high-pressure frozen freeze-substituted root sections of 6-day-old pAtMCTP4:GFP-AtMCTP4 seedlings, using anti-GFP antibodies. GFP-AtMCTP4-associated gold particle signal was seen along the length of the channel and neck region (Fig 5B). Distribution of the gold labelling showed a strong preference for labelling associated with plasmodesmata. Immunogold labelling of wild-type roots gave no significant labelling (Appendix Fig S11A). To complement immunogold labelling on root sections, we also performed correlative light and electron microscopy (CLEM) on walls purified from pAtMCTP4:GFP-AtMCTP4 seedlings. Calcofluor staining combined with confocal imaging revealed discrete plasmodesmata pit fields characterised by the absence of cellulose staining [65] into which GFP-AtMCTP4 punctate signal was systematically associated (Fig 5C, Appendix Fig S10, yellow arrowheads). We then transferred the wall fragments to electron microscopy, after negative staining with uranyl acetate, to reveal plasmodesmata structures. As shown in Fig 5D and Appendix Fig S11B, the dotted GFP-AtMCTP4 signal was perfectly co-localised with plasmodesmata pit fields. To further confirm the results from the CLEM, we performed immunogold labelling using anti-callose (10 nm gold) and/or anti-PDCB (5 nm gold), two well-established plasmodesmata markers [27,29]. Both antibodies specifically labelled the areas identified as pit fields (Fig 5D, Appendix Fig S11C). In summary, we concluded that whatever the tissue and organ considered, AtMCTP4 is strongly and consistently associated with plasmodesmata but also presents a steady association with the ER.

**The C-terminal transmembrane regions of MCTPs serve as ER anchors**

A requirement for tethers is that they physically bridge two membranes. Often this is achieved through lipid-binding module(s) at one terminus of the protein and transmembrane domain(s) at the other [47,48]. All sixteen *Arabidopsis* MCTPs contain two to three predicted TMDs near their C-terminus (collectively referred to as the transmembrane region, TMR). To test whether the MCTP TMRs are

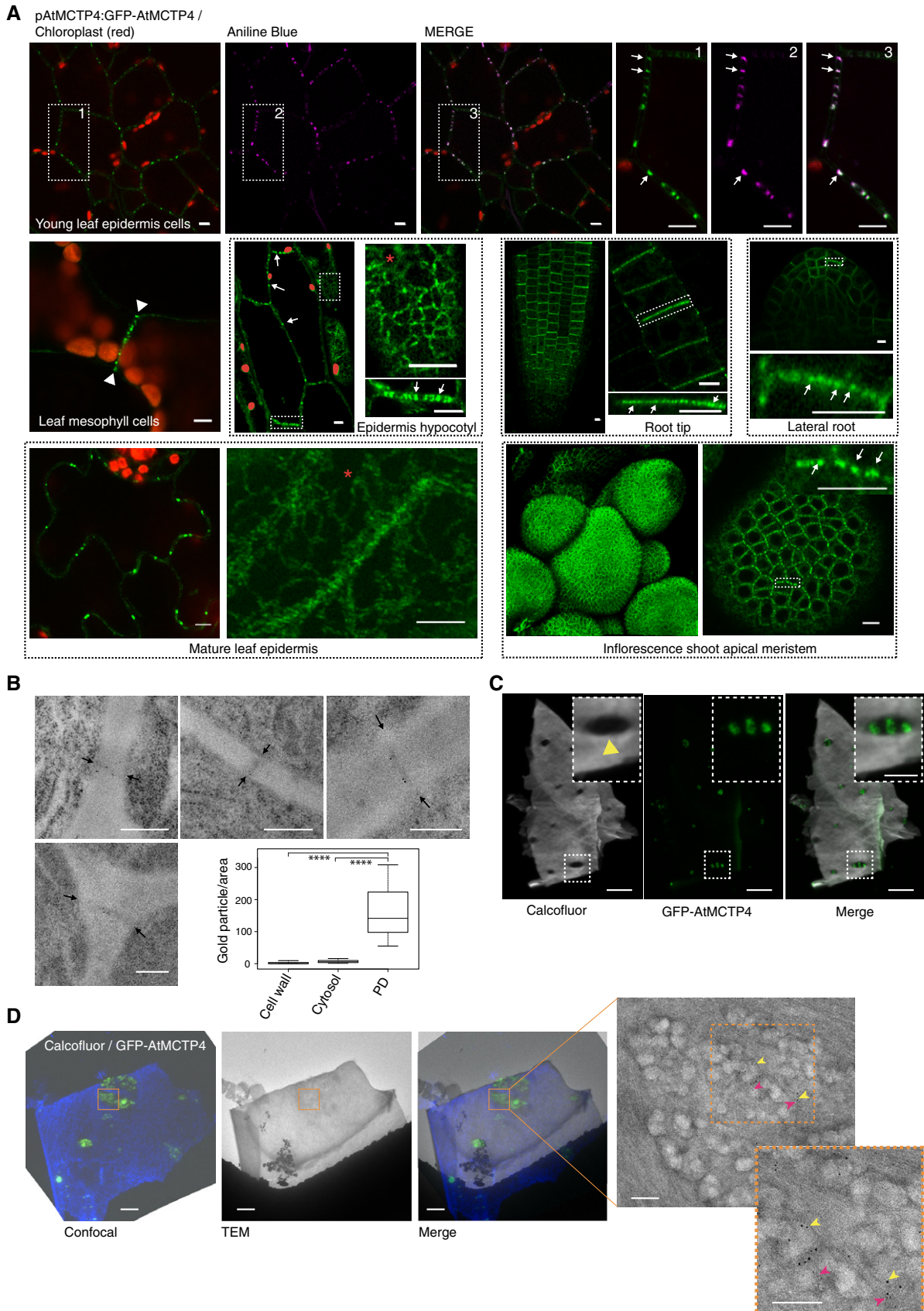


Figure 5.

### Figure 5. AtMCTP4 is a plasmodesmata protein localised at plasmodesmata pit fields.

- A Subcellular localisation of GFP-AtMCTP4 under AtMCTP4 native promoter in *Arabidopsis* transgenic lines visualised by confocal microscopy. In all tissues examined, GFP-MCTP4 shows a typical punctate distribution of plasmodesmata at the cell boundaries (indicated by white arrows). In leaf, spongy mesophyll GFP-AtMCTP4 punctate pattern was visible only on adjoining walls (arrowheads), which contain plasmodesmata but absent from non-adjoining walls. GFP-AtMCTP4 dots at the cell periphery are immobile (see Movie EV2) and co-localise perfectly with aniline blue (top row) confirming plasmodesmata localisation. In most tissues examined, an ER-reticulated pattern was also observable (red stars). Boxed regions are magnified in adjacent panels. Please note that the hypocotyl epidermis was imaged in airy scan mode and chloroplasts were manually outlined in red. Scale bars, 5  $\mu$ m.
- B Immunogold localisation of GFP-AtMCTP4 to plasmodesmata. Thin sections of pAtMCTP4:GFP-AtMCTP4 transgenic *Arabidopsis* roots subjected to immunogold labelling using anti-GFP antibodies (5 and 10 nm gold particles). Electron micrographs showing wall sections with plasmodesmata labelled by gold particles. Gold particles were quantified relative to the area occupied by plasmodesmata, cell wall and cytosol, respectively (see Materials and Methods). \*\*\*\* $P < 0.001$  in pairwise Wilcoxon test (total particles count 298). In the box plot, median is represented by horizontal line, values between quartiles 1 and 3 are represented by box ranges, and minimum and maximum values are represented by error bars. Scale bars, 300 nm
- C Confocal observation of cell walls purified from pAtMCTP4:GFP-AtMCTP4. Cell wall was stained with calcofluor, revealing plasmodesmata pit fields where calcofluor staining, hence cellulose, is absent/reduced (yellow arrowhead). GFP-AtMCTP4 signal is systematically associated with plasmodesmata pit fields (see boxed magnified region and Appendix Fig S10). Scale bars, 5 and 2.5  $\mu$ m in boxed regions.
- D CLEM on cell walls purified from pAtMCTP4:GFP-AtMCTP4 *Arabidopsis* seedlings combined with immunogold labelling against callose (yellow arrow; 10-nm gold particles) and PDCB1 protein (magenta arrow; 5-nm gold particles), two plasmodesmata markers. TEM = transmission electron microscopy. For CLEM, also see Appendix Fig S11. Scale bars, 5  $\mu$ m for confocal images and 200 nm for TEM images.

determinants of ER insertion, we generated truncation mutants lacking the C2 domains for NbMCTP7, AtMCTP3, AtMCTP4, AtMCTP6, AtMCTP9 as well as AtMCTP1/FTIP and AtMCTP15/QKY (Fig 6A). When fused to YFP at their N-terminus, all truncated mutants retained ER association, as demonstrated by co-localisation with RFP-HDEL (Fig 6B left panels). Meanwhile, plasmodesmata association was completely lost and the plasmodesmata index of all truncated MCTP\_TMRs dropped below one, comparable to RFP-HDEL (Fig 6B right panels and c), quantitatively confirming the loss of plasmodesmata association when the C2 modules were deleted. For AtMCTP15/QKY, this is in agreement with a previous study [20]. We therefore concluded that, similar to the HsE-Syt and AtSYT ER-PM tether families [57,58,66], MCTPs insert into the ER through their TMRs, but the TMR alone is not sufficient for MCTP plasmodesmal localisation.

### MCTP C2 domains can bind membranes in an anionic lipid-dependent manner

Members of the HsE-Syt and AtSYT tether families bridge across the intermembrane gap and dock to the PM via their C2 domains [57,58,67,68]. *Arabidopsis* MCTPs contain three to four C2 domains, which may also drive PM association through interactions with membrane lipids. C2 domains are independently folded structural and functional modules with diverse modes of action, including membrane docking, protein–protein interactions and calcium sensing [69].

To investigate the function of MCTP C2 modules, we first searched for homologs of AtMCTP individual C2 domains (A, B, C, and D) amongst all human and *A. thaliana* proteins using the HHpred web server [70] for remote homology detection. The searches yielded a total of 1,790 sequence matches, which contained almost all human and *A. thaliana* C2 domains. We next clustered the obtained sequences based on their all-against-all pairwise similarities in CLANS [71]. In the resulting map (Appendix Fig S12A), the C2 domains of *Arabidopsis* MCTPs (AtMCTPs, coloured cyan) most closely match the C2 domains of membrane-trafficking and membrane-tethering proteins, including human MCTPs (HsMCTPs, green), human synaptotagmins (HsSyts, orange), human Ferlins (HsFerlins, blue), human HsE-Syts (HsE-Syts, magenta) and *Arabidopsis* SYTs (AtSYTs, red), most of which dock to membranes through direct interaction with anionic lipids [58,68,72–74]. By

comparison to the C2 domains of these membrane-trafficking and membrane-tethering proteins, the C2 domains of most other proteins do not make any connections to the C2 domains of AtMCTPs at the  $P$ -value cut-off chosen for clustering ( $1e-10$ ). Thus, based on sequence similarity, the plant AtMCTP C2 domains are expected to bind membranes.

We next asked whether the C2 modules of MCTPs are sufficient for PM association *in vivo*. Fluorescent protein fusions of the C2A-D or C2B-D modules without the TMR were generated for NbMCTP7, AtMCTP3, AtMCTP4, AtMCTP6, AtMCTP9 as well as AtMCTP1/FTIP and AtMCTP15/QKY and expressed in *N. benthamiana*. We observed a wide range of subcellular localisations from cytosolic to PM-associated and in all cases plasmodesmata association was lost (Appendix Fig S12B–D).

To further investigate the potential for MCTP C2 domains to interact with membranes, we employed molecular dynamic modelling. We focussed on AtMCTP4, as a major plasmodesmal constituent and whose loss of function in conjunction with AtMCTP3 induces severe plant developmental and plasmodesmata defects [52] (Fig 3). We first generated the 3D structures of all three C2 domains of AtMCTP4 using 3D homology modelling and then tested the capacity of individual C2 domains to dock to membrane bilayers using coarse-grained dynamic simulations (Fig 7A; Movie EV3). Molecular dynamic modelling was performed on three different membranes: (i) a neutral membrane composed of phosphatidylcholine (PC), (ii) a membrane with higher negative charge composed of PC and phosphatidylserine (PS; 3:1) and (iii) a PM-mimicking lipid bilayer, containing PC, PS, sitosterol and the anionic phosphoinositide phosphatidyl inositol-4-phosphate (PI4P; 57:19:20:4). The simulations showed that all individual C2 domains of AtMCTP4 can interact with lipids and dock on the membrane surface when a “PM-like” lipid composition was used (Fig 7A). The PC-only membrane showed only weak interactions, while the PC:PS membrane allowed only partial docking (Fig 7A). Docking of AtMCTP4 C2 domains arose mainly through electrostatic interactions between lipid polar heads and basic amino acid residues at the protein surface. We also confirmed membrane docking and stable anionic lipid interaction for individual AtMCTP4 C2 domains using all atom simulation. For that, coarse-grained systems were transformed back to all atom representations and simulation was run for 100 ns to check the stability of membrane

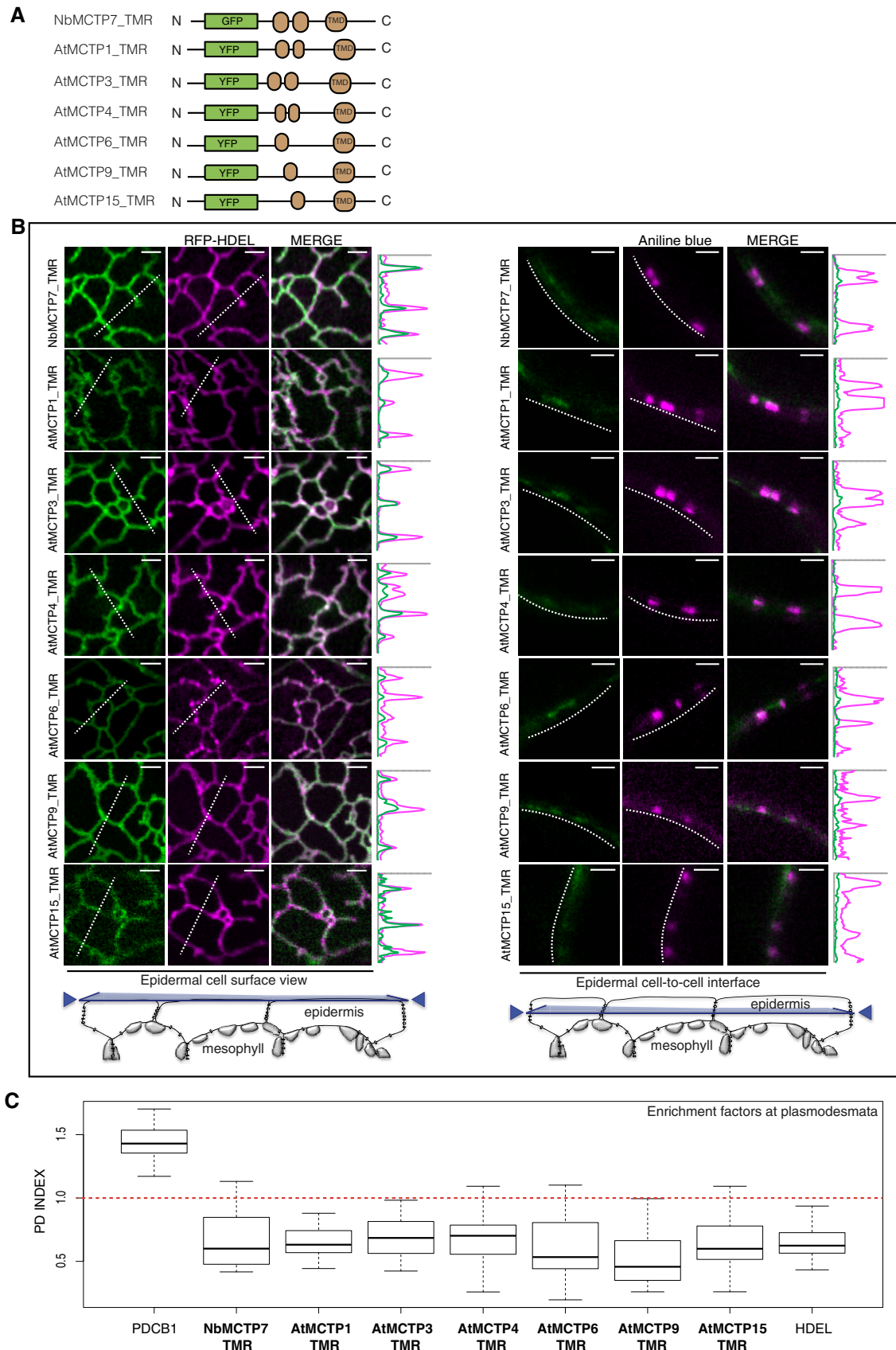


Figure 6.

**Figure 6. MCTPs insert into the ER membrane via their C-terminal transmembrane region.**

Localisation of truncated AtMCTP1, AtMCTP3, AtMCTP4, AtMCTP6, AtMCTP9, AtMCTP15 and NbMCTP7 transmembrane regions (TMR) in *N. benthamiana* leaf epidermal cells. TMRs were tagged at their N-terminus with GFP/YFP and expressed transiently under moderate UBIQUITIN10 promoter.

- A Schematic representation of truncated MCTPs tagged with GFP/YFP.  
 B Optical sections at cell surface (left) and cell-to-cell interface (right) showing the co-localisation between GFP/YFP-MCTP\_TMR constructs and the ER marker RFP-HDEL (left) and the plasmodesmata marker aniline blue (right). Intensity plots along the white dashed lines are shown for each co-localisation pattern. When expressed in epidermal cells, GFP/YFP-MCTP\_TMR constructs associate with the ER but plasmodesmata association is lost. Scale bars, 2  $\mu$ m.  
 C The PD index of individual truncated MCTP\_TMR constructs is below 1 (red dashed line), similar to the ER marker RFP-HDEL confirming loss of plasmodesmata localisation. In the box plot, median is represented by horizontal line, values between quartiles 1 and 3 are represented by box ranges, and minimum and maximum values are represented by error bars. Three biological replicates were analysed.

docking (Appendix Fig S13C). We further tested two other MCTP members, namely AtMCTP15/QKY and NbMCTP7, which possess four rather than three C2 domains. We found that similar to AtMCTP4, the individual C2 domains of AtMCTP15/QKY and NbMCTP7 exhibited membrane interaction in the presence of the negatively charged lipids (Appendix Fig S13A and B).

Our molecular dynamic data thus suggest that membrane docking of the AtMCTP4 C2 domains depends on the electrostatic charge of the membrane and more specifically on the presence of PI4P, a negatively charged lipid which has been reported as controlling the electrostatic field of the PM in plants [75].

To confirm the importance of PI4P for MCTP membrane interactions and, thus, potentially subcellular localisation, we used a short-term treatment with phenylarsine oxide (PAO), an inhibitor of PI4-kinases [75]. We focused on *Arabidopsis* root tips where effects of PAO have been thoroughly characterised [75]. In control-treated roots of *Arabidopsis* plants stably expressing UB10:YFP-AtMCTP4, the fluorescent signal was most prominent at the apical-basal division plane of epidermal root cells, where numerous plasmodesmata are established during cytokinesis [27] (Fig 7B white arrowheads). The YFP-AtMCTP4 fluorescence pattern was punctate at the cell periphery, each spot of fluorescence corresponding to a single or group of plasmodesmata (Fig 7C, white arrows). We found that 40-min treatment with PAO (60  $\mu$ M) induced a loss in the typical spotty plasmodesmata-associated pattern, and instead, AtMCTP4 became more homogeneously distributed along the cell periphery (Fig 7B and C). To confirm the effect of PAO on the cellular PI4P pool, we used a PI4P biosensor (1 $\times$ PH FAPP1) which showed a clear shift from PM association to cytosolic localisation upon treatment with PAO [73] (Fig 7B). This control not only demonstrates that the PAO treatment was successful, but also highlights that the majority of PI4P was normally

found at the PM, rather than the ER, of *Arabidopsis* root cells. Therefore, the effect of PAO on YFP-AtMCTP4 localisation is likely related to a perturbation of PM docking by the MCTP4 C2 domains. When *Arabidopsis* seedlings were grown on PAO (1 and 10  $\mu$ M) for 7 days, we observed root tip phenotypic defects reminiscent of the *Atmctp3/Atmctp4* mutant (Appendix Fig S14).

Altogether, our data suggest that the C2 domains of plant MCTPs can dock to membranes in the presence of negatively charged phospholipids and that PI4P depletion reduced AtMCTP4 stable association with plasmodesmata.

**AtMCTP4 expression is sufficient to partially restore ER-PM contacts in yeast**

To further test the ability of MCTPs to physically bridge across membranes and tether the ER to the PM, we used a yeast  $\Delta$ tether mutant line deleted in six ER-PM tethering proteins resulting in the separation of the cortical ER (cER) from the PM [76] and expressed untagged AtMCTP4. To monitor recovery in cortical ER, and hence, ER-PM contacts, upon AtMCTP4 expression, we used Sec63-RFP [77] as an ER marker combined with confocal microscopy. In wild-type cells, the ER was organised into nuclear (nER) and cER. The cER was visible as a thread of fluorescence along the cell periphery, covering a large proportion of the cell circumference (Fig 8A white arrows). By contrast and as previously reported [76], we observed a substantial reduction of cER in the  $\Delta$ tether mutant, with large areas of the cell periphery showing virtually no associated Sec63-RFP (Fig 8A). When AtMCTP4 was expressed into the  $\Delta$ tether mutant line, we observed partial recovery of cER, visible as small regions of Sec63-RFP closely apposed to the cell cortex. We further quantified the extent of cER in the different lines by measuring the ratio of the length of cER (Sec63-RFP) against the cell perimeter (through

**Figure 7. Anionic lipid-dependent membrane docking of AtMCTP4 C2 domains.**

- A Top: 3D-atomistic model of the individual AtMCTP4 C2 domains. Beta strands are shown in pink, loops in green and alpha helices in orange. Bottom: molecular dynamics of individual AtMCTP4 C2 domains with different biomimetic lipid bilayer compositions: phosphatidylcholine (PC) alone, with phosphatidylserine (PS) (PC/PS 3:1) and with PS, sitosterol (Sito) and phosphoinositol-4-phosphate (PI4P) (PC/PS/Sito/PI4P 57:19:20:4). The plots show the distance between the protein's closest residue to the membrane and the membrane centre, over time. The membrane's phosphate plane is represented by a PO<sub>4</sub> grey line on the graphs and a dark green meshwork on the simulation image captures (above graphs). For each individual C2 domain and a given lipid composition, the simulations were repeated four to five times (runs 1–5). C2 membrane docking was only considered as positive when a minimum of four independent repetitions showed similarly stable interaction with the membrane. All C2 domains of AtMCTP4 show membrane interaction when anionic lipid, in particular PI4P, is present. The amino acid colour code is as follows: red, negatively charged (acidic) residues; blue, positively charged (basic) residues; green, polar uncharged residues; and white, hydrophobic residues.  
 B, C Confocal microscopy of *Arabidopsis* root epidermal cells of UBQ10:YFP-AtMCTP4 transgenic lines after 40-min treatment with DMSO (mock) and PAO (60  $\mu$ M), an inhibitor of PI4 kinase. To confirm PI4P depletion upon PAO treatment, we used the PI4P *Arabidopsis* sensor line 1 $\times$ PH(FAPP1) [74]. (B) PAO treatment leads to a loss of plasmodesmal punctate signal at the cell periphery (apical-basal boundary is highlighted by white arrowheads in B) for YFP-AtMCTP4, and redistribution of PM-localised 1 $\times$ PH(FAPP1) to the cytoplasm. (C) Magnified boxed regions from (B) and profile plot along the cell wall after DMSO (1) or PAO (2) treatment, respectively (arrows: plasmodesmal punctae). Scale bars, 5  $\mu$ m in (B) and 2.5  $\mu$ m in (C).

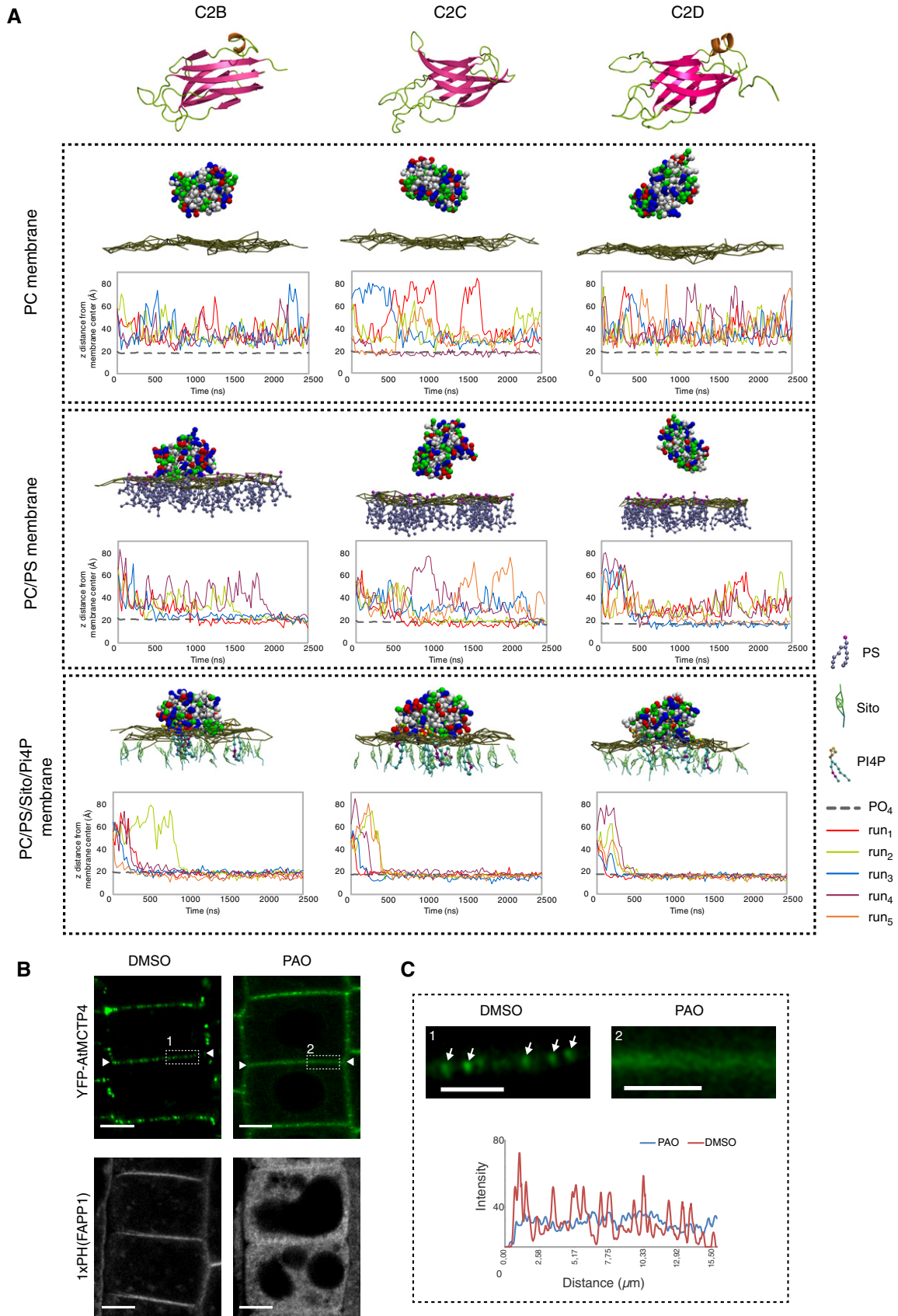


Figure 7.

calcofluor wall staining) and confirmed that AtMCTP4 expression induced an increase in cER from 7.3 to 23.1% when compared to the  $\Delta$ tether mutant (Fig 8B). This partial complementation is similar to results obtained with yeast deletion mutants containing only a single endogenous ER-PM tether, IST2, or all three isoforms of the tricalbin (yeast homologs of HsE-Syts) [76], supporting a role of AtMCTP4 as ER-PM tether.

## Discussion

In plants, communication between cells is facilitated and regulated by plasmodesmata, ~50-nm-diameter pores that span the cell wall and provide cell-to-cell continuity of three different organelles: the PM, cytoplasm and ER. The intercellular continuity of the ER and the resulting architecture of the pores make them unique amongst eukaryotic cellular junctions and qualify plasmodesmata as a

specialised type of ER-PM MCS [1,33]. Like other types of MCS, the membranes within plasmodesmata are physically connected, but so far, the molecular components and function of the ER-PM tethering machinery remain an enigma.

Here, we provide evidence that members of the MCTP family, some of which have been described as key regulators of intercellular trafficking and cell-to-cell signalling [20,51,52], also act as ER-PM tethers inside the plasmodesmata pores.

### MCTPs are functionally important plasmodesmal components

To identify ER-PM tether candidates acting specifically at plasmodesmata, we produced a refined plasmodesmata proteome. We combined label-free proteomic analysis and subcellular fractionation, and reduce the complexity of the plasmodesmata proteome from about 1,400 proteins [49] to 115 proteins. For that, we purified plasmodesmata from *Arabidopsis* liquid cell culture,

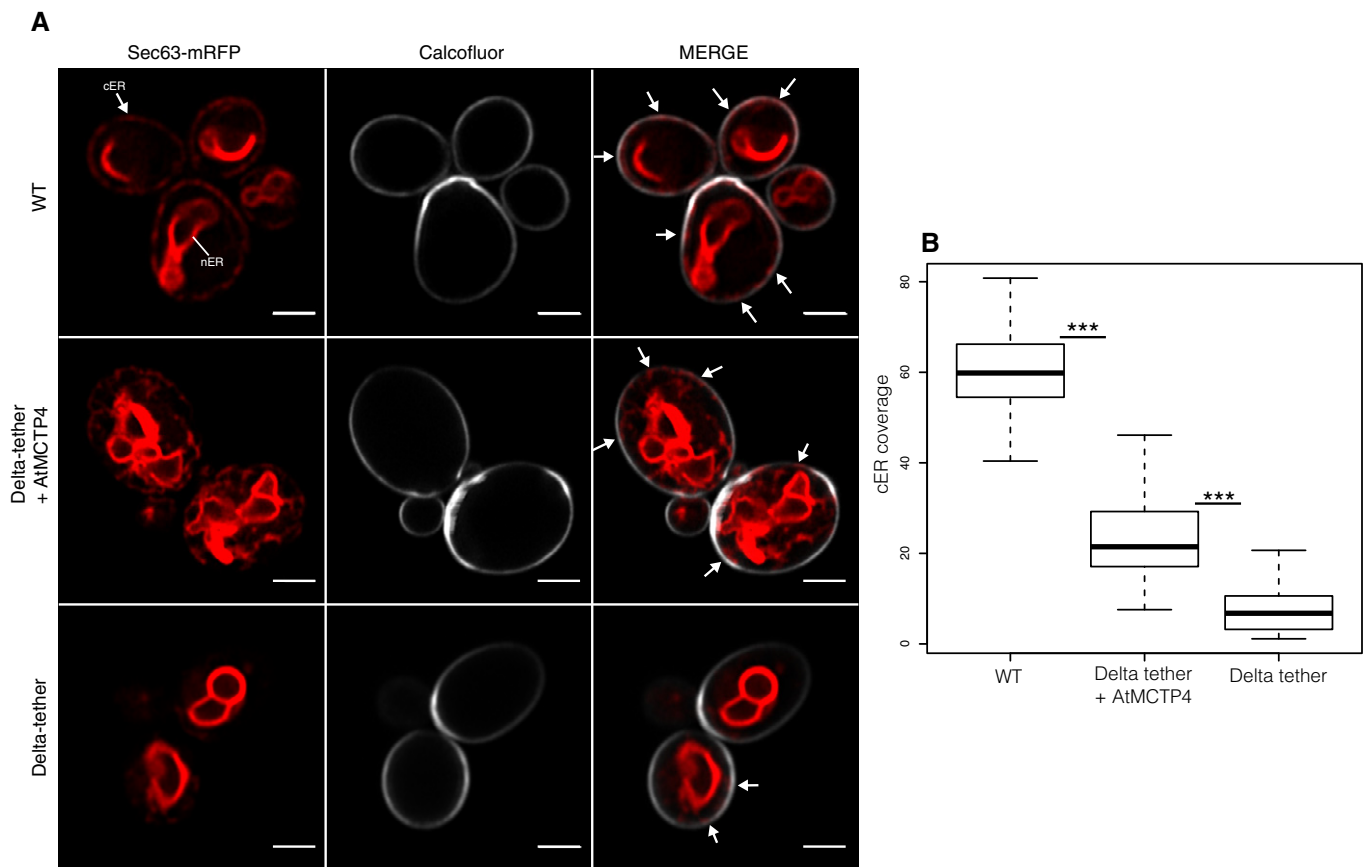


**Figure 8. AtMCTP4 expression in yeast partially restores ER-PM membrane contact sites.**

Expression of AtMCTP4 in yeast  $\Delta$ tether cells (*ist2* $\Delta$ , *scs2/22* $\Delta$  and *tcbl1/2/3* $\Delta$ ) [76] followed by confocal microscopic analysis of cortical ER.

**A** Top to bottom: Wild-type (WT) cell,  $\Delta$ tether expressing untagged AtMCTP4 and  $\Delta$ tether cells, respectively. The cortical ER (cER) and nuclear ER (nER) are labelled by the ER marker Sec63-RFP (red), while the cell periphery is stained by calcofluor (white). In WT cells, both nER and cER are visible, whereas in  $\Delta$ tether cell only remains of the cER are visible (arrows), due to the loss of ER-PM tethering factors. When AtMCTP4 is expressed in the yeast  $\Delta$ tether, partial recovery of cER is observable (arrows). Scale bars, 2  $\mu$ m.

**B** Quantification of cER expressed as a ratio of the length of cER to length of the PM in WT,  $\Delta$ tether+AtMCTP4 and  $\Delta$ tether cells. Numbers of cells used for quantifying the cER:  $n = 39$  for WT,  $n = 49$  for  $\Delta$ tether+AtMCTP4 and  $n = 61$  for  $\Delta$ tether strains. Wilcoxon test was used to compare the extent of cER between the different strains, i.e. WT versus  $\Delta$ tether+AtMCTP4 and  $\Delta$ tether+AtMCTP4 versus  $\Delta$ tether ( $***P < 0.001$ ). In the box plot, median is represented by horizontal line, values between quartiles 1 and 3 are represented by box ranges, and minimum and maximum values are represented by error bars.

employing a protocol previously used to determine the lipid composition of these structures and which gives rise to pure plasmodesmata-derived membrane fractions [27,50,54]. We also took advantage of a label-free proteomic approach to simultaneously analyse plasmodesmata, PM, microsomal, cell wall and total cell extracts with the aim to discriminate plasmodesmata constituents from potential contaminants. Compared to the previously published *Arabidopsis* plasmodesmata proteome [49], our refined proteomic analysis is more stringent yet includes most of the well-established plasmodesmata protein residents such as members of the PDLP, PDCB,  $\beta$ 1-3 glucanase and callose synthase families [4,6,29,60,78,79] (Appendix Table S1).

Using this proteomic approach, we identified several members of the MCTP family as plasmodesmata-enriched constituents, which we confirmed by confocal analysis using fluorescently tagged protein fusion, immunogold labelling and CLEM.

So far, two members of the MCTP family, AtMCTP1/FTIP and AtMCTP15/QKY, have been conclusively identified as plasmodesmata-associated proteins in *Arabidopsis*, both proteins acting as regulators of cell-to-cell signalling [20,51]. A recent study in Maize [80] also reports the localisation of CPD33 (AtMCTP15/QKY homolog) in plasmodesmata and at the ER, with *cdp33* loss of function mutant exhibiting defects in plasmodesmata-mediated carbohydrate distribution. Here, we localise several further family members to plasmodesmata, including some for which other subcellular localisations were previously reported [52,53]. In particular, a recent paper by Liu *et al* [52] identified AtMCTP3 and AtMCTP4 as endosomal but also golgi, plasma membrane and cytosolic proteins whereas our data indicate that both proteins are plasmodesmata and ER-located. We fused GFP or YFP to the N-terminus of AtMCTP3 and AtMCTP4. This is in contrast to Liu *et al* [52], who inserted either GFP or RFP internally within the coding sequence or a 4xHA tag at the N-terminus, and reported both fusions as complementing *Atmctp3/Atmctp4*. AtMCTP4 fused to GFP at the N-terminus localised to plasmodesmata in transient expression in *N. benthamiana* leaves [63]. It has previously been shown for AtMCTP15/QKY that a functional, N-terminal GFP fusion is located at plasmodesmata, a subcellular localisation supported by immunogold electron microscopy, whereas a non-functional, C-terminal fusion shows a PM localisation [20,81]. On the other hand, a C-terminal GFP fusion and a N-terminal 4xHA tag fusion of AtMCTP1/FTIP were both located at plasmodesmata and the ER and functional [51]. Internally [52] or N-terminally (this study) fused AtMCTP constructs both complemented *Atmctp3/Atmctp4* double mutant. Thus, fusions at different positions may affect localisation of various MCTPs differently, and the proteins may also function at more than one subcellular localisation. Similarly to Liu *et al* [52], we found that a *Atmctp3/Atmctp4* loss-of-function *Arabidopsis* mutant displays severe developmental defects, which include stem cell specification defects in the shoot, but also in the root which had not been investigated by Liu *et al* [52]. We further show that the double *Atmctp3/Atmctp4* mutant is impaired in plasmodesmata trafficking, with reduced size exclusion limit, and has an altered plasmodesmal proteome.

### MCTPs as plasmodesmata-specific ER-PM tethers

While ER-PM contacts within plasmodesmata have been observed for decades [22–24,82], the molecular identity of the tethers has

remained elusive. Here, we propose that MCTPs are prime plasmodesmal membrane tethering candidates as they possess all required features: (i) strong association with plasmodesmata; (ii) structural similarity to known ER-PM tethers such as HsE-Syts and AtSYTs [57,58,66] with an ER-inserted TMR at one end and multiple lipid-binding C2 domains at the other for PM docking; and (iii) the ability to partially restore ER-PM tethering in a yeast  $\Delta$ tether mutant.

Similarly to other ER-PM tethers [15,47,48,58], MCTP C2 domains dock to the PM through electrostatic interaction with anionic lipids, especially PI4P and to a lesser extent PS. In contrast with animal cells, PI4P is found predominantly at the PM in plant cells and defines its electrostatic signature [75]. Although PI4P depletion reduces AtMCTP4 association with the pores, it is unlikely that the lipid acts alone as a sole determinant of plasmodesmata targeting, as MCTP C2 domains without the TMR did not localise to the pores. Instead, a combination of protein/protein and protein/lipid interactions at both the ER and PM may collectively contribute to plasmodesmata targeting of the MCTP family. Although plasmodesmata are MCS, they are also structurally unique: both the ER and the PM display extreme, and opposing membrane curvature inside the pores; the ER tubule is linked to the PM on all sides; and the membrane apposition is unusually close (2–3 nm in type I post-cytokinetic pores [25]). Thus, while structurally related to known tethers, MCTPs are also expected to present singular properties. For instance, similar to the human MCTP2, plant MCTPs could favour ER membrane curvature through their TMR [83]. Plasmodesmata also constitute a very confined environment, which, together with the strong negative curvature of the PM, may require the properties of MCTP C2 domains to differ from that of HsE-Syts or AtSYTs. All of these aspects will need to be investigated in the future.

### Interorganellar signalling at the plasmodesmal MCS?

In yeast and animals, MCS have been shown to be privileged sites for interorganelle signalling by promoting fast, non-vesicular transfer of molecules such as lipids [15,40,68]. Unlike the structurally analogous tethering proteins AtSYTs and HsE-Syts, MCTPs do not harbour known lipid-binding domains that would suggest that they participate directly in lipid transfer between membranes. However, MCTPs are likely to act in complex with other proteins [81,84] which may include lipid-shuttling proteins. For instance, AtSYT1, which contains a lipid-shuttling SMP (synaptotagmin-like mitochondrial-lipid-binding protein) domain [85], is recruited to plasmodesmata during virus infection and promotes virus cell-to-cell movement [66]. MCS tethers typically interact with other MCS components and locally regulate their activity, act as  $\text{Ca}^{2+}$  sensors or modulate membrane spacing to turn lipid shuttling on or off [37,38,41–46,58,68,86,87]. Similar activities could be performed by MCTPs at plasmodesmata and might contribute to the altered plasmodesmal proteome of the *Atmctp3/Atmctp4* mutant. To date however, ER-PM cross-talk at plasmodesmata remains hypothetical.

### Combining organelle tethering and cell-to-cell signalling functions

Several members of the MCTP family have previously been implicated in regulating either macromolecular trafficking or intercellular



signalling through plasmodesmata. AtMCTP1/FTIP interacts with and is required for phloem entry of the Flowering Locus T (FT) protein, triggering transition to flowering at the shoot apical meristem [51]. Similarly, AtMCTP3/AtMCTP4 regulate trafficking of SHOOTMERISTEMLESS in the shoot apical meristem; however, in this case they prevent cell-to-cell trafficking [52]. In this study, we have shown that an *Atmctp3.Atmctp4* mutant displays reduced macromolecular trafficking between leaf epidermal cells, though it remains to be investigated how this relates to trafficking of specific developmental signals. AtMCTP15/QKY promotes the transmission of an unidentified non-cell-autonomous signal through interaction with the plasmodesmata/PM-located receptor-like kinase STRUBBELIG [20]. Thus, previously characterised MCTP proteins regulate intercellular trafficking/signalling either positively or negatively.

While the mechanisms by which these MCTP proteins regulate intercellular transport/signalling have not been elucidated, MCTP physical interaction with mobile factors or receptor is critical for proper function [20,51–53]. In AtMCTP1/FTIP, the interaction is mediated by the C2 domain closest to the TMR [53]. For the C2 domains of HsE-Syts, conditional membrane docking is critical for

their function and depends on intramolecular interactions, cytosolic  $\text{Ca}^{2+}$  and the presence of anionic lipids [58,68,87–89]. With three to four C2 domains, it is conceivable that MCTPs assume different conformations within the cytoplasmic sleeve in response to changes in the plasmodesmal PM composition,  $\text{Ca}^{2+}$  and the presence of interacting mobile signals (Fig 9), which could link membrane tethering to cell-to-cell signalling. Understanding in detail how MCTPs function in the formation and regulation of the plasmodesmal MCS will be an area of intense research in the coming years.

## Materials and Methods

### Biological material and growth conditions

*Arabidopsis* (*Columbia*) and transgenic lines were grown vertically on solid medium composed of *Murashige and Skoog* (MS) medium including vitamins (2.15 g/l), MES (0.5 g/l) and plant agar (7 g/l), pH 5.7, and then transferred to soil under long-day conditions at 22°C and 70% humidity.

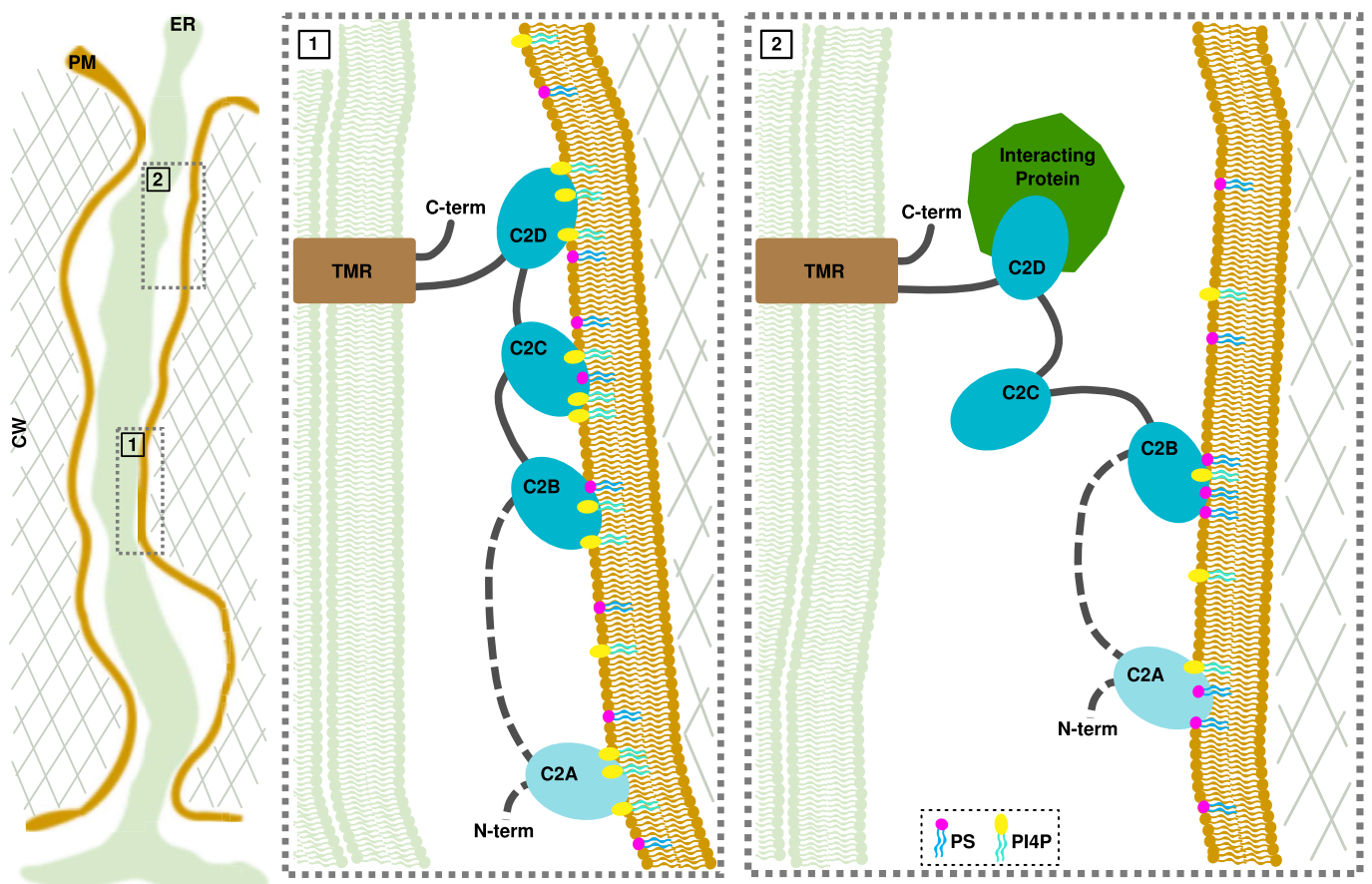


**Figure 9. Model of MCTP arrangement within plasmodesmata and hypothetical conditional docking events.**

Inside plasmodesmata, MCTPs insert into the ER via their transmembrane regions (TMR), while docking to the PM by interacting with the negatively charged phospholipids, PS and PI4P via their C2 domains. In condition of high PI4P/PS levels, all C2 domains interact with the PM, maintaining the ER close to the PM (panel 1). Decrease in the PI4P pool and/or protein interaction causes a detachment of some but not all C2 domains, which then modulate the space between the two membranes and the properties of the cytoplasmic sleeve. Please note that the exact topology of the TMR is not currently known.

*Arabidopsis* (*Landsberg erecta*) culture cells were cultivated as described in [Ref. 26] under constant light (20  $\mu$ E/m/s) at 22°C. Cells were used for experimentation at various ages ranging from 4 to 7 days old (mentioned in individual experiment).

### MCTP sequence alignment and phylogenetic tree

The 16 members of *Arabidopsis thaliana* MCTP family, gathering a total of 59 C2 domains, were dissected using a combination of several bioinformatic tools. The alignment of *A. thaliana* MCTP members from [Ref. 53] combined with Pfam predictions was used as a first step to segregate the MCTP members into “subfamilies”: the short MCTPs, which contain three C2 domains (C2B to C2D), and the long MCTPs, which contain four C2 domains (C2A to C2D). The short MCTPs lack the C2A domain, whereas the C2B, C2C and C2D are conserved in all members.

The prediction and delimitation of C2 domains in proteins, including MCTPs, from databases such as Pfam are rather imprecise. In order to provide stronger and more accurate predictions for the delimitation of each C2 domain, we used both the PSIPRED [90,91] protein sequence analysis (<http://bioinf.cs.ucl.ac.uk/psipred/>) and hydrophobic cluster analysis [92] (HCA; <http://www-ext.impmc.upmc.fr/~callebau/HCA.html>). Multiple sequence alignment was performed using Clustal Omega (<http://www.ebi.ac.uk/Tools/msa/clustalo/>).

### Cluster map of human and *A. thaliana* C2 domains

To generate a C2 cluster map, we first collected all *A. thaliana* and human C2 domains, using the HHpred web server [92,93]. The obtained set was filtered to a maximum of 100% pairwise sequence identity at a length coverage of 70% using MMseqs2 [95] to eliminate all redundant sequences. The sequences in the filtered set, comprising almost all human and *A. thaliana* C2 domains (~1,800 in total), were next clustered in CLANS [71] based on their all-against-all pairwise sequence similarities as evaluated by BLAST P-values.

### Cloning of MCTPs and transformation into *Arabidopsis*

The different constructs used in this study were either PCR amplified from cDNA or genomic DNA (Col-0) using gene-specific primers (Appendix Table S2), or were synthesised and cloned into donor vectors by GenScript® (Appendix Table S2). For N-terminal tag fusion, the PCR/DNA products were cloned into the MultiSite Gateway® donor vectors pDONR-P2RP3 (Invitrogen, Carlsbad, CA) and then subcloned into pB7m34GW or pK7m34GW using the multisite LR recombination system [96], the moderate promoter UBIQUITIN10 (UBQ10/pDONR-P4P1R previously described in [97]) and eYFP/pDONR221. For C-terminal tag fusion, the PCR/DNA products were first cloned into pDONR221, and then, was recombined using multisite recombination system using mVenus/pDONR-P2RP3 and UB10/pDONR-P4P1R.

For the expression of GFP-AtMCTP4 driven by its native promoter, we used the binary vector pRBbar-OCS harbouring a BASTA resistance, a multiple cloning side (MCS) and an octopine synthase (OCS) terminator within the left and right borders. The vector is derived from the pB2GW7 [96] by cutting out the expression cassette with the

restriction enzymes SacI and HindIII and replacing it with a synthesised MCS and an OCS terminator fragment. To combine promoter region and GFP-AtMCTP4 coding sequence, we used In-Fusion Cloning (Takara Bio Europe). To PCR amplify the coding sequence for GFP-AtMCTP4 with its respective primers (Appendix Table S2), we used the plasmid coding for GFP-AtMCTP4 as template (previously described as GFP-C2-89 by [63]). The resulting pRBbar-pAtMCTP4: plasmid was linearised with BamHI/PstI, and the amplified GFP-MCTP4 was fused in to generate the MCTP4 promoter-driven GFP-AtMCTP4 construct (pAtMCTP4:GFP-AtMCTP4).

Expression vectors were transformed in *Arabidopsis* Col-0 by floral dip [98], and transformed seeds were selected based on plasmid resistance.

*Nicotiana benthamiana* homologs of *Arabidopsis* MCTP isoforms were identified by protein BLAST searches against the SolGenomics *N. benthamiana* genome (<https://solgenomics.net>). An ortholog of AtMCTP7, NbMCTP7 (Niben101Scf03374g08020.1), was amplified from *N. benthamiana* leaf cDNA. The recovered cDNA of NbMCTP7 differed from the SolGenomics reference by the point mutation G287D and three additional silent nucleotide exchanges, as well as missing base pairs 1,678–1,716 which correspond to thirteen in-frame codons (encoding the amino acid sequence LKKEKFSSRLHLR). We note that this nucleotide and amino acid sequence is exactly repeated directly upstream (bp 1,639–1,677) in the SolGenomics reference and may thus represent an error in the *N. benthamiana* genome assembly. The recovered NbMCTP7 sequence has been submitted to database.

### Generation of *Atmctp3/Atmctp4* loss of function *Arabidopsis* mutant

*Atmctp3* (Sail\_755\_G08) and *Atmctp4* (Salk\_089046) T-DNA insertion *Arabidopsis* mutants (background Col-0) were obtained from the *Arabidopsis* Biological Resource Center (<http://www.arabidopsis.org/>). Single T-DNA insertion lines were genotyped, and homozygous lines were crossed to obtain double homozygous *Atmctp3/Atmctp4*.

For genotyping, genomic DNA was extracted from Col-0, *Atmctp3* (GABI-285E05) and *Atmctp4* (SALK-089046) plants using chloroform:isoamyl alcohol (ratio 24:1), genomic DNA isolation buffer (200 mM Tris-HCl PH7.5, 250 mM NaCl, 25 mM EDTA and 0.5% SDS) and isopropanol. PCR was performed with primers indicated in Appendix Table S2. For transcript expression, total mRNA was extracted from Col-0 and *Atmctp3/Atmctp4* using RNeasy® Plant Mini Kit (Qiagen) and cDNA was produced using random and oligodT primers. The expression level of AtMCTP3, AtMCTP4 and ubiquitous Actin2 (ACT2) transcript was tested by PCR amplification using primers listed in Appendix Table S2.

### Macromolecular cell-to-cell trafficking assay

60 ng of a plasmid encoding GFP-sporamin under control of a 35S promoter [62] was mixed with 1- $\mu$ m gold particles (Bio-Rad) suspended in ethanol and bombarded into fully expanded *Arabidopsis* leaf rosettes from approximately 1.5- to 2-cm distance using a home-built non-vacuum nitrogen pressure gun [99]. Leaves were detached and imaged at 72 h after bombardment. Clusters of fluorescent cells were counted manually on maximum projections.

### Label-free proteomic analysis of plasmodesmata

To establish the plasmodesmata core proteome, the identification and the relative amount of proteins in different cellular fractions, namely, the plasmodesmata, PM, total cell (TP) extract, microsomal and cell wall (CW) fractions, were determined with a label-free quantification method. Four to six biological replicates of each fraction were used for quantification. The plasmodesmata, PM and microsomal fractions were purified from liquid cell cultures of *Arabidopsis thaliana* (ecotype Landsberg *erecta*) as described in [Ref. 27,54] and the cell wall protein extract as in [Ref. 100].

Ten micrograms of each protein sample was solubilised in Laemmli buffer and deposited onto an SDS-PAGE gel for concentration and cleaning purposes. Separation was stopped after proteins entered the resolving gel, and following colloidal blue staining, the bands were excised and cut into 1-mm<sup>3</sup> pieces. Gel pieces were destained in 25 mM ammonium bicarbonate and 50% acetonitrile (ACN), rinsed twice in ultrapure water and shrunk in ACN for 10 min. After ACN removal, gel pieces were dried at room temperature, covered with trypsin solution (10 ng/ml in 40 mM NH<sub>4</sub>HCO<sub>3</sub> and 10% ACN), rehydrated at 4°C for 10 min and finally incubated overnight at 37°C. Gel pieces were then incubated for 15 min in 40 mM NH<sub>4</sub>HCO<sub>3</sub> and 10% ACN at room temperature. The supernatant was collected, and a water:ACN:HCOOH (47.5:47.5:5) extraction solution was added to gel slices for 15 min. The extraction step was repeated twice. Supernatants were concentrated by vacuum centrifugation to a final volume of 100 µl and acidified. The peptide mixture was analysed with the UltiMate 3000 Nano LC System (Dionex, Amsterdam, The Netherlands) coupled to an Electrospray Q-Exactive quadrupole Orbitrap benchtop mass spectrometer (Thermo Fisher Scientific, San Jose, CA). Ten microlitres of peptide digests was loaded onto a 300-µm-inner diameter × 5-mm C<sub>18</sub> PepMap™ trap column (LC Packings) at a flow rate of 30 µl/min. The peptides were eluted from the trap column onto an analytical 75-mm id × 25-cm C<sub>18</sub> PepMap™ column (LC Packings) with a 4–40% linear gradient of solvent B in 48 min (solvent A was 0.1% formic acid in 5% ACN, and solvent B was 0.1% formic acid in 80% ACN). The separation flow rate was set at 300 nl/min. The mass spectrometer was operated in positive ion mode at a 1.8-kV needle voltage. Data were acquired using Xcalibur 2.2 software in a data-dependent mode. MS scans (*m/z* 300–2,000) were recorded at a resolution of *R* = 70,000 (@ *m/z* 200) and an AGC target of 10<sup>6</sup> ions collected within 100 ms. Dynamic exclusion was set to 30 s, and top 15 ions were selected from fragmentation in HCD mode. MS/MS scans with a target value of 1 × 10<sup>5</sup> ions were collected with a maximum fill time of 120 ms and a resolution of *R* = 35,000. Additionally, only +2 and +3 charged ions were selected for fragmentation. Other settings were as follows: no sheath nor auxiliary gas flow, heated capillary temperature, 250°C; normalised HCD collision energy of 25%; and an isolation width of 3 *m/z*. Data were searched by SEQUEST through Proteome Discoverer 1.4 (Thermo Fisher Scientific) against a subset of the version 11 of the Araport (<https://www.araport.org/>) protein database (40,782 entries). Spectra from peptides higher than 5,000 Da or lower than 350 Da were rejected. The search parameters were as follows: the mass accuracy of the monoisotopic peptide precursor and peptide fragments was set to 10 ppm and 0.02 Da, respectively. Only b- and y ions were considered for mass calculation. Oxidation of methionines (+16 Da) was considered as variable

modification and carbamidomethylation of cysteines (+57 Da) as fixed modification. Two missed trypsin cleavages were allowed. Peptide validation was performed using the Percolator algorithm [101], and only “high-confidence” peptides were retained, corresponding to a 1% false-positive rate at peptide level.

For label-free quantitative data analysis, raw LC-MS/MS data were imported in Progenesis QI for Proteomics 2.0 (Nonlinear Dynamics Ltd, Newcastle, U.K.). Data processing includes the following steps: (i) features detection; (ii) features alignment across the twenty-six samples; (iii) volume integration for two to six charge-state ions; (iv) normalisation on ratio median; (v) import of sequence information; and (vi) calculation of protein abundance (sum of the volume of corresponding peptides). Only non-conflicting features and unique peptides were considered for calculation at the protein level. Quantitative data were considered for proteins quantified by a minimum of two peptides. Protein enrichment ratios were calculated between each protein in the plasmodesmata fraction and the same protein in the four other cellular fractions. Before that, a relative normalised abundance was established for each protein to the most abundant protein in the fraction of interest. Protein enrichment was estimated by calculating the ratio between the relative normalised abundance of a given protein in the fraction of interest compared to other fractions.

Cut-offs for enrichment ratios were determined using a reference list of previously identified plasmodesmata proteins (see Appendix Table S1 with previously characterised plasmodesmal proteins outlined in orange). Cut-off scores of 8 for plasmodesmata/PM, 40 for plasmodesmata/microsome, 30 for plasmodesmata/TP and 30 for plasmodesmata/CW were selected in order to filter out the false positives, as most well-established plasmodesmal proteins display similar or higher enrichment ratios. Please note that while LysM domain-containing GPI-anchored protein 2 (LYM2) has been characterised as a plasmodesmal protein [12], its enrichment ratio value was below our cut-off limit. We manually added this protein to the core plasmodesmata proteome.

ER proteomic dataset was extracted from [Ref. 55,56].

To estimate differential abundance of *Arabidopsis* plasmodesmal proteins type II (7-day-old cells) versus type I (4-day-old cultured cells), label-free proteomic analysis was carried out as described above. Four biological replicates for each condition were used. Enrichment ratios were calculated for individual protein in the seven (type II)- versus 4 (type I)-day-old plasmodesmata fraction. Cut-off absolute value of enrichment ratio was set at 1.3-fold. A *t*-test comparing type II protein-normalised abundance to type I protein-normalised abundance was established and the significant limit was fixed at 0.05 and below. Only proteins from the plasmodesmata core proteome, which responded to these two thresholds, were retained. Please note that differential accumulation of type I versus type II plasmodesmata in *Arabidopsis* cultured cells was established in previous work by Nicolas *et al* [25].

The mass spectrometry proteomics data have been deposited to the ProteomeXchange Consortium via the PRIDE [102] partner repository with the dataset identifier PXD006806.

### Comparative proteomic analysis

For comparative proteomic comparison, we used 5 biological replicates of *Atmctp3/Atmctp4* and Col-0 of fully developed leaves and

enriched plasmodesmata-containing cell wall as described by Kraner et al [63]. Following that protocol, the remaining proteins were solubilised and subsequently digested with trypsin. Desalted peptides were separated on a 160-min acetonitrile gradient by ultra-performance liquid chromatography (UPLC). After electron spray ionisation, samples were analysed by an Orbitrap Fusion Tribrid Mass Spectrometer in HCD fragmentation mode. Raw MS data files were analysed by using PEAKS Studio 8.5 (Bioinformatics Solutions, Waterloo, Ontario, Canada; [103]) against the *Arabidopsis* TAIR10 protein database (November 2010, 35 386 entries). For identification, we allowed parent mass tolerance of 10.0 ppm, fragment mass tolerance of 0.5 Da, and two missed cleavages. Carbamidomethylation of cysteines was set as static modification and oxidation of methionine as dynamic modification. For label-free quantification, the FDR threshold was set to 1% and retention time shift tolerance to 10 min.

### Confocal laser scanning microscopy

For transient expression in *N. benthamiana*, leaves of 3-week-old plants were pressure-infiltrated with GV3101 agrobacterium strains, previously electroporated with the relevant binary plasmids. Prior to infiltration, agrobacteria cultures were grown in Luria and Bertani medium with appropriate antibiotics at 28°C for 2 days, then diluted to 1/10 and grown until the culture reached an OD<sub>600</sub> of about 0.8. Bacteria were then pelleted and resuspended in water at a final OD<sub>600</sub> of 0.3 for individual constructs and 0.2 each for the combination of two. The ectopic silencing suppressor 19k was co-infiltrated at an OD<sub>600</sub> of 0.15. Agroinfiltrated *N. benthamiana* leaves were imaged 3–4 days post-infiltration at room temperature. ~ 2 by 2 cm leaf pieces were removed from plants and mounted with the lower epidermis facing up onto glass microscope slides.

Transgenic *Arabidopsis* plants were grown as described above. For primary roots, lateral roots and hypocotyl imaging, 6- to 7-day-old seedlings or leaves of 5- to 8-leaf stage rosette plants were mounted onto microscope slides. For shoot apical meristem imaging, the plants were first dissected under a binocular, then transferred to solid MS media and immediately observed using a long-distance working 40× water-immersion objective.

Confocal imaging was performed on a Zeiss LSM 880 confocal laser scanning microscope equipped with fast AiryScan using Zeiss C PL APO x63 oil-immersion objective (numerical aperture 1.4). For GFP, YFP and mVenus imaging, excitation was performed with 2–8% of 488 nm laser power and fluorescence emission collected at 505–550 nm and 520–580 nm, respectively. For RFP and mCherry imaging, excitation was achieved with 2–5% of 561 nm laser power and fluorescence emission collected at 580–630 nm. For aniline blue (infiltrated at the concentration of 25 µg/ml) and calcofluor white (1 µg/ml), excitation was achieved with 5% of 405 nm laser and fluorescence emission collected at 440–480 nm. For co-localisation, sequential scanning was systematically used.

For quantification of NbMCTP7 co-localisation with VAP27.1, SYT1 and PDCB1, co-expression of the different constructs was done in *N. benthamiana*. An object-based method was used for co-localisation quantification [104]. Images from different conditions are all acquired with same parameters (zoom, gain, laser intensity, etc.), and channels are acquired sequentially. These images are processed and filtered using ImageJ software (<https://imagej.nih.gov/ij/>)

in order to bring out the foci of the pictures. These foci were then automatically segmented by thresholding, and the segmented points from the two channels were assessed for co-localisation using the ImageJ plugin *Just Another Colocalization Plugin (JACoP)* [104]. This whole process was automatised using a macro (available upon demand).

Pseudo-Schiff propidium iodide-stained *Arabidopsis* root tips were performed according to [Ref. 104]. Aniline blue staining was performed according to [Ref. 27]. Brightness and contrast were adjusted on ImageJ software (<https://imagej.nih.gov/ij/>).

### Plasmodesmata (PD) index

Plasmodesmata depletion or enrichment was assessed by calculating the fluorescence intensity of GFP/YFP-tagged full-length MCTP, truncated MCTPs and the proton pump ATPase GFP-PMA2 [106], at (i) plasmodesmata (indicated by mCherry-PDCB1, PDLP1-mRFP or aniline blue) and (ii) the cell periphery (i.e. outside plasmodesmata pit fields). For that, confocal images of leaf epidermal cells (*N. benthamiana* or *Arabidopsis*) were acquired by sequential scanning of mCherry-PDCB1, PDLP1-mRFP or aniline blue (plasmodesmata markers) in channel 1 and GFP/YFP-tagged MCTPs in channel 2 (for confocal setting, see above). About thirty images of leaf epidermis cells were acquired with a minimum of three biological replicates. Individual images were then processed using ImageJ by defining five regions of interest (ROI) at plasmodesmata (using plasmodesmata marker to define the ROI in channel 1) and five ROIs outside plasmodesmata. The ROI size and imaging condition were kept the same. The GFP/YFP-tagged MCTP mean intensity (channel 2) was measured for each ROI and then averaged for single image. The plasmodesmata index corresponds to intensity ratio between fluorescence intensity of MCTPs at plasmodesmata versus outside the pores. For the plasmodesmata index of RFP-HDEL, PDLP1-RFP and mCherry-PDCB1, we used aniline to indicate pit fields. R software was used for making the box plots and statistics.

### FRAP analysis

For FRAP analysis, GFP-NbMCTP7, RFP-HDEL and mCherry-PDCB1-expressing *N. benthamiana* leaves were used. The experiments were performed on a Zeiss LSM 880 confocal microscope equipped with a Zeiss C PL APO x63 oil-immersion objective (numerical aperture 1.4). GFP and mCherry were respectively excited at 488 nm and 561 nm with 2% of argon or DPSS 561-10 laser power, and fluorescence was collected with the GaAsp detector at 492–569 nm and 579–651 nm, respectively. To reduce as much as possible scanning time during FRAP monitoring, the acquisition window was cropped to a large rectangle of 350 by 50 pixels, with a zoom of 2.7 and pixel size of 0.14 µm. By this mean, pixel dwell time was of 0.99 µs and total frame scan time could be reduced down to 20 ms approximately. Photobleaching was performed on rectangle ROIs for the ER network and on circle ROIs for the pit fields with the exciting laser wavelengths set to 100%. The FRAP procedure was the following: 30 pre-bleach images, 10 iterations of bleaching with a pixel dwell time set at 1.51 µs and then 300 images post-bleach with the “safe bleach mode for GaAsp”, bringing up the scan time up to approximately 200 ms. The recovery profiles were background subtracted and then double normalised (according to the last

pre-bleach image and to the reference signal, in order to account for observational photobleaching) and set to full scale (last pre-bleach set to 1 and first post-bleach image set to 0), as described by Kote Miura in his online FRAP-teaching module (EAMNET-FRAP module, <https://embl.de>). Plotting and curve fitting were performed on GraphPad Prism (GraphPad Software, Inc.).

### 3D-SIM imaging

For 3D structured illumination microscopy (3D-SIM), an epidermal peel was removed from a GFP-NbMCTP7-expressing leaf and mounted in perfluorocarbon PP11 [106] under a high-precision ( $170\ \mu\text{m} \pm 5\ \mu\text{m}$ ) coverslip (Marie Enfield). The sample chamber was sealed with non-toxic Exaktosil N 21 (Bredent, Germany). 3D-SIM images were obtained using a GE Healthcare/Applied Precision OMX v4 BLAZE with a 1.42NA Olympus PlanApo N 60 $\times$  oil-immersion objective. GFP was excited with a 488 nm laser and imaged with emission filter 504–552 nm (528/48 nm). SR images were captured using DeltaVision OMX software 3.70.9220.0. SR reconstruction, channel alignment and volume rendering were done using softWoRx V. 7.0.0.

### Immunogold labelling on high-pressure frozen *Arabidopsis* roots

pAtMCTP4:GFP-AtMCTP4 roots were high-pressure frozen, freeze-substituted and embedded into HM20 resin as described in [Ref. 27]. Immunogold labelling was performed on 90-nm sections with the following antibodies: polyclonal anti-GFP antibody (Invitrogen A-11122 and Torrey lines TP-401) diluted at 1:200. Antibody binding was detected with 5 or 10 nm gold-conjugated goat anti-rabbit antibodies diluted 1:40. Quantification of immunogold labelling was performed by counting gold particles in plasmodesmata, at the cell wall outside plasmodesmata and endomembrane/cytosolic compartments. The numbers of gold particles were then normalised to the relative area of each compartment (compartment area/total analysed area). Statistical analysis was performed with the software R using the non-parametrical Wilcoxon test ( $n = 30$  images; a total of 298 gold particles were counted).

### Correlative light and electron microscopy (CLEM)

Cell wall purification from 10-day-old seedlings (pAtMCTP4:GFP-AtMCTP4) was performed according to [Ref. 108]. The purified walls were washed twice for 10 min with 0.2  $\mu\text{m}$  filtered deionised water before observation by confocal and electron microscopy. Wall fragments were directly deposited onto electron microscopy grids (T-400 mesh Cu, EMS) filmed with 2% parlalidion and carbon-coated, incubated for 3 min before removing water excess. The grid was then mounted in deionised water between glass slide and coverslip for confocal microscopy observation. The acquisition was performed using a Zeiss LSM 880 confocal microscope. The cell wall fragments were detected at 20 $\times$  magnification and imaged as z-stack at 63 $\times$  magnification (1.4 N.A., C-Plan-Apochromat, oil-immersion objective) with a pinhole (airy) of 1, excitation and emission filters at 405 nm and 415–490 nm, and at 488 nm and 500–560 nm for calcofluor white and GFP, respectively. The imaged wall fragments were identified by their overall position and shape on the grid which was then

recovered, dried and negative stained with 2% (w/v) uranyl acetate for transmission electron microscopy observation. The data acquisition was done on a FEI Tecnai G2 Spirit TWIN TEM with axial Eagle 4K camera at different magnifications to identify the wall fragment previously observed by confocal before focusing onto the region of interest. Afterwards, the low magnification images of both confocal and electron microscopy were superimposed for correlation (Photoshop).

Subsequent immunogold labelling was combined with CLEM. This requires blocking cell walls with 5% Natural Donkey Serum (NDS) in Tris-buffered saline (TBS) 1 $\times$  for 1 h before incubation overnight at 4 $^{\circ}\text{C}$  with monoclonal mouse antibodies against callose ( $\beta$ -(1-3)-glucan antibody; Biosupplies, Parkville, Victoria, Australia) diluted at 1:20. Antibody excess was washed four times (10 min) with TBS 1 $\times$ . For callose and PDCB1 co-labelling, the cell walls were then blocked a second time with 5% NDS in TBS 1 $\times$  for 1 h before incubation overnight at 4 $^{\circ}\text{C}$  with polyclonal rabbit anti-PDCB1 antibodies [27] diluted at 1:300. Antibody excess was washed four times (10 min) with TBS 1 $\times$ . Antibody binding was detected by 5 nm diameter gold-conjugated goat anti-rabbit antibodies (PDCB1) diluted at 1:30 (BB international) incubated for 2 h or 10 nm diameter gold-conjugated goat anti-mouse antibodies for callose and 5 nm diameter gold-conjugated goat anti-rabbit antibodies for PDCB1, both diluted at 1:30 and incubated for 2 h at room temperature. The control conditions for each immunogold labelling were performed following the same protocol without primary antibody incubation. After immunogold labelling, the cell wall fragments were washed twice 10 min with 0.2  $\mu\text{m}$  filtered deionised water before observation by confocal and electron microscopy.

### PAO treatment

Short-term phenylarsine oxide (PAO) treatment was performed on 7-day-old *Arabidopsis* seedlings expressing pAtMCTP4:GFP-AtMCTP4 grown on solid agar plates containing MS salt (2.2 g/l) supplemented with vitamins, 1% sucrose and MES (0.5 g/l) at pH 5.8. For PAO treatment, seedlings were transferred to liquid MS media containing 60  $\mu\text{M}$  PAO for 30–40 min before imaging. Controls were performed by replacing PAO with DMSO.

Long-term PAO treatment was performed by growing *Arabidopsis* Col-0 onto solid agar plates containing MS salt (2.2 g/l) supplemented with vitamins, 1% sucrose, MES (0.5 g/l) and 1 or 10  $\mu\text{M}$  PAO for 7 days before imaging.

### 3D structure modelling and molecular dynamic simulations

The delimitation of each individual C2 domain of the MCTP family members was done by combining PSIPRED [89,90] secondary structure prediction, hydrophobic cluster analysis (HCA) [91] and multiple sequence alignment tools (Clustal Omega) [108], allowing a better definition of structured domains [109]. C2 domains are 130- to 140-residue water-soluble domains characterised by two facing beta-sheets of each four beta strands, with a hydrophobic core and loops connecting the beta strands.

AtMCTP4 C2 domain models were obtained using the automated ROSETTA server [110]. The three domains were aligned and built by comparative modelling from parents extended-synaptotagmin 2 (PDB id: 4npj) for C2B and C2C and Munc13-1 (PDB id: 3kwu) for C2D.

AtMCTP15 C2A, C2C and C2D domain models were obtained using T-COFFEE multiple sequence alignment [111,112], which served as input for Modeller [113] for homology modelling, with human E3 ubiquitin-like ligase NEDD4-like protein (PDB id : 2nsq), Munc13-1 (PDB id : 3kwt) and E3 ubiquitin-protein ligase NEDD4 (PDB id: 3b7y) for C2A; human E3 ubiquitin-like ligase NEDD4-like protein (PDB id : 2nsq), human Intersectin 2 (PDB id: 3jzy) and extended-synaptotagmin 2 (PDB id: 4npj) for C2C; and human MCTP2 (PDB id : 2ep6), human Intersectin 2 (PDB id: 3jzy) and extended-synaptotagmin 2 (PDB id: 4npj) for C2D. AtMCTP15 C2B domain was modelled using ROSETTA server [110] with alignment and comparative building from parent *Arabidopsis thaliana* CAR4 (PDB id: 5a51).

NbMCTP7 C2A domain was modelled using T-COFFEE multiple sequence alignment [111,112], which served as input for Modeller [113] for homology modelling, with human MCTP2 (PDB id: 2ep6), human E3 ubiquitin-like ligase NEDD4-like protein (PDB id: 2nsq) and Munc13-1 (PDB id: 3kwt). NbMCTP7 C2B, C2C and C2D were aligned and built by comparative modelling using ROSETTA server [110] from parents, C2 domain-containing protein from putative elicitor-responsive gene (PDB id: 1wfi) for C2B, the first C2 domain of human myoferlin (PDB id: 2dmh) for C2C and extended-synaptotagmin 2 (PDB id: 4npj) for C2D. Either ROSETTA [110] server or Modeller [113] was used for C2 domains modelling, depending on the quality of the template alignment. All the obtained C2 models were quality-verified using ProSA-web server [114].

The structural models were then used for molecular dynamic simulations with GROMACS v5 software [115]. Atomistic simulations have been performed with the GROMOS96 54a7 force field [117–119]. The systems were first minimised by steepest descent for 5000 steps. Then, NVT and NPT equilibrations were carried on for 1 ns with the protein under position restraints. Production runs were performed for 50 ns. The systems were solvated with SPC water [120]. All simulations were performed with a 2-fs time step, a short-range electrostatic cut-off and a short-range van der Waals cut-off of 1.0 nm. Bond lengths were maintained with the LINCS algorithm [121]. A Verlet cut-off scheme was used. Particle mesh Ewald (PME) [121] was used for long-range electrostatics. Temperature coupling was set to 300 K using v-rescale algorithm [123] with  $\tau_T = 0.1$  ps. For the NPT equilibration and the production run, pressure coupling was set to 1 bar using isotropic Parrinello-Rahman [124] with  $\tau_P = 2$  ps and compressibility at  $4.5 \times 10^{-5}$  (bar<sup>-1</sup>). Atomistic simulations showed that the characteristic beta sheet structure of C2 domains was stable along the 50-ns trajectories (RMSD < 0.15 nm) while the loops presented a greater mobility.

For the simulation of protein–membrane interactions, the models were converted to a coarse-grained (CG) representation suitable for the MARTINI 2.1 force field [125] with ELNEDIN [126] elastic network. To render the protein behaviour in CG, the ELNEDIN network was trimmed off at the high-mobility loop regions using the dom\_ELNEDIN.tcl script [127] in VMD software [128]. Behaviour validation was performed by comparing the RMSF from the 50-ns atomistic simulation to a mean RMSF over three 50-ns CG simulations.

The CG structures were placed above PLPC (1-palmitoyl,2-linoleoyl-sn-glycero-3-phosphocholine), PLPC:PLPS (1-palmitoyl,2-linoleoyl-sn-glycero-3-phosphoserine) (3:1) or PLPC:PLPS:Sitosterol:PI4P (1-palmitoyl,2-linoleoyl-sn-glycero-3-phosphoinositol-4-phosphate)

(57:19:20:4) bilayers built with the insane tool [129]. A 2000-step steepest descent energy minimisation and an equilibration of 1 ns with Berendsen [130] pressure coupling were carried out, followed by five production repetitions of 2.5  $\mu$ s with a 20-fs time step. Temperature and pressure were coupled at 300 K and 1 bars using the v-rescale [123] and Parrinello-Rahman [124] algorithm, respectively, with  $\tau_T = 1$  ps and  $\tau_P = 12$  ps. Pressure was coupled semi-isotropically in XY and Z. A Verlet cut-off scheme was used, with a buffer tolerance of 0.005. Electrostatic interactions were treated with a reaction field, a Coulomb cut-off of 1.1 nm and dielectric constant of 15. van der Waals interactions; had a cut-off of 1.1 nm; and used a potential shift Verlet modifier [131]. Bond lengths were maintained with the LINCS algorithm [121].

The trajectories were analysed with the GROMACS v5 tools as well as with homemade scripts and MDA software [132,133]. 3D structures were analysed with both PyMOL (DeLano Scientific, <http://www.PyMOL.org>) and VMD softwares.

Once the proteins were in interaction with the lipid bilayer, the systems were transformed to an atomistic resolution with backwards [134,135]. Atomistic simulations have been performed with the GROMOS96 54a7 force field [117–119]. All the systems studied were first minimised by steepest descent for 5,000 steps. Then, NVT and NPT equilibrations were carried on for 0.1 and 1 ns, respectively. The protein was under position restraints, and periodic boundary conditions (PBC) were used with a 2-fs time step. Production runs were performed for 100 ns. Temperature was maintained by using the Nose–Hoover method [135] with  $\tau_T = 0.2$  ps during equilibration processes and v-rescale [123] with  $\tau_T = 2.0$  ps for production run. All the systems were solvated with SPC water [120], and the dynamics were carried out in the NPT conditions (300 K and 1 bar). A semi-isotropic pressure was maintained by using the Parrinello-Rahman barostat [124] with a compressibility of  $4.5 \times 10^{-5}$  (1/bar) and  $\tau_P = 1$  ps. Verlet cut-off scheme was used for neighbour searching with fast smooth particle mesh Ewald (PME) [122] for electrostatics and twin range cut-offs for van der Waals interactions. Bond lengths were maintained with the LINCS algorithm [121].

## Yeast

Wild-type (SEY6210) and delta-tether yeast strain [76] were transformed with Sec63.mRFP (pSM1959). Sec63.mRFP [77] was used as an ER marker and was a gift from Susan Mickaelis (Addgene plasmid #41837). Delta-tether/Sec63.mRFP strain was transformed with AtMCTP4 (pCU416 : pCU between SacI and SpeI sites, Cyc1 terminator between XhoI and KpnI sites and AtMCTP4 CDS between BamHI and SmaI sites, Appendix Table S2). Calcofluor white was used to stain the cell wall of yeast. All fluorescent microscopy was performed on midlog cells, grown on selective yeast media (-URA -LEU for AtMCTP4 and Sec63 expression, and -LEU for Sec63). Images were acquired with AiryScan module, using a 63 $\times$  oil-immersion lens and sequential acquisition. Brightness and contrast were adjusted on ImageJ software (<https://imagej.nih.gov/ij/>).

Sequence data for genes in this article can be found in the GenBank/EMBL databases using the following accession numbers: AtMCTP1, At5g06850; AtMCTP2, At5g48060; AtMCTP3, At3g57880; AtMCTP4, At1g51570; AtMCTP5, At5g12970; AtMCTP6, At1g22610; AtMCTP7, At4g11610; AtMCTP8, At3g61300; AtMCTP9, At4g00700;

AtMCTP10, At1g04150; AtMCTP11, At4g20080; AtMCTP12, At3g61720; AtMCTP13, At5g03435; AtMCTP14, At3g03680; AtMCTP15, At1g74720; AtMCTP16, At5g17980 and NbMCTP7, Niben101Scf03374g08020.1.

## Data availability

Proteomic data: PRIDE PXD006800 (<http://www.ebi.ac.uk/pride/archive/projects/PXD006800>), PRIDE PXD006806 (<http://www.ebi.ac.uk/pride/archive/projects/PXD006806>) and PRIDE PXD013999 (<http://www.ebi.ac.uk/pride/archive/projects/PXD013999>).

**Expanded View** for this article is available online.

## Acknowledgements

This work was supported by the National Agency for Research (Grant ANR-14-CE19-0006-01 to E.M.B.), “Osez l’interdisciplinarité” OSEZ-2017-BRIDGING CNRS programme to E.M.B., the European Research Council (ERC) under the European Union’s Horizon 2020 research and innovation programme (grant agreement No 772103-BRIDGING) to E.M.B., the EMBO Young Investigator Program to E.M.B., and Fonds National de la Recherche Scientifique (NEAMEMB PDR T.1003.14, BRIDGING CDR J.0114.18 and RHAMEMB CDR J.0086.18) to L. L. and M.D. J.D.P. is funded by a PhD fellowship from the Belgian “Formation à la Recherche dans l’Industrie et l’Agriculture” (FRIA grant no. 1.E.096.18). Work in J.T. laboratory is supported by grant BB/M007200/1 from the U.K. Biotechnology and Biomedical Sciences Research Council (BBSRC) and by the Scottish Government’s Rural and Environment Science and Analytical Services Division (RESAS). Fluorescence microscopy analyses were performed at the plant pole of the Bordeaux Imaging Centre (<http://www.bic.u-bordeaux.fr>). For electron microscopy, the Region Aquitaine also supported the acquisition of the electron microscope (grant no. 2011 13 04 007 PFM), and FranceBioImaging Infrastructure supported the acquisition of the AFS2 and ultramicrotome. The proteomic analyses were performed at the Functional Genomic Center of Bordeaux, (<https://proteome.cgfb.u-bordeaux.fr>). We thank Steffen Vanneste and Abel Rosado for providing the VAP27.1.RFP and SYT1.GFP binary vectors and Yvon Jaillais for providing the 1xPH(FAPP1) *Arabidopsis* transgenic lines. The plasmid pRBbar-OCS was kindly provided by Prof. Frederik Börnke (IGZ—Leibniz Institute of Vegetable and Ornamental Crops, Großbeeren, Germany). We thank Christophe Trehin and Patrice Morel for providing the AtMCT15\_C2s construct and Alenka Copic for providing the yeast WT and  $\Delta$ tether strains. We thank Fabrice Cordelières for his help for the fluorescence image quantification and Paul Gouget, Yvon Jaillais, Andrea Paterlini and Yrjo Helariutta for critical review of the article prior to submission.

## Author contributions

Fl, MSG, MF and SC carried out the label-free proteomic analysis of plasmodesmata fractions isolated from *Arabidopsis* cell cultures. MLB cloned the MCTPs, produced and phenotyped the *Arabidopsis* transgenic lines, with the exception of AtMCTP4:GFP-AtMCTP4 and 35S:GFP-AtMCTP6 which were generated by MK. MLB and JDP imaged the MCTP reporter lines. WJN carried out the FRAP analysis and image quantification for co-localisation with the help of LB. MG and JDP performed the CLEM and immunogold labelling approaches. JT, MR and VG performed the plasmodesmata cell-to-cell trafficking assay. MK carried out the proteomic comparison and AP the data integration. AG performed the phylogenetic analysis. JDP and MLB carried out the PAO experiments. MLB performed the yeast experiments. TJH and JT performed

the 3D-SIM. VA carried out the C2 cluster map analysis. JDP carried out the molecular dynamic analysis with the help of J-MC, LL and MD. EMB conceived the study and designed experiments with the help of JT and LL. EMB, JDP, JT, MLB and YH wrote the manuscript. All the authors discussed the results and commented on the manuscript.

## Conflict of interest

The authors declare that they have no conflict of interest.

## References

1. Tilsner J, Nicolas W, Rosado A, Bayer EM (2016) Staying tight: plasmodesmata membrane contact sites and the control of cell-to-cell connectivity. *Annu Rev Plant Biol* 67: 337–364
2. Gallagher KL, Sozzani R, Lee C-M (2014) Intercellular protein movement: deciphering the language of development. *Annu Rev Cell Dev Biol* 30: 207–233
3. Ross-elliott TJ, Jensen KH, Haaning KS, Wager BM, Knoblauch J, Howell AH, Mullendore DL, Monteith AG, Paultre D, Yan D *et al* (2017) Phloem unloading in *Arabidopsis* roots is convective and regulated by the phloem-pole pericycle. *Elife* 6: e24125
4. Vatén A, Dettmer J, Wu S, Stierhof YD, Miyashima S, Yadav SR, Roberts CJ, Campilho A, Bulone V, Lichtenberger R *et al* (2011) Callose biosynthesis regulates symplastic trafficking during root development. *Dev Cell* 21: 1144–1155
5. Carlsbecker A, Lee J-Y, Roberts CJ, Dettmer J, Lehesranta S, Zhou J, Lindgren O, Moreno-Risueno MA, Vatén A, Thitamadee S *et al* (2010) Cell signalling by microRNA165/6 directs gene dose-dependent root cell fate. *Nature* 465: 316–321
6. Benitez-Alfonso Y, Faulkner C, Pendle A, Miyashima S, Helariutta Y, Maule A (2013) Symplastic intercellular connectivity regulates lateral root patterning. *Dev Cell* 26: 136–147
7. Wu S, O’Lexy R, Xu M, Sang Y, Chen X, Yu Q, Gallagher KL (2016) Symplastic signaling instructs cell division, cell expansion, and cell polarity in the ground tissue of *Arabidopsis thaliana* roots. *Proc Natl Acad Sci USA* 113: 11621–11626
8. Han X, Hyun T, Zhang M, Kumar R, Koh EJ, Kang BH, Lucas W, Kim JY (2014) Auxin-callose-mediated plasmodesmal gating is essential for tropic auxin gradient formation and signaling. *Dev Cell* 28: 132–146
9. Daum G, Medzihradzky A, Suzuki T, Lohmann JU (2014) A mechanistic framework for non-cell autonomous stem cell induction in *Arabidopsis*. *Proc Natl Acad Sci USA* 111: 14619–14624
10. Nakajima K, Sena G, Nawy T, Benfey PN (2001) Intercellular movement of the putative transcription factor SHR in root patterning. *Nature* 413: 307–311
11. Xu XM, Wang J, Xuan Z, Goldshmidt A, Borrill PGM, Hariharan N, Kim JY, Jackson D (2011) Chaperonins facilitate KNOTTED1 cell-to-cell trafficking and stem cell function. *Science* 333: 1141–1144
12. Faulkner C, Petutschnig E, Benitez-Alfonso Y, Beck M, Robatzek S, Lipka V, Maule AJ (2013) LYM2-dependent chitin perception limits molecular flux via plasmodesmata. *Proc Natl Acad Sci USA* 110: 9166–9170
13. Wang X, Sager R, Cui W, Zhang C, Lu H, Lee J-Y (2013) Salicylic acid regulates Plasmodesmata closure during innate immune responses in *Arabidopsis*. *Plant Cell* 25: 2315–2329
14. Lim GH, Shine MB, De Lorenzo L, Yu K, Cui W, Navarre D, Hunt AG, Lee JY, Kachroo A, Kachroo P (2016) Plasmodesmata localizing proteins

- regulate transport and signaling during systemic acquired immunity in plants. *Cell Host Microbe* 19: 541–549
15. Wong LH, Levine TP, Wirtz KW, Zilversmit DB, Pagano RE, Vance JE, Bernhard W, Rouiller C, Prinz WA, Vihtelic TS et al (2016) Lipid transfer proteins do their thing anchored at membrane contact sites. . . but what is their thing? *Biochem Soc Trans* 44: 517–527
  16. Sager R, Lee J-Y (2014) Plasmodesmata in integrated cell signalling: insights from development and environmental signals and stresses. *J Exp Bot* 65: 6337–6358
  17. Caillaud M-C, Wirthmueller L, Sklenar J, Findlay K, Piquerez SJM, Jones AME, Robatzek S, Jones JDG, Faulkner C (2014) The plasmodesmal protein PDLP1 localises to haustoria-associated membranes during downy mildew infection and regulates callose deposition. *PLoS Pathog* 10: e1004496
  18. Stahl Y, Faulkner C (2016) Receptor complex mediated regulation of symplastic traffic. *Trends Plant Sci* 21: 450–459
  19. Stahl Y, Grabowski S, Bleckmann A, Kühnemuth R, Weidtkamp-Peters S, Pinto KG, Kirschner GK, Schmid JB, Wink RH, Hülsewede A et al (2013) Moderation of *Arabidopsis* root stemness by CLAVATA1 and *Arabidopsis* CRINKLY4 receptor kinase complexes. *Curr Biol* 23: 362–371
  20. Vaddepalli P, Herrmann A, Fulton L, Oelschner M, Hillmer S, Stratil TF, Fastner A, Hammes UZ, Ott T, Robinson DG et al (2014) The C2-domain protein QUIRKY and the receptor-like kinase STRUBBELIG localize to plasmodesmata and mediate tissue morphogenesis in *Arabidopsis thaliana*. *Development* 141: 4139–4148
  21. Lee J-Y (2015) Plasmodesmata: a signaling hub at the cellular boundary. *Curr Opin Plant Biol* 27: 133–140
  22. Nicolas W, Grison MS, Bayer EMF (2017) Shaping intercellular channels of plasmodesmata: the structure-to-function missing link. *J Exp Bot* 69: 91–103
  23. Tilsner J, Amari K, Torrance L (2011) Plasmodesmata viewed as specialised membrane adhesion sites. *Protoplasma* 248: 39–60
  24. Ding B, Turgeon R, Parthasarathy MV (1992) Substructure of freeze-substituted plasmodesmata. *Protoplasma* 169: 28–41
  25. Nicolas W, Grison M, Trépout S, Gaston A, Fouché M, Cordelières F, Oparka K, Tilsner J, Brocard L, Bayer E (2017) Architecture and permeability of post-cytokinesis plasmodesmata lacking cytoplasmic sleeve. *Nat Plants* 3: 17082
  26. Bayer EM, Mongrand S, Tilsner J (2014) Specialized membrane domains of plasmodesmata, plant intercellular nanopores. *Front Plant Sci* 5: 507
  27. Grison MS, Brocard L, Fouillen L, Nicolas W, Wewer V, Dörmann P, Nacir H, Benitez-Alfonso Y, Claverol S, Germain V et al (2015) Specific membrane lipid composition is important for plasmodesmata function in *Arabidopsis*. *Plant Cell* 27: 1228–1250
  28. Thomas CL, Bayer EM, Ritzenthaler C, Fernandez-Calvino L, Maule AJ (2008) Specific targeting of a plasmodesmal protein affecting cell-to-cell communication. *PLoS Biol* 6: 0180–0190
  29. Simpson C, Thomas C, Findlay K, Bayer E, Maule AJ (2009) An *Arabidopsis* GPI-anchor plasmodesmal neck protein with callose binding activity and potential to regulate cell-to-cell trafficking. *Plant Cell* 21: 581–594
  30. Zavaliev R, Dong X, Epel BL (2016) Glycosylphosphatidylinositol (GPI) modification serves as a primary plasmodesmal sorting signal. *Plant Physiol* 172: 1061–1073
  31. Knox K, Wang P, Kriechbaumer V, Tilsner J, Frigerio L, Sparkes I, Hawes C, Oparka K (2015) Putting the squeeze on plasmodesmata: a role for reticulons in primary plasmodesmata formation. *Plant Physiol* 168: 1563–1572
  32. Zavaliev R, Ueki S, Epel BL, Citovsky V (2011) Biology of callose ( $\beta$ -1,3-glucan) turnover at plasmodesmata. *Protoplasma* 248: 117–130
  33. Bayer EM, Sparkes I, Vanneste S, Rosado A (2017) From shaping organelles to signalling platforms : the emerging functions of plant ER–PM contact sites. *Curr Opin Plant Biol* 40: 89–96
  34. Yan D, Yadav SR, Paterlini A, Nicolas WJ, Petit JD, Brocard L, Belevich I, Grison MS, Vaten A, Karami L et al (2019) Sphingolipid biosynthesis modulates plasmodesmal ultrastructure and phloem unloading. *Nat Plants* 5: 604–615
  35. Burgoyne T, Patel S, Eden ER (2015) Calcium signaling at ER membrane contact sites. *Biochim Biophys Acta - Mol Cell Res* 1853: 2012–2017
  36. Prinz WA (2014) Bridging the gap: membrane contact sites in signaling, metabolism, and organelle dynamics. *J Cell Biol* 205: 759–769
  37. Zhang SL, Yu Y, Roos J, Kozak JA, Deerinck TJ, Ellisman MH, Stauderman KA, Cahalan MD (2005) STIM1 is a Ca<sup>2+</sup> sensor that activates CRAC channels and migrates from the Ca<sup>2+</sup> store to the plasma membrane. *Nature* 437: 902–905
  38. Omrus DJ, Manford AG, Bader JM, Emr SD, Stefan CJ (2016) Phosphoinositide kinase signaling controls ER-PM cross-talk. *Mol Biol Cell* 27: 1170–1180
  39. Phillips MJ, Voeltz GK (2016) Structure and function of ER membrane contact sites with other organelles. *Nat Rev Mol Cell Biol* 17: 69–82
  40. Gallo A, Vannier C, Galli T (2016) ER-PM associations: structures and functions. *Annu Rev Cell Dev Biol* 32: 279–301
  41. Eden ER, White IJ, Tsapara A, Futter CE (2010) Membrane contacts between endosomes and ER provide sites for PTP1B-epidermal growth factor receptor interaction. *Nat Cell Biol* 12: 267–272
  42. Eden ER, Sanchez-Heras E, Tsapara A, Sobota A, Levine TP, Futter CE (2016) Annexin A1 tethers membrane contact sites that mediate ER to endosome cholesterol transport. *Dev Cell* 37: 473–483
  43. Ho C-MK, Paciorek T, Abrash E, Bergmann DC (2016) Modulators of stomatal lineage signal transduction alter membrane contact sites and reveal specialization among ERECTA Kinases. *Dev Cell* 38: 345–357
  44. Chang CL, Hsieh TS, Yang TT, Rothberg KG, Azizoglu DB, Volk E, Liao JC, Liou J (2013) Feedback regulation of receptor-induced Ca<sup>2+</sup> signaling mediated by E-Syt1 and Nir2 at endoplasmic reticulum-plasma membrane junctions. *Cell Rep* 5: 813–825
  45. Kim YJ, Guzman-Hernandez ML, Wisniewski E, Balla T (2015) Phosphatidylinositol-phosphatidic acid exchange by Nir2 at ER-PM contact sites maintains phosphoinositide signaling competence. *Dev Cell* 33: 549–561
  46. Petkovic M, Jemaïel A, Daste F, Specht CG, Izeddin I, Vorkel D, Verbatz J-M, Darzacq X, Triller A, Pfenninger KH et al (2014) The SNARE Sec22b has a non-fusogenic function in plasma membrane expansion. *Nat Cell Biol* 16: 434–444
  47. Eisenberg-Bord M, Shai N, Schuldiner M, Bohnert M (2016) A tether is a tether: tethering at membrane contact sites. *Dev Cell* 39: 395–409
  48. Henne WM, Liou J, Emr SD (2015) Molecular mechanisms of inter-organelle ER–PM contact sites. *Curr Opin Cell Biol* 35: 123–130
  49. Fernandez-Calvino L, Faulkner C, Walshaw J, Saalbach G, Bayer E, Benitez-Alfonso Y, Maule A (2011) *Arabidopsis* plasmodesmal proteome. *PLoS ONE* 6: e18880
  50. Faulkner C, Bayer EMF (2017) Isolation of plasmodesmata. *Methods Mol Biol* 1511: 187–198
  51. Liu L, Liu C, Hou X, Xi W, Shen L, Tao Z, Wang Y, Yu H (2012) FTIP1 is an essential regulator required for florigen transport. *PLoS Biol* 10: e1001313



52. Liu L, Li C, Song S, Wang Y, Jackson D, Yu H, Liu L, Li C, Song S, Wei Z et al (2018) FTIP-dependent STM trafficking regulates shoot meristem development in *Arabidopsis*. *Cell Rep* 23: 1879–1890
53. Liu L, Li C, Liang Z, Yu H (2017) Characterization of multiple C2 domain and transmembrane region proteins in *Arabidopsis*. *Plant Physiol* 176: 01144.2017
54. Grison MS, Fernandez-calvino L, Mongrand S, Bayer EMF (2015) Isolation of Plasmodesmata from *Arabidopsis* suspension culture cells. *Methods Mol Biol* 1217: 83–93
55. Nikolovski N, Rubtsov D, Segura MP, Miles GP, Stevens TJ, Dunkley TPJ, Munro S, Lilley KS, Dupree P (2012) Putative glycosyltransferases and other plant golgi apparatus proteins are revealed. *Plant Physiol* 160: 1037–1051
56. Dunkley TPJ, Hester S, Shadforth IP, Runions J, Weimar T, Hanton SL, Griffin JL, Bessant C, Brandizzi F, Hawes C et al (2006) Mapping the *Arabidopsis* organelle proteome. *Proc Natl Acad Sci USA* 103: 6518–6523
57. Pérez-Sancho J, Vanneste S, Lee E, McFarlane HE, Esteban Del Valle A, Valpuesta V, Friml J, Botella MA, Rosado A (2015) The *Arabidopsis* synaptotagmin 1 is enriched in endoplasmic reticulum-plasma membrane contact sites and confers cellular resistance to mechanical stresses. *Plant Physiol* 168: 132–143
58. Giordano F, Saheki Y, Idevall-Hagren O, Colombo SF, Pirruccello M, Milosevic I, Gracheva EO, Bagriantsev SN, Borgese N, De Camilli P (2013) PI(4,5)P<sub>2</sub>-dependent and Ca<sup>2+</sup>-regulated ER-PM interactions mediated by the extended synaptotagmins. *Cell* 153: 1494–1509
59. Wang P, Hawkins TJ, Richardson C, Cummins I, Deeks MJ, Sparkes I, Hawes C, Hussey PJ (2014) The plant cytoskeleton, NET3C, and VAP27 mediate the link between the plasma membrane and endoplasmic reticulum. *Curr Biol* 24: 1397–1405
60. Thomas CL, Bayer EM, Ritzenthaler C, Fernandez-Calvino L, Maule AJ (2008) Specific targeting of a plasmodesmal protein affecting cell-to-cell communication. *PLoS Biol* 6: e7
61. Fitzgibbon J, Bell K, King E, Oparka K (2010) Super-resolution imaging of plasmodesmata using three-dimensional structured illumination microscopy. *Plant Physiol* 153: 1453–1463
62. Oparka KJ, Roberts AG, Boevink P, Cruz SS, Roberts I, Pradel KS, Imlau A, Kotlizky G, Sauer N, Epel B (1999) Simple, but not branched, plasmodesmata allow the nonspecific trafficking of proteins in developing tobacco leaves. *Cell* 97: 743–754
63. Kraner ME, Müller C, Sonnewald U (2017) Comparative proteomic profiling of the choline transporter-like 1 (CHER1) mutant provides insights into plasmodesmata composition of fully developed *Arabidopsis thaliana* leaves. *Plant J* 92: 696–709
64. Wille AC, Lucas WJ (1984) Ultrastructural and histochemical studies on guard cells. *Planta* 160: 129–142
65. Faulkner C, Akman OE, Bell K, Jeffrey C, Oparka K (2008) Peeking into pit fields: a multiple twinning model of secondary plasmodesmata formation in tobacco. *Plant Cell* 20: 1504–1518
66. Levy A, Zheng JY, Lazarowitz SG (2015) Synaptotagmin SYTA forms ER-plasma membrane junctions that are recruited to plasmodesmata for plant virus movement. *Curr Biol* 25: 1–8
67. Pérez-sancho J, Schapire AL, Botella MA, Rosado A (2016) Analysis of protein-lipid interactions using purified C2 domains. *Methods Mol Biol* 1363: 175–187
68. Saheki Y, Bian X, Schauder CM, Sawaki Y, Surma MA, Klose C, Pincet F, Reinisch KM, De Camilli P (2016) Control of plasma membrane lipid homeostasis by the extended synaptotagmins. *Nat Cell Biol* 18: 504–515
69. Corbalan-Garcia S, Gómez-Fernández JC (2014) Signaling through C2 domains: more than one lipid target. *Biochim Biophys Acta - Biomembr* 1838: 1536–1547
70. Zimmermann L, Stephens A, Nam S, Rau D, Kübler J, Lozajic M, Gabler F, Söding J, Lupas AN, Alva V (2018) A completely reimplemented MPI bioinformatics toolkit with a new HHpred server at its core. *J Mol Biol* 430: 2237–2243
71. Frickey T, Lupas A (2018) CLANS: a Java application for visualizing protein families based on pairwise similarity. *Bioinformatics* 20: 3702–3704
72. Pérez-Lara Á, Thapa A, Nyenhuis SB, Nyenhuis DA, Halder P, Tietzel M, Tittmann K, Cafiso DS, Jahn R (2016) PtdInsP<sub>2</sub> and PtdSer cooperate to trap synaptotagmin-1 to the plasma membrane in the presence of calcium. *Elife* 5: 1–22
73. Abdullah N, Padmanarayana M, Marty NJ, Johnson CP (2014) Quantitation of the calcium and membrane binding properties of the C2 domains of dysferlin. *Biophys J* 106: 382–389
74. Marty NJ, Holman CL, Abdullah N, Johnson CP (2014) The C2 domains of otoferlin, dysferlin, and myoferlin alter the packing of lipid bilayers. *Biochemistry* 52: 5585–5592
75. Simon MLA, Platre MP, Marquès-Bueno MM, Armengot L, Stanislas T, Bayle V, Caillaud M, Jaillais Y (2016) APTdIns(4)P-driven electrostatic field controls cell membrane identity and signalling in plants. *Nat Plants* 2: 16089
76. Manford AG, Stefan CJ, Yuan HL, MacGurn JA, Emr SD (2012) ER-to-plasma membrane tethering proteins regulate cell signaling and ER morphology. *Dev Cell* 23: 1129–1140
77. Metzger MB, Maurer MJ, Dancy BM, Michaelis S (2008) Degradation of a cytosolic protein requires endoplasmic reticulum-associated degradation machinery. *J Biol Chem* 283: 32302–32316
78. Levy A, Erlanger M, Rosenthal M, Epel BL (2007) A plasmodesmata-associated beta-1,3-glucanase in *Arabidopsis*. *Plant J* 49: 669–682
79. Cui W, Lee J-Y (2016) *Arabidopsis* callose synthases CalS1/8 regulate plasmodesmal permeability during stress. *Nat Plants* 2: 16034
80. Tran TM, Mccubbin TJ, Bihmidine S, Julius BT, Frank R, Schauflinger M, Weil C, Springer N, Chomet P, Woessner J et al (2019) Maize carbohydrate partitioning defective 33 encodes a MCTP protein and functions in sucrose export from leaves. *Mol Plant* <https://doi.org/10.1016/j.molp.2019.05.001>
81. Trehin C, Schrempp S, Chauvet A, Berne-Dedieu A, Thierry A-M, Faure J-E, Negrutiu I, Morel P (2013) QUIRKY interacts with STRUBBELIG and PAL OF QUIRKY to regulate cell growth anisotropy during *Arabidopsis* gynoecium development. *Development* 140: 4807–4817
82. Tilney LG, Cooke TJ, Connelly PS, Tilney MS (1991) The structure of plasmodesmata as revealed by plasmolysis, detergent extraction, and protease digestion. *J Cell Biol* 112: 739–747
83. Joshi AS, Nebenfuehr B, Choudhary V, Satpute-Krishnan P, Levine TP, Golden A, Prinz WA (2018) Lipid droplet and peroxisome biogenesis occur at the same ER subdomains. *Nat Commun* 9: 2940
84. Fulton L, Batoux M, Vaddepalli P, Yadav RK, Busch W, Andersen SU, Jeong S, Lohmann JU, Schneitz K (2009) DETORQUEO, QUIRKY, and ZERZAUST represent novel components involved in organ development mediated by the receptor-like kinase STRUBBELIG in *Arabidopsis thaliana*. *PLoS Genet* 5: e1000355
85. Reinisch KM, De Camilli P (2016) SMP-domain proteins at membrane contact sites: structure and function. *Biochim Biophys Acta - Mol Cell Biol Lipids* 1861: 924–927

86. Idevall-Hagren O, Lü A, Xie B, De Camilli P (2015) Triggered Ca<sup>2+</sup> influx is required for extended synaptotagmin 1-induced ER-plasma membrane tethering. *EMBO J* 34: 1–15
87. Fernández-Busnadiego R, Saheki Y, De Camilli P (2015) Three-dimensional architecture of extended synaptotagmin-mediated endoplasmic reticulum–plasma membrane contact sites. *Proc Natl Acad Sci USA* 112: E2004–E2013
88. Idevall-Hagren O, Lü A, Xie B, De Camilli P (2015) Triggered Ca<sup>2+</sup> + influx is required for extended synaptotagmin 1-induced ER-plasma membrane tethering. *EMBO* 34: 2291–2305
89. Bian X, Saheki Y, De Camilli P (2018) Ca<sup>2+</sup> releases E-Syt1 autoinhibition to couple ER-plasma membrane tethering with lipid transport. *EMBO J* 37: 219–234
90. Buchan DWA, Minneci F, Nugent TCO, Bryson K, Jones DT (2013) Scalable web services for the PSIPRED protein analysis workbench. *Nucleic Acids Res* 41: W349–W357
91. Jones DT (1999) Protein secondary structure prediction based on position-specific scoring matrices. *J Mol Biol* 292: 195–202
92. Callebaut I, Labesse G, Durand P, Poupon A, Canard L, Chomilier J, Henrissat B, Mormon JP (1997) Deciphering protein sequence information through hydrophobic cluster analysis (HCA): current status and perspectives. *Cell Mol Life Sci* 53: 621–645
93. Alva V, Nam S, Johannes S, Lupas AN (2016) The MPI bioinformatics Toolkit as an integrative platform for advanced protein sequence and structure. *Nucleic Acids Res* 44: 410–415
94. Söding J, Biegert A, Lupas AN (2005) The HHpred interactive server for protein homology detection and structure prediction. *Nucleic Acids Res* 33: 244–248
95. Steinegger M, Söding J (2017) MMseqs2 enables sensitive protein sequence searching for the analysis of massive data sets. *Nat Biotechnol* 35: 1026–1028
96. Karimi M, Inzé D, Depicker A (2002) GATEWAYTM vectors for *Agrobacterium*-mediated plant transformation. *Trends Plant Sci* 7: 193–195
97. Marqués-Bueno MM, Morao AK, Cayrel A, Platre MP, Barberon M, Cailieux E, Colot V, Jaillais Y, Roudier F, Vert G (2016) A versatile multisite gateway-compatible promoter and transgenic line collection for cell type-specific functional genomics in *Arabidopsis*. *Plant J* 85: 320–333
98. Clough SJ, Bent AF (1998) Floral dip: a simplified method for *Agrobacterium*-mediated transformation of *Arabidopsis thaliana*. *Plant J* 16: 735–743
99. Gal-On A, Meiri E, Elma C, Gray DJ, Gaba V (1997) Simple hand-held devices for the efficient infection of plants with viral-encoding constructs by particle bombardment. *J Virol Methods* 64: 103–110
100. Bayer EM, Bottrill AR, Walshaw J, Vigouroux M, Naldrett MJ, Thomas CL, Maule AJ (2006) *Arabidopsis* cell wall proteome defined using multidimensional protein identification technology. *Proteomics* 6: 301–311
101. Käll L, Canterbury JD, Weston J, Noble WS, MacCoss MJ (2007) Semi-supervised learning for peptide identification from shotgun proteomics datasets. *Nat Methods* 4: 923–925
102. Vizcaino JA, Csordas A, Del-Toro N, Dianas JA, Griss J, Lavidas I, Mayer G, Perez-Riverol Y, Reisinger F, Ternent T et al (2016) 2016 update of the PRIDE database and its related tools. *Nucleic Acids Res* 44: D447–D456
103. Zhang J, Xin L, Shan B, Chen W, Xie M, Yuen D, Zhang W, Zhang Z, Lajoie GA, Ma B (2012) PEAKS DB: *de novo* sequencing assisted database search for sensitive and accurate peptide identification. *Mol Cell Proteomics* 11: M111.010587
104. Bolte S, Cordelières FP (2006) A guided tour into subcellular colocalization analysis in light microscopy. *J Microsc* 224: 213–232
105. Truernit E, Bauby H, Dubreucq B, Grandjean O, Runions J, Barthélémy J, Palauqui J-C (2008) High-resolution whole-mount imaging of three-dimensional tissue organization and gene expression enables the study of phloem development and structure in *Arabidopsis*. *Plant Cell* 20: 1494–1503
106. Gronnier J, Crowet J-M, Habenstein B, Nasir MN, Bayle V, Hosy E, Platre MP, Gouguet P, Raffaele S, Martinez D et al (2017) Structural basis for plant plasma membrane protein dynamics and organization into functional nanodomains. *Elife* 6: e26404
107. Littlejohn GR, Mansfield JC, Christmas JT, Witterick E, Fricker MD, Grant MR, Smirnoff N, Everson RM, Moger J, Love J (2014) An update: improvements in imaging perfluorocarbon-mounted plant leaves with implications for studies of plant pathology, physiology, development and cell biology. *Front Plant Sci* 5: 1–8
108. Bayer E, Thomas CL, Maule AJ (2004) Plasmodesmata in *Arabidopsis thaliana* suspension cells. *Protoplasma* 223: 93–102
109. Sievers F, Wilm A, Dineen D, Gibson TJ, Karplus K, Li W, Lopez R, McWilliam H, Remmert M, Söding J et al (2011) Fast, scalable generation of high-quality protein multiple sequence alignments using clustal omega. *Mol Syst Biol* 7: 1–6
110. Lins L, Couvineau A, Rouyer-fessard C, Nicole P, Maoret J-J, Benhamed M, Brasseur R, Thomas A, Laburthe M (2001) The human VPAC 1 receptor. *J Biol Chem* 276: 10153–10160
111. Song Y, DiMaio F, Wang RY-R, Kim D, Miles C, Brunette TJ, Thompson J, Baker D (2013) High resolution comparative modeling with RosettaCM. *Structure* 21: 1–15
112. Di Tommaso P, Moretti S, Xenarios I, Orobitg M, Montanyola A, Chang J-M, Taly J-F, Notredame C (2011) T-Coffee: a web server for the multiple sequence alignment of protein and RNA sequences using structural information and homology extension. *Nucleic Acids Res* 39: 13–17
113. Notredame C, Higgins DG, Heringa J (2000) T-Coffee: a novel method for fast and accurate multiple sequence alignment. *J Mol Biol* 302: 205–217
114. Sali A, Potterton L, Yuan F, van Vlijmen H, Karplus M (1995) Evaluation of comparative protein modeling by MODELLER. *Proteins* 326: 318–326
115. Wiederstein M, Sippl MJ (2007) ProSA-web: interactive web service for the recognition of errors in three-dimensional structures of proteins. *Nucleic Acids Res* 35: W407–W410
116. Abraham MJ, Murtola T, Schulz R, Pall S, Smith JC, Hess B, Lindahl E (2015) GROMACS: high performance molecular simulations through multi-level parallelism from laptops to supercomputers. *SoftwareX* 2: 19–25
117. Schmid N, Eichenberger AP, Choutko A, Riniker S, Winger M, Mark AE, van Gunsteren WF (2011) Definition and testing of the GROMOS force-field versions 54A7 and 54B7. *Eur Biophys J* 40: 843–856
118. Poger D, van Gunsteren WF, Mark AE (2009) A new force field for simulating phosphatidylcholine bilayers. *J Comput Chem* 31: 1117–1125
119. Poger D, Mark AE (2010) On the validation of molecular dynamics simulations of saturated and cis-monounsaturated phosphatidylcholine lipid bilayers: a comparison with experiment. *J Chem Theory Comput* 6: 325–336
120. Berendsen HJC, Postma JPM, van Gunsteren WF, Hermans J (1981) Interaction models for water in relation to protein hydration. In, *Intermolecular forces* pp 331–342

121. Hess B, Bekker H, Berendsen HJC, Fraaije JGEM (1997) LINCS: a linear constraint solver for molecular simulations. *J Comput Chem* 18: 1463–1472
122. Darden T, York D, Pedersen L (1993) Particle mesh Ewald: an N.log(N) method for Ewald sums in large systems. *J Chem Phys* 98: 10089–10092
123. Bussi G, Donadio D, Parrinello M (2007) Canonical sampling through velocity rescaling. *J Chem Phys* 126: 014101-1-014101–014107
124. Parrinello M, Rahman A (1981) Polymorphic transitions in single crystals: a new molecular dynamics method. *J Appl Phys* 52: 7181–7190
125. Marrink SJ, Risselada JH, Yefimov S, Tieleman DP, de Vries AH (2007) The MARTINI force field: coarse grained model for biomolecular simulations. *J Phys Chem B* 111: 7812–7824
126. Periole X, Cavalli M, Marrink S, Ceruso MA (2009) Combining an elastic network with a coarse-grained molecular force field : structure, dynamics, and intermolecular recognition. *J Chem Theory Comput* 5: 2531–2543
127. Siuda I, Thøgersen L (2013) Conformational flexibility of the leucine binding protein examined by protein domain coarse-grained molecular dynamics. *J Mol Model* 19: 4931–4945
128. Humphrey W, Dalke A, Schulten K (1996) VMD: visual molecular dynamics. *J Mol Graph* 14: 33–38
129. Marrink SJ (2015) Computational lipidomics with insane: a versatile tool for generating custom membranes for molecular simulations. *J Chem Theory Comput* 11: 2144–2155
130. Berendsen HJC, Postma JPM, van Gunsteren WF, DiNola A, Haak JR (1984) Molecular dynamics with coupling to an external bath. *J Chem Phys* 81: 3684–3690
131. de Jong DH, Baoukina S, Ingólfsson HI, Marrink SJ (2016) Martini straight: boosting performance using a shorter cutoff and GPUs. *Comput Phys Commun* 199: 1–7
132. Michaud-Agrawal N, Denning EJ, Woolf TB, Beckstein O (2011) Software news and updates MDAnalysis: a toolkit for the analysis of molecular dynamics simulations. *J Comput Chem* 32: 2319–2327
133. Gowers RJ, Linke M, Barnoud J, Reddy TJE, Melo MN, Seyler SL, Doman-ski J, Dotson DL, Buchoux S, Kenney IM et al (2016) MDAnalysis : a Python package for the rapid analysis of molecular dynamics simulations. *Proc 15th PYTHON Sci conf* 98–105
134. Wassenaar TA, Pluhackova K, Böckmann RA, Marrink SJ, Tieleman DP (2013) Going Backward: a flexible geometric approach to reverse transformation from coarse grained to atomistic models. *J Chem Theory Comput* 10: 676–690
135. Nosé S (1984) A unified formulation of the constant temperature molecular dynamics methods. *J Chem Phys* 81: 511–519

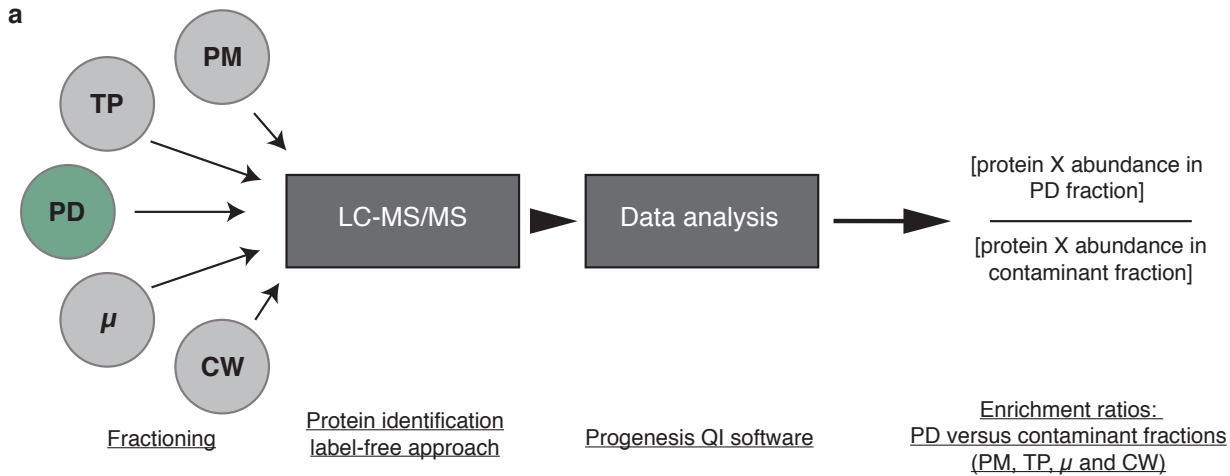


**License:** This is an open access article under the terms of the Creative Commons Attribution 4.0 License, which permits use, distribution and reproduction in any medium, provided the original work is properly cited.

## **Table of content**

<b>Appendix Figure S1</b>	<b>2-3</b>
<b>Appendix Figure S2</b>	<b>4-5</b>
<b>Appendix Figure S3</b>	<b>6</b>
<b>Appendix Figure S4</b>	<b>7-8</b>
<b>Appendix Figure S5</b>	<b>9</b>
<b>Appendix Figure S6</b>	<b>10-11</b>
<b>Appendix Figure S7</b>	<b>12-13</b>
<b>Appendix Figure S8</b>	<b>14</b>
<b>Appendix Figure S9</b>	<b>15</b>
<b>Appendix Figure S10</b>	<b>16</b>
<b>Appendix Figure S11</b>	<b>17-18</b>
<b>Appendix Figure S12</b>	<b>19-20</b>
<b>Appendix Figure S13</b>	<b>21-22</b>
<b>Appendix Figure S14</b>	<b>23</b>
<b>Appendix Table S1</b>	<b>24-25</b>
<b>Appendix Table S2</b>	<b>26</b>

## Appendix Figure S1



**b**

Description	Abundance	Enrichment ratios				ER proteomes		PD association references
		PD/PM	PD/TP	PD/ $\mu$	PD/CW	1.	2.	
<b>Multiple C2 domains and Transmembrane region Protein 4,10,14 (MCTP4,10,14)</b>	<b>2093561645</b>	<b>351,0</b>	<b>223,6</b>	<b>360,1</b>	<b>70,2</b>	x	x	—
Beta-1-3-glucanase (AtBG_PAPP)	1638015771	164,0	247,2	580,8	45,0			3.
<b>Multiple C2 domains and Transmembrane region Protein 6,9 (MCTP6,9)</b>	<b>776007012</b>	<b>315,5</b>	<b>115,1</b>	<b>285,3</b>	<b>61,7</b>			—
Plasmodesmata callose-binding protein 1 (PDCB1)	328259264	219,2	1052,3	623,0	48,0			4.
Plasmodesmata-located protein 1 (PDLP1)	311480268	309,0	119,0	307,6	46,4			5.
Glucan synthase-like 12 (CALS3)	257637656	14,5	56,4	67,3	65,2			6.
O-Glycosyl hydrolases family 17 protein (beta1-3 glucanase, PdBG2)	232481254	26,9	73,3	89,6	48,4			7.
Plasmodesmata-located protein 6 (PDLP6)	159384568	193,7	126,1	637,9	52,3			5.
Plasmodesmata callose-binding protein 3 (PDCB3)	100145419	101,4	63,2	76,5	46,8			4.
Plasmodesmata callose-binding protein 4 (PDCB4)	79562157	107,9	133,1	129,2	47,5			4.
O-Glycosyl hydrolases family 17 protein (beta1-3 glucanase, PdBG3)	71917917	32,9	204,2	237,4	59,5			7.
Plasmodesmata-located protein 3 (PDLP3)	71730983	251,4	90,8	325,4	60,7			5.
O-Glycosyl hydrolases family 17 protein (beta1-3 glucanase, PdBG1)	65897722	42,7	148,4	287,3	52,3			7.
Tetraspanin 3 (TET3)	47760446	65,3	102,4	242,7	51,0			10.
LysM domain-containing GPI-anchored protein 2 (LYM2)	40630549	2,7	18,3	10,3	35,9			8.
Plasmodesmata-located protein 2 (PDLP2)	38475248	172,0	78,7	74,5	44,9			5.
Callose synthase 1 (CALS1, GSL6)	29840182	14,0	39,5	40,0	69,2			9.
Probable receptor-like protein kinase	25515183	4,9	29,4	23,8	58,0			10.
<b>Multiple C2 domains and Transmembrane region Protein 16 (MCTP16)</b>	<b>23482273</b>	<b>59,7</b>	<b>33,5</b>	<b>126,7</b>	<b>34,9</b>	x	x	—
<b>Multiple C2 domains and Transmembrane region Protein 3,7 (MCTP3,7)</b>	<b>20441820</b>	<b>47,5</b>	<b>44,3</b>	<b>96,9</b>	<b>81,7</b>	x	x	—
<b>Multiple C2 domains and Transmembrane region Protein 15 (MCTP15, QUIRKY, QKY)</b>	<b>15148937</b>	<b>79,0</b>	<b>47,9</b>	<b>82,9</b>	<b>73,1</b>			11.
<b>Multiple C2 domains and Transmembrane region Protein 5 (MCTP5)</b>	<b>9974540</b>	<b>102,5</b>	<b>516,4</b>	<b>171,4</b>	<b>152,6</b>			—
Receptor kinase 3 (SD18)	8493304	14,4	6,1	7,2	34,6			10.
Leucine-rich repeat protein kinase family protein (SUB)	6660962	31,8	40,7	68,3	55,6			11.
Plasmodesmata-located protein 8 (PDLP8)	2101866	365,8	32,1	214,6	48,5			5.

- Nikolovski, N. et al. Putative glycosyltransferases and other plant golgi apparatus proteins are revealed. *Plant Physiol.* 160, 1037–1051 (2012).
- Dunkley, T. P. J. et al. Mapping the Arabidopsis organelle proteome. *PNAS* 103, 6518–6523 (2006).
- Levy, A., Erlanger, M., Rosenthal, M. & Epel, B. L. A plasmodesmata-associated beta-1,3-glucanase in Arabidopsis. *Plant J.* 49, 669–682 (2007).
- Simpson, C., Thomas, C., Findlay, K., Bayer, E. & Maule, A. J. An Arabidopsis GPI-anchor plasmodesmal neck protein with callose binding activity and potential to regulate cell-to-cell trafficking. *Plant Cell* 21, 581–594 (2009).
- Thomas, C. L., Bayer, E. M., Ritzenthaler, C., Fernandez-Calvino, L. & Maule, A. J. Specific targeting of a plasmodesmal protein affecting cell-to-cell communication. *PLoS Biol.* 6, 0180–0190 (2008).
- Vatén, A. et al. Callose biosynthesis regulates symplastic trafficking during root development. *Dev. Cell* 21, 1144–1155 (2011).
- Benitez-Alfonso, Y. et al. Symplastic intercellular connectivity regulates lateral root patterning. *Dev. Cell* 26, 136–147 (2013).
- Faulkner, C. et al. LYM2-dependent chitin perception limits molecular flux via plasmodesmata. *Proc. Natl. Acad. Sci. U. S. A.* 110, 9166–70 (2013).
- Cui, W. & Lee, J.-Y. Arabidopsis callose synthases CalS1/8 regulate plasmodesmal permeability during stress. *Nat. Plants* 2, 16034 (2016).
- Fernandez-Calvino, L. et al. Arabidopsis plasmodesmal proteome. *PLoS One* 6, e18880 (2011).
- Vaddepalli, P. et al. The C2-domain protein QUIRKY and the receptor-like kinase STRUBBELIG localize to plasmodesmata and mediate tissue morphogenesis in Arabidopsis thaliana. *Development* 141, 4139–4148 (2014).

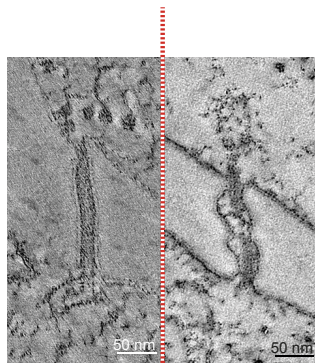
## Appendix Figure S1.

MCTP members are highly enriched in the *Arabidopsis* plasmodesmata core proteome.

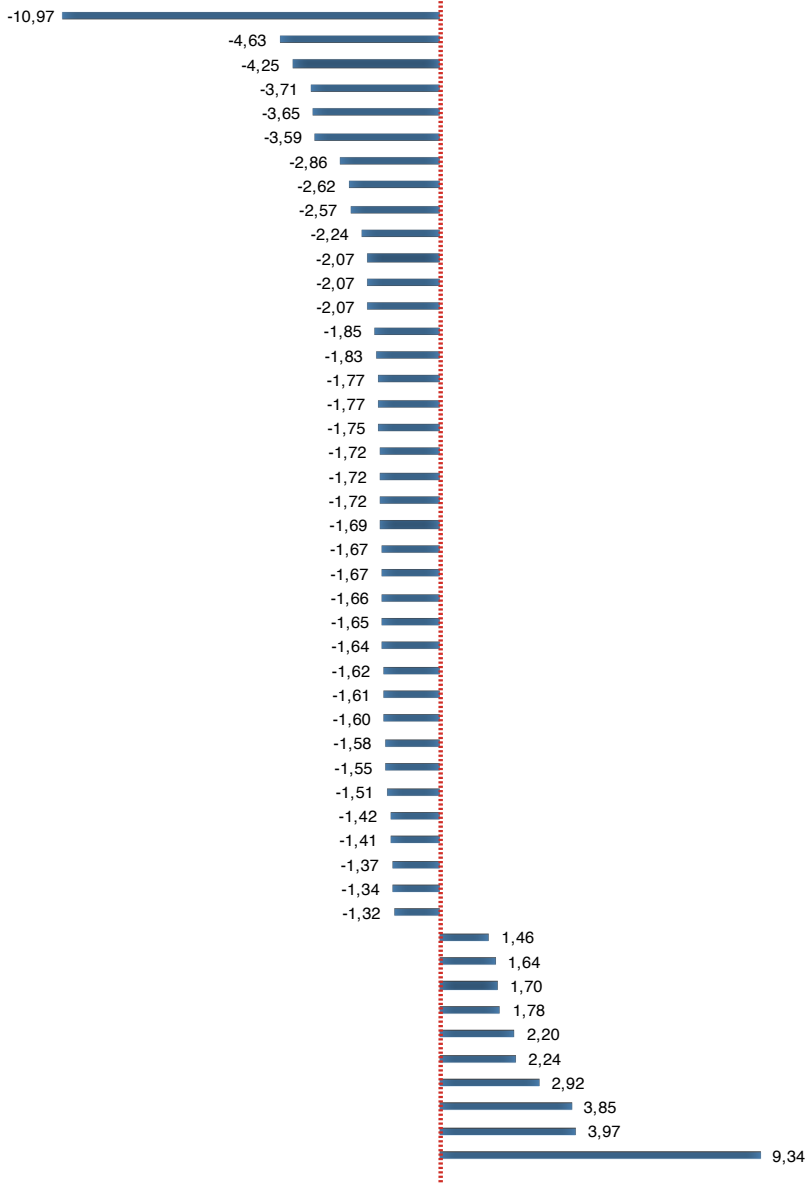
(a) Label-free quantitation strategy was used to determine the relative abundance of proteins in the plasmodesmata (PD) fraction *versus* contaminant subcellular fractions namely, the PM, total extract (TP), microsomes ( $\mu$ ) and cell wall (CW).

(b) Selected set of proteins from the plasmodesmata core proteome (see Supplementary Table1 for the complete list) showing the abundance and enrichment ratios of known plasmodesmal proteins (reference to published papers is indicated below the table) and MCTP members (in bold). MCTP members are present in the plasmodesmal core proteome being both abundant and highly enriched (from 47.5- to 351-folds compared to the PM) similar to known plasmodesmata proteins. Please note that in some cases, the identified peptides did not permit unambiguous identification of MCTP isoforms due to high sequence homology between several members. The different shades (light to dark) of brown represent different enrichment levels (0-10; 10-20; 20-100 and above 100).

## Appendix Figure S2



**Type I** **Type II**



- HAD superfamily subfamily IIIB acid phosphatase (53)
- LOW protein: exocyst complex component-like protein (96)
- NHL domain-containing protein (68)
- NHL domain-containing protein (108)
- Exocyst complex component (SEC15A) (94)
- MCTP5 (77)**
- Glucan synthase-like 1 (CAL511, GSL1) (80)
- Glucan synthase-like 12 (CAL53) (14)
- Exocyst subunit exo70 family protein G1(103)
- Glucan synthase-like 3 (CAL52, GSL3) (83)
- MCTP15 QKY (70)**
- O-Glycosyl hydrolases family 17 protein (31)
- Plasmodesmata callose-binding protein 4 (PDCB4) (29)
- Leucine-rich repeat protein kinase family protein (TMK3)(13)
- Auxin efflux carrier family protein (82)
- Hypothetical protein (112)
- Heavy metal transport/detoxification superfamily protein (57)
- Calcium-dependent lipid-binding family protein (115)
- NDR1/HIN1-like 2 (NHL2) (52)
- Plasmodesmata-located protein 2 (PDLP2) (50)
- Glucan synthase-like 8 (CAL510, GSL8) (44)
- Transmembrane protein (22)
- MCTP4, 10, 14 (4)**
- EPS15 homology domain 2 (78)
- Plasmodesmata-located protein 1 (PDLP1) (12)
- Xanthine/uracil permease family protein (AtNAT1) (34)
- Callose synthase 1 (CAL51, GSL6) (55)
- Leucine-rich repeat protein kinase family protein (SUB) (85)
- ABC2 homolog 14 (56)
- Xanthine/uracil permease family protein (AtNAT3) (36)
- U-box domain-containing protein (66)
- MCTP6,9 (8)**
- MCTP16 (60)**
- ABC2 homolog 11 (54)
- MCTP3,7 (64)**
- Pmr5/Cas1p GD5L/SGNH-like acyl-esterase family protein (106)
- Nucleobase-ascorbate transporter 12 (AtNAT12) (81)
- Eukaryotic aspartyl protease family protein (69)
- Probable receptor-like protein kinase (59)
- Transmembrane protein (91)
- Farnesylated protein 3 (30)
- Neutral/alkaline non-lysosomal ceramidase (61)
- Plant cadmium resistance 2 (101)
- Glycine-rich protein family (73)
- Plasmodesmata callose-binding protein 3 (PDCB3) (24)
- Xyloglucan endotransglucosylase/hydrolase 15 (120)
- RING/U-box superfamily protein (116)
- Pectin lyase-like superfamily protein (117)

## Appendix Figure S2.

Differential abundance of core *Arabidopsis* plasmodesmal proteins in type I (four day old cultured cells) versus type II (seven day old cells) plasmodesmata.

In *Arabidopsis* cultured cells, transition from type I to type II plasmodesmata is associated with a change in ER-PM contact site architecture, from very tight contact (~3 nm) with no visible cytoplasmic sleeve (type I) to larger ER-PM distance (10 nm to more) with an electron lucent cytosolic sleeve and sparse spoke-like elements (type II) [1]. We analysed the plasmodesmata proteome from four days old cultured cells where type I plasmodesmata represent 70% of the total plasmodesmata population and at seven days where this proportion is reversed and type II become predominant [1]. Results show that 47 proteins from the plasmodesmata core proteome are differentially enriched at either type I or type II plasmodesmata, including all members of MCTPs (in bold), which are more abundant (1.4 to 3.6 folds) in type I plasmodesmata. Numbers in brackets correspondent to the protein numbering in Suppl. Table 1.



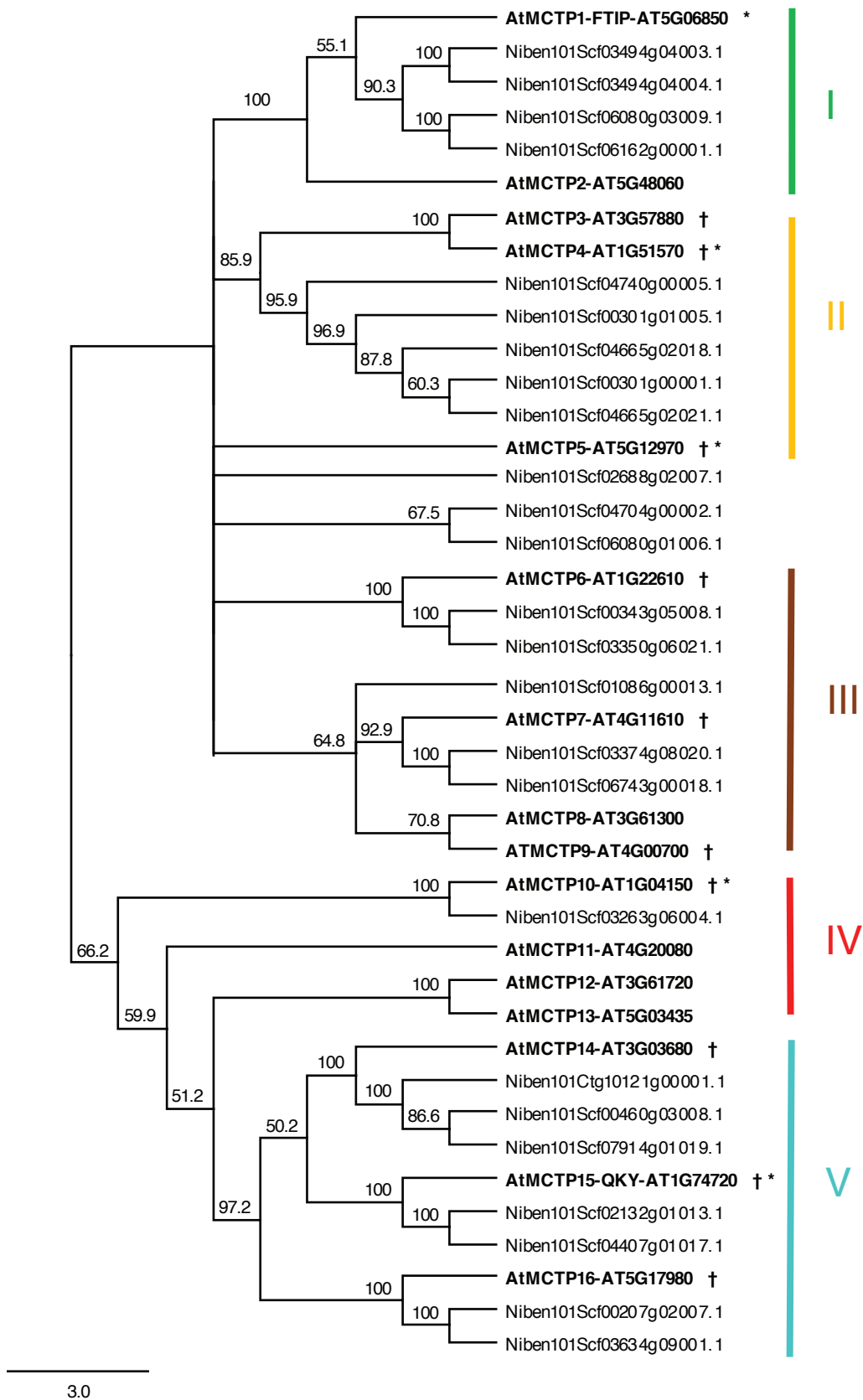


### Appendix Figure S3.

Domain organisation of the *Arabidopsis* MCTP protein family.

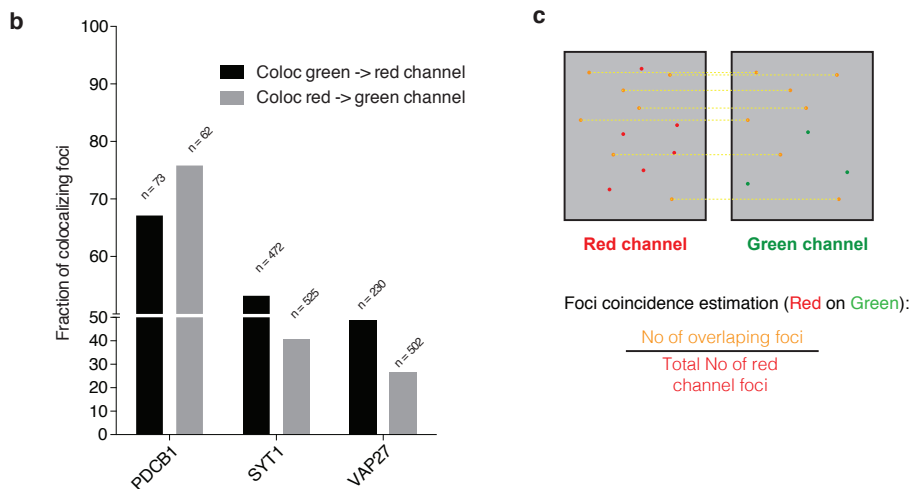
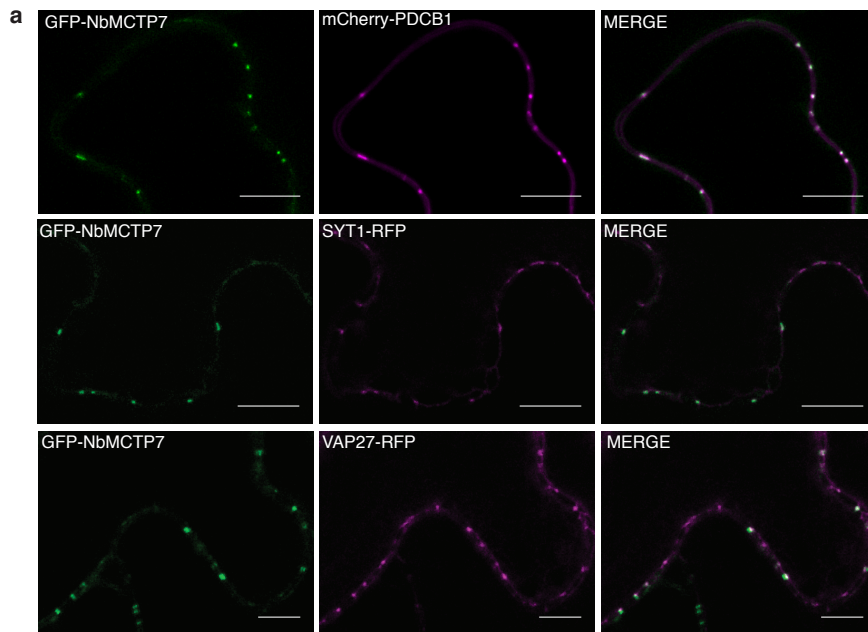
Alignment of the 16 MCTP proteins of *A. thaliana*. C2 domains are represented in blue and transmembrane domains (TMD) in yellow. Each coloured vertical bars represents specific amino acid. The consensus sequence and the percentage of identity are represented on the top of the alignment. Note that for every MCTP member the C2 domains were individually delimited using a combination of prediction methods (see M&M for details).

Appendix Figure S4



#### **Appendix Figure S4.**

Phylogenetic tree of *A. thaliana* and *N. benthamiana* MCTP proteins. Amino acid sequences of MCTP family from *A. thaliana* and *N. benthamiana* were aligned with CLUSTALW [2]. The resulting alignment was adjusted manually and used to construct an unrooted phylogenetic tree using the neighbour-joining algorithm with Geneious 8.0.5 (<https://www.geneious.com>). Bootstrap values for 1000 re-samplings are shown on each branch. † indicates the MCTP members enriched in the plasmodesmata proteome and \* indicates the MCTP members enriched in type I plasmodesmata. The five clades defined in Liu *et al.* 2017 [3] are indicated from I to V.



### Appendix Figure S5.

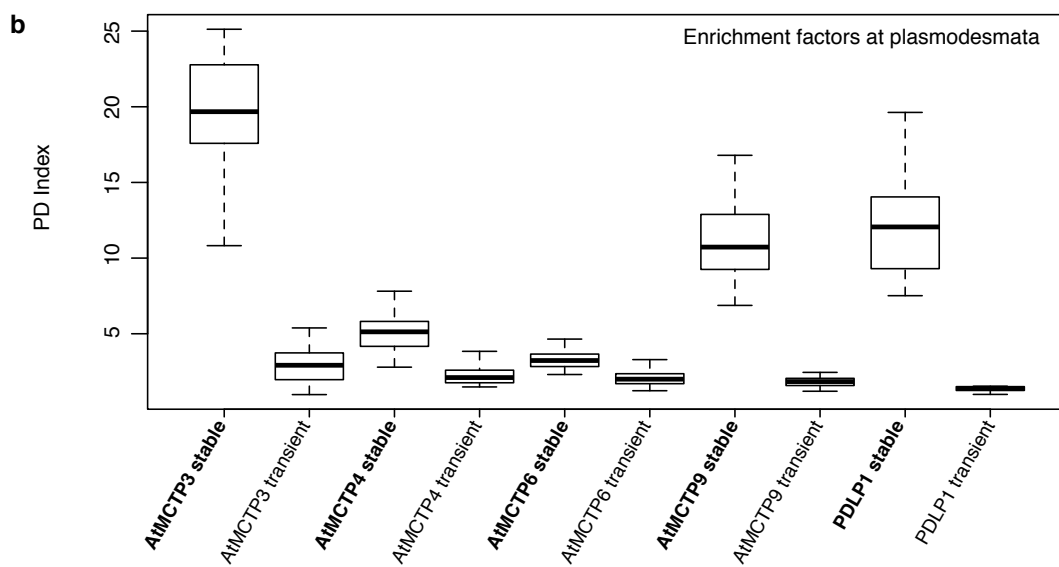
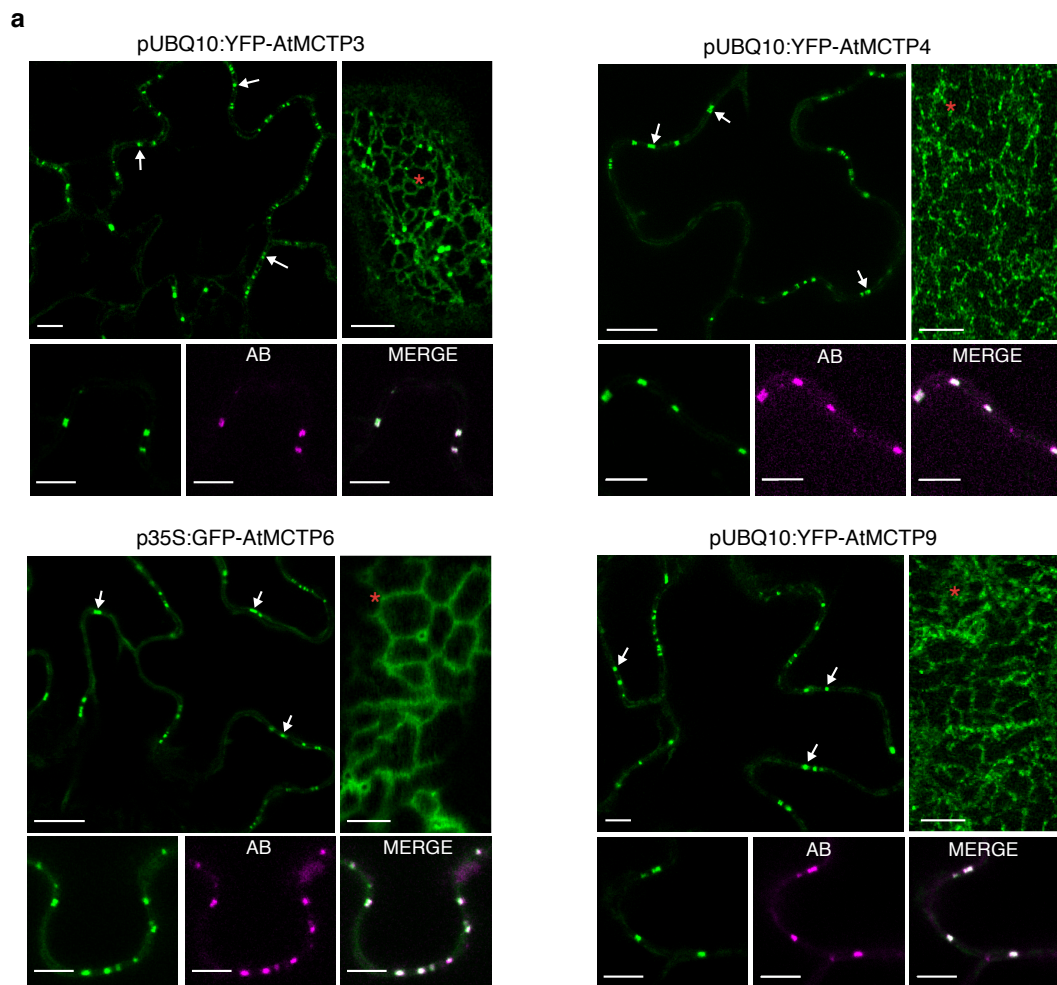
NbMCTP7 only partially co-localise with peripheral ER-PM contact sites.

(a) Co-localisation between GFP-NbMCTP7 with mCherry-PDCB1 and two well-established markers of peripheral ER-PM contact sites, VAP27.1 [4] and SYT1 [5,6], in *N. benthamiana* epidermal cells visualised by confocal microscopy. Scale bars, 10  $\mu\text{m}$ .

(b) Plot of the coincidence ratios. “Coloc green -> red channel” depicts the proportion of foci in the green channel overlapping with foci of the red channel over the total number of foci in the green channel. “Coloc red -> green channel” depicts this same proportion but of the red foci over the green foci. Coefficients range from 0 (complete exclusion) to 100% (complete colocalization of all foci). N indicated is the number of foci counted over 10 images of a given condition acquired over multiple co-expression/imaging sessions.

(c) Cartoon schematic on how the Coincidence ratio is calculated.

# Appendix Figure S6



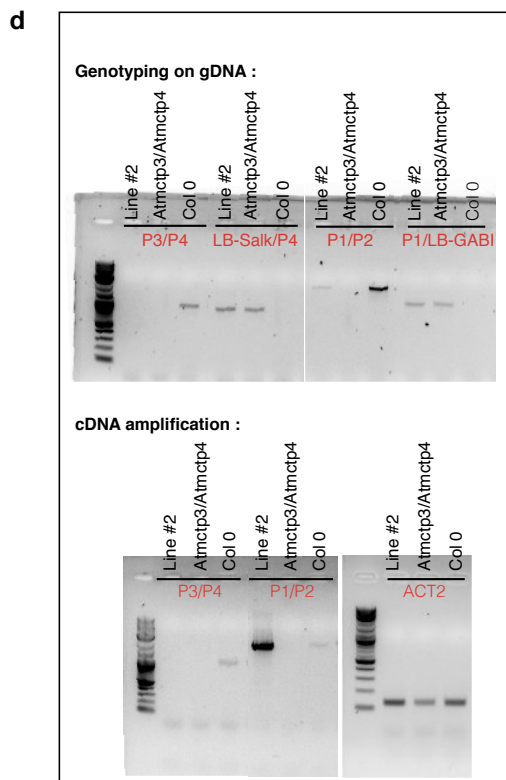
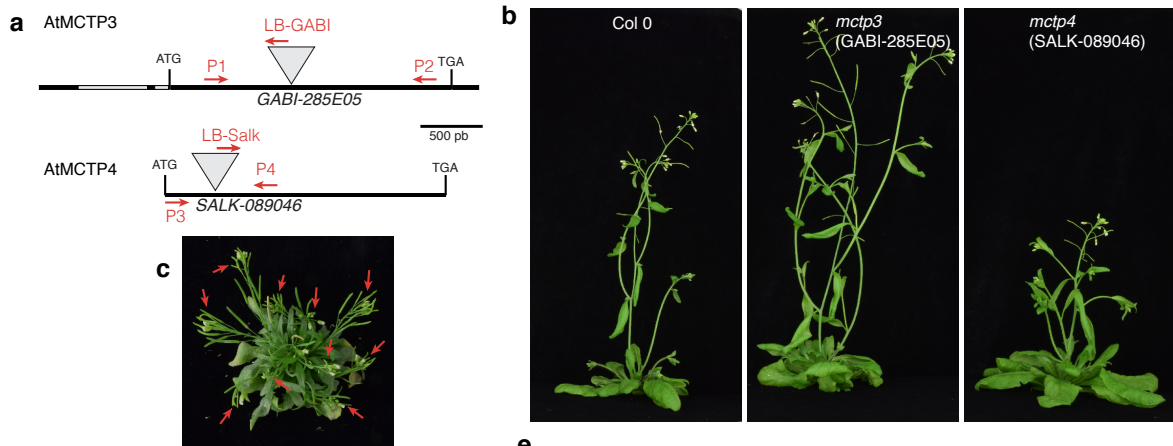
### Appendix Figure S6.

Subcellular localisation pattern of AtMCTP3, AtMCTP4, AtMCTP6 and AtMCTP9 when stably expressed in *Arabidopsis*.

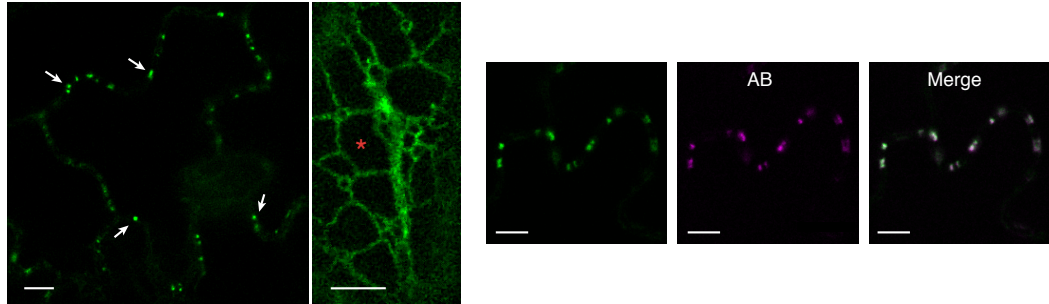
(a) Subcellular localisation of pUBQ10:YFP-AtMCTP3, pUB10:YFP-AtMCTP4, 35S:GFP-MCTP6 and pUB10:YFP-AtMCTP9 in transgenic *Arabidopsis* epidermal cells showing typical plasmodesmata punctate pattern at the cell periphery (white arrows) and reticulated ER pattern at the cell surface (red stars). Plasmodesmal localisation was confirmed by aniline blue (AB) co-staining. Scale bars, 5  $\mu\text{m}$ .

(b) Plasmodesmata (PD) index of *Arabidopsis* MCTPs and 35S:PDLP1-RFP when either stably expressed transgenic *Arabidopsis*, or transiently expressed in *N. benthamiana*, showing consistently increased plasmodesmata association in transgenic lines. Three biological replicates were analysed. In the box plot, median value is represented by horizontal line, values between quartil 1 to 3 are represented by box ranges, minimum and maximum values are represented by error bars.

# Appendix Figure S7



**f** *Atmctp3/Atmctp4* + pUBQ10:eYFP-AtMCTP3 (Line #2)



## Appendix Figure S7

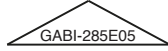
YFP-AtMCTP3 expression complements *Atmctp3/Atmctp4* loss-of-function double mutant.

(a) Schematic representation of T-DNA insertions in AtMCTP3 and AtMCTP4. LB, left border. In red, primers used for genotyping and RT-PCR. (b) Inflorescence stage of Col 0 *Atmctp3* (GABI-285E05) and *Atmctp4* (SALK-089046). (c) *Atmctp3/Atmctp4* double mutant shows multiple inflorescences (red arrows). (d) Top, genotyping of *Atmctp3/Atmctp4* complemented with pUBQ10:YFP-AtMCTP3 (Line #2), *Atmctp3/Atmctp4* double mutant and Col-0, showing the presence of AtMCTP3 and AtMCTP4 T-DNA inserts. Bottom, RT-PCR analysis of AtMCTP3, AtMCTP4 and Actin2 (ACT2) on cDNA extracted from complemented *Atmctp3/Atmctp4* line #2, *Atmctp3/Atmctp4* double mutant and Col-0 showing the absence of full-length AtMCTP4 transcripts and the over expression of AtMCTP3. (e) Rosette and inflorescence stage of Col 0, *Atmctp3/Atmctp4* double mutant and the complemented line #2. (f) Subcellular localization of YFP-AtMCTP3 in the complemented *Atmctp3/Atmctp4* line visualised by confocal microscopy. Arrows indicate plasmodesmata pitfields. \* indicates ER strand. Scale bar, 5  $\mu$ m.



AtMCTP3 protein sequence

MQRPPPEDFS LKETRPHLGG GKLSGDKLTS TYDLVEQMZY LYVRVVKAKE LPGKDMTGSC DPYVEVKLGN YKGTTRHFEK  
KSNPEWNQVF AFSKDRIQAS FLEATVKDKD FVKDDLIGRV **VFDLNEVPKR** VPPDSPLAPQ WYRLEDKGD KVKGELMLAV  
WFGTQADEAF PEAWHSDAAT VSGTDALANI RSKVYLSPLK WYLRVNVIEA QDLIPTDK**QR** **YPEVYVKAIV** GNQALRTRVS  
QSRTINPMWN EDLMFVAAEP FEEPLLSVE DRVAPNKDEV LGRCAIPLQY LDRRFDHKPV NSRWYNLEKH IMVDGEKKET  
KFASRIHMRI CLEGGYHVLD ESTHYSSDLR PTAKQLWKPN IGVLELGILN ATGLMPMKTG DGRGTDDAYC VAKYGQKWIR



TRTIIDSFTP RWNEQYTWEV FDPCTVVTVG VFDNCHLHGG EKIGGAKDSR IGKVRIRLST LETDRVYTHS YPLLVLHPNG  
VKKMGEIHLA VRFTCSLLN MMYMYSQPLL PKMHYIHPLT VSQLDNLRHQ ATQIVSMRLT RAEPPLRKEV VEYMLDVGSH  
MWSMRRSKAN FFRIMGVLSG LIAVGKWFQ ICNWKNPITT VLIHLLFIIL VLYPELILPT IFLYFLIGI WYYRWRPRHP  
PHMDTRLSHA DSAHPDELDE EFDTFPTS RP SDIVRMRYDR LRSIAGRIQT VVGDLATQGE RLQSLLSWRD PRATALFVLF  
CLIAAVILYV TPFQVVALCI GIYALRHPRF RYKLPSPVPLN FFRRLPARTD CML

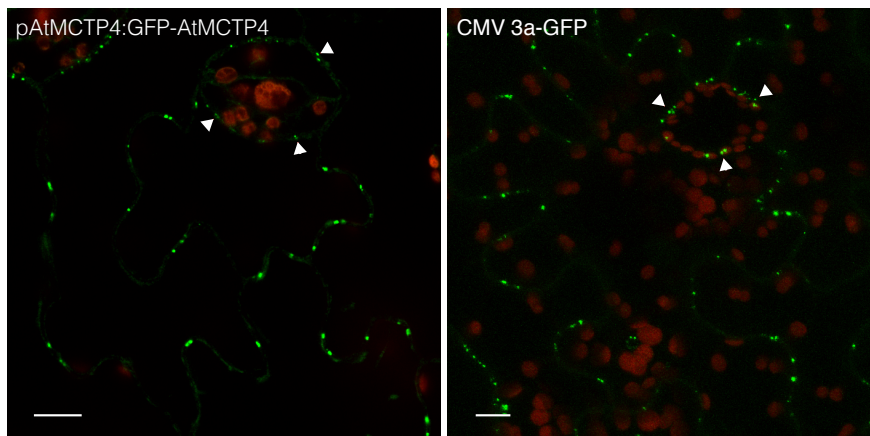
## Appendix Figure S8

AtMCTP3 protein sequence with in green the unique peptides identified in proteomics (Fig. 4) and position of the T-DNA.

**a** pAtMCTP4:GFP-AtMCTP4

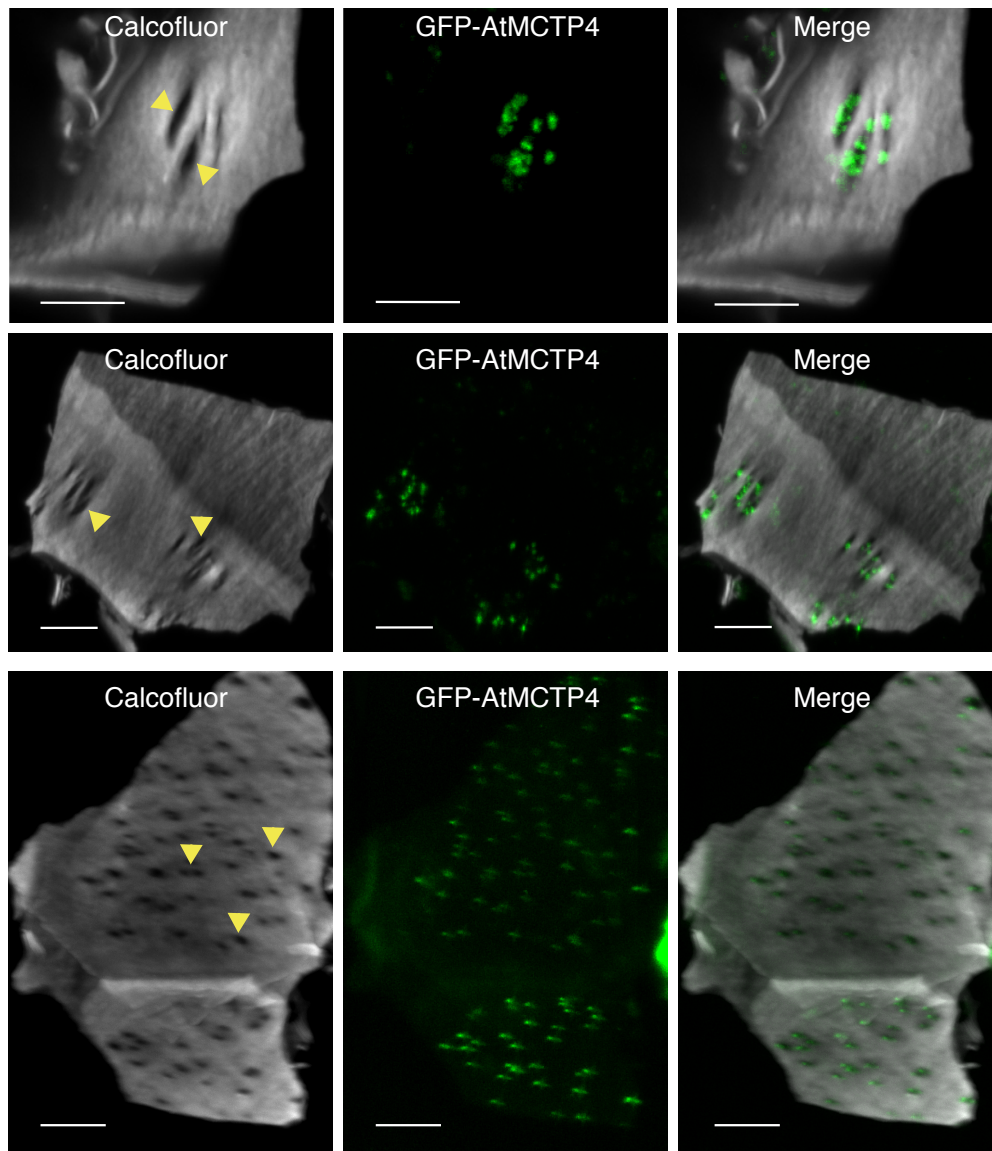


**b** Mature epidermis cells and stomata



**Appendix Figure S9**

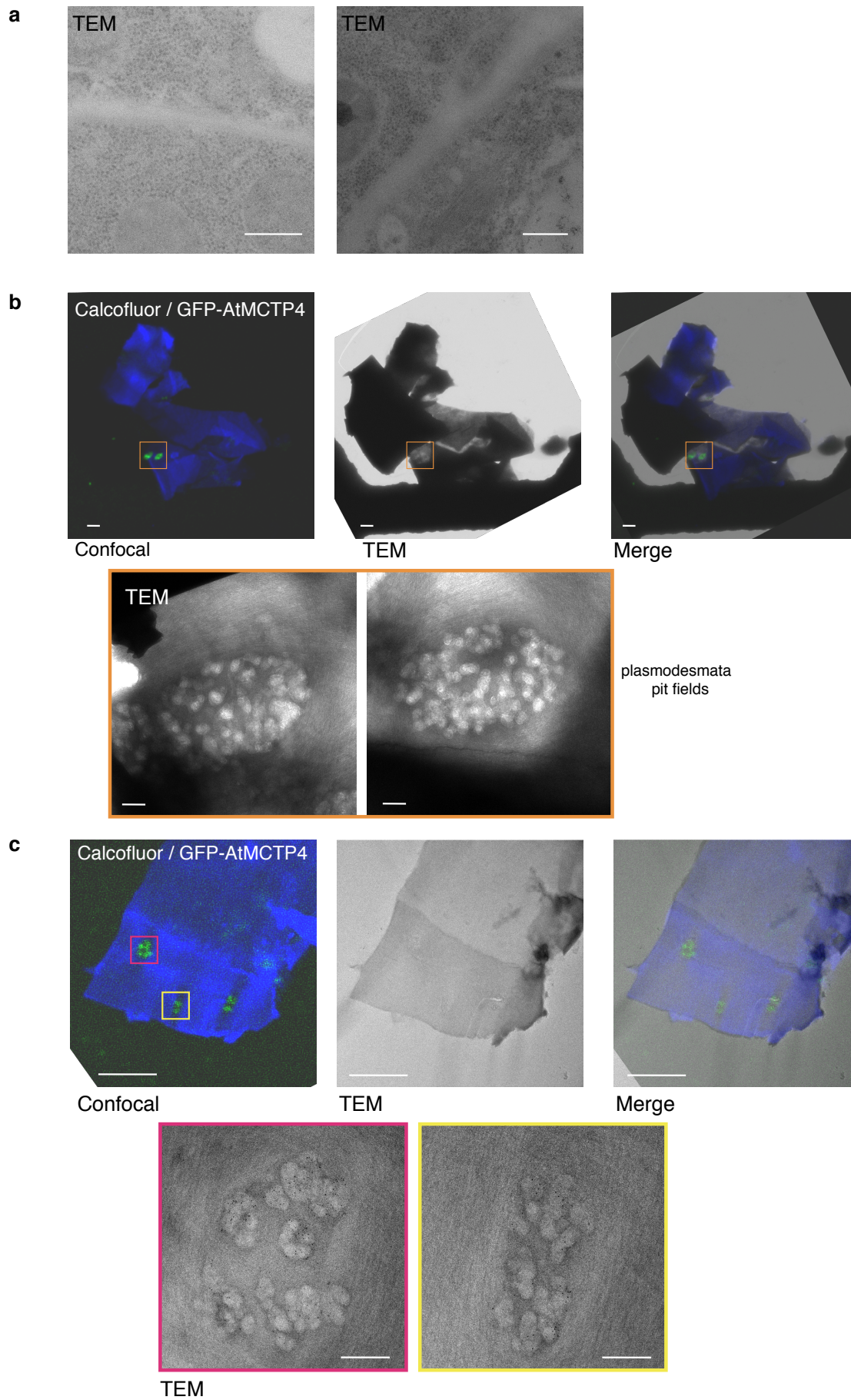
Overview of *Arabidopsis* seedlings showing the expression pattern of GFP-AtMCTP4 protein under native promoter visualised by confocal microscopy. (a) GFP-AtMCTP4 is strongly expressed in young leaf primordia, in root tip and lateral root of *Arabidopsis*. Scale bars, root tip and lateral root 10  $\mu\text{m}$ ; young leaf 100  $\mu\text{m}$ . (b) Localisation pattern of GFP-AtMCTP4 (in *Arabidopsis thaliana*) and Cucumber mosaic virus movement protein CMV 3a-GFP (in *Nicotiana benthamiana*) in leaf epidermal cells is similar. Both proteins display a characteristic plasmodesmata-punctate localisation pattern at the cell periphery and stomata. Arrowhead indicate punctate signal in stomata. Scale bar, 10 $\mu\text{m}$ .



### Appendix Figure S10

Confocal observation of cell walls purified from pAtMCTP4:GFP-AtMCTP4. Cell walls were stained with calcofluor, revealing plasmodesmata pit fields where calcofluor staining, hence cellulose, is absent/reduced (yellow arrowheads). GFP-AtMCTP4 signal is always associated with plasmodesmata pit fields. Scale bars, 5  $\mu\text{m}$

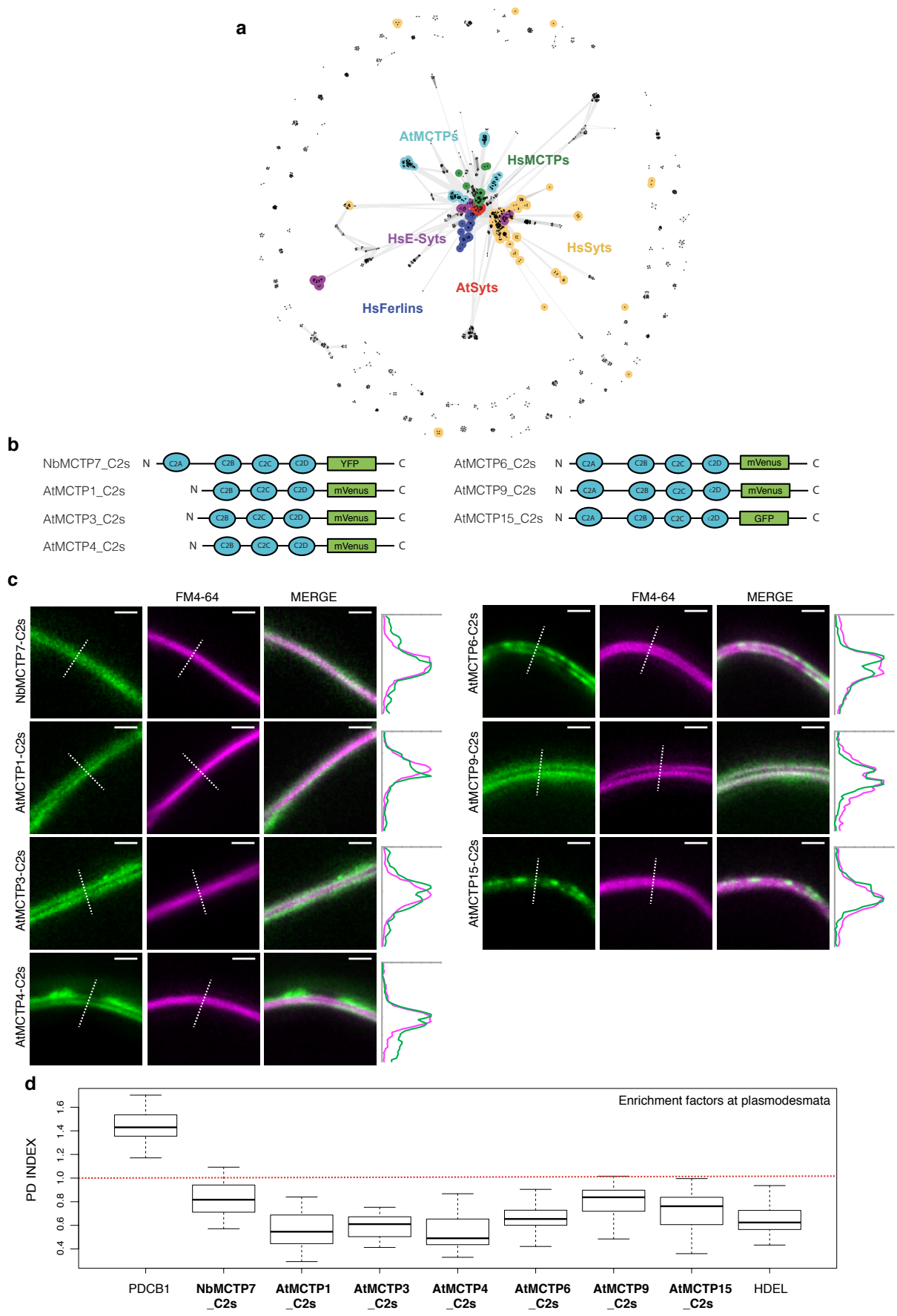
# Appendix Figure S11



### **Appendix Figure S11**

(a) Immunogold labelling for GFP on Col-0 wild type roots. Scale bar, 300 nm. (b) CLEM on cell walls purified from pAtMCTP4:GFP-AtMCTP4 *Arabidopsis* seedlings (c) CLEM combined with immunogold labelling against callose (10 nm gold particles). TEM = transmission electron microscopy. Scale bars, 5  $\mu\text{m}$  for confocal images and 300 nm for TEM images.

# Appendix Figure S12



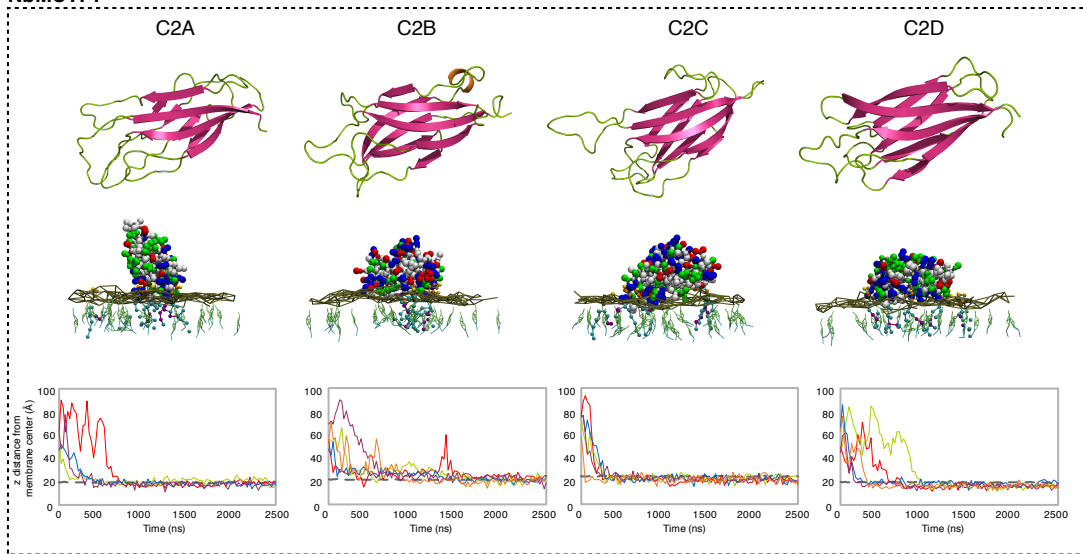
## Appendix Figure S12

(a) Cluster map of human and *A. thaliana* C2 domains. Homologs of the four *A. thaliana* MCTP C2 domains were searched for in the human and *A. thaliana* proteomes using HHpred with a probability cut-off of 50% and with 'No. of target sequences' set to 10000. The obtained sequences were filtered to a maximum pairwise sequence identity of 100%, at a length coverage of 70%, using MMseqs2 (cite PMID: 29035372) to eliminate redundant sequences. The sequences in the filtered set, comprising almost all human and *A. thaliana* C2 domains, were next clustered in CLANS based on their all-against-all pairwise sequence similarities as evaluated by BLAST P-values (PMID: 9254694). Clustering was done to equilibrium in 2D at a P-value cutoff of e-10 using default settings. In the map, dots represent sequences and line coloring reflects the strength of sequence similarity between them; the darker a line, the lower the P-value. Proteins not discussed in the manuscript are not colored.

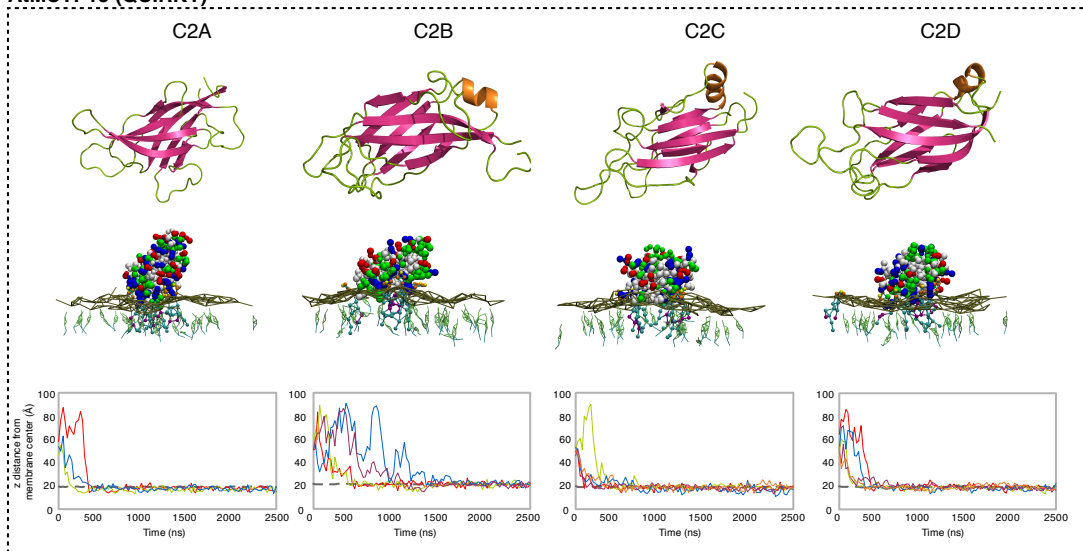
(b-d) The C2 blocks (C2A-D or C2B-D) of AtMCTP1, 3, 4, 6, 9, 15 and NbMCTP7 were tagged at their C-terminus with a fluorescent tag and expressed transiently in *N. benthamiana* leaves under moderate ubiquitin 10 promoter. b, Schematic representation of truncated MCTPs tagged with a fluorescent tag. c, Localisation of truncated AtMCTP1, 3, 4, 6, 9, 15 and NbMCTP7 C2 blocks (MCTP-C2s) in *N. benthamiana* epidermal cells by confocal microscopy. The PM was stained using short-term (up to 15 min) FM4-64 staining (magenta). Intensity plots are shown for each co-localisation pattern. When expressed in epidermal cells, MCTP-C2s-YFP constructs only partially associate with the PM and cytosolic localisation is also apparent. Scale bars, 5  $\mu\text{m}$ . d, The PD index of individual truncated MCTP\_C2s constructs is below 1 (red dashed line), indicating loss of plasmodesmata localisation. In the box plot, median value is represented by horizontal line, values between quartil 1 to 3 are represented by box ranges, minimum and maximum values are represented by error bars. 3 biological replicates were analysed.

## Appendix Figure S13

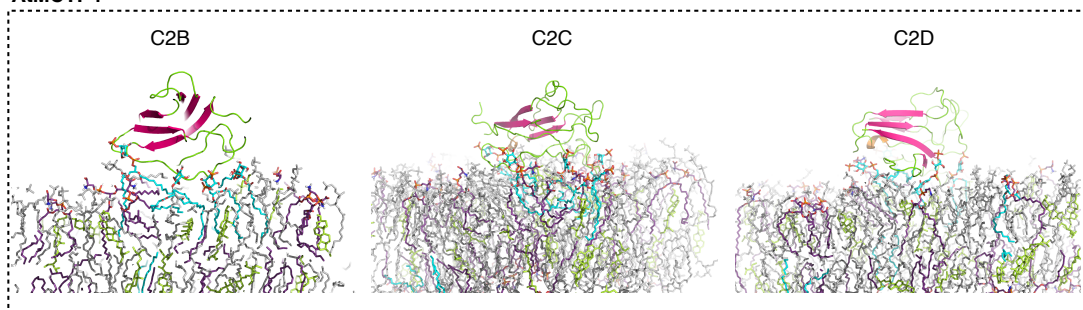
### a NbMCTP7



### b AtMCTP15 (QUIRKY)



### c AtMCTP4

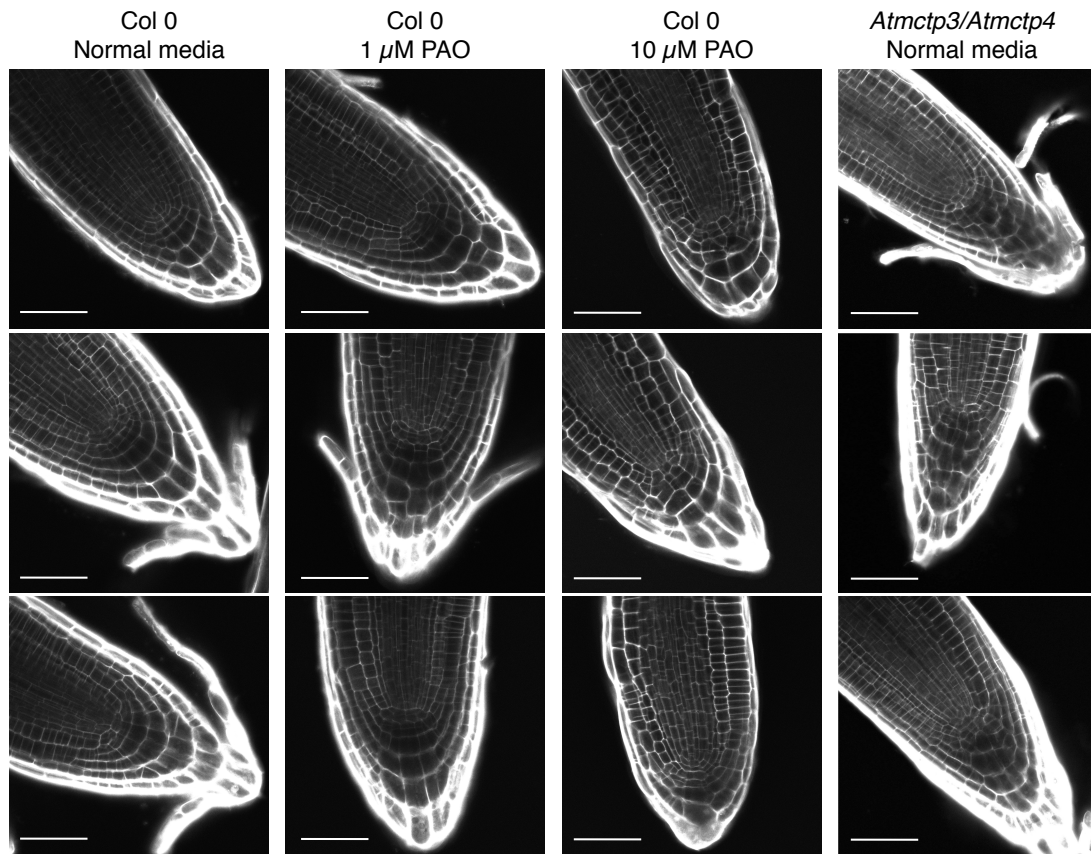




### Appendix Figure S13

Membrane docking of NbMCTP7 and AtMCTP15/QKY C2 domains on a PM-like membrane.

In (a) and (b); Top: 3D-atomistic model of the individual AtMCTP4 C2 domains. Beta strands are shown in pink, loops in green and alpha helices in orange. Bottom: molecular dynamics of individual NbMCTP7 (a) and AtMCTP15/QKY (b) C2 domains with phosphatidylcholine (PC), phosphatidylserine (PS), sitosterol (Sito) and phosphoinositol-4-phosphate (PI4P) (PC/PS/Sito/PI4P 57:19:20:4) biomimetic lipid bilayer. The plots show the minimal distance between the protein's closest residue to the membrane and the membrane center, over time. The membrane's phosphate plane is represented by a PO<sub>4</sub> grey line on the graphs and a dark green meshwork on the simulation image captures (above graphs). For individual C2 domain, the simulations were repeated three to five times (runs 1-5). C2 membrane docking was only considered as positive when a minimum of three independent repetitions showed similarly stable interaction with the membrane. All C2 domains of NbMCTP7 and AtMCTP15/QKY show membrane interaction with a "PM-like" membrane composition, mainly due to the presence of PI4P. The amino acid colour code is as follow: red, negatively charged (acidic) residues; blue, positively charged (basic) residues; green, polar uncharged residues; and white, hydrophobic residues. (c) All atom simulation of AtMCTP4 C2 domains. 3D representation of the AtMCTP4 C2 domains still interacting with lipids after 100 ns all atom simulations. The C2 domain color code used is the same as in (a). PC is represented in grey, PS in purple, sitosterol in green and PI4P in blue.



**Appendix Figure S14**

PAO treated Col-0 *Arabidopsis* seedlings. After 7 days on MS solid media containing 1  $\mu\text{M}$  or 10  $\mu\text{M}$  PAO, root organisation was visualised by propidium iodide staining. At 1  $\mu\text{M}$  PAO cell organisation at the root tip was aberrant in 4 out of 12 plants against 12 out of 12 in 10  $\mu\text{M}$  PAO conditions. Scale bar, 50 $\mu\text{m}$ .

# Appendix Table S1

Candidate number	Primary Accession	Secondary Accessions	Description	Abundance	Enrichment ratios				Presence in published ER proteomes		PD association in Arabidopsis references
					PDPM	PDTP	PDly	PDWC	Nikolovski et al. 1	Dunkley et al. 2	
1	AT1G051570.1	AT2G31570.1, AT3G04130.1, AT3G03680.1, AT5G43740.1, AT5G44760.1	<b>Multiple C2 domains and Transmembrane region Protein 4, 10, 14 (MCTP4, 10, 14)</b>	203201610	331.0	223.6	300.1	70.2	x	x	
2	AT5G24100.2	AT5G42100.1, AT5G42100.1	<b>Beta 1-3-glucanase (ABG, PAPB)</b>	183801571	184.0	247.2	580.8	45.0			3
3	AT4G16380.1	AT4G16380.1, AT4G16380.1, AT4G16380.4, AT4G16380.4	Heavy metal transport/ detoxification superfamily protein	135301110	1022.7	478.1	1318.4	72.8			
4	AT5G26280.1	AT5G26280.1, AT5G26280.4	Xanthine/larval permease family protein (ANAT6)	113551318	772.6	730.3	1308.9	96.0	x		
5	AT1G22610.1	AT1G22610.1, AT4G00700.1	<b>Multiple C2 domains and Transmembrane region Protein 5.9 (MCTP5.9)</b>	776007012	315.5	115.1	285.3	61.7			
6	AT3G52470.1	AT3G52470.1, AT2G35980.1, AT5G06330.1	Alpha-ubiquitin proteinase (LEA) hydroxyproline-rich glycoprotein family	643336566	123.3	137.5	323.3	97.4			
7	AT5G16510.1	AT5G16510.1	Late embryogenesis abundant (LEA) protein synthase family protein	494288348	661.2	206.1	772.3	886.8			
8	AT5G01130.1	AT5G01130.1	Plasmodemata callose-binding protein 1 (PDCB1)	328259264	219.2	1052.3	623.0	48.0			4
9	AT5G43980.1	AT5G43980.1	Plasmodemata-located protein 1 (PDLP1)	311480268	309.0	119.0	307.6	46.4			5
10	AT2G01820.1	AT2G01820.1	Leucine-rich repeat protein kinase family protein (TMK3)	285991310	28.9	60.4	137.5	241.7			
11	AT5G32600.1	AT5G32600.1, AT3G14570.1, AT3G14570.2, AT3G14570.3, AT3G14780.1, AT5G13000.2	<b>Glucan synthase 2 (GALS2)</b>	297697666	14.5	58.4	67.3	65.2			6
12	AT5G05200.1	AT5G05200.1	NR1H1-like 3 (NHL3)	251252320	47.8	184.2	95.4	41.6			
13	AT3G51740.1	AT3G51740.1, AT5G55100.1	Inferolensene meristem receptor-like kinase 2 (IMK2)	245842528	17.5	43.5	57.1	52.5			
14	AT2G01630.1	AT2G01630.1, AT2G01630.2, AT2G01630.3	<b>O-Glycosyl hydrolases family 17 protein (beta1-3 glucanase, PdBG2)</b>	233481254	26.9	73.3	89.6	48.4			7
15	AT5G48450.1	AT5G48450.1, AT5G48450.2	SKUS similar 3	204842485	62.4	42.9	75.0	52.7			
16	AT5G46700.1	AT5G46700.1	Tetraspanin family protein (TRN2, TET1)	190712794	92.2	278.8	253.6	120.1			
17	AT1G06030.1	AT1G60030.1	Nucleobase-ascorbate transporter 7 (ANAT7)	175342944	228.0	548.4	468.1	42.0			
18	AT2G01660.1	AT2G01660.1, AT2G01660.2, AT2G01660.3	Plasmodemata-located protein 6 (PDLP6)	159384568	163.7	126.1	637.9	52.3			5
19	AT2G25270.1	AT2G25270.1	Transmembrane protein	139590159	182.4	186.1	198.2	74.8			
20	AT1G03290.1	AT1G03290.1, AT1G62320.1, AT1G62320.2, AT1G62320.3, AT1G62320.4	Early-responsive to dehydration stress protein (ERD4)	111499705	17.7	40.0	82.5	68.4			
21	AT2G01820.1	AT1G18650.1, AT1G18650.2	Xanthine/larval permease family protein (ANAT1)	109145419	701.8	63.2	76.5	46.8			4
22	AT2G23810.1	AT2G23810.1	Tetraspanin 8 (TET8)	97572093	58.9	73.8	180.0	60.9			
23	AT3G11660.1	AT3G11660.1	NR1H1-like 1 (NHL1)	83423848	57.1	62.0	70.9	77.1			
24	AT3G54200.1	AT3G54200.1	Late embryogenesis abundant (LEA) hydroxyproline-rich glycoprotein family	81984458	16.9	197.0	89.5	48.8			
25	AT4G29360.1	AT4G29360.1, AT4G29360.2	O-Glycosyl hydrolases family 17 protein	79706419	68.0	70.0	155.6	47.5			
26	AT1G06295.1	AT1G06295.1, AT1G26450.1, AT1G66295.2	Plasmodemata callose-binding protein 4 (PDCB4)	79562157	107.9	133.1	129.2	47.5			4
27	AT5G06330.2	AT5G06330.2, AT5G06330.1	Farnesylated protein 3	76940500	153.5	63.4	157.5	41.7			
28	AT1G66250.1	AT1G66250.1	O-Glycosyl hydrolases family 17 protein (beta1-3 glucanase, PdBG3)	71917917	32.9	204.2	237.4	59.5			7
29	AT2G33330.1	AT2G33330.1	Plasmodemata-located protein 3 (PDLP3)	71730983	251.4	90.8	355.4	60.7			5
30	AT1G03290.1	AT1G03290.1	Phosphothiolase	71318252	19.8	76.5	134.0	789.2			
31	AT2G05760.1	AT2G05760.1	Xanthine/larval permease family protein (ANAT1)	69482206	574.8	658.3	702.1	46.0			
32	AT3G34150.1	AT4G34150.1	Callose-dependent lipid-binding family protein Soc C-term domain charged block	67976864	270.5	92.9	235.3	178.7			
33	AT2G26510.1	AT2G26510.1, AT2G26510.2, AT2G26510.3	Xanthine/larval permease family protein (ANAT3)	66876643	87.1	54.6	41.8	67.5			
34	AT2G12400.1	AT2G12400.1	Plasma membrane fusion protein	66330049	25.9	80.8	107.0	91.4			
35	AT5G49990.1	AT5G49990.1	Xanthine/larval permease family protein (ANAT4)	66145014	112.7	171.7	277.7	77.3			
36	AT3G13560.1	AT3G13560.1	O-Glycosyl hydrolases family 17 protein (beta1-3 glucanase, PdBG1)	65897722	42.7	148.4	287.3	52.3			7
37	AT1G64760.1	AT1G64760.1, AT3G04010.1, AT5G18220.1	O-Glycosyl hydrolases family 17 protein	64825238	12.3	63.2	48.9	38.1			
38	AT5G58090.1	AT5G58090.1	O-Glycosyl hydrolases family 17 protein	62685626	27.8	88.9	96.6	45.0			
39	AT2G31810.1	AT2G31810.1, AT2G31810.2, AT2G31810.3	ACT domain-containing small subunit of acetylacetate synthase protein	61594943	74.3	34.3	229.6	46.6			
40	AT4G25400.1	AT4G25400.1	SKUS similar 1	58538994	17.3	61.9	94.1	60.8			
41	AT2G36850.1	AT2G36850.1	Glucan synthase-like 8 (GALS10, GSL8)	52455867	8.0	20.8	25.4	23.9			
42	AT3G45200.1	AT3G45200.1, AT3G45200.2, AT5G60220.1	<b>Tetraspanin 3 (TET3)</b>	47750446	65.3	102.4	242.7	51.0			10
43	AT5G61030.1	AT5G61030.1	Glycine-rich RNA-binding protein 3	45152284	165.8	40.8	211.6	183.0			
44	AT1G68700.1	AT1G68700.1	HVA22 homologous C	43597164	222.7	137.1	204.2	86.5			
45	AT2G17120.1	AT2G17120.1	LysM domain-containing GPI-anchored protein 2 (LYM2)	40630549	2.7	18.3	10.3	35.9			8
46	AT3G53780.2	AT3G53780.2, AT3G53780.1, AT3G53780.3	RHOMBOLD-like protein 4	40497867	103.2	104.2	195.7	57.7			
47	AT1G04520.1	AT1G04520.1	Plasmodemata-located protein 2 (PDLP2)	38473248	172.0	78.7	74.5	44.9			5
48	AT4G31140.1	AT4G31140.1, AT5G20870.1	O-Glycosyl hydrolases family 17 protein	36893093	21.7	75.7	127.0	48.3			
49	AT3G11650.1	AT3G11650.1	NR1H1-like 2 (NHL2)	34003434	308.4	66.8	306.7	50.3			
50	AT1G06460.1	AT1G06460.1, AT5G44020.1	HAD superfamily subfamily IIIB acid phosphatase	33114051	292.6	119.0	261.1	378.2			
51	AT5G61730.1	AT5G61730.1, AT5G61990.1, AT5G61990.2, AT5G61730.1	ABC2 homolog 11	32559047	10.7	36.3	51.4	83.7			
52	AT1G05570.1	AT1G05570.1, AT1G05570.2, AT1G06490.1, AT1G06490.2	Callose synthase 1 (CALS1, GSL6)	29840182	14.0	39.5	40.0	69.2			
53	AT5G61740.1	AT5G61740.1, AT3G47740.1, AT3G47750.1, AT3G47760.1, AT3G47760.2, AT3G47760.3	ABC2 homolog 14	26706448	9.6	43.5	63.1	69.4			
54	AT3G53060.1	AT3G53060.1	Heavy metal transport/ detoxification superfamily protein	26431305	20.7	136.7	137.9	57.9			
55	AT2G35960.1	AT2G35960.1	NR1H1-like 12 (NHL12)	25292331	186.4	46.6	186.0	66.5			
56	AT5G17890.1	AT5G17890.1	<b>Multiple C2 domains and Transmembrane region Protein 16 (MCTP16)</b>	23482273	59.7	33.5	128.7	34.9	x	x	
57	AT2G38010.1	AT2G38010.1, AT1G07380.1, AT1G07380.2, AT2G38010.3	Neutral/alkaline non-lysosomal ceramidase	22829457	107.4	56.4	68.5	44.4			
58	AT1G74010.1	AT1G74010.1, AT5G53810.1	Calcium-dependent phosphotriesterase superfamily protein	21457306	133.9	61.0	207.8	75.2			
59	AT5G03300.1	AT5G03300.1, AT5G03300.2	Adenosine kinase 2	21310306	195.4	34.8	149.9	86.8			
60	AT3G17890.1	AT3G17890.1, AT4G11610.1, AT4G11610.2, AT4G11610.3	<b>Multiple C2 domains and Transmembrane region Protein 3, 7 (MCTP3, 7)</b>	26444826	47.5	44.3	25.9	61.7	x	x	
61	AT2G01080.1	AT2G01080.1	Late embryogenesis abundant (LEA) hydroxyproline-rich glycoprotein family	20172878	91.7	33.8	112.7	45.3			
62	AT5G15400.1	AT5G15400.1	U-box domain-containing protein	18414844	237.2	33.9	256.6	232.3			
63	AT2G42010.1	AT2G42010.1, AT2G42010.2, AT4G00240.1, AT4G00240.2, AT4G00240.3, AT4G11830.1	Phospholipase D beta 1 (PLD2BETA1)	18265056	169.7	46.1	149.7	35.4			
64	AT1G23880.1	AT1G23880.1, AT1G23880.2	NHL domain-containing protein	16952398	186.3	52.5	134.8	107.1			
65	AT1G08210.1	AT1G08210.1, AT1G08210.2, AT1G08210.3, AT1G08210.4	Eukaryotic aspartyl protease family protein	15438818	162.3	132.8	172.9	50.4			
66	AT1G74720.1	AT1G74720.1	<b>Multiple C2 domains and Transmembrane region Protein 15 (MCTP5, QUIRKY, OK)</b>	15148837	79.0	47.9	82.9	73.1			11
67	AT5G67130.1	AT5G67130.1	PLC-like phosphodiesterase superfamily protein	15053353	22.9	43.0	64.9	52.1			
68	AT5G55050.1	AT5G55050.1	GDSL-like Lipase/Acylhydrolase superfamily protein	14212548	267.7	56.2	236.3	83.1			
69	AT1G64800.1	AT1G64800.1	Glycine-rich protein family	14151963	201.6	104.5	418.2	99.4			
70	AT1G74520.1	AT1G74520.1	HVA22 homologous A	14588843	144.1	38.6	75.2	78.5			
71	AT4G25550.1	AT4G25550.1	Cleavage/polyadenylation specificity factor 250Da subunit	12059569	553.2	56.8	292.5	41.0			
72	AT2G32080.1	AT2G32080.1, AT2G32080.2	STRUBBELIG-receptor family 1 (SFR1)	11280796	8.0	60.7	63.0	60.8			
73	AT5G12970.1	AT5G12970.1	<b>Multiple C2 domains and Transmembrane region Protein 5 (MCTP5)</b>	9974540	1025.2	516.4	171.4	152.6			
74	AT4G05520.1	AT4G05520.1, AT4G0520.2	EPS15 homolog domain 2	9223837	24.2	63.0	91.8	57.6			
75	AT4G04970.1	AT4G04970.1, AT4G13690.1	Glucan synthase-like 1 (CALS11, GSL1)	8134750	53.8	55.1	93.0	90.2			
76	AT2G27810.1	AT2G27810.1, AT2G27810.2, AT2G27810.3, AT2G27810.4	Nucleobase-ascorbate transporter 12 (ANAT12)	8121544	18.2	50.9	109.0	57.2			
77	AT1G73590.1	AT1G73590.1	Auxin efflux carrier family protein	7752624	12.8	180.1	59.8	158.8			
78	AT2G31960.1	AT2G31960.1, AT2G31960.2, AT2G31960.3	Glucan synthase-like 3 (CALS3, GSL3)	7719612	24.4	81.2	57.1	68.2			
79	AT2G07860.1	AT2G07860.1	Late embryogenesis abundant (LEA) hydroxyproline-rich glycoprotein family	7372929	828.0	186.0	288.6	69.7			
80	AT1G11130.1	AT1G11130.1, AT1G11130.2	<b>Leucine-rich repeat protein kinase family protein (SLB)</b>	6262052	51.8	40.7	63.3	55.6			11
81	AT3G17350.1	AT3G17350.1, AT3G20560.1, AT4G27080.2	Wall-associated receptor kinase carboxy-terminal protein	6485007	48.3	38.0	86.7	55.9			
82	AT4G27080.1	AT4G27080.1, AT3G20560.1, AT4G27080.2	PKI-like 5-4	6261964	327.2	121.2	61.0	646.1			
83	AT5G02750.1	AT5G02750.1, AT5G02750.1	RHOMBOLD-like protein 3	5887061	27.6	81.9	296.7	101.2	x		
84	AT4G25810.1	AT4G25810.1	Xyloglucan endotransglycosylase 6	5353773	815.6	77.1	361.2	40.8			
85	AT3G06030.1	AT3G06030.1	bZIP domain class transcription factor	5213727	83.5	51.9	156.7	92.9			
86	AT2G21185.1	AT2G21185.1	Transmembrane protein	5171328	877.8	69.7	1668.4	158.8			
87	AT4G01410.1	AT4G01410.1	Late embryogenesis abundant (LEA) hydroxyproline-rich glycoprotein family	4702568	136.6	151.5	600.1	61.1			
88	AT1G14940.1	AT1G14940.1	RNA-binding (RHM/RBD/RNP motifs) family protein	4578430	61.2	75.6	103.3	67.4			
89	AT3G35490.1	AT3G35490.1	Eucytoplasmic complex component (SEC15A)	4425140	51.8	53.1	175.4	181.5			
90	AT4G36860.1	AT4G36860.1, AT4G36860.2	LIM domain-containing protein	4418701	83.4	40.8	62.2	45.2			
91	AT1G10180.1	AT1G10180.1	LOW protein; exocyst complex component-like protein	3755718	28.8	37.2	126.3	212.4			
92	AT4G35730.1	AT4G35730.1, AT1G25420.1, AT1G25420.2, AT2G21340.1, AT2G21340.2	Regulator of Yps2 activity in the MVB pathway protein</								

### **Appendix Table S1. Proteins of the core *Arabidopsis* plasmodesmata proteome**

Label-free quantitation strategy was used to determine the relative abundance of proteins in the plasmodesmata (PD) fraction *versus* contaminant subcellular fractions namely, the PM, total extract (TP), microsomes ( $\mu$ ) and cell wall (CW), see Methods for details. Only proteins presenting minimum enrichment ratios of 8, 40, 30 and 30 in plasmodesmata *versus* PM, TP, microsomal and CW fractions, respectively were selected. Previously characterised plasmodesmal proteins are in orange and MCTP members in green. First row indicates the main accession and second row all possible isoforms potentially identified. The different shades (light to dark) of brown represent different enrichment levels (0-10; 10-20; 20-100 and above 100).

CLONING	MCTP Full length	construction	plasmid	primers Forward / right border	primers Reverse / left border
NbMCTP7	p35S::GFP::NbMCTP7		pGWB406	GGGACAAAGTTTGTACAAAAGAGGcttaATGATCTTAAGTAATCTGAAGCTAGAGTGTGG	GGGACCACTTTTGTACAAAAGAGCTGGGTTACAACATACTATCTGTTCGAGCGAGGAAG
AIMCTP3	pUBQ10::eYFP::AIMCTP3		pK7m34GW	GGGACAGCTTTTCTGTACAAAGTGgaaATGTCAGAGCAACACCTCCTGAAG	GGGACAACTTTGTATAATAAAGTTGctCTACCAAAAACACAAGCTTATCTTAC
AIMCTP4	prom::AIMCTP4::GFP::AIMCTP4		pRbbar::OCS	CGTCCAGCAAGGATCTCATGGTGAAGCAAGGGCGAGGA	AAAGCAGGGCATCCCTCGAGCAAGCTGCAATCAAGTTCTTGCT
AIMCTP4	pUBQ10::eYFP::AIMCTP4		pB7m34GW	GCTCACTAGTGAATCTCCACCTTCCCAATCAAGCTTCCA	TAACGATTTGGTTCCTCGCTGCGAGGAGGTCATATGTTGCT
AIMCTP6	p35S::eGFP::AIMCTP6		pB7WGF2	GGGACAGCTTTCTGTACAAAGTGgaaATGTCAGAGCAACACCTCCTGAAG	GGGACAACTTTGTATAATAAAGTTGctCTACCAAAAACACAAGCTTATCTTAC
AIMCTP9	pUBQ10::eYFP::AIMCTP9		pB7m34GW	ctcctcATATAAACTAGTGTGAAGATC	TTACAGTAGCATCTGAGCTTGGC
MCTP_TMR				GGGACAGCTTTCTGTACAAAGTGgaaATGAGCAATATAAAGCTAGGA	GGGACAACTTTGTATAATAAAGTTGctTCACAGCATAGAGTGGGTCAATG
NbMCTP7_TMR	p35S::GFP::NbMCTP7_TMD		pK7WGY2	GGGACAAAGTTTGTACAAAAGAGGCTbATGTGGTTTGGGAACATGCTTTA	GGGACCACTTTTGTACAAAAGAGCTGGGTTTACAACATACTACTGTGTGG
AIMCTP1_TMR	pUBQ10::eYFP::AIMCTP1_TMD		pB7m34GW	GGGACAGCTTTTGTACAAAAGTGgaaATGCTTGTGTGCAACAAAA	GGGACAACTTTGTATAATAAAGTTGctCAAAAGCATACAATCTGTGTTTTGA
AIMCTP3_TMR	pUBQ10::eYFP::AIMCTP3_TMD		pB7m34GW	GGGACAGCTTTTGTACAAAAGTGgaaATGCTTGTGTGCAACAAAA	GGGACAACTTTGTATAATAAAGTTGctCAAAAGCATACAATCTGTGTTTTGA
AIMCTP4_TMR	pUBQ10::eYFP::AIMCTP4_TMD		pK7m34GW	GGGACAGCTTTTGTACAAAAGTGgaaATGCTTGTGTGCAACAAAA	GGGACAACTTTGTATAATAAAGTTGctCAAAAGCATACAATCTGTGTTTTGA
AIMCTP6_TMR	pUBQ10::eYFP::AIMCTP6_TMD		pB7m34GW	AGGACAAGCAAAAGCTAA1TT	AGTCAAGATAGCTACTGCTGTA
AIMCTP9_TMR	pUBQ10::eYFP::AIMCTP9_TMD		pB7m34GW	ATGGACAAGTGTGCAACATG	TGACCAGACTCTATGCTGTGA
AIMCTP15_TMR	pUBQ10::eYFP::AIMCTP15_TMD		pB7m34GW	AGCAAAAGCGAATTGGTACAG	TGTCGGATCGACTCATCTAA
MCTP_C2s					
AIMCTP1_C2s	pUBQ10::AIMCTP1_C2B::D::mVenus		pB7m34GW	ATGGCAGCCAAAGATGGAGC	TCAGTTGTCTATCCTTGGCT
AIMCTP3_C2s	pUBQ10::AIMCTP3_C2B::D::mVenus		pB7m34GW	ATGGCAGCCAAAGATGGAGC	TCAGTTGTCTATCCTTGGCT
AIMCTP4_C2s	pUBQ10::AIMCTP4_C2B::D::mVenus		pB7m34GW	ATGGCAGCCAAAGATGGAGC	TCAGTTGTCTATCCTTGGCT
AIMCTP6_C2s	pUBQ10::Ab C2::mVenus		pB7m34GW	ATGGCAGCCAAAGATGGAGC	TCAGTTGTCTATCCTTGGCT
AIMCTP9_C2s	pUBQ10::Ab C2::mVenus		pB7m34GW	ATGGCAGCCAAAGATGGAGC	TCAGTTGTCTATCCTTGGCT
AIMCTP15_C2s	p35S::A15 C2 A-D::eGFP		pK7FWG2	GGGACAAAGTTTGTACAAAAGAGGCTbATGAATAAACTAGTGTAGAAATCG	GGGACCACTTTTGTACAAAAGAGCTGGGTTaGCGCGGTGCAAGGTGTACCTCAG
NbMCTP7_C2s	p35S::NbMCTP7 C2A-D::eYFP		pH7YWG2	ATGAGCAATAATAAAGCTAGG	GCACATGGGCTCTCCAGTATG
GENOTYPING					
AIMCTP3				GTGGAACCAAGTTTTGGCCT	GAGAACTCGGCGCAATCA
AIMCTP4				GTGGAACCAAGTTTTGGCCT	ATATTGACCATCACTCAATTGC
				P1 (Fw) / LB-SAB1	ACCSAGTTAGGGCTCCACA
				Fw / Rv	ACCSAGTTAGGGCTCCACA
				LBb1-3-Salk / Rv	
Transcript expression					
AIMCTP3				GTGGAACCAAGTTTTGGCCT	AAATTGAGAGGAAACGGATGG
AIMCTP4				GTGGAACCAAGTTTTGGCCT	CTTGGTGGGAAATTTGAT
ACT2 (AT1.G49240)				CGGAGAGCATGAAGATTAAG	CATACTCTGGCTTAGAGATCCACA
YEAST EXPERIMENT					
AIMCTP4	pCUA16			GGTGGTGGATCCATGCAGAGACCACTCCTCTGAAG	GGTGGTCCGGGCTATCAGAGCATGCAATCAAGTTCT

Appendix Table S2  
Primers used for MCTP cloning.

## Quantification of Protein Enrichment at Plasmodesmata

Magali S. Grison<sup>1, \*</sup>, Jules D. Petit<sup>1, 2</sup>, Marie Glavier<sup>1</sup> and Emmanuelle M. Bayer<sup>1</sup>

<sup>1</sup>Laboratoire de Biogenèse Membranaire, UMR5200 CNRS, Université de Bordeaux, Villenave d'Ornon, France; <sup>2</sup>Laboratoire de Biophysique Moléculaire aux Interfaces, TERRA Research Centre, GX ABT, Université de Liège, Gembloux, Belgium

\*For correspondence: [magali.grison@u-bordeaux.fr](mailto:magali.grison@u-bordeaux.fr)

**[Abstract]** Intercellular communication plays a crucial role in the establishment of multicellular organisms by organizing and coordinating growth, development and defence responses. In plants, cell-to-cell communication takes place through nanometric membrane channels called plasmodesmata (PD). Understanding how PD dictate cellular connectivity greatly depends on a comprehensive knowledge of the molecular composition and the functional characterization of PD components. While proteomic and genetic approaches have been crucial to identify PD-associated proteins, *in vivo* fluorescence microscopy combined with fluorescent protein tagging is equally crucial to visualise the subcellular localisation of a protein of interest and gain knowledge about their dynamic behaviour. In this protocol we describe in detail a robust method for quantifying the degree of association of a given protein with PD, through ratiometric fluorescent intensity using confocal microscopy. Although developed for *N. benthamiana* and *Arabidopsis*, this protocol can be adapted to other plant species.

**Keywords:** Plasmodesmata, PD Index, Protein enrichment, Confocal data analysis, Confocal microscopy

**[Background]** Currently, confirmation of protein localization to PD by confocal imaging is based primarily on two different approaches. On the one hand, the molecular composition of the cell wall surrounding PD differs. While the cell wall is highly enriched in cellulose, the environment near the PD is enriched in callose, a beta (1-3) glucan polymer that can easily and specifically be stained with fluorophore Aniline Blue. This staining presents the considerable advantage of being used as a PD marker without crossed lines. On the other hand, proteomic studies have identified specific PD proteins and led to their characterization (Faulkner *et al.*, 2005; Fernandez-Calvino *et al.*, 2011; Grison *et al.*, 2015; Brault *et al.*, 2019). These proteins can be used as PD markers in subsequent studies when tagged with fluorescent proteins in transient or stable expression in plants (Thomas *et al.*, 2008; Simpson *et al.*, 2009). Note that PD proteins can be exclusively associated with PD but can also present a dual localization within different cellular compartments as for Synaptotagmin1 (SYT1), Multiple C2 domains and Transmembrane regions Protein 4 (MCTP4) which associate with both the Endoplasmic Reticulum and PD (Levy *et al.*, 2015; Brault *et al.*, 2019). Since PD are dynamic structures responding to developmental and environmental cues, their molecular constituents may vary conditionally (Benitez-Alfonso *et al.*, 2013; Stahl *et al.*, 2013; Han *et al.*, 2014; Sager and Lee, 2014; Otero *et al.*, 2016; Stahl and Faulkner, 2016). Thus, Receptor Like Kinases (RLKs), such as the Leucine-Rich-Repeat RLKs Qian

Shou Kinase 1 (QSK1) and Inflorescence Meristem Kinase 2 (IMK2) or the Cystein-Rich Receptor Kinase 2 (CRK2), are able to dynamically relocate to PD upon osmotic stress conditions (Grison *et al.*, 2019; Hunter *et al.*, 2019). The study of the dynamic localization of protein *in vivo* requires the development of quantification methodologies. Using confocal microscopy, we developed a ratiometric calculations to evaluate the PD enrichment of a given protein using PD markers, hereinafter referred as “PD Index”. The PD Index can be used for co-localization experiments but also as reference points for characterizing mutants, drugs or growing conditions that could modify the degree of proteins PD association (Perraki *et al.*, 2018; Brault *et al.*, 2019; Grison *et al.*, 2019).

## **Materials and Reagents**

1. Syringe without needle (1 ml, Dutscher, catalog number: 8SS01H1)
2. Razorblade (19 x 38 x 0.27 mm, Dutscher, catalog number: 320529)
3. Slides (76 x 26 mm, Dutscher, catalog number: 06962)
4. Coverslips (22 x 32 mm, Dutscher, catalog number: 100034M)
5. Tweezer (Pince à écharde forme pointue, Dutscher, catalog number: 711197)
6. Plant material (see Procedure A)
7. Aniline Blue (Biosupplies Australia, catalog number: 100.1), storage at 4 °C

*Note: The Aniline Blue stock solution is 1 mg/ml in water. The Aniline Blue working solution is 0.025 mg/ml. Do not use higher concentration of aniline bleu when the protein of interest is GFP tagged otherwise the Aniline Blue signal will crosstalk with the GFP signal.*

8. Distilled water
9. Luria and Bertani medium (LB broth Miller, Sigma-Aldrich, catalog number: L3152)
10. Sucrose (Sigma-Aldrich, catalog number: S7903)

## **Equipment**

1. Confocal Microscope: plant imaging was performed using a ZEISS microscope (ZEISS, model: LSM880)
2. 28 °C Shaking Incubator (Dutscher, MaxQ 4000, catalog number: 078381)
3. Centrifuge (Dutscher, Spectrafuge 6 C for 10 ml tubes, catalog number: 096610)

## **Software**

1. FIJI (<https://imagej.net/Fiji>) (Schindelin *et al.*, 2012)
2. R (<https://www.r-project.org>) (R Core Development Team, 2015)

## **Procedure**

### A. Plant material preparation

#### ***In Arabidopsis seedlings***

##### 1. Aniline Blue staining

This method allows PD staining in the cotyledon and the hypocotyl, the aniline blue staining in roots gives a resolution and staining efficiency that we find difficult to combine with PD Index calculation.

*Note: For roots, we advise the users to do immunolocalization in whole mount roots using monoclonal antibody: Biosupplies Australia, (1-3)-beta-glucan-directed monoclonal, catalogue number 400-2 and the protocol described in Boutté and Grebe, 2014.*

- a. Grow *Arabidopsis* seedlings during 4 to 6 days on ½ MS 1% sucrose agar plate under 16/8 h day/night photoperiodic condition (150 µE/m<sup>2</sup>/s, 22 °C).
- b. Take 0.2 ml of Aniline blue solution at a concentration of 0.025 mg/ml in water with the 1 ml syringe.

*Note: Abiotic or biotic stress conditions can be tested to compare the PD Index of the protein of interest, in that case the aniline blue can be diluted in water supplemented with different molecules (such as NaCl, Mannitol, ...) or can be apply before the aniline blue staining (such as viral infection where the plant is infected few days before aniline blue infiltration). Note that leaves or seedlings cannot be infiltrated twice.*

- c. Remove the air from the syringe.
- d. Carefully take the seedling with tweezers.
- e. Gently push the seedling into the syringe, so that the aerial parts of the seedling (*i.e.*, the cotyledons and hypocotyl) are immersed in the solution (Figures 1A-1D). The seedling's root should protrude from the syringe in order to be able to extract the seedling from the syringe after infiltration.
- f. Position your finger at the extremity of the syringe and slowly pull the piston out of the syringe and reach the 0.21 graduation, bubbles should appear at the surface of the cotyledons (Figures 1E-1H).
- g. Count to 5 and then release the piston very slowly (Figures 1I).
- h. Carefully remove the seedling from the syringe by grasping the root of it with tweezers (Figures 1J-1K).
- i. Place the seedling on a slide in a drop of water, and gently mount the coverslip.
- j. Immediately proceed to the acquisition under the confocal microscope.

*Note: Aniline Blue bleaches rapidly. Direct observation should be done with a low power of the mercury lamp to avoid the bleaching of the sample. In confocal mode, please use a*



405 nm laser power as low as possible for the same reason. With the ZEISS 880 confocal device, the laser power is generally set around 0.2 to 5%, but of course this may vary depending on the microscope used. Aniline blue staining can be visualised immediately and is stable during 10 to 15 min.

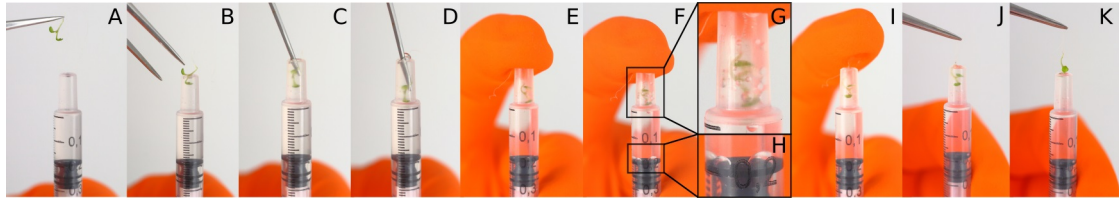


**Figure 1. Arabidopsis seedling infiltration.** Illustration of the different steps of an Arabidopsis seedling infiltration using a 1 ml syringe.

## 2. Using PD proteins as PD marker

In addition to aniline blue, fluorescently tagged PD proteins such as Plasmodesmata Located Protein 1 (PDLP1) or Plasmodesmata Callose Binding Protein 1 (PDCB1) can be used as PD markers for the PD Index calculation both in transient and stable expression (Thomas *et al.*, 2008; Simpson *et al.*, 2009). However, we highly recommend crossing the Arabidopsis lines expressing the protein of interest with the available Arabidopsis lines expressing a fluorescent tagged PD marker protein.

*Notes:*

- Over expression of PD associated proteins can lead to callose deposition at PD.
- Transient expression of fluorescent tagged PD protein markers in Arabidopsis seedlings may be used but the efficiency rate of transformation is low. We do not recommend this method.

## In *Nicotiana benthamiana*

### 1. Aniline Blue staining

- Three days before imaging, infiltrate *Nicotiana benthamiana* leaves only with agrobacteria previously electroporated with the relevant binary plasmid of the protein of interest (as described in Step A1a of **In Arabidopsis seedlings**).
- Take a small volume, around 0.2 ml, of aniline blue at a concentration of 0.025 mg/ml in water in a 1 ml syringe.
- Gently return the leaf to show its abaxial side.
- Apply the syringe on the leaf and position your finger at the same location on the other side in order to block the syringe (Figures 2A-2B).

*Note: Avoid infiltration in veins area of the leaf, the area to infiltrate should be as flat as possible. Also avoid the puncture site from the previous Agrobacterium infiltration.*

- Apply a small pressure on the leaf with the syringe and push slowly the piston in order to infiltrate (Figures 2C-2F).

*Note: When the liquid penetrates and migrates in the leaf, a darker area should appear and expand around the syringe. If the pressure applied is correct, the infiltration should be smooth, without resistance nor loss of liquid, and without wounding the surface of the leaf.*

- f. Do not infiltrate the whole leaf, a small area of 1 cm<sup>2</sup> is sufficient.
- g. With a sharp razor blade, cut the infiltrated area of the leaf.
- h. Place the sample on a mounting slide, abaxial side of the leaf facing up.
- i. Add a drop of water on the sample.
- j. Cover it with the coverslip.
- k. Immediately proceed to the acquisition under the confocal microscope.



**Figure 2. *Nicotiana benthamiana* leaf infiltration.** Illustration of the different steps (A-F) of *Nicotiana benthamiana* leaf infiltration using a 1 ml syringe.

2. Using PD proteins as PD marker
  - a. Grow *Agrobacterium* previously electroporated with the relevant binary plasmids of the protein of interest and of the PD marker (Table 1) in liquid Luria and Bertani medium with appropriate antibiotics, at 28 °C and 250 rpm, for 1 day.
  - b. Perform a 1/10 dilution of each culture and grow again at 28 °C and 250 rpm until the culture reach an OD<sub>600</sub> of about 0.8
  - c. Centrifuge the culture at 3,500 x g, discard carefully the supernatant and resuspend in water for a final OD<sub>600</sub> of 0.3.
  - d. Mix 1:1 volume of both the *agrobacteria* cultures transformed with the protein of interest and with the PD marker.
  - e. Use 5 to 6 leaves stage plant and make a very small puncture on the abaxial side of each selected leaf. Avoid the leaf veins.
  - f. Apply a 1 ml syringe containing the *agrobacteria* mix in water against the leaf at the puncture site
  - g. Position your finger on the other side to block the syringe and gently push the piston while applying a small pressure on the leaf so the liquid can infiltrate. Here, it is advantageous to infiltrate a large portion of the leaf.
  - h. Place the plant in the appropriate culture room for another 3 days for protein expression.
  - i. Using a razor blade, cut a square of approximately 1 cm<sup>2</sup> in the infiltrated area of the leaf.
  - j. Place the sample on a mounting slide, abaxial side of the leaf facing up.
  - k. Add a drop of water on the sample.
  - l. Cover it with the coverslip.

m. Immediately proceed to the acquisition under the confocal microscope.

## B. Confocal acquisition

1. The use of a water immersion objective 63x (NA  $\geq$  1.4) for observation is recommended to have the same refraction index between immersion and mounting. If water immersion objective is not available, the use of an oil-immersion objective is still possible.
2. The pinhole value needs to be kept at airy 1 to ensure a focal plane as accurate as possible.
3. The excitation wavelength and the spectral acquisition windows should be adjusted according to the fluorescent proteins chosen in your experiment (Table 1).
4. Laser power, photomultiplier (PMT) and photomultiplier offset should be set such that the acquired signals are not saturated. Between experiments and in a same experiment the setting parameters of the PD marker can be modified to obtain the better signal as possible without bleaching. In a same experiment the fluorescent tagged protein of interest channel setting must be kept identical while comparing different mutants or conditions. Between experiments we also recommend keeping the same settings for the fluorescently-tagged protein of interest. However, the PD Index is a ratiometric calculation between Region Of Interest (ROI) in a same picture so changes on the fluorescent protein acquisition setting may be acceptable if really needed.
5. Line average can be applied during image acquisition, the same line average should be kept in all experiments.
6. During image acquisition, the sequential scanning is preferable compared to simultaneous scanning. It is important to control that the excitation wavelength used for one fluorescent protein does not excite the other one, *i.e.*, ensure there is no crosstalk between the PD marker/Aniline blue and the tag of the protein of interest (Table 1).

### Notes:

- a. *The Aniline Blue stock solution is 1 mg/ml in water. The Aniline Blue working solution is 0.025 mg/ml. Do not use higher concentration of aniline bleu when the protein of interest is GFP tagged otherwise the Aniline Blue signal will crosstalk with the GFP signal.*
- b. *To avoid crosstalk of fluorescence between channels, it is necessary to perform independent and combined excitation and detection at the excitation and emission wavelength of the individual fluorochrome or fluorescent protein, respectively. Control samples labeled only with a single fluorescent protein/PD marker should be prepared in order to verify that the laser excitation wavelength used to excite one fluorochrome does not excite the other.*

**Table 1. Fluorescence excitation and emission maximum of Aniline Blue and commonly used fluorescent proteins** (FP: Fluorescent Protein or Dye; Ex: Excitation wavelength in nm; Em: Emission wavelength in nm)

FP or Dye	Ex Maximum	Em Maximum
Aniline Blue	405	450
CFP	433	475
mTurquoise	433	475
mCerulean	433	475
EGFP	488	507
EYFP	514	527
mVenus	515	528
mCitrine	516	529
mRFP	584	607
mCherry	587	610

## **Data analysis**

### A. Data collection using Fiji

1. Open the confocal image with Fiji. Do not split channels.
2. Open ROI Manager (Analyze > Tools > ROI Manager).
3. Use the circle selection tool from main panel and draw a circle on the PD marker channel that is slightly smaller than the size of the PD marker signal (Figure 3A).  
*Note: Only sharp callose signal should be selected as PD ROI. Do not select ROI either for PD ROI and for PM ROI when the "spot" in the aniline blue channel is blurry.*
4. Click "add" on the ROI Manager once the circle is well positioned and selected. A new line should appear in the ROI Manager.
5. Move the circle, without modifying it, to another signal and click "add" again.
6. Repeat Step A4 until you have enough ROI (ROI; best between 5 and 10).
7. Change the view to the other channel (the protein of interest fluorescence channel).
8. Using the same circle resume from step A5 and add regions that do not overlap with the AB signals but are at the cell periphery (Figure 3B).
9. Verify the measurement parameters by going to Analyze > Set parameters. Tick the "Mean gray value" box.
10. Verify that the channel is still on the protein of interest. Then, on the ROI Manager, click on "Measure". A new window appears with the values.
11. Select and copy the values.

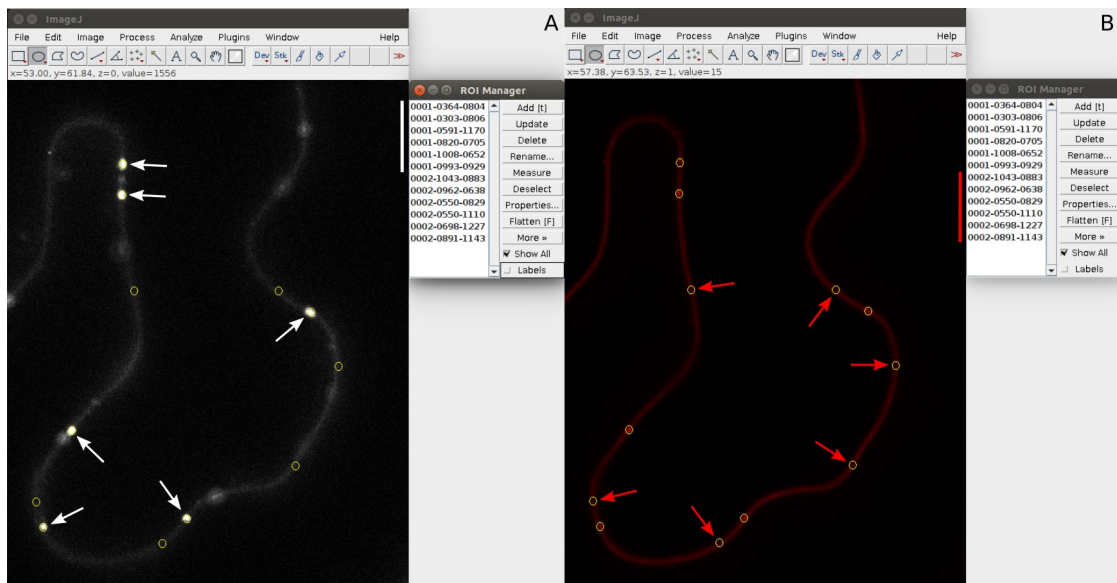


**Figure 3. ROI selection for PD Index calculation.** A. The PD ROI are selected in the PD marker channel (white arrows). B. The PM ROI are selected in the protein of interest fluorescence channel (red arrows). Verify that the ROI selected in the protein of interest fluorescence channel do not correspond to a PD in the PD marker channel.

#### B. PD index calculation using Excel

1. On an Excel sheet, paste the values copied from Fiji (ImageJ)
2. Calculate the mean of the values from “at PD” ROIs and the mean of the values from “outside PD” ROIs
3. Calculate the PD index by doing “At PD ROI mean value/Outside PD ROI mean value”. A PD Index value below or equal to 1 means that there is no specific enrichment nor accumulation of the protein of interest at PD, whereas a PD Index value above 1 is significant from enrichment of a protein at PD.

*Note: For example, a PD resident protein like At-PDCB1, which is also located at the plasma membrane, present a PD Index of 1.45 when transiently expressed in N. benthamiana. QSK1 and IMK2, two PM associated LRR-RLKs which conditionally relocate to PD, display a PD Index rising from 0.9 to 1 in control condition to 1.5 to 2 upon abiotic stress (Grison et al., 2019). It is also important to note that the system of expression may sorely influence the PD Index value. Illustrating this, At-MCTP4 display a PD Index of 1.85 when transiently expressed in N. benthamiana, whereas the PD Index raised to 5 when stably expressed in Arabidopsis (Brault et al., 2019).*

For statistical analysis the use of R software and the Rcmdr package is recommended. Parametrical tests can be use only when  $n \geq 20$  and when the sample distribution respect the normal law. Non-parametrical tests are systematically used when  $n < 20$ .

## **Acknowledgments**

J.D.P. is funded by a PhD fellowship from the Belgian “Formation à la Recherche dans l'Industrie et l'Agriculture” (FRIA grant no. 1.E.096.18).

This work was supported by the National Agency for Research (Grant ANR-14-CE19-0006-01 to E.M.B), “Osez l'interdisciplinarité” OSEZ-2017-BBRIDGING CNRS program to E.M.B., the European Research Council (ERC) under the European Union's Horizon 2020 research and innovation programme (grant agreement No 772103-BRIDGING to E.M.B).

## **Competing interests**

The authors declare no competing financial interests.

## **References**

1. Benitez-Alfonso, Y., Faulkner, C., Pendle, A., Miyashima, S., Helariutta, Y. and Maule, A. (2013). [Symplastic intercellular connectivity regulates lateral root patterning](#). *Dev Cell* 26(2): 136-147.
2. Boutté, Y. and Grebe, M. (2014). [Immunocytochemical fluorescent \*in situ\* visualization of proteins in \*Arabidopsis\*](#). *Methods Mol Biol* 1062: 453-472.
3. Brault, M. L., Petit, J. D., Immel, F., Nicolas, W. J., Glavier, M., Brocard, L., Gaston, A., Fouché, M., Hawkins, T. J., Crowet, J. M., Grison, M. S., Germain, V., Rocher, M., Kraner, M., Alva, V., Claverol, S., Paterlini, A., Helariutta, Y., Deleu, M., Lins, L., Tilsner, J. and Bayer, E. M. (2019). [Multiple C2 domains and transmembrane region proteins \(MCTPs\) tether membranes at plasmodesmata](#). *EMBO Rep* 20(8): e47182.
4. Faulkner, C. R., Blackman, L. M., Cordwell, S. J. and Overall, R. L. (2005). [Proteomic identification of putative plasmodesmatal proteins from \*Chara corallina\*](#). *Proteomics* 5(11): 2866-2875.
5. Fernandez-Calvino, L., Faulkner, C., Walshaw, J., Saalbach, G., Bayer, E., Benitez-Alfonso, Y. and Maule, A. (2011). [Arabidopsis plasmodesmal proteome](#). *PLoS One* 6(4): e18880.
6. Grison, M. S., Kirk, P., Brault, M. L., Wu, X. N., Schulze, W. X., Benitez-Alfonso, Y., Immel, F. and Bayer, E. M. (2019). [Plasma membrane-associated receptor-like kinases relocate to plasmodesmata in response to osmotic stress](#). *Plant Physiol* 181(1): 142-160.
7. Grison, M. S., Brocard, L., Fouillen, L., Nicolas, W., Wewer, V., Dörmann, P., Nacir, H., Benitez-Alfonso, Y., Claverol, S., Germain, V., Boutté, Y., Mongrand, S. and Bayer, E. M. (2015). [Specific membrane lipid composition is important for plasmodesmata function in \*Arabidopsis\*](#). *Plant Cell* 27(4): 1228-1250.
8. Han, X., Kumar, D., Chen, H., Wu, S. and Kim, J. Y. (2014). [Transcription factor-mediated cell-to-cell signalling in plants](#). *J Exp Bot* 65(7): 1737-1749.

9. Hunter, K., Kimura, S., Rokka, A., Tran, H. C., Toyota, M., Kukkonen, J. P. and Wrzaczek, M. (2019). [CRK2 enhances salt tolerance by regulating callose deposition in connection with PLD \$\alpha\$ 1](#). *Plant Physiol* 180(4): 2004-2021.
10. Levy, A., Zheng, J. Y. and Lazarowitz, S. G. (2015). [Synaptotagmin SYTA forms ER-plasma membrane junctions that are recruited to plasmodesmata for plant virus movement](#). *Curr Biol* 25(15): 2018-2025.
11. Otero, S., Helariutta, Y. and Benitez-Alfonso, Y. (2016). [Symplastic communication in organ formation and tissue patterning](#). *Curr Opin Plant Biol* 29: 21-28.
12. Perraki, A., Gronnier, J., Gouguet, P., Boudsocq, M., Deroubaix, A. F., Simon, V., German-Retana, S., Legrand, A., Habenstein, B., Zipfel, C., Bayer, E., Mongrand, S. and Germain, V. (2018). [REM1.3's phospho-status defines its plasma membrane nanodomain organization and activity in restricting PVX cell-to-cell movement](#). *PLoS Pathog* 14(11): e1007378.
13. R Core Development Team. (2015). R: A Language and Environment for Statistical Computing. <https://doi.org/10.1007/978-3-540-74686-7>.
14. Sager, R. and Lee, J. Y. (2014). [Plasmodesmata in integrated cell signalling: insights from development and environmental signals and stresses](#). *J Exp Bot* 65(22): 6337-6358.
15. Schindelin, J., Arganda-Carreras, I., Frise, E., Kaynig, V., Longair, M., Pietzsch, T., Preibisch, S., Rueden, C., Saalfeld, S., Schmid, B., Tinevez, J. Y., White, D. J., Hartenstein, V., Eliceiri, K., Tomancak, P. and Cardona, A. (2012). [Fiji: an open-source platform for biological-image analysis](#). *Nat Methods* 9(7): 676-682.
16. Simpson, C., Thomas, C., Findlay, K., Bayer, E. and Maule, A. J. (2009). [An Arabidopsis GPI-anchor plasmodesmal neck protein with callose binding activity and potential to regulate cell-to-cell trafficking](#). *Plant Cell* 21(2): 581-594.
17. Stahl, Y. and Faulkner, C. (2016). [Receptor complex mediated regulation of symplastic traffic](#). *Trends Plant Sci* 21(5): 450-459.
18. Stahl, Y., Grabowski, S., Bleckmann, A., Kühnemuth, R., Weidtkamp-Peters, S., Pinto, K. G., Kirschner, G. K., Schmid, J. B., Wink, R. H., Hülsewede, A., Felekyan, S., Seidel, C. A. and Simon, R. (2013). [Moderation of Arabidopsis root stemness by CLAVATA1 and ARABIDOPSIS CRINKLY4 receptor kinase complexes](#). *Curr Biol* 23(5): 362-371.
19. Thomas, C. L., Bayer, E. M., Ritzenthaler, C., Fernandez-Calvino, L. and Maule, A. J. (2008). [Specific targeting of a plasmodesmal protein affecting cell-to-cell communication](#). *PLoS Biol* 6(1): e7.

## **Plasmodesmata ultrastructure determination using electron tomography**

Jules D. Petit<sup>1,2</sup>, Marie Glavier<sup>1</sup>, Lysiane Brocard<sup>3\*</sup> and Emmanuelle Bayer<sup>1\*</sup>

1 Univ. Bordeaux, CNRS, Laboratoire de Biogenèse Membranaire, UMR5200, F-33140, Villenave d'Ornon, France.

2 Laboratoire de Biophysique Moléculaire aux Interfaces, TERRA Research Centre, GX ABT, Université de Liège, Gembloux, Belgium.

3 Bordeaux Imaging Centre, Plant Imaging Platform, UMS 3420, INRA-CNRS-INSERM-University of Bordeaux, Villenave-d'Ornon, France.

\* Corresponding authors: Emmanuelle Bayer and Lysiane Brocard.

Running head: Plasmodesmata visualization using electron tomography



## **Summary/Abstract**

Plant plasmodesmata (PD) are complex intercellular channels consisting of a thin endoplasmic reticulum (ER) tubule enveloped by the plasma membrane (PM). PD were first observed by electron microscopy about fifty years ago and, since, numerous studies in transmission and scanning electron microscopy have provided important information regarding their overall organisation, revealing at the same time their diversity in terms of structure and morphology. However, and despite the fact that PD cell-cell communication is of critical importance for plant growth, development, cellular patterning and response to biotic and abiotic stresses, linking their structural organisation to their functional state has been proven difficult. This is in part due to their small size (20-50 nm in diameter) and the difficulty to resolve these structures in three dimensions at nanometer resolution to provide details of their internal organisation.

In this protocol, we provide in detail a complete process to produce high-resolution transmission electron tomograms of PD. We describe the preparation of the plant sample using high-pressure cryofixation and cryo-substitution. We also describe how to prepare filmed grids and how to cut and collect the sections using an ultra-microtome. We explain how to acquire a tilt series and how to reconstruct a tomogram from it using the IMOD software. We also give a few guidelines on segmentation of the reconstructed tomogram.

## **Keywords**

Plasmodesmata, Ultrastructure, Electron tomography, Cryofixation, Segmentation

### **1. Introduction**

In order to obtain information about plasmodesmata (PD) distribution and architecture in different plant tissues, several protocols were established using electron microscopy-based techniques [1-5]. In the case of transmission electron microscopy, protocols involve chemical fixation [1] or cryo-fixation and cryo-substitution [2]. However, most of these protocols are not suitable to access close-to-native

inner structures of PD. Chemical fixations can be very handy for researchers as it allows the preparation of many samples in a relatively short time but it is also impacting the cell physiology. High Pressure Freezing and Freeze Substitution are much more adequate for the cell preservation, but the choice of resin is very important to optimise the observation of the PD architecture embedded in the cell wall.

On the other hand, the development of cryogenic electron microscopy where biological samples are cryo-fixed by vitrification (embedded in vitreous water) and imaged by cryo-electron tomography is very promising to uncover the extremely fine structural elements of PD and macromolecular organization, in a near-native state condition. However, despite their attractiveness, these approaches have, so far, mainly been applied to single particles and biomacromolecules [6-7] and remain challenging for complex plant tissues. In addition, performing cryo-electron microscopy requires expensive equipment that will not be available to all laboratories.

In this chapter, we propose a methodology that relies on high pressure freezing, freeze-substitution and low-temperature staining, to study the inner architecture of PD using transmission electron tomography. This protocol is accessible to most researchers and can be used as a routine tool. We made the choice to describe the entire process, from sample preparation to tomogram analysis and the construction of three-dimensional models, to give a complete guideline of what is necessary material-wise as well as time involvement-wise. It is important to note that adaptations can be made, depending on the available equipment, especially for the tilt series acquisition and the use of the tomogram reconstruction and segmentation software. IMOD software [8] information and tutorials are easily accessible (<https://bio3d.colorado.edu/imod/>), making it possible to optimize usage at best depending on the dataset and the computational equipment.

This protocol was first described in Nicolas et al, *Nature Plant* (2017) [9] and Nicolas et al., *Bio-protocols* (2018) [10], and we acknowledge its complementarity with the current version, mostly by means of the visual support.

## 2. Material

## 2.1. Equipment

1. Liquid nitrogen container and protective gear.
2. Air compressor.
3. Leica EMPACT1 machine.
4. Regular biomolecular pipets and tips from 2  $\mu$ L to 1000  $\mu$ L.
5. Binocular with transmitted light with a high working distance (more than 15 cm).
6. Binocular with lighting from above with a high working distance (more than 15 cm).
7. Heating surface/bench.
8. UV light adapted for AFS2.
9. Leica Automatic Freeze Substitution 2 (EM AFS2) machine.
10. Ventilated chemical hood.
11. Bloc holder.
12. Diamond knives (Trim20 dry, Ultra 45° wet, HISTO 45° wet).
13. Leica Ultracut UC7.
14. Table top microscope.
15. Rubber bellow.
16. Computer with sufficient CPU (and GPU, optional) power.
17. Graphic tablet (optional).

## 2.2. High pressure freezing

1. Liquid nitrogen.
2. Insulated tweezers.
3. Leica loading system with associated platelet holder.
4. 100  $\mu$ m deep 1.5 mm diameter copper membrane carriers.
5. Sample transfer metal containers.
6. Pod holder.
7. Pods.

8. Torque screwdriver.
9. Glass slides.
10. Wooden toothpicks.
11. Razor blades.
12. 1/2 Murashige-Skoog (MS) liquid media (the same used for plant material growth).
13. 20 % Bovine Serum Albumine (BSA) solution in liquid MS medium (the same used for plant material growth).

### 2.3. Freeze substitution

1. Screw top 2 mL tubes.
2. Disposable plastic pipets of 1.5, 2 and 3 mL and thin tip pipets of 1 mL.
3. Glass sample vials with snap-cap.
4. Cartridge half mask.
5. Plastic pills Leica moulds and plastic mould containers.
6. Plastic solvent containers with screw tops for mix with OsO<sub>4</sub>.
7. Glass containers (for dehydration solutions).
8. Aluminum foil.
9. Uranyl acetate solution 20 % in pure methanol (store in dark at -20 °C).
10. Glutaraldehyde 10 % EM-grade anhydrous solution in acetone.
11. Ultrapure 100 % ethanol.
12. Ultrapure 100 % acetone.
13. Osmium tetroxide 0.1 g vials.
14. Nail polish.
15. AFS tube holders.
16. Metal cups for holding cryomix tubes.
17. Metal socket for mould containers for polymerization.
18. Screwdriver for tube/containers transfer.

19. EMS micro-needle and Ted Pella Inc. ultra-micro needle tools.

20. Liquid nitrogen.

#### 2.4. Resin embedding

1. HM20 resin EMS.

#### 2.5. Ultramicrotomy

1. Glass crystallization dish.

2. Glass wand.

3. Fast-absorbent Whatman paper filters.

4. Copper grids (200 and/or 300 mesh thin bars).

5. Glass Pasteur pipet.

6. 0.2  $\mu\text{m}$  syringe filters.

7. Syringe.

8. 0.5 mL Eppendorf tubes.

9. Solid Parlodion.

10. Isoamyl-acetate.

11. 0.05 % toluidine blue solution in water.

12. MilliQ water.

13. Petri dishes of various sizes.

14. Grid containers.

15. EM grade precision tweezers of various styles (2, 5, 5X, 7).

16. Razor blades.

17. Dog hair mounted on a long wooden stick.

#### 2.6. Electron microscopy

1. Electron microscope.
2. Tomo grid holder.
3. Screwdriver for the grid holder clip screws.
4. EM-grade tweezers.
5. Parafilm.
6. 5 nm colloidal gold solution.
7. BSA 0.5 % in filtered MilliQ water.

## 2.7. Softwares

1. Tecnai Imaging and Analysis (TIA) software.
2. Xplore3D (FEI).
3. IMOD (Etomo and 3Dmod).

## 3. Methods

### 3.1. High pressure freezing

1. Start the Leica EMPACT1 and prepare it for usage according to the user manual (*see Note 1*).
2. Once the system is ready (working pressure 4,8-5 bars), shoot an empty pod to remove potential air from the machine circuit.
3. Place a membrane carrier on the Leica loading device and fill it with 20 % BSA in liquid MS medium using a 0,5-2  $\mu$ L pipet (*see Note 2*) while avoiding air bubbles.
4. In the shortest time lapse possible (around 1-2 min): under a binocular with transmitted light, prepare a glass slide with a drop of MS 1/2 solution in order to place the Arabidopsis seedling root. Cut the root tip (~1-1,5 mm) with a sharp razor blade and carefully slide it up using a wooden toothpick. Drop the root by slightly moving the toothpick in the BSA contained in the membrane carrier (*see Note 3*).

5. Push the membrane carrier in the pod, which is positioned in its allocated socket of the Leica loading system. Screw the sapphire tight on the carrier with the TORX screwdriver (set on 2.5 cN.m-1) (*see Note 4*). Screw the white pod holder.
6. Load the ensemble in the Leica EMPACT loading stage and insert the piston. On the screen, tap “prepare”, “lock” and then “start”. The pod and the sample fall in the liquid nitrogen bath.
7. Verify the curves by checking that the maximum pressure (>1900 bars) is reached ~20 ms before the sample is at final temperature (*see Note 5*).
8. From this step, the sample has to be maintained in liquid nitrogen to avoid ice crystallization (occurs between -90 and -80 °C at standard atmosphere pressure). Carefully place the pod holder in the special socket present in the liquid nitrogen bath and unscrew it. Unscrew the clamping from the sapphire to release it and gently tap out the membrane carrier in the bath. Use pre-cooled insulated tweezers to manipulate the membrane carrier and place it in the metal sample container already present in the bath (*see Note 6*).
9. To avoid the blocking of the screw parts due to the freezing of residual water, use a heating surface or a hair dryer to remove all water on the pod and pod holder between each sample. Repeat the process for each sample.
10. When all the samples are ready to be transferred, place a metal lid on the sample container and quickly transfer the container to the already prepared, pre-cooled (-90 °C) and running AFS2 machine (*see Note 7*).

### 3.2. Freeze substitution

During all steps, solutions, containers and tools need to be pre-cooled before entering in contact with samples. Exchange solutions slowly to avoid the loss of samples.

1. In a chemical hood, prepare the cryomix consisting of glutaraldehyde 0.5 %, uranyl acetate 0.1 % and Osmium tetroxide 2 % in pure acetone. To avoid osmium tetroxide reaction, immediately dispatch 200 to 500 µL of the mix in screw top tubes (labelled with a permanent marker) and dip them vertically in liquid nitrogen (*see Note 8*).

2. Place the cryomix tubes in the AFS well, in the metal cups, and dispatch 1 to 3 membrane carriers containing the frozen samples in every tube, as the mix is still in a solid state. Close the tubes with the screw top. The samples will sink as the mix thaw while reaching -90 °C.
3. Set the AFS program at -90 °C for 48 h, followed by a controlled rising of +3 °C/hour for 13 h and a stand-by at -50 °C. To avoid uranyl acetate precipitation, ensure that no light reaches the samples by using an opaque lid or aluminium foil to cover the lid of the AFS2 (*see Note 9*)
4. When the AFS has reached -50 °C and the samples were infiltrated by the cryomix for around 10 h at this temperature, wash thoroughly every tube three times with ultrapure acetone and then three times with ultrapure ethanol (*see Note 10*). For the last wash, transfer the samples into a plastic container (or more if several conditions) containing ultrapure ethanol. Label the containers beforehand with several points of nail polish according to the different conditions (condition 1 with no point, condition 2 with 1 points, etc.)
5. Using the microtools, carefully un mould the frozen sample in BSA from the membrane carrier. To do so, gently poke the BSA at the carrier-sample interface, all around, several times (*see Note 11*).
6. Fill the plastic embedding moulds with cold ultrapure ethanol and let them cool down to -50 °C, then gently transfer the detached sample in the mould with a 3 mL plastic pipet. Sample might need to be repositioned in the center of the embedding mould. Label the moulds beforehand with nail polish according to the different conditions, as before.

### 3.3. Resin embedding

During all steps, solutions, containers and tools need to be pre-cooled before entering in contact with the samples. Exchange solutions slowly to avoid the loss of samples.

1. After all samples have been transferred, pipet out the excess ethanol and replace with a pre-cooled 25 % HM20 in pure ethanol for ~2 h.
2. Always at a working temperature of -50 °C, change the solution for a 50 % HM20 in pure ethanol and let it impregnate ~2 h. Continue with 75 % HM20 in pure ethanol overnight.



3. Replace the solution with fresh pre-cooled 100 % HM20 and incubate at least 2 h. Replace again the resin by fresh pre-cooled 100 % HM20 solution for 2 h. Replace the resin with fresh pre-cooled 100% HM20 one last time. Place the mould containers in the pre-cooled metal piece and adjust the position of samples in the centre of the embedding mould if necessary.
4. Mount the UV lamp on top of the AFS well and set the following program: 8 h at -50 °C without UV (to continue resin embedding), 24 h at -50 °C with UV on, 24 h at +20 °C with UV on.
5. The resin blocks can be removed from the moulds by cutting the plastic with a razor blade and/or punched out from the bottom using a flat tip hexagonal screwdriver.

#### 3.4. Grid preparation

1. Under the hood, place a crystallization dish in a large glass Petri dish and fill it with distilled water until it overflows a little.
2. Roll a glass rod on the top of the crystallization dish to make the water surface even.
3. With a glass Pasteur pipet, let one drop of 2 % parlodion solution (*see note 12*) fall vertically on the water surface and let it spread on the water surface.
4. Using tweezers, remove the parlodion film to clean the water surface from eventual dust.
5. Ensure the hood flux is low and repeat step 3.
6. Gently place the grids on the parlodion film (*see Note 13*).
7. Carefully lay a filter paper on the floating film and grids. Let it slowly soak water.
8. Fold the excess parlodion film from the sides over the filter paper using tweezers.
9. Pinch, at two opposite points the filter paper covered by the parlodion film using two auto-clamping tweezers and flip it (without opening the tweezers) before transferring it into a Petri dish.
10. Place the Petri dish cover over the grids to prevent dust from falling onto them but keeping an opening on one side to allow air flow. Let it under the ventilated hood for 24 h to dry.

### 3.5. Ultramicrotomy

**Important:** Be careful to avoid deformations of the grid.

1. Select the resin block (*see Note 14*) and prepare its face for cutting. First, remove resin excess on each side of the sample with a razor blade. Adjust the cutting surface by using a diamond Trim 20 dry knife for precise trimming. The face must be as small as possible around the biological material and be trapezoidal (parallel sides up and down) with clear and clean edges, especially if serial sectioning is required.
2. When the block face is very close to the sample, switch to a diamond Histo 45° knife (*see Note 15*). Place and secure the knife on the machine, away from the block.
3. Fill the knife boat with filtered distilled water until the water surface is above the knife edges (dome shape). Move the knife manually closer to the block. Do not touch the block with the knife edge, keep a safe distance of a couple of micrometers.
4. Use a wooden stick mounted with a dog hair to gently guide the water to and along all edges and corners. At the diamond knife edge, slide the dog hair tip very gently. Be extra careful not to touch it with the stick.
5. Suck the excess water with a thin syringe needle. Stop removing water when, from the binocular, the water surface reflection is changing, passing through a white reflection to a darker one at the edges and along the diamond knife (*see Note 16*).
6. Approach the knife to the block using the device control panel and the binocular. (*see Note 17*). Stop the approach when a very thin ray of light is still visible between the block face and the knife edge.
7. Cut 250 to 500 nm sections from the block, setting the ultramicrotome speed during the cutting window to 1 mm/s.
8. Once you have entered the sample at desired depth, stop the cutting. Collect the sections using a perfect loop and place them on a glass slide.
9. On a heating bench, dry the glass slide, cover the section with a drop of 0.05 % toluidine blue solution and let dry. Next, wash the excess by dipping the slide and gently moving it

successively into three distilled water baths. Let dry again. The section can be observed under a table microscope.

10. To make the final sections, either continue with the Histo 45° diamond knife for sections between 100 and 150 nm (or more if using a high voltage microscope) or switch to Ultra 45° diamond knife for sections between 60 and 90nm. To cut with the Ultra 45° diamond knife, prepare the knife as in steps 4-7. Cut the sections as required.
11. Collect the sections with the parlodion film coated grids. This is done using auto-clamping tweezers to clamp the grid on one side and plunging it in the water perpendicularly. Then, gently push the sections toward the grid with the dog hair and slowly bring the grid up toward the surface with a small angle (*see Note 18*).
12. Once the sections are on the grid, let them dry still clamped in the tweezers before transferring it into a grid storage box.

### 3.6. Coating sections with fiducial markers

Important: Be careful to avoid deformations of the grid.

1. Prepare the gold particle solution by mixing 1:1 (v:v) the colloidal gold solution with filtered 0.5 % BSA in MilliQ water (*see Note 19*).
2. Clamp the grid with auto-clamping tweezers and place it on the lab bench.
3. Use a pipet to gently lay a drop of 20  $\mu$ L of the gold solution on the grid without touching it. Wait 30 s.
4. Carefully blot the excess solution onto a filter paper from the side of the grid (*see Note 20*).
5. Repeat the steps 3 and 4 on the other face of the grid and let it dry (*see Note 21*).
6. Place the grid back in the grid storage box.

### 3.7. Tilt series acquisition

Important: Be careful to avoid deformations of the grid.

1. Put the grid into the microscope grid holder, depending on the fixing method, the grid can be clipped with a metal ring or tighten by screwing two metal claws.
2. Insert the holder in the electron microscope and wait for the vacuum to go down.
3. Screen the grid to find the root section at low magnification.
4. Set the eucentric height.
5. Perform a coarse alignment of the electron beam.
6. Screen the sample for PD at high magnification. Don't forget to add the diaphragm at the low-Mag/Mag transition to avoid destruction of the section.
7. When a PD is selected, magnify as desired, centre it in the image frame for acquisition and ensure that you have 10 to 30 gold beads in your field of view (*see Note 22*).
8. Set the eucentric focus again.
9. Precisely refine alignment in the following sequence: gun tilt and shift, the focus, the pivot points and the rotation center (*see Note 23*).
10. Open the Xplore3D (FEI) software. It is possible to perform either single or batch acquisitions (*see Note 24*).
11. If you chose to perform batch acquisition, prepare the first area in the software. Continue screening and add as many areas as wanted. Then, or if you decide to perform a single acquisition, follow the software steps: select the working directory and options, choose the acquisition mode and start/end angles (*see Note 25*), center the image when requested by the software.
12. To obtain more resolution, it is possible to perform a dual-axis tomogram. Depending the grid holder and microscope, an automated or manual rotation can be performed. To do the manual rotation, the grid is rotated at a 90° angle from the first tilt series position. Then, start another acquisition along the second axis.

### 3.8. Tomogram reconstruction

IMOD is an open source software available for LINUX, Windows and MAC OS environments.

Software, documentation and tutorials are available on <https://bio3d.colorado.edu/imod/>.

Four files are important for the reconstruction: name.mrc, name.rawltl, name.txt and name\_shifts.txt.

They must be in the same working directory. We are here going to assume a reconstruction from a single axis acquisition.

1. Open the Etomo software. Click on “Build Tomogram”.
2. Browse and select the .mrc file (see **Note 26**). Select “single axis” and click on “Scan Header” and enter the size for the fiducial marker (ex. 5 for a 5 nm diameter fiducial marker). If the .rawltl file is available, click “Tilt angles in existing rawltl file”. Then, click on “Create Com Scripts”. If you chose to start the tilt series acquisition at 0°, enter 0 for the selected parameter “series was bidirectional from:”.
3. On the new window, click on “Pre-processing” (see **Note 27**).
4. To ponderate extreme intensity pixels created during the acquisition step, click on “Create Fixed Stack”. The progress bar is visible at the top of the Etomo window. Then, click on “Use Fixed Stack”. Finish by clicking on “Done”.
5. For the Coarse Alignment, start with “Calculate Cross-Correlation”. Click on the little “A” button of the “Newstack” and deselect the “Convert to bytes” tick box. Continue with “Generate Coarse Aligned Stack”. You can verify the alignment with “View Aligned Stack In 3dmod”. The Z bar at the top of the 3dmod is used to browse through all tilt angles. Finish by clicking on “Done”.
6. Seed tracking method is powerful to optimize the final alignment. First, on the “Seed Model” panel, define which and how many beads will be used for the fine alignment step. Etomo offers two ways to define the fiducial marker: an automatic (“Generate seed model automatically”) and a manual (“Make seed model manually”) one. Select the automatic method. Then, type the number of beads (“Seed Points to Select/Total number: ex.20) for the fiducial tracking. To select the fiducials present on both sides of the sample, click “Select beads on two surfaces”. Then click on “Generate Seed Model”. To verify the quality of the

fiducial selection, click on “Open Seed Model” and check that the software selected only gold beads that are not overlapping and well distributed in the central frame of the series overview (see **Note 28**). Save the “Seed Model”. Keep all the 3dmod windows open.

7. Before the fine alignment, the Etomo software has to track each fiducial on each image of the tilt series. Go on the “Track Beads” panel and click on “Track Seed Model” and “Fix Fiducial Model”. The log window gives the missing points. If the missing point is different from 0, click on “Track with Fiducial Model as Seed” to allow iterative tracking. Stop to click on “Track with Fiducial Model as Seed” when the number of missing points stops to decrease.
8. If the number has not yet reached 0, open the 3dmod model by clicking on “Fix Fiducial model”, for saving bead positions, before going to the Bead Fixer window (3dmod panel/Special/Bead Fixer) and filling manually every gap. To proceed gap by gap, use the button “Go to Next Gap” (in the Bead Fixer window). The concerned bead is highlighted with a green or purple and yellow circle (color code corresponds to the beads on the two surfaces of the sample). Moreover, an arrow indicates if the gap is on the previous or following image, depending on whether it is pointing up or down, respectively (see **Note 29**). Once the point is manually added, click on “Reattach to Gap point”. Repeat for every gap until the main 3dmod window highlights “No more gaps found”. Save the model in the 3dmod software window. Verify there are no missing points by clicking on “Track with Fiducial Model as Seed” one last time in the Etomo window and check the log file. Click on “Done”.
9. In the Fine Alignment step, in the “Global Variables” panel, if the alignment doesn’t show visible shifting and distortion, select “Full solution” in the distortion Solution Type sub-window. If the alignment is not good, select “Disabled”. Then, click on “Compute Alignment”. If the residual error is too high (see **Note 30**), click on “View/Edit Fiducial Model” to correct the fiducial positions.
10. In the Bead Fixer window, click on “Go to Next Big Residual”. The 3dmod visualization panel shows the bead to correct (highlighted with a yellow circle) and the red arrow shows the suggested correction. Magnify the image to have a better view of different fiducial positions. Click on “Move Point by Residual” to move the residual according to the automatic

correction (see **Note 31**). Repeat for every residual until “No more residual” shows in the main 3dmod window. Save the model.

11. Click again on “Compute Alignment” in the Etomo window. The residual error in the log should decrease. New residuals may be needing examination in the 3dmod window. If so, repeat step 10-12 until there are no more residuals to examine or when the residual error and sd are low enough. Then click on “Done”.
12. In the Tomogram Positioning step, change the default “Positioning tomogram thickness” to 1500 in order to access the whole of z view of your section. Click “Create Sample Tomogram” and “Create Boundary Model”. In the 3dmod visualization window, create two parallel lines delimiting the top and bottom of the sample section (include beads). Do this for all three sample sections, top\_rec.mrc, mid\_rec.mrc and bot\_rec.mrc of one Z position (available with the black right/left arrowheads at the top of the window). Save the model.
13. In the Etomo window, change the “Added border thickness (unbinned)” to your sample thickness in nm and click “Compute Z Shift & Pitch Angles” followed by “Create Final Alignment”. Finish by clicking on “Done”.
14. In the Final Alignment Stack step, activate “Use linear interpolation” (select “Aligned image stack binning: 4” to generate a 4 x binned tomogram useful for illustration and no binning for fully resolved tomograms for image analysis) before clicking on “Create Full Aligned Stack”. “View Full Aligned Stack” allows to open the Final Aligned Stack. Click on “Done”.
15. Choose Tomogram Generation options (see **Note 32**) and click on “Generate Tomogram”. “View Tomogram In 3dmod” enables verification and allows to note the beginning and end sections for the trimming (see **Note 33**). Click on “Done”.
16. In the Post-processing step, unnecessary sections present before and after the sample could be trimmed away by defining the Z min and Z max in “Trim vol” panel, section “Volume Trimming/Volume Range”. Deselect “Convert to bytes” in the Scaling section. Then Click on “Trim Volume”. Click on “Done”.
17. The final window enables the deletion of temporary files created during the reconstruction process. Click on “Done”.

18. Close Etomo and find the final reconstructed tomogram in the working directory with the .rec file extension (under Linux) or rec.mrc file extension (under Windows).

### 3.9 Three-dimensional segmentation

In this section, we give limited guidance since every segmentation is dependent on the sample and the researcher objectives. We still share important features to use in the software as well as a few tips. To perform segmentation on a regular basis, the use of a graphic tablet can save time. Segmentation step is relatively interpretative but permits access to the 3D visualisation of individual PD compartments.

1. Open 3dmod and select the .rec file in the Image file browser and click ok. Press “V” on the keyboard to open the Model View window (*see Note 34*).
2. Under “Edit”, “Object”, go to “Type”. Select the object type : Closed or Open (in which case we advise selecting “Start New contour at new Z”).
3. In the 3dmod main window, search for “Drawing Tools” under “Special” and choose the Drawing Mode (*see Note 35*).
4. Trace the elements every five to ten sections and then interpolate for in-between sections using the “Interpolator” tool under “Special” of the main 3dmod window (*see Note 36*).
5. Render the segmentation from the 3dmod Model View window, under “Edit”, “Objects” and select “Meshing” on the bottom left of the new window. Then, select the mesh type and click on “Mesh One” or “Mesh All” (*see Note 37*).

### 4. Notes

1. Keep liquid nitrogen source at proximity in case of need during the process, especially during long sessions of cryofixation. Be aware that liquid nitrogen is dangerous, it can cause burns and asphyxiation, we thus recommend wearing a lab coat, protective gloves, protective goggles and working in a well ventilated space.
2. The solution must form a clean dome in the socket, without any air bubbles nor spilling on the edges.



3. Once the sample is cut, the steps until the sample is cryofixed must be done very rapidly (~1 min) to avoid bias due to tissue damage and stress responses in the cells. Moreover, the sample has to be kept in solution as much as possible to avoid air drying. When the sample is placed in the carrier, it is best if it is completely submerged in BSA, centered in the socket and that no air bubble is present.
4. The tightening is the best when hearing 2 or 3 “clicks” from the screwdriver.
5. From the moment the sample is plunged in liquid nitrogen, it must not be taken out of it.
6. Be attentive to prepare everything you need in advance in the liquid nitrogen bath to avoid bringing room temperature objects in the bath when samples are present. Be sure to cool down the tweezers in a remote corner of the bath before handling the carriers.
7. To easily move containers without transferring heat, a special handle can be screwed to the container while in the bath, and then unscrewed once in the AFS2. If the distance from the EMPACT to the AFS2 is more than a few meters, use an intermediate container filled with liquid nitrogen to put the sample container without risk.
8. Starting from the preparation of the cryosubstitution mix, the procedure involves the handling of many very dangerous chemicals such as acetone, osmium tetroxyde, glutaraldehyde, uranyl acetate and lowicryl resin. We advise clear awareness of the risks and the related safety rules, and a handling of the chemicals in appropriate conditions (vented hood, special gloves, cartridge mask for manipulation outside the hood and in the AFS, protective eyewear, etc.) as well as appropriate waste disposal and management.
9. We encourage checking the tubes the next day, to ensure all samples are in the solution and not covering each other.
10. Every solution and tool that will be used must be pre-cooled in the AFS well for a good 15-20 min. In order to remove and add new solution, pipet out the solution with a thin tip 1mL pipet (avoid pipetting in and out or any other turbulence; always leave some solution in the bottom as a security against air-drying) then add the fresh solution gently with a classic plastic pipet, by letting it drip on the side of the tube. This is true for the entire protocol, but it is very

important here that everything is done with calm and patience because of both the sensitivity of the samples and the dangerousness of the chemicals.

11. This step is certainly the most tedious task of the protocol. Depending on the number of samples, experience and preciseness of the person, it can take up to several hours. If the unmoulding step is difficult with a risk of breaking the sample, skipping this step can be considered. Nevertheless, the resin embedding will require an increase of the times in steps 3.3.1 and 3.3.2. The carrier can later be removed from the polymerized block by doing repetitive cold/heat shocks.
12. 2 % parlodion solution is made from solid parlodion (nitrocellulose) dissolved in isoamyl-acetate. This solution needs to be done at least 24 h in advance to allow proper dissolution. Note that this solution is very easily contaminated with water from the air, which makes bubbles on the film of the grids. To avoid this, it is best to prepare under the vented hood, in a container that won't have much air remaining on top of the solution, to avoid agitation procedures that would bring air into the solution, to limit as much as possible the opening time of the container and to seal the lid with Parafilm between uses. It is also recommended that the container is made of stained glass and wrapped in tinfoil.
13. As the parlodion is transparent, it can be difficult to see the film. However, the edges of the film can be seen by the presence of tiny wrinkles. If the parlodion is not flat or present several visible folds in the middle, remove it and repeat step 3 until it is adequate. For the placement of the grids, the best is to select a homogeneous area on the film and arrange the grids as tight as possible. We advise you to choose one side of the grid (shiny or opaque) to face the film and always work that way. The choice of the grids is as desired, but 200 or 300 mesh/ $\mu\text{m}^2$  thin bars is, to us, optimal for tomography.
14. Check every block under a binocular and select the ones containing a biological sample in a good condition (some roots might have disappeared or being damaged during the sample preparation process). It is possible to carefully smooth the block surface using a dry diamond knife, to see the sample more clearly.

15. Diamond knives are extremely fragile, and very expensive, and must be handled with extra care and calm. Any hit or bump of the knife or tool against the knife might cause irremediable damage to the knife edge and then cause unwanted stripes on the sections. It is crucial to keep that in mind during the whole process, from taking the knife out of the box to the cleaning at the end.
16. If the water is disrupted from the diamond knife edge during this process, maybe there was too much water removed. Fill again the knife boat with new filtered distilled water and level the water again.
17. For the approach phase, the reflection of the knife edge onto the block face can be used to monitor and optimize distances. The light reflected on the block permits to adjust the lateral inclination and orientation of the block. The block needs to be parallel to the diamond knife blade and every point of the block face must be at the same distance from the blade as the block is moved up and down.
18. This necessitates calm and patience as the process is very delicate. This step could be facilitated by hydrophilizing the grids using a glow discharge device. The process takes 2 min and the grids will be hydrophile for about 30 min.
19. This solution can be stored at -20 °C between uses.
20. It is easier to use gravity in the blotting process by folding the paper at a 90° angle and placing it with the fold up on the bench, then bring the grid on top of one of the paper faces (90° angle between the paper face and the grid).
21. Another method consists in putting a drop of the solution onto a parafilm placed on a flat surface and then carefully lay the grid on top of the drop. The grid should not fall in the drop nor touch the parafilm. After 30s, remove the grid, blot the excess solution and let dry. Repeat on the other side of the grid.
22. If there are not enough beads, you can repeat the coating section. We usually work between 30000x and 42000x for tilt series acquisition on PD.
23. We advise to refine the microscope alignment in an area close to the area of interest but not to do it directly above it.

24. The Batch/Single processes are fairly similar but the choice needs to be made when opening the software. Note that single acquisition can be done using either continuous or discontinuous mode, batch acquisition can only be done using the discontinuous mode. The holder calibration file must be chosen accordingly to the selected mode.
25. Tilt angles can be verified manually before starting the acquisition to ensure that there are no grid bars passing on the area of interest at high angles.
26. Because the Etomo software modifies the original files, we advise to copy all original files as “archives”, to be able to start again from them if necessary. The most important file for the reconstruction is the .mrc
27. All reconstruction steps are visible on the left of the Etomo window, they have a colour code and a mention of their advancement (red – step not processed, purple – step is being processed, green – step processed).
28. We typically use around 20-25 nicely segregated and well-spread fiducials but this number can be adjusted depending on the number of beads present on the section (the minimum is 3) and the precision of the reconstruction that is needed. Selecting more fiducials can improve the tomogram alignment. Problematic fiducials can be eliminated by suppressing corresponding “Contour” in the 3dmod tool window before saving the model.
29. In 3dmod, keyboard shortcuts come very handy for rapidly switching from one image to the other in the tilt series. Mouse settings for adding and moving objects are important to know.
30. The log window indicates the residual error mean and sd which represent the number of pixels of uncertainty for the image alignment. Thus, the acceptable values for residual error and standard deviation depend on the pixel size of your image. In our case, the pixel size is usually 0.22 nm since we acquire the tilt series at 4096x4096 resolution. In this condition, correct fine alignment is obtained when the mean residual error is around or below 1 and the sd around or below 0.6 (non binned images).
31. If the automatic correction isn't correct, it is possible to manually adjust the residual position or to keep the position as it is. Moves can be undone by clicking “Undo Move”. When the bead is difficult to see, tracking its movement by going up and down in the tilt series can help.

32. We typically use the Back Projection Method, using the “SIRT-like filter equivalent to ... iterations”. The number of iterations to choose depends on the signal-to-noise ratio. We generally use from 10 to 50 iterations.
33. The quality of the general reconstruction is evaluated by looking at the shape of reconstructed beads. In the XZ view, beads have to have a symmetric X shape.
34. Under “Edit”, “Options”, it is possible to change the mouse and behaviour preferences.
35. New straight lines are made with “Normal” whereas “Warp” and “Sculpt” can be used to adjust lines afterwards. Pressing CTRL+Z undo the last action. Depending on the number and the continuity of the elements (typically the ER and PM membranes), it is possible to create as many objects as necessary. New objects can be created under “Edit”, “Object”, “New” and the object color can be modified in “Edit”, “Object”, “Color”. Working with different colours for different organelles is usually more convenient. In the object window, each object can be off (no visible) or on (visible).
36. We generally use the linear interpolation with a Z-Bridge of 10 or 5. Note that the interpolation only works for one object at the time. When the object switch from a continuous to a discontinuous line, the interpolation can easily go wrong. This usually happens for the PM, which is split in two, at the PD site. To avoid any problem, trace the object on two consecutive sections at the “continuous to discontinuous” line transition.
37. We usually work with “Tube” meshing (with a diameter of 3 or 5, for open objects only) or “Surface” meshing (for closed objects only). It is important to note that object rendering can be different depending on the object type (open or closed).

## **5. Acknowledgements**

This work was supported by the National Agency for Research (Grant ANR-18-CE13-0016 STAYING-TIGHT to E.M.B), the European Research Council (ERC) under the European Union’s Horizon 2020 research and innovation programme (grant agreement No 772103-BRIDGING) to E.M.B, the EMBO Young Investigator Program to E.M.B, J.D.P. is funded by the Belgian “Formation

à la Recherche dans l'Industrie et l'Agriculture" (FRIA grant no. 1.E.096.18). The development of this protocol was performed at the Bordeaux Imaging Centre (<http://www.bic.u-bordeaux.fr/>). The Region Aquitaine supported the acquisition of the electron microscope (grant no. 2011 13 04 007 PFM).

The authors would also like to thank William J. Nicolas, who actively participated in the development of the original protocol, and Sylvain Trépout for his help.

## 6. References

1. Hepler P K (1982) Endoplasmic reticulum in the formation of the cell plate and plasmodesmata. *Protoplasma* 111:121-133. doi:10.1007/BF01282070
2. Ding B, Turgeon R, Parthasarathy M V (1992) Substructure of freeze-substituted plasmodesmata. *Protoplasma* 169:28-41. doi:10.1007/BF01343367
3. Bell K, Oparka K (2011) Imaging plasmodesmata. *Protoplasma* 248:9-25. doi:10.1007/s00709-010-0233-6
4. Brecknock S, Dibbayawan T P, Vesik M et al (2011) High resolution scanning electron microscopy. *Planta* 234:749-758. doi:10.1007/s00425-011-1440-x
5. Barton D A, Overall R (2015) Imaging plasmodesmata with high resolution scanning electron microscopy. In: Heinlein M (ed) *Plasmodesmata: methods and protocols*. Humana Press, New York.
6. Frank J (2017) Advances in the field of single-particle cryo-electron microscopy over the last decade. *Nat Protoc* 12:209-212. doi:10.1038/nprot.2017.004
7. Luque D, Castón J R (2020) Cryo-electron microscopy for the study of virus assembly. *Nat Chem Biol* 16:231-239. doi:10.1038/s41589-020-0477-1
8. Kremer J R, Mastrorarde D N, McIntosh J R (1996) Computer visualization of three-dimensional image data using IMOD. *J Struct Biol* 116:71-76. doi:10.1006/jsbi.1996.0013
9. Nicolas W J, Grison M S, Trépout S et al (2017) Architecture and permeability of post-cytokinesis plasmodesmata lacking cytoplasmic sleeves. *Nat Plants* 3: 17082. doi:10.1038/nplants.2017.82

10. Nicolas W J, Bayer E, Brocard L (2018) Electron tomography to study the three-dimensional structure of plasmodesmata in plant tissues - from high pressure freezing preparation to ultrathin section collection. *BioProtoc* 8(1): e2681. doi: 10.21769/BioProtoc.2681